Protection of CTR First Structural Walls by Neutron Spectrum Shifting

Halil Ibrahim Avci

July 1978

UWFDM-255

Ph.D. thesis.

FUSION TECHNOLOGY INSTITUTE

UNIVERSITY OF WISCONSIN

MADISON WISCONSIN

Protection of CTR First Structural Walls by Neutron Spectrum Shifting

Halil Ibrahim Avci

Fusion Technology Institute
University of Wisconsin
1500 Engineering Drive
Madison, WI 53706

http://fti.neep.wisc.edu

July 1978

UWFDM-255

Ph.D. thesis.

PROTECTION OF CTR FIRST STRUCTURAL WALLS BY NEUTRON SPECTRUM SHIFTING

BY

HALIL IBRAHIM AVCI

A thesis submitted in partial fulfillment of the requirements for the degree of

DOCTOR OF PHILOSOPHY

(Nuclear Engineering)

at the

UNIVERSITY OF WISCONSIN-MADISON

1978

ABSTRACT

PROTECTION OF CTR FIRST STRUCTURAL WALLS
BY NEUTRON SPECTRUM SHIFTING

HALIL IBRAHIM AVCI

Under the Supervision of Professor Gerald L. Kulcinski

The main objective of this thesis has been to explore the means of increasing the fusion reactor first structural wall lifetimes in both the magnetic and inertial confinement systems by the employment of ISSECs (Internal Spectral Shifter and Energy Converters). To accomplish this objective existing radiation damage theories had to be modified and models to more precisely quantify the damage state in the fusion reactor first structural wall materials had to be developed.

The materials studied for the ISSECs were Carbon, and the refractory metals, Mo, Nb, W and V for tokamak applications. Liquid metals such as Li, Pb and a low temperature Pb-Li eutectic, Pb_4Li, were examined for ISSEC in laser fusion reactors. The first wall materials considered were Al, V, 316 SS, Nb, Mo, and Ta.

All ISSECs have been shown to reduce displacement damage and gas production rates in any first wall and thus increase the first wall lifetime. Depending on whether the isotopes causing radioactivity are produced as a result of fast or thermal neutron activation, the first wall radioactivity has been shown to decrease or increase respectively as the ISSEC thickness is increased. A com-

parison study of tokamaks operating on D-T and D-D plasma cycles showed that there is no significant advantage of D-D cycle over the D-T cycle with respect to radiation damage.

ISSECs also affect the blanket parameters such as tritium breeding ratio, energy deposition, and radioactivity. In general, the breeding ratio is reduced by carbon and solid metallic ISSECs, but increased by liquid metal ISSECs. ISSECs of Mo, Nb, W, Pb and Pb_4Li increase the energy multiplication in the cylindrical model blanket of this study, V and C ISSECs decrease it while a Li ISSEC keeps it about constant. The total blanket radioactivity at shutdown is increased by metallic ISSECs while it is being reduced by a carbon ISSEC. At long time after shutdown (>100 years), Mo and Nb ISSEC systems have higher radioactivity than systems employing carbon, V, W ISSEC or no ISSEC at all.

Among the four solid metallic ISSECs studied, Mo is considered to be superior to Nb, W and V. Mo and C both seem to be suitable for an ISSEC in tokamaks. In inertial confinement systems the liquid ISSEC material with the best overall characteristics has been found to be the Pb-Li eutectic and the thickness to be used for best results is 50-70 cm.

Another advantage of the ISSECs is that they produce a PKA spectrum as well as gas production to displacement damage ratio in the first wall close to that found in fast or thermal fission test reactors. This means that the materials data obtained in those reactors become much more meaningful in the design of future fusion

facilities employing ISSECs.

Modifications made in the radiation damage theories and models to more accurately quantify the damage state in fusion reactor first structural walls indicate that the inclusion or omission of the low energy (n,γ) capture and high energy $(n,n'c)$ neutron-charged particle emission reactions from the analysis has negligible effects on the calculated spectral averaged displacement cross sections and PKA energy probability distributions in hard fusion neutron spectra. However, the inclusion of the (n,γ) and $(n,n'c)$ reactions in the calculational models for ISSEC protected systems has been found to increase the spectral averaged displacement cross sections by 1-2% and alter the PKA energy probability distributions by appreciable amounts at low (<1 keV) PKA energies.

Date: July 20, 1978 Signed: _____

Gerald L. Kulcinski
Professor of Nuclear Engineering

ACKNOWLEDGEMENT

I would like to thank Professor Gerald L. Kulcinski for his continuous help and supervision of this study for the last 4.5 years. I am greatly indebted to him for his many helpful suggestions, encouragement and guidance.

I am also grateful to Professor Peter Wilkes and the entire Radiation Effects group at the University of Wisconsin-Madison, particularly H. Attaya, T. Hunter, B. Knoll, R. Lott, K. McLaurin, J. Whitley and R. Zee for their many constructive comments and discussions. I am also appreciative of the help I have received from the members of the Fusion Research program in the Nuclear Engineering Department at the University of Wisconsin-Madison. I would particularly like to thank Professors Conn, Maynard, Vogelsang and Dr. E. Cheng. I would also like to extend my thanks to the rest of the staff and faculty members of the Nuclear Engineering Department. I have had the opportunity to learn from each and every one of them during my eight years of undergraduate and graduate study at the University of Wisconsin.

Finally I wish to express my appreciation to Mary Jane Carr for her neat and diligent work in typing the manuscript of this thesis.

TABLE OF CONTENTS

	Page
Abstract	ii
Acknowledgement	v
List of Tables	ix
List of Figures	xiv
I. INTRODUCTION	1
II. GENERAL REVIEW OF THE ISSEC CONCEPTS	6
II.A. Introduction	6
II.B. General Results from Earlier Work on the ISSEC Concept	9
II.B.1. Description of Design Approaches	9
II.B.2. General Effects of ISSEC Designs on Material Response Functions	17
II.B.3. Summary	29
III. DISPLACEMENT CROSS SECTION AND PKA DISTRIBUTION CALCULATIONS	32
III.A. Secondary Displacement Functions $\nu(T)$	33
III.B. Primary Interaction Mechanisms and Calculations of PKA Spectra	37
III.B.1. Review of Previous Theoretical Work in PKA Distribution Calculations	38
III.B.2. PKA Distribution Calculations for (n,γ) and $(n,n'c)$ Neutron-Charged Particle Emission Reactions	52
III.B.3. Effects of the (n,γ) and $(n,n'c)$ Neutron-Charged Particle Out Reactions on the Calculated Displacement Cross Sections and PKA Spectra.	60
III.B.4. Discussion	67
IV. CALCULATIONAL METHODS	72
IV.A. INPUTPM	72
IV.B. DISCSM	80
IV.C. DPLOT	88
IV.D. NSPECAVE	91
IV.E. APLOT	93

Table of Contents (cont.)

	Page
IV.F. XGRPAVE	97
IV.G. ANISN	99
IV.H. DKR	102
IV.I HEAT and FEM2D	103
V. RESULTS AND ANALYSIS	107
V.A. The Response of the Anticipated First Wall Materials to Fusion Neutron Spectra Degraded by a Carbon ISSEC	108
V.A.1. Introduction	108
V.A.2. Results and Analysis	112
V.A.3. Discussion on Normalization	136
V.A.4. Conclusions of Section V.A.	138
V.B. A Comprehensive Study of Graphite and Solid Metal ISSECs in Tokamak Fusion Reactors	142
V.B.1. Introduction	142
V.B.2. Effects of ISSEC on the 316 SS Structural First Wall	146
V.B.3. Effects of ISSEC on the Total Blanket	154
V.B.4. Radiation Damage in ISSEC	159
V.B.5. Mechanical Design and Heat Transfer of ISSECs	168
V.B.6. Other Considerations Affecting ISSECs	182
V.B.7. Discussion	197
V.B.8. Conclusions of Section V.B.	201
V.C. The Effects of Liquid ISSECs; Li, Pb, and Pb_4Li Eutectic in In Inertial Confinement Fusion Reactors	204
V.C.1. Introduction	204
V.C.2. Results and Analysis	207
V.C.2.a. Damage Parameters	207
V.C.2.b. Breeding Ratio	212
V.C.2.c. Energy Extraction	212
V.C.3. Discussion on Results Obtained in Section V.C.	217
V.C.4. Conclusions of Section V.C.	221

Table of Contents (cont.)

Page

V.D. The Effect of Displacement Cross Sections Calculated by the DISCSM Code on the Reduction of Displacement Damage in Various First Wall Materials Protected by ISSECs 223

V.E. Discussion on Results Presented in Sections V.A., V.B., and V.C. 225

VI. DISCUSSION ON THE POSSIBILITY OF FUSION REACTOR MATERIALS TESTING IN FISSION REACTORS 236

VII. CONCLUSIONS AND RECOMMENDATIONS 264

VII.A. Summary and Conclusions 265

VII.B. Recommendations for Future Research 274

REFERENCES 277

APPENDIX A 287

APPENDIX B 301

LIST OF TABLES

Table		Page
I.1	Summary of Previous Publications of Work Related to this Thesis	5
II.1	ISSEC Concepts with Lithium Cooled External Blankets	10
II.2	ISSEC Concepts with He Cooled, Solid Breeder, External Blankets	12
II.3	ISSEC Concepts with Internal Breeding	13
II.4	ISSEC Burner Concepts	14
II.5	ISSEC Concepts with Liquid Metals Li, Pb and Pb-Li Eutectic	15
II.6	Comparison of Important Reaction Rates in Reference Systems and in Designs Using ISSEC Concepts/E.B., Li-cooled	19
II.7	Comparison of Radioactivity in the First Structural Wall at Shutdown and One Week After Shutdown of Reference Systems and ISSEC Design Concepts	22
II.8	Comparison of Important Reaction Rates in Reference Systems and in Designs Using ISSEC Concepts/E.B., He Cooled	24
II.9	Comparison of Important Reaction Rates in Reference Systems and in Designs Using ISSEC Concepts/I.B.	27
II.10	Comparison of Important Reaction Rates in Reference Systems and in Designs Using ISSEC Concepts/Bu.	30
III.1	The Effects of the (n,γ) and $(n,n'c)$ Reactions on the Calculated Displacement Cross Sections	61
III.2	The Effect of the (n,γ) Reactions on the Spectral Averaged Ni Displacement Cross Sections in Various Neutron Spectra	63
IV.1	Card Input Data for INPUTPM	75
IV.2	Description of the Input to the DISCSM Code	82

LIST OF TABLES (cont.)

Table		Page
IV.3	Input from Cards for the DPLOT Program	89
IV.4	Description of the Card-Input to the NSPECAVE Program	92
IV.5	Description of the Card-Input to APLOT	94
V.1	Factors of ISSEC Produced Reduction in Displacement Damage in Various CTR First Wall Materials in D-T and D-D Fusion Environments	113
V.2	Effect of Carbon ISSEC on the Helium Gas Production Rate in Potential CTR Materials in D-D Fusion Environment	119
V.3	Effect of Carbon ISSEC on the Hydrogen Gas Production Rate in Potential CTR First Wall Materials in D-D Fusion Environment	120
V.4	Effect of Carbon ISSEC Thickness on the Gas Production Rates in Potential CTR Materials/ D-T Plasma	124
V.5	Appm He Generated in 316 SS from $Ni^{58}(n,\gamma)Ni^{59}(n,\alpha)$ Reaction Sequence Only/D-D and D-T	125
V.6	Total Appm He Generated in 316 SS/D-D and D-T	128
V.7	Level of Neutron Induced Radioactivity at Various Times After Shutdown in the First Wall of Carbon ISSEC Protected System After 2 Years of Operation/ D-D Plasma	129
V.8	Level of Neutron Induced Radioactivity at Various After Shutdown Times in the First Wall of an ISSEC Protected System After 20 Years of Operation/D-D Plasma	129
V.9	Level of Neutron Induced Radioactivity at Shutdown in First Wall in an ISSEC Protected System After 2 Years of Irradiation/D-T and D-D	133
V.10	Level of Neutron Induced Radioactivity 100 Years After Shutdown in the First Wall of ISSEC Protected System After 2 Years of Irradiation/ D-T and D-D	134

LIST OF TABLES (cont.)

Table		Page
V.11	A Comparison of Possible Normalization Procedures for D-D and D-T Fusion Systems - 316 SS First Wall	139
V.12	Specific Radioactivity of First Wall (Ci/cm^3)	152
V.13	Specific BHP of First Wall (km^3 of air/W-cm^3)	152
V.14	First Wall Afterheat Density ($Watt/cm^3$)	153
V.15	Nuclear Heating in the Model Blanket and ISSEC Used in This Study	158
V.16	Helium and Hydrogen Production in Various ISSEC Materials	163
V.17	Front and Back Surface Temperatures in the Radiation Cooled 5, 10 and 25 cm ISSECs	170
V.18	Maximum Allowable ISSEC Thicknesses in Three Limiting Cases With Radiation Cooling Only	173
V.19	Generation and Conduction of Heat from ISSECs to 316 SS First Wall and the Thermal Stress Generated in the First Wall	181
V.20	Current Materials Costs for ISSECs	183
V.21	Free Vaporization Rate of Various ISSEC Materials	183
V.22	Summary of Particles Striking the ISSEC Surface for UWMAK-III Conditions	193
V.23	Flux of Sputtered Atoms From Various ISSEC Surfaces	193
V.24	Relative Figure of Merit for Thermal Shock Resistance of Potential ISSEC Materials	196
V.25	Comparison of the Five ISSEC Materials Considered in This Study	198
V.26	Comparison of Various ISSEC Materials Considered in This Study	200

LIST OF TABLES (cont.)

Table		Page
V.27	Summary of Radiation Damage in 316 SS First Wall Behind Various ISSECs	209
V.28	Estimate of Damage Limitations in 316 SS Irradiated in a Fusion Neutron Spectrum	218
V.29	Summary of Liquid Metal ISSEC Thickness Required to Extend 316 SS First Wall Life to Reactor Life	218
V.30	Summary of Necessary Liquid ISSEC Thicknesses Required to Extend Useful Lifetime of 316 SS to 30 Years at 70% P.F. and 5 MW/m^2 Wall Loading	219
V.31	Effect of the Displacement Cross Sections Calculated by the DISCSM Code on the Reduction of Displacement Damage in Nb and 316 SS First Walls by a Carbon ISSEC	226
V.32	Effect of Displacement Cross Sections Calculated by the DISCSM Code on the Reduction of D-T Displacement Damage in 316 SS First Wall by Carbon and Metallic ISSECs	227
V.33	Effect of Displacement Cross Sections Calculated by the DISCSM Code on the Reduction of Displacement Damage in 316 SS First Wall by Liquid ISSECs	228
VI.1	Calculated Ratio of appm He Gas Production to Displaced Atom Density in Potential CTR First Structural Wall Materials	256
VI.2	Appm He/dpa Ratio in the 316 SS First Structural Wall in ISSEC Protected Systems	259
A.1	Sample Card Input to the INPUTPM Program for the Element Niobium	287
A.2	Part of an Output from the INPUTPM (Input to DISCSM) for the Element Nb	288
A.3.1	Damage Cross Sections for Niobium at 14.9 MeV Neutron Energy Calculated by the DISCSM Code	289

LIST OF TABLES (cont.)

Table		Page
A.3.2	$\chi(T)$ Versus the Nb PKA Energy, T at 14.9 MeV Neutron Energy as Calculated by the DISCSM Code	290
A.4	Pointwise Nb Displacement Cross Sections as Calculated by the DISCSM Code	292
A.5	Group Averaged Displacement Cross Sections of Niobium as Calculated by the XGRPAVE Program	293
B.1	Neutron 46 Multigroup Structure in eV	301
B.2	Gamma 21 Multigroup Structure in MeV	302

LIST OF FIGURES

Figure		Page
II.1	Schematic Drawing of a Full ISSEC System	8
II.2	Schematic Drawing of a Partial ISSEC System	8
II.3	Effect of Carbon ISSEC on Neutron Spectrum from a D-T Plasma	18
II.4	Fraction of Be_2C in Spectral Shaper of Model 2 Blankets	25
III.1	Comparison of Ni PKA Energy Distribution Results from the DISCS and DISCSM Codes in a Hard Fusion Neutron Spectrum	65
III.2	Comparison of Ni PKA Energy Distribution Results from the DISCS and DISCSM Codes in a Fusion Neutron Spectrum Softened by 25 cm of Carbon	66
III.3	Comparison of $\chi^{n,\alpha}(E,T)$ Distributions from the Isotropic-Emission Compound-Nucleus Model and Calculations Using Experimental Data for ^{63}Cu and ^{93}Nb at 14 MeV	69
IV.1	Layout of MODISS	73
IV.2	Flow Diagram of INPUTPM	78
IV.3	Flow Diagram of DISCSM	85
V.1	Model Blanket Design Used to Study the Effect of Graphite Spectral Shifter on the Radiation Damage Parameters in the First Wall	109
V.2	Reduction of Displacement Damage by Carbon ISSEC in D-D Fusion Environment	114
V.3	Normalized dpa Rate in ISSEC Protected D-T Systems	115
V.4	The Comparison Effect of Carbon ISSEC on Displacement Damage with D-T and D-D Fusion Neutrons	116
V.5	Reduction of Helium Generation Rates with Carbon ISSEC in D-T Systems	121

LIST OF FIGURES (cont.)

Figure		Page
V.6	Normalized Helium Production Rates in ISSEC Protected Systems. D-D and D-T	123
V.7	The Comparison Effect of Thermal $Ni^{59}(n,\alpha)$ Reaction on the Helium Production in 316 SS First Wall in D-D and D-T ISSEC Systems	126
V.8	Normalized Short Term (Shutdown) Radioactivity in ISSEC Protected D-D Systems After 2 Years of Irradiation	130
V.9	Normalized Mid-term (1 Year) Radioactivity in ISSEC Protected D-D Systems After 2 Years of Irradiation	131
V.10	Normalized Long Term Radioactivity in ISSEC Protected D-D Systems After 2 Years of Irradiation	132
V.11	1-Dimensional Cylindrical Blanket Model Used in This Study	143
V.12	Reduction of Displacement Damage in ISSEC Protected 316 SS First Wall	147
V.13	Effect of Various Kinds of ISSEC on the Helium Production in 316 SS First Wall From High Energy Threshold Reactions	149
V.14	Reduction of Hydrogen Production in 316 SS First Wall by ISSEC	150
V.15	Effect of ISSEC Thickness on Tritium Breeding Ratio in the Model Blanket Used in This Study	156
V.16	Radioactivity of Total Blanket (Including ISSEC) After Shutdown	160
V.17	Displacement Damage in ISSEC	162
V.18	Radioactivity of ISSEC (5 cm Thick)	165
V.19	Biological Hazard Potential of ISSEC (5 cm Thick)	166
V.20	Afterheat of ISSEC (5 cm Thick)	167

LIST OF FIGURES (cont.)

Figure		Page
V.21	Vapor Pressure of Potential ISSEC Materials vs. Temperature	172
V.22	A Radiation Plus Conduction Cooled ISSEC Plate and Its Attachment to the First Wall	175
V.23	Incorporation of ISSEC into Moveable Blanket Concept	176
V.24	Nodal Point Temperatures (^{o}C) in 5 cm Thick, 15 cm Wide ISSECs Cooled by Conduction Only	178
V.25	Nodal Point Temperatures (^{o}C) in 10 cm Thick, 15 cm Wide ISSECs Cooled by Conduction Only	179
V.26	Sputtering Yields for Normal Incidence of Different Ions on Molybdenum (Molten Material)	187
V.27	Chemical Sputtering of Pyrolitic Graphite	189
V.28	Effect of Temperature and Crystal Orientation on the Reaction Probability of Carbon	190
V.29	Pb-Li Phase Diagram	205
V.30	Vapor Pressure vs. Temperature for Liquid Lithium and Lead	206
V.31	Reduction of Displacement Damage in ISSEC Protected 316 SS First Wall	210
V.32	Effect of Various Kinds of ISSEC on the Helium Production in 316 SS First Wall From High Energy Threshold Reactions	211
V.33	Effect of ISSEC Thickness on Tritium Breeding Ratio in the Model Blanket Used in This Study	213
V.34	Energy Multiplication in Liquid ISSEC System	214
V.35	Energy Absorption in Liquid ISSEC	216
V.36	Change in the 316 SS Displacement Cross Sections Due to More Recent Calculations	224

LIST OF FIGURES (Cont.)

Figure		Page
V.37	Effect of Neutron Source and Geometry on the Displacement Damage in 316 SS First Wall	232
VI.1	Differential Fe PKA Distributions in Various Neutron Spectra	237
VI.2	Differential Fe PKA Distributions in Various Neutron Spectra	238
VI.3	Fractional Fe PKA Distributions in Various Neutron Spectra	239
VI.4	Fractional Fe PKA Distributions in Various Neutron Spectra	240
VI.5	Differential Cr PKA Distributions in Various Neutron Spectra	241
VI.6	Differential Cr PKA Distributions in Various Neutron Spectra	242
VI.7	Fractional Cr PKA Distributions in Various Neutron Spectra	243
VI.8	Fractional Cr PKA Distributions in Various Neutron Spectra	244
VI.9	Differential Ni PKA Distributions in Various Neutron Spectra	245
VI.10	Fractional Ni PKA Distributions in Various Neutron Spectra	246
VI.11	Fractional Nb PKA Distributions in Various Neutron Spectra	247
VI.12	Fractional Nb PKA Distributions in Various Neutron Spectra	248
VI.13	Fractional V PKA Distributions in Various Neutron Spectra	249
VI.14	Fractional V PKA Distributions in Various Neutron Spectra	250

LIST OF FIGURES (cont.)

Figure		Page
VI.15	Normalized He/Dpa Ratios for ISSEC Protected System/HFIR	257
VI.16	Normalized He/Dpa Ratios for ISSEC Protected Systems/EBR-II	258
VI.17	Ratio of (Appm He/Dpa) in 316 SS First Structural Wall of CTR ÷ (Appm He/Dpa) in 316 SS in EBR-II	261
A.1	Differential Nb PKA Spectrum at 14.9 MeV Neutron Energy	294
A.2	Normalized Nb PKA Spectrum at 14.9 MeV Neutron Energy	295
A.3	Fractional Nb PKA Distribution at 14.9 MeV Neutron Energy	296
A.4	Niobium Displacement Cross Sections Calculated by the DISCSM Code	297
A.5	Differential Nb PKA Probability Distribution in Hard Fusion Neutron Spectrum	298
A.6	Fractional Nb PKA Probability Distribution in Hard Fusion Neutron Spectrum	299
A.7	Comparison Nb Fractional PKA Distribution in Various Neutron Spectra	300

CHAPTER I

INTRODUCTION

One of the major obstacles to the successful operation of a nuclear fusion power reactor will be the ability of its structural components to withstand the extremely harsh radiation damage environment and to maintain their structural integrity over an extended period of time. In a tokamak fusion reactor, the first structural wall around a D-T plasma will be required to maintain vacuums of $\sim 10^{-8}$ to 10^{-5} torr while its inner surfaces are being bombarded, in a cyclic fashion, with 14.1 MeV neutrons and low Z(D,T,He) particles. In addition to the above environment, the first wall in a laser fusion reactor will also be subjected to intense X-ray bombardment and high Z pellet debris, at a 0.1 to 10 Hertz frequency. Such a severe radiation environment can cause considerable property degradation and erosion of the first wall such that it will probably have to be replaced before the design lifetime of the plant has been achieved. Several studies have concluded that the periodic replacement of a 316 SS first structural wall in a tokamak fusion reactor might take place at intervals anywhere between 2 to 4 years under typical 1-5 MW/m^2 neutron wall loadings.[1-3] One early economic assessment study of fusion reactors concluded that for the UWMAK-I[4] and UWMAK-II[5] reactors, the cost of electricity is significantly increased when the first wall lifetime drops below $\sim$5-10 $MW\text{-}yr/m^2$.[6] In fact, it was

shown that in these reactors the cost of electricity is increased by 17-28% over the 10 MW-yr/m^2 first wall lifetime value if the wall life is only 2 MW-yrs/m^2 and it is 35-65% higher for a wall life of 1 MW-yr/m^2. Therefore, it is apparent that a great incentive exists for seeking ways to increase the first wall lifetimes.

The main objects of this thesis are to:

1. Demonstrate how one might go about achieving higher first wall lifetimes in both magnetic and inertially confined D-D and D-T fusion reactors.
2. Develop models and apply radiation damage theories to more precisely quantify the damage state in first wall materials.
3. Investigate the engineering feasibility of in-situ structures that might be profitably utilized in fusion reactors.

The first objective is accomplished by expanding the original ideas of the Carbon Internal Spectral Shifter and Energy Converter (ISSEC) first proposed in 1974[8] in conjunction with vanadium first walls. The use of varying thickness of C with other first wall materials (i.e., 316 SS, Nb, Mo, Ta, Al) will be investigated with respect to the "normal" response functions such as dpa, gas production, and radioactivity. The use of other solid ISSECs (such as Mo, Nb, V and W) with a single first wall and blanket material (316 SS) is then presented. Finally, the idea of a liquid ISSEC (Li, Pb, or a low temperature Pb-Li eutectic, Pb_4Li) is explored in relation to the "waterfall" laser fusion concept recently proposed.[7,12]

The second objective is accomplished by modifying existing displacement cross section models to include the (n,γ), and $(n, n'x)$ reactions. The Primary Knock-on-Atom (PKA) spectra from all the nuclear reactions (elastic and inelastic) will then be calculated for the neutron spectra behind various solid and liquid ISSECs. These PKA spectra, for various potential CTR materials, will be compared to those characteristic spectra of current fission reactor test facilities. In this way it will be shown that one can have more confidence in associating future wall life predictions with current data obtained in such facilities.

Finally, the third objective is accomplished by examining some of the thermal stress, breeding ratio, and physical property limitations on the realizable benefits of various solid ISSEC concepts in fusion reactors. The format of the thesis is as follows. In Chapter II various ISSEC concepts and their advantages and disadvantages are reviewed. Chapter III reviews the basic theory of displacement cross sections and PKA spectra calculations and it indicates the improvements made in these models for this thesis. The description of the MODISS computer package developed to implement the calculations for this study and the various sources of data used in these calculations are outlined in Chapter IV. The results for carbon, metallic and liquid ISSECs with various first wall materials and blanket structures are presented in Chapter V. Chapter VI has a discussion based on the PKA spectra and He/dpa ratio calculations in various

neutron spectra for possible testing of fusion reactor materials in fission reactors. The implications and conclusions of this study are listed in Chapter VII.

Finally, the reader should be aware that much of this work has previously been published in more detail in various journals and reports listed in Table I.1. The material in Chapter IV and most of Chapters III and VI have not been published before. This list of references is provided early in the thesis here to give the interested reader the opportunity to obtain more detailed information if so desired.

Table I.1

Summary of Previous Publications of Work Related to this Thesis

Ref. #	UWFDM #	Date	Title
8	115[a]	Oct. 1974	New Concepts for Controlled Fusion Reactor Blanket Design
9	127[b]	June 1975	Protection of CTR Metallic First Walls by Neutron Spectral Shifting
10	135[c]	Oct. 1975	The Response of ISSEC Protected First Walls to DT and DD Plasma Neutrons
11	202[d]	April 1977	The Use and Performance of Graphite and Metal ISSECs in Tokamak Fusion Reactors
12	205	April 1977	The Effect of a Liquid ISSEC on Radiation Damage Parameters in Laser Fusion Reactor First Walls
13	208	May 1977	Comparison of Liquid ISSECs, Li, Pb and Pb_4Li for Use in Laser Fusion Reactors
14	---[e]	June 1978	Advantages of Liquid Pb-Li Alloy Spectrum Shifters in Laser Fusion Reactors

[a] Published in Nucl. Tech. 26, 125 (1975).

[b] Also in Trans. Am. Nucl. Soc. 21, 50 (1975).

[c] Published in Proc. Int. Confer. on Rad. Eff. and Tritium Tech. for Fusion Reactors at Gatlinburg, Tenn., Oct. 1-3 (1975), pp. 437-473.

[d] Nuclear Engineering and Design, 45, 285 (1978).

[e] Trans. Am. Nucl. Soc., 28, 40 (1978).

CHAPTER II

GENERAL REVIEW OF THE ISSEC CONCEPTS

II.A. Introduction

It was previously shown that the inclusion of a thin (<1 cm) carbon curtain between a D-T plasma and the first structural wall in a magnetic confinement fusion reactor system can effectively protect the first wall from charged particle erosion and protect the plasma from deleterious effects of the high Z impurity ions and neutrals originating in the first wall.[15] It was later shown that increasing the thickness of the curtain degrades the neutron spectrum sufficiently such that the bulk radiation damage and the long term radioactivity is also reduced in a vanadium first structural wall of a tokamak fusion reactor.[8] The concept was given the name ISSEC, for Internal Spectral Shifter and Energy Converter.

The early studies considered only the carbon or graphite as the ISSEC material[8-10,16] but later metallic elements Mo, Nb, V, and W[11] and liquid metals Li and Pb[7,12] and a Pb-Li eutectic[13] were included among the potential ISSEC materials. In tokamak applications two separate ideas were developed; the full and the partial ISSEC.[16] In the case of full ISSEC, the spectral shifter extends all the way around the plasma and the plasma or its emitted neutrons are never exposed directly to the first wall. In the partial ISSEC concept, the spectral shifter is used to protect only the inner blanket,

nearest to the axis of a tokamak where access and maintenance is most difficult. One advantage of the partial ISSEC concept is that if the ISSEC is restricted to transfer its heat to the first wall by thermal radiation only, the allowable thickness of the ISSEC is much larger in the partial ISSEC case than it is in the full ISSEC case. The maximum temperatures in the ISSEC are much lower because a partial ISSEC can radiate its heat from both inner and outer surfaces to different parts of the first wall. Figures II.1 and II.2 illustrate the full and partial ISSEC concepts, respectively. In this study, unless specified otherwise, a full ISSEC will be studied.

Five separate classes of blanket designs have been considered that utilize the concept of a neutron spectral shifter. They are:

1) Systems that breed tritium in the blanket behind the first structural wall and utilize liquid lithium as the coolant and the breeding material.

2) Systems that also breed tritium in the blanket behind the first structural wall but utilize solid breeders like $LiAlO_2$ and gas coolants such as helium.

3) Systems that breed tritium inside the first structural wall, in the vacuum chamber.

4) Systems that do not breed tritium.

5) Systems that utilize liquid metals such as Li, Pb and their alloys as internal spectral shifter and energy converters (ISSECs) and may breed tritium either internally or externally to the first structural wall.

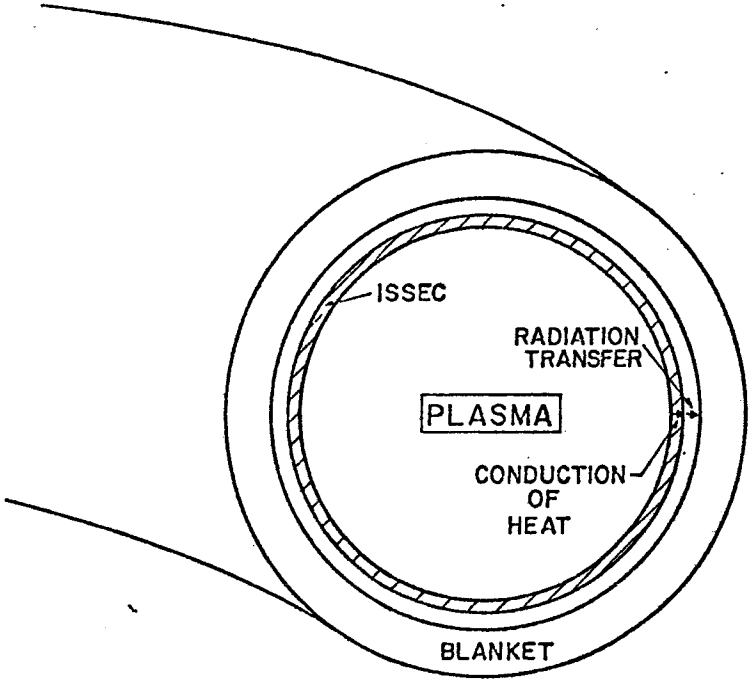

SCHEMATIC DRAWING OF A FULL ISSEC SYSTEM

Figure II.1

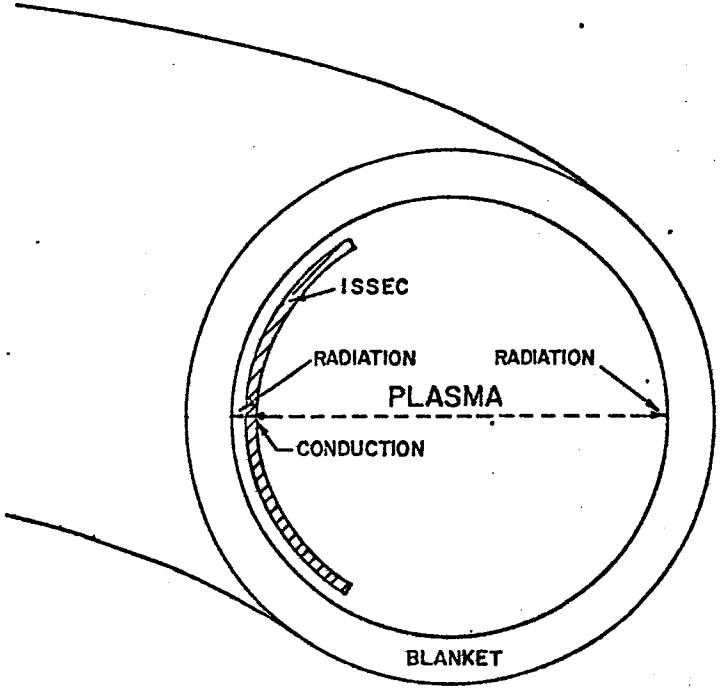

SCHEMATIC DRAWING OF A PARTIAL ISSEC SYSTEM

Figure II.2

The first four designs above have been intended to simulate tokamak or mirror systems and the last one is for a laser fusion system. However, it is conceivable that ISSECs can be used in other magnetic confinement systems as well as in other inertial confinement schemes such as in electron or heavy ion beam fusion systems.

Systems 1, 4 and 5 are fully discussed in Chapter V and they will only be briefly reviewed here. Those aspects regarding the use of internal neutron multipliers and absorbers such as Be_2C and B_4C, which are not covered in Chapter V, will also be highlighted here. More detailed information on systems 1 through 4 can also be obtained in reference 8.

II.B. General Results from Earlier Work on the ISSEC Concept

II.B.1. Description of Design Approaches

In order to illustrate the general features of the ISSEC concept and acquaint the reader with the potential advantages of this approach, five generic blanket systems were studied.[8] These designs are briefly summarized below.

Table II.1 lists the design of blanket systems in which the first structural wall and the blanket behind it are cooled with liquid lithium. System 1A is used as a reference for this type of system and is modeled after previous blanket designs[4,17,18] which utilize liquid lithium as the coolant, moderator, and tritium breeding material. Systems 1B and 1C are used to study the effect

Table II.1

FUSION REACTOR BLANKET DESIGNS USED TO STUDY THE INTERNAL SPECTRAL SHIFTER AND ENERGY CONVERTER (ISSEC) CONCEPTS

ISSEC Concepts with Lithium Cooled External Blankets

(W(cm) = Zone Thickness; Comp = Zone Composition by Volume; D.F. = Zone Density Factor)

Model Number	Internal Blanket						First Structural Wall			External Blanket								
	Zone 1			Zone 2			Zone 3			Zone 4			Zone 5			Zone 6		
	W(cm)	Comp	D.F.	W(cm)	Comp	D.F.	W(cm)	Comp	D.F.	W(cm)	Comp	D.F.	W(cm)	Comp	D.F.	W(cm)	Comp	D.F.
1A	-	Void	-	-	Void	-	1	V	1.0	30	95% Li (nat) + 5% V	1.0	15	"	0.8	5	95% Li (nat) + 5% V	1.0
1B	-	Void	-	12.5	C	1.0	"	"	"	"	95% Li (90% ^{6}Li) + 5% V	"	"	"	"	"	95% Li (90% ^{6}Li) + 5% V	"
1C	-	Void	-	25	C	1.0	"	"	"	"	"	"	"	"	"	"	"	"
1D	-	Void	-	25	50% C + 50% Be_2C	0.5	"	"	"	"	"	"	"	"	"	"	"	"

of placing different thicknesses of three-dimensionally woven carbon elements in front of the first structural wall. Clearly, the neutron moderating properties of carbon suggests the use of lithium enriched in ^{6}Li to maximize the potential breeding ratio. Nevertheless, as will be shown, such systems will not provide enough breeding although conversion ratios can be close to one. However, the radiation damage and induced radioactivity in the first structural wall is greatly reduced. Case 1D has been included to show how tritium breeding ratios of more than 1.0 can be produced with the ISSEC concept and a lithium cooled external blanket. By external blanket, we shall mean the region of the blanket behind the first wall away from the plasma. The internal blanket referred to in Tables II.1 to II.5 is the blanket region between the plasma and the first structural wall. A density factor of 1.0 was used in the calculations in the internal blanket. However, from a neutronics standpoint, these models are equivalent to three-dimensional weaves of twice the thickness at a density factor of 0.5.

Table II.2 summarizes three blanket designs used to illustrate the use of ISSEC concepts with external blankets that use solid breeding materials, such as LiAl or $LiAlO_2$, and high pressure helium cooling. One example of such a system is UWMAK-II.[5] Cases 2B and 2C are used to study the dependence of the breeding ratio on the amount of beryllium (in the form of Be_2C) in the internal spectral

Table II.2

FUSION REACTOR BLANKET DESIGNS USED TO STUDY THE INTERNAL SPECTRAL SHIFTER AND ENERGY CONVERTER (ISSEC) CONCEPTS

ISSEC Concepts with He Cooled, Solid Breeder, External Blankets

(W(cm) = Zone Thickness; Comp = Zone Composition by Volume; D.F. = Zone Density Factor)

Model Number	Internal Blanket				First Structural Wall			External Blanket														
	Zone 1	Zone 2			Zone 3			Zone 4			Zone 5			Zone 6			Zone 7			Zone 8		
		W	Comp	D.F.	W	Comp	D.F.	W	Comp	D.F.	W	Comp	D.F.	W	Comp	D.F.	W	Comp	D.F.	W	Comp	D.F.
2A	Void	-	Void	-	2	V	0.5	3	$90\%LiAlO_2$ $(90\%^6Li)$ + 10% V	0.5	18	90% Be + 10% V	0.5	10	$90\%LiAlO_2$ $(90\%^6Li)$ + 10% V	0.5	38	90% C + 10% V	0.8	8	V	0.9
2B	Void	25	Be_2C	0.5	2	V	0.5	13	$90\%LiAlO_2$ $(90\%^6Li)$ + 10% V	"	35	90% C + 10% V	0.8	4	V	0.9	Void			Void		
2C	Void	25	50% C + 50% Be_2C	0.5	2	V	0.5	13	"	"	35	90% C + 10% V	0.8	4	V	0.9	Void			Void		

Table II.3

FUSION REACTOR BLANKET DESIGNS USED TO STUDY THE INTERNAL SPECTRAL SHIFTER AND ENERGY CONVERTED (ISSEC) CONCEPTS

ISSEC/I.B. Concepts with Internal Breeding

(W(cm) = Zone Thickness; Comp = Zone Composition by Volume; D.F. = Zone Density Factor)

Model Number	Internal Blanket						First Structural Wall			External Blanket		
	Zone 1			Zone 2			Zone 3			Zone 4		
	W(cm)	Comp	D.F.	W(cm)	Comp	D.F.	W(cm)	Comp	D.F.	W(cm)	Comp	D.F.
3A	-	Void	-	-	Void	-	2	V	0.5	50	C	0.8
3B	20	Be_2C	0.5	10	50% $LiAlO_2$ (90% ^6Li) + 50% C	0.5	2	V	0.5	50	C	0.8
3C	20	50% C + 50% Be_2C	0.5	10	50% $LiAlO_2$ (90% ^6Li) + 50% C	0.5	2	V	0.5	50	C	0.8

Table II.4

FUSION REACTOR BLANKET DESIGNS USED TO STUDY THE INTERNAL SPECTRAL SHIFTER AND ENERGY CONVERTER (ISSEC) CONCEPTS

ISSEC/Burner Concepts

(W(cm) = Zone Thickness; Comp = Zone Composition by Volume; D.F. = Zone Density Factor)

Model Number	Internal Blanket						First Structural Wall			External Blanket		
	Zone 1			Zone 2			Zone 3			Zone 4		
	W(cm)	Comp	D.F.	W(cm)	Comp	D.F.	W(cm)	Comp	D.F.	W(cm)	Comp	D.F.
4A	-	Void	-	-	Void	-	2	V	0.5	60	30% B_4C (92% ^{10}B) + 70% C	0.8
4B	-	Void	-	12.5	C	1.0	2	V	0.5	"	"	"
4C	11.5	C	1.0	1	50% B_4C (92% ^{10}B) + 50% C	1.0	2	V	0.5	"	"	"
4D	11.5	50% Be_2C + 50% C	1.0	1	50% B_4C (92% ^{10}B) + 50% C	1.0	2	V	0.5	"	"	"

Table II.5

ISSEC Concepts with Liquid Metals Li, Pb and Pb_4Li Eutectic

(W(cm) = Zone Thickness; Comp = Zone Composition by Volume; D.F. = Zone Density Factor)

Model Number	Internal Blanket			First Structural Wall			External Blanket					
	Zone 1			Zone 2			Zone 3			Zone 4		
	W(cm)	Comp	D.F.	W(cm)	Comp	D.F.	W(cm)	Comp	D.F.	W(cm)	Comp	D.F.
5A	-	Void	-	1	316SS	1.0	60	95% Li (Nat.) + 5% 316SS	1.0	30	95% C + 5% 316SS	1.0
5B	20-100	Liq.Li	1.0	1	316SS	1.0	60	95% Li (Nat.) + 5% 316SS	1.0	30	95% C + 5% 316SS	1.0
5C	20-100	Liq.Pb	1.0	1	316SS	1.0	60	95% Li (Nat.) + 5% 316SS	1.0	30	95% C + 5% 316SS	1.0
5D	20-100	Liq. Pb_4Li Eutectic	1.0	1	316SS	1.0	60	95% Li (Nat.) + 5% 316SS	1.0	30	95% C + 5% 316SS	1.0

shifter. The 2 cm first structural wall has a density factor of 0.5 to account for direct cooling in that zone.

Table II.3 summarizes ISSEC blanket designs which illustrate the potential for both neutron spectral shifting and tritium breeding internal to the first structural wall. Such an approach has an advantage in that all tritium will be handled by a single gas control system already provided to handle gases in the vacuum chamber. This would remove tritium from contact with the primary coolant system and thus eliminate the main potential path for tritium release from the proposed fusion power reactors.[4]

Systems 4A to 4D summarized in Table II.4 illustrate fusion burner blanket concepts designed for energy conversion without tritium breeding. Such systems may be used with D-T fuel if minimizing tritium inventory and associated environmental hazards is an overriding consideration. Relatively near term experimental power reactors are prime candidates for such blanket designs. Of course, such blankets could also be used for fusion reactors based on other fuel cycles, such as D-D, which do not require fuel breeding. In these cases, the external blanket is designed as a helium cooled system which utilizes graphite and boron carbide in a form used in high temperature gas cooled (HTGR) reactor systems.[19] The presence of boron in a system also affects the neutron spectrum and the radioactivity induced by thermal neutron reactions. The beryllium carbide and carbon zone in design 4D multiplies the incident neutrons

and tends to maximize energy production in such ISSEC burners.

Finally, the concept of employing liquid metals such as Li, Pb or a Pb-Li eutectic Pb_4Li as ISSECs in laser fusion reactors is illustrated in Table II.5. System 5A is a base design and in systems 5B, 5C and 5D the thickness of the ISSEC zone (zone 1) has been varied up to 100 cm while the other thicknesses are kept constant. (The first wall is moved back by the corresponding thickness of the ISSEC.) The performance of these class 5 systems will be discussed in Chapter V.

In systems 1-4, models 1A, 2A, 3A and 4A are reference designs with which the performance of other designs will be compared.

II.B.2. General Effects of ISSEC Designs on Material Response Functions

The shift in neutron spectrum at the first structural wall that occurs as a result of using ISSEC is illustrated in Figure II.3. These results are for the blanket design shown later in Figure V.1 and a 316 SS structure is assumed. The results are similar for other structural materials such as V, Nb, Mo, etc. Notice the large amount of decrease in the high energy end and increase in the low energy end of the spectrum. Naturally the thicker the carbon ISSEC, the larger is the shift in the spectrum. Examples of the reduction in the displacement damage rates, gas production rates and long-term radioactivity for a vanadium first structural wall are summarized in Table II.6 for a liquid lithium cooled externally breeding system.

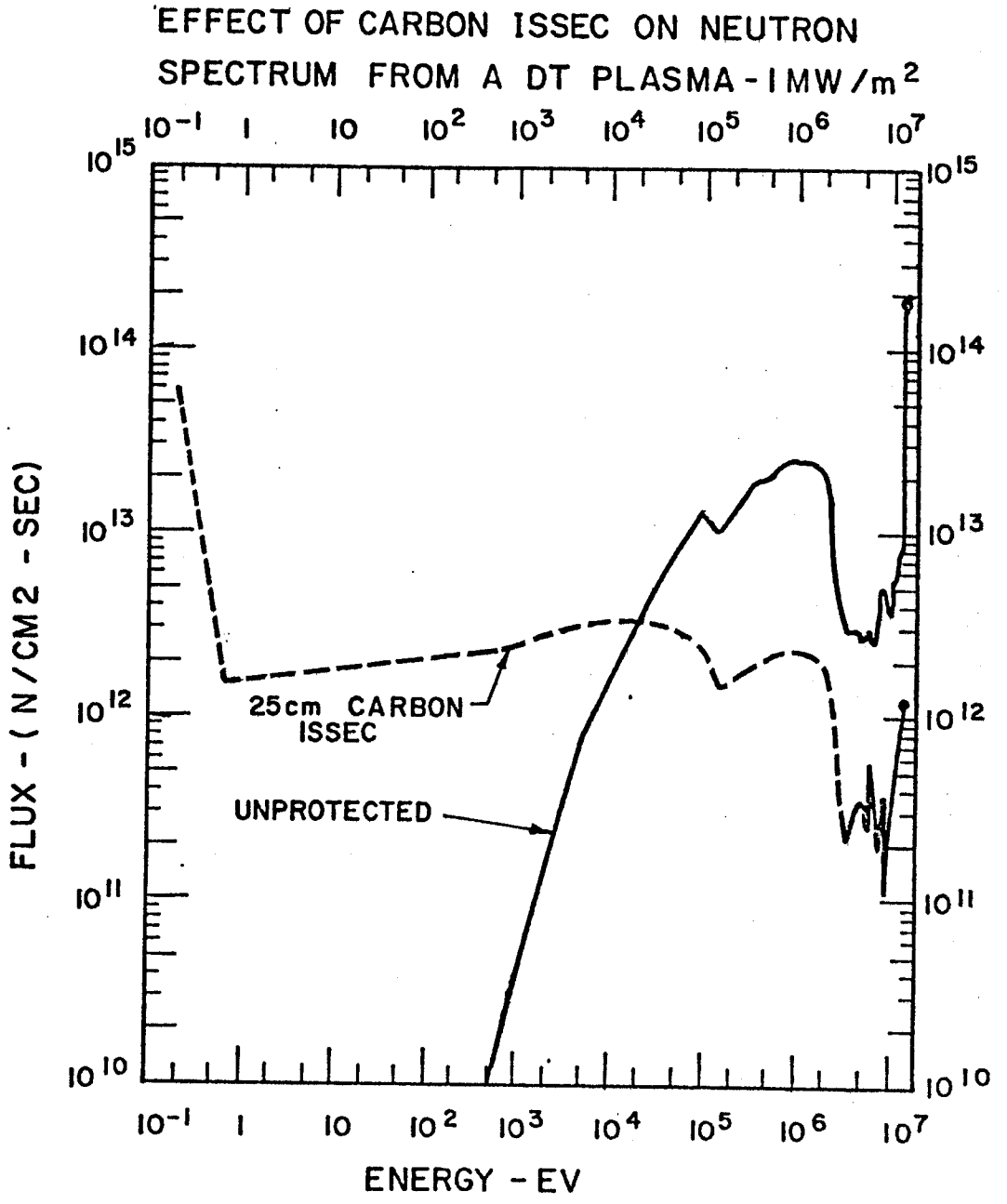
EFFECT OF CARBON ISSEC ON NEUTRON SPECTRUM FROM A DT PLASMA - 1 MW/m2
FLUX - (N/CM2 - SEC)
ENERGY - EV
25cm CARBON ISSEC
UNPROTECTED
10-1
1
10
10 2
10 3
10 4
10 5
10 6
10 7
10 15
10 14
10 13
10 12
10 11
10 10

Figure II.3

Table II.6

Comparison of Important Reaction Rates in Reference Systems and in Designs Using ISSEC Concepts

Model Number	Model Class	Breeding Ratio	Energy Per Fusion (MeV)	He Prod. Rate in First Wall (zone 3) appm/yr*	H Prod. Rate in First Wall (zone 3) appm/yr*	DPA Rate in First Wall (zone 3) dpa/yr*
1A	Reference Li Cooled Blanket	1.29	17.85	72.1	134.4	14.7
1B	ISSEC + Li Cooled External Blanket	0.75	17.33	10.6	26.1	3.92
1C	ISSEC + Li Cooled External Blanket	0.536	17.03	2.71	7.9	1.59
1D	ISSEC + Li Cooled External Blanket	1.05	20.0	7.77	20.89	3.49

* Normalized to 14.1 MeV neutron wall loading of 1 MW/m^2.

(For a more detailed analysis of the reduction of radiation damage parameters see Chapter V.)

A 12.5 cm carbon ISSEC leads to about a factor of 7 reduction in the H and He production rates and about a factor of 3.5 reduction in the displacement damage rates in the first wall (zone 3). A 25 cm carbon shaper produces about a factor of 15 reduction in H and He production rates while the dpa rate in the vanadium is reduced by an order of magnitude. Since the first wall lifetime tends to vary inversely with these response rates, (particularly the dpa and helium production rates) one can expect extended structural wall lifetimes as compared with previous approaches. Note that if the spectral shaper is made of three-dimensional woven carbon fibers, these neutronics results still apply. For a density factor of 0.5, model 1B corresponds to a 25 cm spectral shaper while model 1C would be a 50 cm internal blanket.

Of course, the softening of the neutron spectrum by the carbon leads to a reduction in the breeding ratio, even though the lithium is enriched to 90% in ^{6}Li. As suggested earlier, this may be remedied by including beryllium as a neutron multiplier in the spectral shaper. For example, the use of beryllium carbide pellets coated with pyrolytic carbon and embedded in the 3-D carbon weave is one possible approach. Model 1D has been analyzed to illustrate such a blanket design. The spectral shaper zone is assumed to be composed of 50% Be_2C and 50% C, at one half of actual density to

model carbon coated pellets embedded in a weave system. As indicated in Table II.6 the breeding ratio is above 1.0 in this case, and the energy per fusion is also substantially increased. Both these quantities can be increased even further by increasing the thickness of the lithium breeding zone in the external blanket. For example, in model 1A, an increase in zone 4 from 30 cm to 50 cm increases the breeding ratio from 1.29 to about 1.45.

It is interesting to compare the nuclear performance of cases 1B and 1D since they both include a 12.5 cm internal blanket using a density factor of 1.0. As seen in Table II.6 both the He production rate and the dpa rate are lower when Be_2C is used together with carbon. The reason is that the Be_2C slows down neutrons more effectively than pure C particularly via the (n,2n) reaction, so that the flux above 1 MeV in the first wall is lower in model 1D than in model 1B. This is a general result and is found to hold in all cases with Be_2C.

An important characteristic of all fusion reactors will be the amount of induced radioactivity and afterheat that is generated. This is typically very small in carbon[20] but quite substantial in metallic structural materials.[21-24] The radioactivity in the vanadium first wall of all the models examined in this Chapter is summarized in Table II.7. The level of short-lived radioactivity is assessed by considering only the main contributing isotopes (namely, $^{48}Sc(t_{1/2}=1.82\ d)$, $^{51}Ti(t_{1/2}=5.76\ m)$, and $^{52}V(t_{1/2}=3.75\ m)$) at shutdown and at one week after shutdown. For models 1B, 1C, and 1D, there is a substantial reduction in the ^{48}Sc and ^{51}Ti activities com-

Table II.7

Comparison of Radioactivity in the First Structural Wall (Zone 3) at Shutdown and One Week After Shutdown of Reference Systems and ISSEC Design Concepts

(After 10 years of Operation; In Units of Ci/cm^3 per 1 MW/m^2 of 14.1 MeV neutrons)

Model Number	Model Class	Activity from ^{48}Sc ($t_{1/2}$ = 1.82d)		Activity from ^{51}Ti ($t_{1/2}$ = 5.76m)		Activity from ^{52}V ($t_{1/2}$ = 3.75m)		Total Radioactivity	
		t=0	1 WK	t=0	1 WK	t=0	1 WK	t=0	1 WK
1A	Reference-Li Cooled	4.34	0.302	8.1	-----	30.5	-----	32.8	0.302
1B	ISSEC/EB	0.67	0.0466	1.57	-----	28.3	-----	30.5	0.0466
1C	ISSEC/EB	0.16	0.011	0.47	-----	110	-----	110.6	0.011
1D	ISSEC/EB	0.47	0.033	1.25	-----	128	-----	129.4	0.033
2A	Reference-He Cooled Solid Breeder	4.56	0.317	8.33	-----	18.3	-----	31.2	0.317
2B	ISSEC/EB	0.24	0.0167	0.71	-----	316	-----	317.5	0.0167
2C	ISSEC/EB	0.34	0.0237	0.96	-----	169	-----	170	0.0237
3A	Reference	4.3	0.3	7.97	-----	341.2	-----	353.5	0.30
3B	ISSEC/IB	0.28	0.0195	0.82	-----	50.3	-----	51.4	0.0195
3C	ISSEC/IB	0.34	0.024	0.97	-----	49.2	-----	50.5	0.024
4A	Reference-Burner	4.32	0.30	7.97	-----	1.0	-----	13.3	0.30
4B	ISSEC/Ab	0.64	0.0445	1.61	-----	30.5	-----	32.8	0.045
4C	ISSEC/Ab	0.61	0.0424	1.55	-----	12.7	-----	14.8	0.0424
4D	ISSEC/Ab	0.46	0.032	1.26	-----	2.07	-----	4.79	0.032

pared to case 1A and this leads to reduction by a factor of 10 or more in the long-term radioactivity (greater than 1 week). The reason is that both the ^{48}Sc and ^{51}Ti activities are produced by high energy neutrons, which are moderated by a spectral shaper. On the other hand, the ^{52}V activity, which is induced by the (n,γ) reaction, is increased sharply in cases 1B, 1C, and 1D because of the increase in the number of slow neutrons. These specific results illustrate the general effects that can be expected regardless of the structural material.

There have been several reactor studies that utilize solid breeders and gas coolants, typically helium.[5,26] Model 2A outlined in Table II.2 is an example of such a system.[5] It includes pure Be for neutron multiplication, ($LiAlO_2$) as the solid breeding compound and He as coolant. This is the reference model for this class.

As we can see in Table II.8, the reductions in displacement and gas production rates are even higher than in the previous case. Calculations have been made to determine the amount of Be_2C required to achieve a breeding ratio of more than one. Figure II.4 shows the breeding ratio as a function of the fraction of Be_2C in the spectral shaper. The spectral shaper thickness was taken to be 12.5 cm. It appears that about 85% of the shaper must be Be_2C to obtain a breeding ratio greater than one with such an external blanket design. This is in contrast with the results for model 1D where 50% Be_2C is adequate to achieve breeding. Of course, the reason is the relatively low Li

Table II.8

Comparison of Important Reaction Rates in Reference Systems and in Designs Using ISSEC Concepts

Model Number	Model Class	Breeding Ratio	Energy Per Fusion (MeV)	He. Prod. Rate in First Wall (zone 3) appm/yr*	H Prod. Rate in First Wall (zone 3) appm/yr*	DPA Rate in First Wall (zone 3) dpa/yr*
2A	Reference He Cooled Blanket with Solid Breeder	1.35	21.9	75.8	138.4	15.2
2B	ISSEC + He Cooled External Blanket	1.06	22.3	4.2	12.4	2.9
2C	ISSEC + He Cooled External Blanket	0.87	20.0	6.0	17.6	3.5

* Normalized to 14.1 MeV neutron wall loading of 1 MW/m^2.

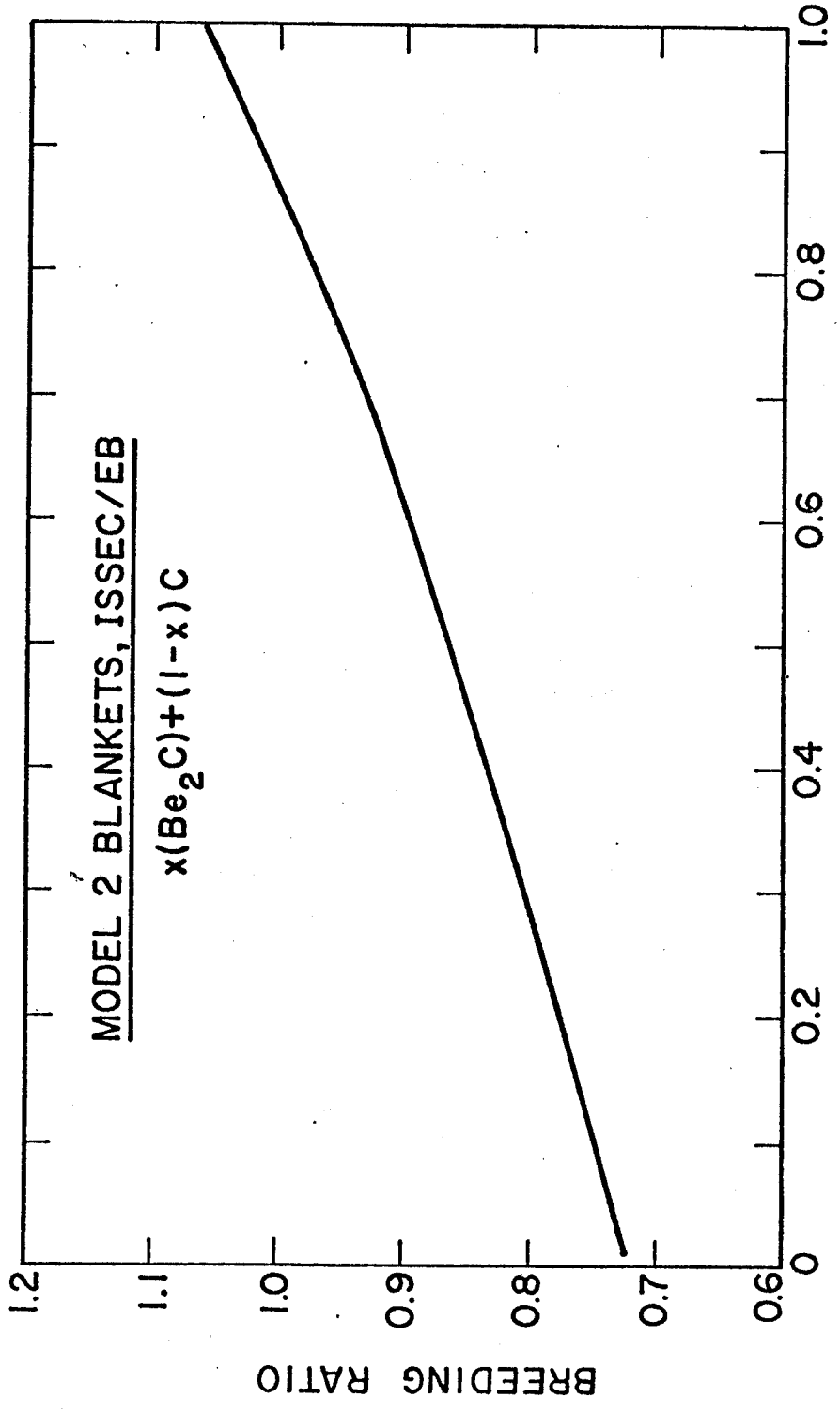
MODEL 2 BLANKETS, ISSEC/EB
x(Be2C)+(1-x)C
BREEDING RATIO
1.2
1.1
1.0
0.9
0.8
0.7
0.6
0
0.2
0.4
0.6
0.8
1.0
X, FRACTION OF Be2C IN SPECTRAL SHAPER

Figure II.4

atom density in the breeding zones when $LiAlO_2$ is the breeding material and the corresponding increase in parasitic absorption. Other materials, such as LiAl or Li_2O, would yield higher Li atom densities and thus somewhat higher breeding ratios.

The effect of the spectral shaper on the radioactivity in the vanadium of the series 2 models is shown in Table II.7. The results are quite similar to those found for models 1A-1D and the explanation of the results is the same.

Table II.9 summarizes the nuclear performance of the ISSEC systems with internal breeding. There are several advantages of these systems over the ones that breed externally to the first structural wall. One is that it can allow all tritium in the system to be handled by a single gas control system already provided for the vacuum chamber. This will remove tritium from contact with the primary coolant and thereby eliminate the main flow path for potential tritium release to the environment. A difficulty with such designs is that there will be high heat deposition rates in the internal blanket, particularly in the breeding zones. This will limit the practical thickness of such systems but a detailed heat transfer analysis is required to establish a maximum thickness accurately. It is also quite possible that an effective heat transfer scheme can be designed such that one does not have to depend solely on radiation to transport heat from the ISSEC zone to the first wall. Then the thickness of this ISSEC zone could be as large as or larger than shown on Tables II.1 to II.4 for a full as well as partial ISSEC.

Table II.9

Comparison of Important Reaction Rates in Reference Systems and in Designs Using ISSEC Concepts

Model Number	Model Class	Breeding Ratio	Energy Per Fusion (MeV)	He Prod. Rate in First Wall (zone 3) appm/yr*	H Prod. Rate in First Wall (zone 3) appm/yr*	DPA Rate in First Wall (zone 3) dpa/yr*
3A	Reference Burner: He Cooled Blanket Without Boron	-----	15.3	71.6	132.4	14.2
3B	ISSEC/I.B.**	1.21	18.3	4.58	13.6	2.93
3C	ISSEC/I.B.**	0.9	18.4	5.69	16.1	3.26

* Normalized to 14.1 MeV neutron wall loading of 1 MW/m^2.

** An ISSEC/I.B. (ISSEC/Internal Breeder) system designed for tritium breeding inside the first structural wall (zone 3 in Table II.1).

Since the tritium breeding and most of the heat deposition occur on the vacuum side of the first structural wall, the external blanket design can be flexible and various coolant - material combinations can be used. For illustrative purposes, a helium cooled, solid graphite system is considered as the external blanket, much like the structures employed in high temperature gas cooled (HTGR) reactors.[19,20]

For the early calculations the solid breeder material used in the ISSEC is $LiAlO_2$ although one might also consider Li_2O. The basic properties of the $LiAlO_2$ and its potential use in fusion reactors has been discussed elsewhere.[25] Lithium aluminate (using Li enriched to 90% ^6Li) has good high temperature properties but at the temperatures expected in the internal blanket (around 2000°C), its vapor pressure is quite high. It would therefore be coated with a material having acceptably low vapor pressure as well as reasonable permeation properties for tritium. Pyrolitic carbon may be acceptable for this role in the 1500-2000°C range. For this reason, and because such composites could be in the form of pellets embedded in graphite or a 3-D carbon weave, the composition of zone 2 in models 3B and 3C is taken as a 50-50 mixture of $LiAlO_2$ and carbon.

From an interpolation of the breeding ratio between models 3B and 3C in Table II.9, it appears that the ratio of Be_2C to total Be_2C plus C content in the first 20 cm of the internal blanket must be approximately 0.65 to achieve a breeding ratio of 1.0. Note,

however, that this is very much dependent on both the thickness of zones 1 and 2 in models 3B and 3C and the lithium bearing compound. As stated earlier, compounds with higher Li atom density, such as Li_2O, would yield higher breeding ratios for the same thickness of the tritium breeding zone.

The performance of ISSEC systems that do not breed tritium (ISSEC Burner Concepts) is discussed fully in Chapter V. Here the effects of B_4C and Be_2C used in models 4C and 4D on Table II.4 will briefly be considered. The external blanket in all these class 4 models is 30% B_4C (Boron enriched to 92% in B^{10}) plus 70% which acts as a neutron absorber and shield and is cooled by helium.

It is clear from Table II.7 that the 1 cm boron carbide zone has a significant effect on the thermal component of the neutron flux in the first wall so that V^{52} activity which is caused by thermal neutron captures is reduced by a factor of 2.4 and 14.7 in models 4C and 4D, respectively, when compared to model 4B. As can be seen from Table II.10, Be_2C in the ISSEC not only increases the reduction in displacement damage and gas production rates for the same thickness as carbon in model 4C, but also increases the energy per fusion. In a way it allows one to "burn" boron to enhance the energy production.

II.B.3. Summary

The results of earlier work on the ISSEC concept have shown that it has a great potential for reducing damage in a vanadium first wall

Table II.10

Comparison of Important Reaction Rates in Reference Systems and in Designs Using ISSEC Concepts

Model Number	Model Class	Breeding Ratio	Energy Per Fusion (MeV)	He Prod. Rate in First Wall (zone 3) appm/yr*	H Prod. Rate in First Wall (zone 3) appm/yr*	DPA Rate in First Wall (zone 3) dpa/yr*
4A	Reference Burner: He Cooled Blanket Containing Boron	-----	15.3	71.8	132.9	12.9
4B	ISSEC/Bu**	-----	15.7	10.7	26.8	4.08
4C	ISSEC/Bu**	-----	15.6	10.1	25.7	3.75
4D	ISSEC/Bu**	-----	18.3	7.67	20.9	3.48

* Normalized to 14.1 MeV neutron wall loading of 1 MW/m^2.

** An ISSEC - Burner System designed for energy conversion without tritium breeding.

of a fusion reactor. It has also been shown that other properties such as short- and long-lived radioactivity, tritium breeding ratio, and energy per neutron emitted can be greatly affected by these concepts. Novel schemes for breeding tritium in the vacuum chamber and using the ISSEC concept in a burner mode have also been shown to have great promise. With such a potential benefit clearly established, other considerations such as the effect of neutron damage on the ISSEC itself, the method of transferring heat, the effect of different ISSEC materials and the response of different first walls need to be examined.

CHAPTER III

DISPLACEMENT CROSS SECTION AND PKA DISTRIBUTION CALCULATIONS

The displacement of atoms from their normal lattice sites as the result of neutron-nucleus interactions is an important source of irradiation damage in reactor materials. The atom that gets forced off from its normal lattice site as a result of such a nuclear interaction is called a Primary Knock-on-Atom (PKA). Depending on the energy of the neutron causing displacements the energy of the PKA can vary between a small value, on the order of 10-100 eV up to several MeV. Succeeding collisions between lattice atoms result in a branching chain of secondary recoiling atoms until the recoils approach the minimum energy needed to cause an atomic displacement. Isolated and clustered defects are produced over a region of the lattice, which is known as displacement cascade.

In calculating the displacement cross sections for a material usually two steps are involved. First, the differential primary Knock-on-Atom (PKA) production cross section $\chi(E,T)$ is determined as a function of neutron energy E and PKA energy T. A secondary defect production function, $\nu(T)$ is then used with $\chi(E,T)$ to define a neutron energy dependent displacement cross section, F(E), as[27]

$$F^i(E) = \int_{T_d}^{T^i_{mx}} \chi^i(E,T)\ \nu(T)\ dT \qquad 3.1$$

where i refers to a particular type of reaction, e.g., elastic, inelastic, (n,2n), (n,p), etc.,

T_d is the minimum energy required to displace an atom, and

T^i_{mx} is the maximum recoil energy from the i^{th} reaction.

The PKA differential cross section $\chi^i(E,T)$ for the i^{th} reaction is expressed as

$$\chi^i(E,T) = \sigma^i(E) \quad K^i(E,T) \tag{3.2}$$

where $\sigma^i(E)$ is the primary neutron interaction cross section for the i^{th} reaction at the neutron energy E, and

$K^i(E,T)$ is the probability that a reacting neutron of energy E will produce a recoil of energy T in the laboratory system, and is called the recoil energy transfer kernel for the i^{th} reaction.

The total displacement cross section at a particular neutron energy E is then the sum of the contributions from all possible nuclear reactions, i.e.,

$$F(E) = \sum_i F^i(E) \tag{3.3}$$

Let us now examine the primary and secondary interactions and it is more convenient to address them in reverse order.

III.A. Secondary Displacement Functions $\nu(T)$

There have been several secondary displacement production functions proposed by different authors[28-34] but there are two that have found widespread use. One of them is the simple model due to Kinchin and Pease.[33] They formulated $\nu(T)$ as follows:

$$\begin{aligned} \nu(T) &= 0 && \text{if} \quad T < E_d \\ \nu(T) &= 1 && \text{if} \quad E_d \leq T < 2E_d \\ \nu(T) &= \frac{T}{2E_d} && \text{if} \quad 2E_d \leq T < A \\ \nu(T) &= \frac{A}{2E_d} && \text{if} \quad T \geq A \end{aligned} \qquad 3.4$$

where E_d is the displacement threshold energy, and

A is the atomic weight of the target element in KeV.

The other widely used secondary displacement model which has been recommended by the International Atomic Energy Agency (IAEA)[30] and the ERDA Working Group on Displacement Calculations[31] is due to Robinson.[28] It is based on the Lindhard, et al.,[35] (LSS) theory of slowing down of energetic atoms in solids and has the following form:

$$\begin{aligned} \nu(T) &= 0 && \text{if} \quad T < E_{d_{eff}} \\ \nu(T) &= 1 && \text{if} \quad E_{d_{eff}} \leq T < 2E_{d_{eff}} \\ \nu(T) &= \beta \frac{T_{dam}}{2E_{d_{eff}}} && \text{if} \quad T \geq 2E_{d_{eff}} \end{aligned} \qquad 3.5$$

where $E_{d_{eff}}$ is the effective displacement threshold and is approximately equal to $\frac{5}{3} E_d$,

β is a numerical factor to account for displacement efficiency and is equal to ~ 0.8, and

T_{dam} is the damage energy; that part of the kinetic energy, T of the recoil atom that goes to displacing atoms. The rest is lost in electron excitations and is assumed

to cause no permanent damage to the metal. T_{dam} is given by:

$$T_{dam} = \frac{T}{1+k_L g(\varepsilon)} \tag{3.6}$$

where the dimensionless energy ε is

$$\varepsilon = A_L T \tag{3.7}$$

and

$$A_L = \frac{0.8853\ A_2}{(27.2)\ Z_1 Z_2 (Z_1^{2/3}+Z_2^{2/3})^{1/2}(A_1+A_2)}\ (eV)^{-1} \tag{3.8}$$

where A_1 and Z_1 are atomic weight and number of the moving particle and A_2 and Z_2 are like quantities for the matrix atoms.

$$k_L = \frac{(0.0793)Z_1^{2/3}Z_2^{1/2}(A_1+A_2)^{3/2}}{(Z_1^{2/3}+Z_2^{2/3})^{3/4}A_1^{3/2}A_2^{1/2}} \tag{3.9}$$

$$g(\varepsilon) = \varepsilon + 0.40244\ \varepsilon^{3/4} + 3.4008\ \varepsilon^{1/6} \tag{3.10}$$

For the case of a pure material rather than an alloy $A_1 = A_2 = A$, $Z_1 = Z_2 = Z$ and the expressions for A_L and k_L simplify to

$$A_L = \frac{0.01151}{(Z)^{7/3}}\ (eV)^{-1} \tag{3.11}$$

and

$$k_L = \frac{0.1334(Z)^{2/3}}{(A)^{1/2}} \tag{3.12}$$

Defects are produced in pairs of interstitials and vacancies in a displacement cascade. Due to the thermal motion and interaction between defects newly created or already present in the matrix, some of the interstitials and vacancies recombine and others form vacancy or interstitial clusters. The amount of recombination and degree of clustering depends on the recoil energy and temperature. It would be desirable to obtain secondary defect production functions for free and clustered vacancies and interstitials. The actual damage state of the material would be better described by such displacement functions. Several theoretical studies[36-39] have attempted to arrive at such displacement functions for iron at recoil energy 1-100 KeV and $\sim 500^{o}$C temperature.

For example, Beeler[36] found that the production of free vacancies in α-iron can be described as

$$\nu_{fv}^{b}(T) = 1.23T^{0.48} \qquad 1 < T < 100 \text{ KeV} \tag{3.13}$$

while in γ-iron, Doran[37] found

$$\nu_{fv}^{d}(T) = 0.52\ (T^{2}+42T)^{1/2} \qquad 1 < T < 100 \text{ KeV} \tag{3.14}$$

The same expression for clustered vacancies from Beeler is

$$\nu_{cv}^{b}(T) = 3.78T^{0.83} - 1.23T^{0.48} \tag{3.15}$$

and from Doran is

$$\nu_{cv}^{d}(T) = 5.0T^{0.80} - 0.38 - 0.52\ (T^2+42T)^{1/2} \qquad 3.16$$

Similar expressions were derived for free and clustered interstitials.

Due to the preliminary nature of the results above and to have a common basis for comparison with earlier calculations, the displacement functions for residual defects were not used in this study. The results of this study will be reported in terms of the secondary displacement model given in equation 3.5. At times in this work we will compare the results given by both the Kinchin and Pease (Eq. 3.4) and Lindhard (Eq. 3.5) secondary displacement models.

III.B. Primary Interaction Mechanisms and Calculations of PKA Spectra

One of the major displacement cross section and PKA distribution calculation codes widely available today was originally written by G. R. Odette and D. R. Doiron.[27] The code was given the name DISCS and the nuclear reactions that Odette and Doiron considered were elastic scattering (n,n), inelastic scattering (n,n'), (n,p), (n,α) and (n,2n). The PKA spectra and displacement cross sections were calculated at any given neutron energy. However, the input data to the code, including all the cross section data, had to be supplied separately for each neutron energy. Later L. R. Greenwood[40] wrote another code that processed the nuclear data from the ENDF files directly and put them in a suitable form for use in DISCS. That made DISCS code more attractive and easier to use.

Odette and Doiron did not include such reactions as (n,γ), $(n,n'\alpha)$ and $(n,n'p)$ in their analysis. As part of work for this study both codes written by L. R. Greenwood, and Odette and Doiron have been modified in such a way that (n,γ), $(n,n'\alpha)$ and $(n,n'p)$ reactions are included in the displacement cross sections and PKA spectra calculations.

In Section III.B.1. the previous theoretical work on the calculation of PKA spectra will be reviewed. Section III.B.2. will outline the improvements made in L. R. Greenwood's and DISCS codes as part of this study. The effects of including the (n,γ) and $(n,n'c)$ charge particle emission reactions on the calculated displacement cross sections and PKA spectra will be given in Section III.B.3. Section III.B.4. will give a discussion on the validity of nuclear models used in these calculations.

III.B.1. Review of Previous Theoretical Work in PKA Distribution Calculations

There have been several attempts to calculate the energy distribution of PKAs in a neutron environment.[27,41-46] Earlier calculations considered only elastic[41] or elastic plus inelastic[42] nuclear reactions. That was adequate for calculating the PKA spectrum in a fission reactor environment. However, with the introduction of fusion reactor concepts[4] where neutrons can have energies of 14 MeV or higher, other high energy threshold reactions such as (n,p) (n,α), $(n,2n)$ had to be considered.

At present there are three major codes designed to calculate the displacement cross sections and PKA spectra in neutron environments.[27,44,45] Of the three codes, the most available and with the best documentation is the one by G. R. Odette and D. R. Doiron.[27] The two codes in references 27 and 44 are believed to be similar in treatment of various nuclear reactions. Gabriel[45] apparently uses a somewhat different physics approach and has concentrated on preparing a very wide data base. His displacement cross section results seem to agree with those of references 27 and 44 to within 20%.

We will now go through a brief review of the Odette-Doiron approach to dpa cross-section calculations to lay the ground work for modifications made in this work described in Section III.B.2. More detailed information on the subject can be found in references 27, 43 and 44.

The procedure used to calculate $K^i(E,T)$ depends on the reaction considered. For single-particle emission reactions, conservation of momentum and total energy give a relationship[42]

$$T(E,E_x,\phi) = \mu_3 E_x + \mu_1\mu_4 E - 2(EE_x\mu_1\mu_3\mu_4)^{\frac{1}{2}} \cos\phi, \qquad 3.17$$

where E_x is the total kinetic energy of reaction products in center-of-mass system, also known as the deexcitation energy,

ϕ is the angle between incident neutron direction and emitted particle direction in center-of-mass,

$\mu_1 = m_1/(m_1 + m_2)$,

$\mu_2 = m_2/(m_1 + m_2)$,

$$\mu_3 = m_3/(m_1 + m_2) \ ,$$

$$\mu_4 = m_4/(m_1 + m_2) \ ,$$

where

m_1 is the mass of incident neutron,

m_2 is the mass of target nucleus,

m_3 is the mass of emitted particle, and

m_4 is the mass of recoil nucleus.

The quantity E_x is related to the energy of the emitted particle in the center-of-mass, E_{3c}, by

$$E_{3c} = \mu_4 E_x \ . \qquad 3.18$$

For single-particle emission reactions, the energy transfer kernel in dT about T can be expressed as[42]

$$\int E_x \text{ (probability of deexcitation energy } E_x) \text{ x}$$
$$\text{(probability that } E_x \text{ produces a recoil of energy T) x} dE_x dT$$

Defining the deexcitation normalized probability as $P_1(E,E_x)$ and the normalized energy transfer probability as $P_2(E,E_x,T)$ we find,

$$K(E,T)dT = \int_{E_x^-}^{E_x^+} P_1(E,E_x)P_2(E,E_x,T)dTdE_x \ . \qquad 3.19$$

The probability $P_2(E,E_x,T)$ is related to the normalized angular emission probability distribution $P_3(E,E_x,\cos\phi)$ as

$$P_2(E,E_x,T) = P_3(E,E_x,\cos\phi)\,\frac{d\cos\phi}{dT}\,, \qquad 3.20$$

where $\cos\phi$ is a function of T, E, E_x found by solving Eq. (3.17). The $E_x^{\pm}$ values are the energetically allowed deexcitation limits. The probability distributions depend on the reaction type and mechanism and can be found from experimental data or nuclear models.

III.B.1.a. Elastic Scattering

The recoil energy distribution of PKAs from elastic scattering is described by the energy-dependent Legendre polynomial coefficients that result from the Legendre expansion of the scattered neutron angular distributions in the center-of-mass system. This gives $K^{el}(E,T)dT$ as[41-43]

$$K^{el}(E,T)dT = \sum_{\ell=0}^{L} \frac{(2\ell+1)}{4\mu_1\mu_2 E} L_\ell(E) P_\ell\left(1 - \frac{T}{2\mu_1\mu_2 E}\right), \qquad 3.21$$

where ℓ is the order of Legendre polynomial term,

L is the order of Legendre expansion used,

$L_\ell(E)$ is the ℓ'th Legendre polynomial coefficient of the angular distribution in center-of-mass system (It is understood that $L_0 = 1.0$.), and

$P_\ell(1-T/2\mu_1\mu_2 E)$ is the ℓ'th-order Legendre polynomial.

III.B.1.b. Inelastic Scattering

Inelastic scattering is handled in two ways depending on the information available on the resolved inelastic scattering levels. If

the discrete resolved cross sections are known, individual level analysis of $K^{inr}(E,T)$ is carried out. When both continuum and resolved cross sections are available, two methods are used over their respective energy ranges.

For isotropic inelastic scattering to M resolved nuclear energy levels, $K^{inr}(E,T)$ is[41-43]

$$K^{inr}(E,T) = \frac{1}{\sigma^{rt}(E)} \sum_{\ell=1}^{M} \frac{\sigma^{r\ell}(E)}{T_\ell^+ - T_\ell^-} , \qquad 3.22$$

where $\sigma^{r\ell}(E)$ is the individual level scattering cross section and where

$$\sigma^{rt}(E) = \sum_{\ell=1}^{M} \sigma^{r\ell}(E) . \qquad 3.23$$

The recoil energy limits are

$$T^{\pm} = 2\mu_1\mu_2\{E \pm [E(E - Q_\ell/\mu_2)]^{\frac{1}{2}}\} - Q_\ell\mu_1 , \qquad 3.24$$

where

$Q_\ell = \mu_2 E - E_x$, and

$Q_\ell = \ell$'th resolved nuclear energy level

The ℓ'th level for a specific T is added to $K^{inr}(E,T)$ if $T_\ell^- \leq T \leq T_\ell^+$.

For scattering to the continuum[42,43]

$$K^{inc}(E,T) = \frac{\theta(E)}{4C_1\mu_1(E\mu_2)^{\frac{1}{2}}} \times \left(\frac{[\theta_1(E)\pi]^{\frac{1}{2}}}{2} \{\mathrm{erf}\{[E_x^+/\theta_1(E)]^{\frac{1}{2}}\} - \mathrm{erf}\{[E_x^-/\theta_1(E)]^{\frac{1}{2}}\}\right.$$

$$\left. - \{(E_x^+)^{\frac{1}{2}} \exp[-E_x^+/\theta_1(E)] - (E_x^-)^{\frac{1}{2}} \exp[-E_x^-/\theta_1(E)]\}\right) \qquad 3.25$$

Here the nuclear temperature $\theta_1(E)$ is approximated as

$$\theta_1(E) = \left(\frac{\mu_2 E}{a}\right)^{\frac{1}{2}}, \qquad 3.26$$

where a is the nuclear density level parameter (i.e., $a \approx m_2/10$) and m_2 is the mass of the recoiling atom. The normalization constant C_1 is given as

$$C_1 = \theta_1^2(E)\left\{1 - \left[\frac{E_x^{mx}}{\theta_1(E)} + 1\right] \exp\left[-E_x^{mx}/\theta_1(E)\right]\right\}. \qquad 3.27$$

The term E_x^{mx} is determined by energy balance consideration, giving

$$E_x^{mx} = \mu_2 E + Q_m , \qquad 3.28$$

where Q_m = Q of highest resolved level that a cross section for a neutron of energy E is available. The term E_x^{mx} is equal to the Q of lowest level if no resolved level cross section data is available and

$$E_x^{\pm}(E,T) = \mu_2 E + T/\mu_1 \pm 2(ETm_2/m_1)^{\frac{1}{2}} \qquad 3.29$$

Due to the upper limit of E_x from energy balance considerations, E_x^+ from Eq. (3.29) must be checked for validity and

$$E_x^+ = E_x^{mx} \quad \text{if } E_x^+ \text{ [from Eq. (3.29)]} > E_x^{mx} , \qquad 3.30$$

that is, if Eq. (3.29) indicates that $E_x^+ > E_x^{mx}$.

III.B.1.c. Charged-Particle Emission

For charged-particle emission reactions, $K^{ch}(E,T)$ is determined by much the same basic procedure as used in the inelastic continuum case except for accounting for differences in mass of incident and emitted particle, the reaction Q value, and effects due to the charge of the emitted particle. With a nonzero lower limit of E_x arising from coulomb barrier $P_1(E,E_x)$, the evaporation model for this case becomes[47]

$$P_1(E,E_x) = \frac{1}{C_2}(E_x - E_{CB})\exp[-(E_x - E_{CB})/\theta_2(E)], \qquad 3.31$$

where

$$\theta_2(E) = \left(\frac{\mu_2 E+Q-E_{CB}}{a}\right)^{\frac{1}{2}} \qquad 3.32$$

E_{CB} = effective coulomb barrier energy.

For isotropic CM angular emission, all recoils between the allowed energy limits are equally probable; thus

$$P_2(E,E_x,T) = \frac{1}{T^+(E,E_x) - T^-(E,E_x)}$$

$$\text{for} \quad T^-(E,E_x) \leq T \leq T^+(E,E_x) \; . \qquad 3.33$$

The terms $T^+(E,E_x)$ and $T^-(E,E_x)$ are found from Eq. (3.17) with ϕ = 180 deg and ϕ = 0 deg, respectively. Substituting from Eq. (3.17) into Eq. (3.33),

$$P_2(E,E_x,T) = \frac{1}{4(EE_x\mu_1\mu_3\mu_4)^{\frac{1}{2}}}. \qquad 3.34$$

Inserting the expressions for $P_1(E,E_x)$ and $P_2(E,E_x,T)$ into Eq. (3.19),

$$K^{ch}(E,T) = \frac{\exp[+E_{CB}/\theta_2(E)]}{4C_2(E\mu_1\mu_3\mu_4)^{\frac{1}{2}}} \int_{E_x^-}^{E_x^+} \frac{(E_x - E_{CB})}{(E_x)^{\frac{1}{2}}}$$

$$x \exp[-E_x/\theta_2(E)]dE_x . \qquad 3.35$$

Evaluation of the integral gives

$$K^{ch}(E,T) = \frac{\exp[+E_{CB}/\theta_2(E)]}{4C_2(E\mu_1\mu_3\mu_4)^{\frac{1}{2}}} \; x \; \{-\theta_2(E)E_x^{\frac{1}{2}}\exp[-E_x/\theta_2(E)]$$

$$+ \theta_2(E)\pi^{\frac{1}{2}} \left[\frac{\theta_2(E)^{\frac{1}{2}}}{2} - E_{CB}/\theta_2(E)^{\frac{1}{2}}\right]$$

$$x \; \{\text{erf } E_x/\theta_2(E)]^{\frac{1}{2}}\}\Big|_{E_x^-}^{E_x^+} . \qquad 3.36$$

The normalization constant in this case is given by the requirement that

$$\int_{E_x} P_1(E,E_x)dE_x \equiv 1 ,$$

or from Eq. (3.31)

$$C_2 = \int_{E_{CB}}^{E_x^{mx}} (E_x - E_{CB}) \exp[-(E_x - E_{CB})/\theta_2(E)]dE_x , \qquad 3.37$$

which is

$$C_2 = \exp[E_{CB}/\theta_2(E)]\theta_2^2(E) \times \left(\frac{E_{CB}}{\theta(E)} \exp[-E_x/\theta_2(E)] - \{\exp[-E_x/\theta_2(E)]\} \times \left[\frac{E_x}{\theta_2(E)} + 1\right]\right)\Bigg|_{E_{CB}}^{E_x^{mx}} . \quad 3.38$$

The term E_x^{mx} comes from energy balance considerations and is

$$E_x^{mx} = \mu_2 E + Q \quad 3.39$$

The term E_{CB} is calculated using the formulation[47]

$$E_{CB} = C_k(1.14418 \times 10^{-13} Z_3 Z_4)/(R_o + R_C) , \quad 3.40$$

where Z_3 is the atomic number of emitted particle,

Z_4 is the atomic number of recoil nucleus,

C_k is the correction to actual coulomb barrier to give an effective value,

R_o is the radius of compound nucleus $= 1.5 \times 10^{-13}(m_2+m_1)^{1/3}$ cm, and

R_c is the correction factor due to size of particle.

Values of C_k and R_c are given in the literature.[47]

To find E_x^+ and E_x^-, Eq. (3.17) is solved for E_x in terms of E and T with ϕ = 180 or 0 deg. This gives

$$E_x^{\pm} = \mu_1 \frac{m_4}{m_3} E + T/\mu_3 \pm 2 \left(ET \frac{m_1}{m_3} \mu_4\right)^{\frac{1}{2}}. \quad 3.41$$

The values of $E_x^{\pm}$ are also limited by E_x^{mx} and E_{CB} so that the

following validity checks must be made:

$$E_x^+ = E_x^{mx} \quad \text{if } E_x^+ \text{ [from Eq. (3.41)]} > E_x^{mx}$$
$$E_x^- = E_{CB} \quad \text{if } E_x^- \text{ [from Eq. (3.41)]} < E_{CB} \qquad 3.42$$

The maximum value of $T(E,E_x,\phi)$, T^{mx}, is determined from Eq. (3.17) with ϕ = 180 deg and $E_x = E_x^{mx}$. The minimum value of T is determined with ϕ = 0 deg. However, due to the quadratic form of the equation and the negative square root term, the E_x value that gives the lowest T^{mn} is not always E_{CB}. To determine the correct E_x for T^{mn}, Eq. (3.17) is differentiated and set equal to zero and solved for $E_x^{T^{mn}}$ giving

$$E_x^{T^{mn}} = \frac{m_4}{m_3}\ \mu_1 E \qquad 3.43$$

The value of $E_x^{T^{mn}}$ is also bounded by E_x^{mx} and E_{CB} so that

$$E_x^{T^{mn}} = E_x^{mx} \quad \text{if } E_x^{T^{mn}} \text{ [from Eq. (3.43)]} > E_x^{mx}$$
$$E_x^{T^{mn}} = E_{CB} \quad \text{if } E_x^{T^{mn}} \text{ [from Eq. (3.43)]} < E_{CB} \qquad 3.44$$

This gives a transfer kernel of

$$K^{ch}(E,T) = \frac{\theta_2(E)\ \exp[E_{CB}/\theta_2(E)]}{C_2 4(E\mu_1\mu_3\mu_4)^{\frac{1}{2}}}$$

$$x\ (\{\ (E_x^-)^{\frac{1}{2}}\ \exp[-E_x^-/\theta_2(E)]$$

$$-\ (E_x^+)^{\frac{1}{2}}\ \exp[-E_x^+/\theta_2(E)]\}\ +\ \pi^{\frac{1}{2}}$$

$$x\ \{\frac{[\theta_2(E)]^{\frac{1}{2}}}{2}\ -\ E_{CB}/[\theta_2(E)]^{\frac{1}{2}}\}$$

$$x\ (\mathrm{erf}\{[E_x^+/\theta_2(E)]^{\frac{1}{2}}\}$$

$$-\ \mathrm{erf}\{[E_x^-/\theta_2(E)]^{\frac{1}{2}}\})), \qquad 3.45$$

where

$$C_2 = \theta_2(E)\ \exp[E_{CB}/\theta_2(E)]$$

$$x\ (E_{CB}\{\exp[-E_x^+/\theta_2(E)]\ -\ \exp[-E_{CB}/\theta_2(E)]\}$$

$$+\ \theta_2(E)\{\exp[-E_{CB}/\theta_2(E)][\frac{E_x}{\theta_2(E)}\ +\ 1]$$

$$-\ \exp[-E_x^+/\theta_2(E)][\frac{E_{CB}}{\theta_2(E)}\ +\ 1]\})\ . \qquad 3.46$$

A slight problem arises in this formulation because finite reaction cross sections can exist below an effective threshold energy $E_o = (E_{CB}-Q)/\mu_2$ at which the nuclear temperature goes to zero. Physically, this means some particles can escape below E_{CB}. Since cross sections are always very small below E_o, they are set at zero for $E < E_o$ in these calculations.

III.B.1.d. (n,2n) Reaction

Odette and Doiron[27] treat the (n,2n) reaction as a multiple particle reaction based on a sequential emission evaporation model and corresponding Monte Carlo evaluation of the conditional probability distributions.

For a (n,2n) reaction to take place, the deexcitation energy of the first neutron emission E_{x_1} must be $<E_x^*$, where

$$E_x^* = E_{ex} - E_b$$

$$E_{ex} = \mu_2 E = \text{excitation energy} \qquad 3.47$$

$$E_b = \text{binding energy of the last neutron in the } m_2 \text{ nucleus.}$$

If $E_{x_1} < E_x^*$, the reaction is taken to be pure (n,2n), while if $E_{x_1} \geq E_x^*$, inelastic scattering is assumed. Because of this, the total $\chi(E,T)$ from incident neutrons in the (n,2n) reaction energy range should be considered as the sum of the part due to the (n,2n) mechanism when $E_{x_1} < E_x^*$ plus the part due to the inelastic mechanism (n,n') for $E_x^* \leq E_{x_1} \leq E_{ex}$. Thus, the (n,2n) kinematics model implies that the ratio of the (n,2n) and (n,n') reactions is given by

$$\sigma^{n,2n}(E)/\sigma^{inc}(E) = \int_{E_x^*}^{E_{ex}} P_1(E,E_{x_1})dE_{x_1} \Big/ \int_0^{E_x^*} P_1(E,E_{x_1})dE_{x_1} \qquad 3.48$$

if (n,2n) is the dominant nonelastic reaction.

When $E_x^* \leq E_{x_1} \leq E_{ex}$, $K^{inp}(E,T)$ for the (n,n') partial reaction is calculated by the same procedure used for the unresolved inelastic reaction. However, a lower limit of deexcitation energy check is made for E_x^- as in Eq. (3.42) with E_x^* substituted for E_{CB}. For the (n,2n) mechanisms, both neutrons are assumed to be emitted nearly simultaneously, viz., before the nucleus has a chance to move significantly.

Using the evaporation model, the deexcitation energy distribution of first neutron emission from the A+1 compound nucleus is[47]

$$P_1(E,E_{x_1}) = \frac{1}{C_3(E_x^*)} E_{x_1} \exp[-E_{x_1}/\theta_3(E_{ex})], \qquad 3.49$$

where

$$\theta_3(E_{ex}) = \left(\frac{E_{ex}}{a}\right)^{\frac{1}{2}} \qquad 3.50$$

The normalization constant $C_3(E_x^*)$ is determined by the requirement that

$$\int E_{x_1} P(E,E_{x_1}) \equiv 1 , \qquad 3.51$$

thus

$$C_3(E_x^*) = \theta_3^2(E_{ex}) \times \{1-[1+E_x^*/\theta_3(E_{ex})]\exp[-E_x^*/\theta_3(E_{ex})]\}. \qquad 3.52$$

The probability distribution of the second neutron emission deexcitation energy is determined by the excitation level of the A nucleus, which is dependent on E_{x_1}, and is given by

$$P_1(E,E_{x_2}) = \frac{1}{C_3(E_x^*)} \int_0^{E_x^*-E_{x_2}} \frac{\{E_{x_2}\exp[-E_{x_2}/\theta_4(E_{x_1})]\}\{E_{x_1}\exp[-E_{x_1}/\theta_3(E_{ex})]\}}{C_4(E_{x_1})} dE_{x_1}, \quad 3.53$$

where

$$0 \leq E_{x_2} \leq E_x^*$$

$$\theta_4(E_{x_1}) = \left(\frac{E_x^* - E_{x_1}}{a}\right)^{\frac{1}{2}}, \quad a = \frac{A-1}{10} \quad 3.54$$

and

$$C_4(E_{x_1}) = \theta_4^2(E)\{1 - [1 + \frac{(E_x^* - E_{x_1})}{\theta_4(E_{x_1})}] \times \exp[-(E_x^*-E_{x_1})/\theta_4(E_{x_1})]\} \quad 3.55$$

A Monte Carlo simulation is used to solve for $K^{n,2n}(E,T)$ based on the following procedures:

1. The first neutron deexcitation energy is randomly selected from the probability distribution in Eq. (3.49) using standard methods. A CM system emission angle cosine for the first neutron is selected randomly between -1 and +1.

2. The conditional probability distribution for the second neutron is calculated using the first neutron deexcitation energy as described by Eq. (3.53). The second neutron deexcitation energy is then also randomly selected from this conditional probability distribution. The second neutron emission angle cosine is also randomly selected between -1 and +1.

3. Conservation of momentum principles are applied to calculation of the recoil velocity vector for each of the sequential emis-

sions, giving a PKA recoil energy as a function of E_{x_1}, E_{x_2}, and the emission angle cosines.

4. Steps 1, 2, and 3 are repeated a large number of times using the random selection procedure. A histogram is built up by sorting recoils into appropriate energy bins.

For a small number of simulation experiments, the resulting $K^{n,2n}(E,T)$ spectrum is erratic in shape. At least several thousand simulations should be used for reasonably smooth results.

III.B.2. PKA Distribution Calculations for (n,γ) and (n,n'c) Neutron-Charged Particle Emission Reactions

III.B.2.a. (n,γ) Reaction

The recoil energy distribution function for the (n,γ) reaction is calculated using the data given in file 15 in ENDF-B/IV.[49] In this file the continuous energy distribution of secondary photons from (n,γ) reaction is given, as a function of incoming neutron energy. The energy distributions, $f(E_\gamma \leftarrow E)$, are in units of $(eV)^{-1}$ and are normalized so that

$$\int_0^{E_\gamma^{max}} f(E_\gamma \leftarrow E)\, dE_\gamma = 1 \qquad 3.56$$

where E_γ^{max} is the maximum possible secondary photon energy and its value depends on the incoming neutron energy as well as the particular nuclei involved. The energy distribution $f(E_\gamma \leftarrow E)$ can be broken

down into the weighted sum of several different normalized distributions in the following manner:

$$f(E_\gamma \leftarrow E) = \sum_{j=1}^{NC} P_j(E)\, q_j(E_\gamma \leftarrow E) \quad (eV)^{-1} \qquad 3.57$$

where

NC = the number of partial distributions used to represent $f(E_\gamma \leftarrow E)$,

$q_j(E_\gamma \leftarrow E)$ = the j^{th} normalized partial distribution in units of $(eV)^{-1}$, and

$P_j(E)$ = the probability of weight given to the j^{th} partial distribution, $q_j(E_\gamma \leftarrow E)$.

The following normalization condition is imposed

$$\int_0^{E_\gamma^{max}} q_j(E_\gamma \leftarrow E)\, dE_\gamma = 1 \qquad 3.58$$

Thus,

$$\sum_{j=1}^{NC} P_j(E) = 1 \qquad 3.59$$

The reaction cross sections as a function of neutron energy are obtained from ENDF-B/IV files 3 and 2. Appropriate resonance parameters are read from file 2 and using the formulae given in appendix D of the ENDF manual,[49] contributions from both resolved and unresolved resonance regions are calculated and added to cross sections given in file 3. For resolved resonance region calculations only single level and multi-level Breit-Wigner resonance parameters are accepted. The

code does not handle Reich-Moore and Adler-Adler resonance parameters in this region. Most of the calculations for obtaining the neutron energy dependent (n,γ) reaction cross sections from ENDF-B/IV were provided by L. R. Greenwood[40] in his input preparation program (hereafter referred to as INPUTPP) for DISCS.

A new subroutine written by the author and added to the INPUTPP is used to read from file 15 of ENDF-B/IV the parameters that characterize the secondary photon energy distributions from the (n,γ) reactions at discrete neutron energies, namely it collects the parameters NC and P and the function values q vs. E_γ (see Eqs. (3.57)-(3.59)) at each neutron energy given in ENDF-B/IV. Those values are later passed on to the DISCS, the displacement cross section and PKA spectrum calculation program, along with the neutron energy dependent reaction cross sections. In the DISCS program first the normalized gamma energy distribution function values, $f(E_\gamma \leftarrow E)$, are calculated by using Eq. (3.57). Then the PKA spectrum for the (n,γ) reaction is calculated as described below.

From the data obtained from file 15 in ENDF, two arrays are set up. For each incident neutron energy one array contains the photon energies and the other contains normalized photon energy distribution function values at corresponding photon energies. Gamma energies are converted to PKA energies using the formula

$$T = \frac{E_\gamma^{\,2}}{2(m+1)^2} = \frac{[E_\gamma\ (\mathrm{MeV})]^2}{(0.00186)(m+1)} \qquad 3.60$$

where m is the mass of target nucleus in amu.

The recoil energy transfer kernel for the (n,γ) reaction, $K^{n,\gamma}(E,T)$ is then

$$K^{n,\gamma}(E,T)dT = f(E_\gamma \leftarrow E)dE_\gamma \qquad 3.61$$

and the differential PKA cross section, $\chi^{n,\gamma}(E,T)$

$$\chi^{n,\gamma}(E,T) = \sigma^{n,\gamma}(E)\, K^{n,\gamma}(E,T) = \sigma^{n,\gamma}(E)\, \frac{f(E_\gamma \leftarrow E)dE_\gamma}{dT} \qquad 3.62$$

where $\sigma^{n,\gamma}(E)$ is the reaction cross section at neutron energy E.

III.B.2.b. <u>(n,n'c) Neutron-Charged Particle Emission Reactions</u>

The treatment of these reactions differ from the treatment of (n,2n) reaction in the way that the coulomb barrier effects have to be taken into account. For a (n,n'c) reaction to take place the deexcitation energy of the emitted neutron, E_{xn}, has to be $< E_x^*$, where

$$E_x^* = E_{ex} - SECP - ECB \qquad 3.63$$

$E_{ex} = \mu_2 E$ - excitation energy

SECP = Separation energy of the charged particle from the m_2 nucleus

ECB = Coulomb barrier energy for the charged particle to escape from the m_2 nucleus

As for the (n,2n) reaction, the evaporation model gives the deexcitation energy distribution of the neutron emitted from the A+1 compound nucleus as[47,48]

$$P_1(E,E_{xn}) = \frac{1}{C_3(E_x^*)} E_{xn} \exp[-E_{xn}/\theta_3(E_{ex})] \qquad 3.64$$

where

$$\theta_3(E_{ex}) = \left(\frac{E_{ex}}{a}\right)^{\frac{1}{2}}, \quad a = \frac{A}{10} \qquad 3.65$$

The normalization constant $C_3(E_x^*)$ is determined by the requirement that

$$\int_0^{E_x^*} P(E,E_{xn})dE_{xn} \equiv 1 \qquad 3.66$$

Thus

$$C_3(E_x^*) = \theta_3^2(E_{ex}) \left\{1 - \left[1 + \frac{E_x^*}{\theta_3(E_{ex})}\right] \exp\left[-\frac{E_x^*}{\theta_3(E_{ex})}\right]\right\} \qquad 3.67$$

The probability distribution of the charged particle emission deexcitation energy is determined by the excitation level of the A nucleus, which is dependent on E_{xn}, and is given by

$$P_1(E,E_{xc}) = \frac{1}{C_4(E_{xc}^*)} E_{xc} \left(1 - \frac{ECB}{E_{xc}}\right) \exp\left[-\frac{E_{xc}}{\theta_4(E_{xcex})}\right] \qquad 3.68$$

where

$$E^*_{xc} = E^*_x - E_{xn} \quad \text{- maximum charged particle energy} \tag{3.69}$$

$E_{xcex} = E^*_x - E_{xn}$ - maximum excitation energy of the residual nucleus, same as E^*_{xc}

$$\theta_4(E_{xcex}) = \left(\frac{E_{xcex}}{a}\right)^{\frac{1}{2}}, \quad a = \frac{m_4}{10} \tag{3.70}$$

where m_4 is the mass of the residual nucleus.

The coulomb barrier energy ECB is calculated using the formula[47]

$$ECB = K_c\ (1.4418 \times 10^{-13}\ Z_3 Z_4)/(R_o + R_c) \tag{3.71}$$

Z_3 = atomic number of emitted charged particle,

Z_4 = atomic number of recoil nucleus,

K_c = correction to actual coulomb barrier to give an effective value,

R_o = radius of the m_2 nucleus

$= 1.5 \times 10^{-13}\ (m_2)^{1/3}$ cm, and

R_c = correction factor due to size of particle.

Values of K_c and R_c are given in the literature.[47,48]

The normalization constant $C_4(E^*_{xc})$ is determined by the requirement that

$$\int_{ECB}^{E^*_{xc}} P(E,E_{xc})dE_{xc} \equiv 1 \tag{3.72}$$

Then

$$C_4(E^*_{xc}) = \theta_4^2(E_{xcex}) \{\exp\left[-\frac{ECB}{\theta_4(E_{xcex})}\right] - \left(1 + \frac{E^*_{xc} - ECB}{\theta_4(E_{xcex})}\right)$$

$$x \exp\left[-\frac{E^*_{xc}}{\theta(E_{xcex})}\right]\}. \qquad 3.73$$

Using a Monte Carlo simulation model, $K^{n,n'c}(E,T)$ is calculated as follows:

1. The neutron energy is randomly selected from the probability distribution in Eq. (3.64). This is done by assigning a random number between 0 and 1 to $P_1(E,E_{xn})$ and calculating E_{xn} by iterative procedures. Then a CM system emission angle cosine for the neutron is selected randomly between -1 and +1.

2. The energy of the emitted charged particle is calculated from Eq. (3.68) using a procedure similar to the one used for the neutron in step 1. The charged particle emission angle cosine is also randomly selected between -1 and +1.

3. Conservation of momentum principles are applied to calculation of the recoil velocity vector for each of the sequential emissions, giving a PKA recoil energy as a function of E_{xn}, E_{xc}, and the emission angle cosines.

4. Steps 1, 2, and 3 are repeated 2-3 thousand times using the random selection procedure. A histogram is built up by sorting recoils into appropriate energy bins.

Appropriate changes were made in the INPUTPP routine so that (n,n'c) reactions cross sections are collected from ENDF-B/IV, along with the rest of the reactions considered, and included in the input prepared for DISCS. Three new subroutines were written in DISCS. One subroutine performed the evaporation model analysis for the charged particle emission part, one subroutine obtained the PKA energy from reaction kinematics for each Monte Carlo experiment and the main NN'C subroutine calculated the PKA energy distributions from these (n,n'c) neutron-charged particle out reactions.

Besides including four new subroutines, one for (n,γ) and three for (n,n'c) reactions, in DISCS, almost all other subroutines had to be modified for various reasons. The new versions of the DISCS and INPUTPP codes are given the names DISCSM and INPUTPM, respectively. Presently the INPUTPM and DISCSM codes together are capable of generating neutron displacement cross sections and PKA energy distribution spectra at any number of neutron energies. The amount of input data to be supplied to INPUTPM by hand is minimal. Most of the input comes from ENDF files. There is no input preparation for DISCSM, it is all done by INPUTPM. For both the cross sections and the PKA spectra, the contributions from individual reactions, namely elastic, inelastic (n,2n), (n,p), (n,α), (n,n'α), (n,n'p) and (n,γ) are calculated. Four other smaller routines have been written to perform various functions using the output of DISCSM. One routine is used to calculate neutron spectrum averaged displacement cross sections, and differential and

normalized PKA spectra in a neutron flux. Two kinds of normalizations are used. One gives the percent probability of having a PKA with energy T in dT as a function of T and the other gives the probability of getting a PKA with energy greater than T as a function of T.

The second routine can be used to plot the displacement cross sections as a function of neutron energy and PKA probability distributions as a function of PKA energy at discrete neutron energies. The third routine is used to plot the neutron spectral averaged PKA probability distributions and the fourth routine is used to generate neutron group averaged displacement cross sections. On all plots, the specific contributions from individual nuclear reactions can be shown if so desired.

III.B.3. The Effects of the (n,γ) and (n,n'c) Neutron-Charged Particle Out Reactions on the Calculated Displacement Cross Sections and PKA Spectra

Table III.1 lists the displacement cross sections for Nb and Ni calculated by DISCS and DISCSM codes. The main differences between the two sets of data from DISCS and DISCSM are in the low neutron energy end due to (n,γ) reactions and in the very high energy end due to (n,n'α) and (n,n'p) reactions. Table III.2 gives the Ni displacement cross sections averaged in various fusion first wall and fission reactor neutron spectra. The effect of both the (n,γ) and (n,n'c) reactions is to make the spectral averaged displacement cross

Table III.1

The Effects of the (n,γ) and (n,n'c) Reactions on the Calculated Displacement Cross Sections

Barns

Neutron Energy (MeV)	Nb DISCS	Nb DISCSM	Ni DISCS	Ni DISCSM
2.2000-08	0.0	0.234	0.0	10.49
4.1400-07	0.0	0.047	0.0	2.101
8.7643-07	0.0	0.033	0.0	1.444
1.8554-06	0.0	0.022	0.0	0.993
3.9279-06	0.0	0.015	0.0	0.682
8.3153-06	0.0	0.011	0.0	0.469
1.7603-05	0.0	0.007	0.0	0.322
3.7267-05	0.0	0.005	0.0	0.222
7.8893-05	0.0	0.003	0.0	0.152
1.6702-04	0.0	0.002	0.0	0.105
3.5358-04	0.0	0.002	0.0	0.072
7.4852-04	0.0	0.015	3.487	3.537
1.5848-03	0.655	0.684	9.352	9.386
3.3546-03	6.299	6.341	13.19	13.22
7.1017-03	6.153	6.181	20.34	20.40
1.5034-02	11.99	12.00	91.99	92.06
3.1828-02	24.37	24.38	71.35	71.38
6.7379-02	55.43	55.44	117.3	117.4
1.2277-01	119.9	119.9	274.2	274.3
1.6573-01	148.5	148.5	255.7	255.7
2.2371-01	184.0	184.0	339.3	339.3
3.0197-01	225.2	225.2	316.1	316.1
4.0762-01	266.6	266.6	391.2	391.2
5.5023-01	312.1	312.1	422.3	422.3
7.4274-01	319.0	319.0	393.6	393.6
1.0026+00	335.8	335.8	698.8	698.8
1.3534+00	382.3	382.3	547.2	547.2
1.8268+00	463.9	463.9	696.8	696.8
2.4660+00	616.0	616.0	979.7	979.7
2.7253+00	647.0	647.1	1082	1082
3.0199+00	681.1	681.1	1089	1089
3.3282+00	705.7	705.7	1184	1184
3.6788+00	754.6	754.6	1217	1217
4.0657+00	812.1	812.1	1293	1293
4.4933+00	888.7	888.7	1348	1348
4.9659+00	953.6	953.9	1527	1527
5.4881+00	991.0	991.0	1724	1724
6.0653+00	1112	1112	1791	1791
6.7032+00	1239	1239	1873	1873
7.4082+00	1203	1203	1896	1896
8.1873+00	1240	1240	1900	1900
9.0484+00	1279	1279	2290	2290
1.0000+01	1394	1394	2721	2721
1.1052+01	1427	1427	2823	2823
1.2214+01	1585	1585	2916	2916

Table III.1 (cont.)

Neutron Energy (MeV)	Nb DISCS	Nb DISCSM	Ni DISCS	Ni DISCSM
1.3499+01	1842	1842	2995	3072
1.4918+01	2003	2003	3051	3215
1.6000+01	2101	2103	3077	3344
1.7000+01	2169	2172	3039	3446
1.8000+01	2204	2207	2971	3558
1.9000+01	2259	2263	2877	3681

Table III.2

The Effect of the (n,γ) Reactions on the Spectral Averaged Ni Displacement Cross Sections in Various Neutron Spectra

Neutron Environment	Spectral Averaged Displacement Cross Section (barns) DISCS	DISCSM
Hard Fusion	1177	1177
Softened Fusion		
behind 25 cm carbon	474.8	475.7
behind 25 cm Mo	230.7	230.7
behind 112 cm Pb	73.74	73.94
behind 91 cm Pb_4Li	100.2	100.3
behind 115 cm Li	267.6	267.6
EBR-II	465.1	465.1
HFIR	200.2	202.2

sections from DISCSM higher than the DISCS values. However, in this case, the main difference is expected to come from the (n,γ) reactions because the (n,n'c) reactions do not become operative until after 13.5 MeV neutron energy and none of the neutron spectra considered have neutrons of energy >14.9 MeV. As we see in Table III.2 there is little difference in the spectral averaged Ni displacement cross sections even in a softened fusion or thermal fission reactor neutron environment. The difference is even less in the Nb displacement cross sections. However, as discussed below, the difference in the PKA probability distributions can be appreciably high.

Figure III.1 shows the normalized PKA probability distribution in a hard fusion neutron spectrum with and without the (n,γ) and (n,n'c) reactions. Similar curves in a soft (behind 25 cm solid carbon) fusion neutron spectrum are shown in Figure III.2. The (n,γ) and (n,n'c) reactions are competing in this case. The (n,γ) reactions tend to shift the PKA spectrum to lower energies and the (n,n'c) reactions tend to make it go in the opposite direction. In the hard fusion neutron spectrum the two effects tend to cancel each other with hardly any difference between the DISCM and DISCS curves in Figure III.1. In softened fusion neutron spectrum, however, the (n,γ) reactions take over and the PKA distribution from DISCSM is shifted to lower energies.

The effect of the (n,n'c) reactions on the calculated spectral averaged displacement cross sections and PKA distributions was not

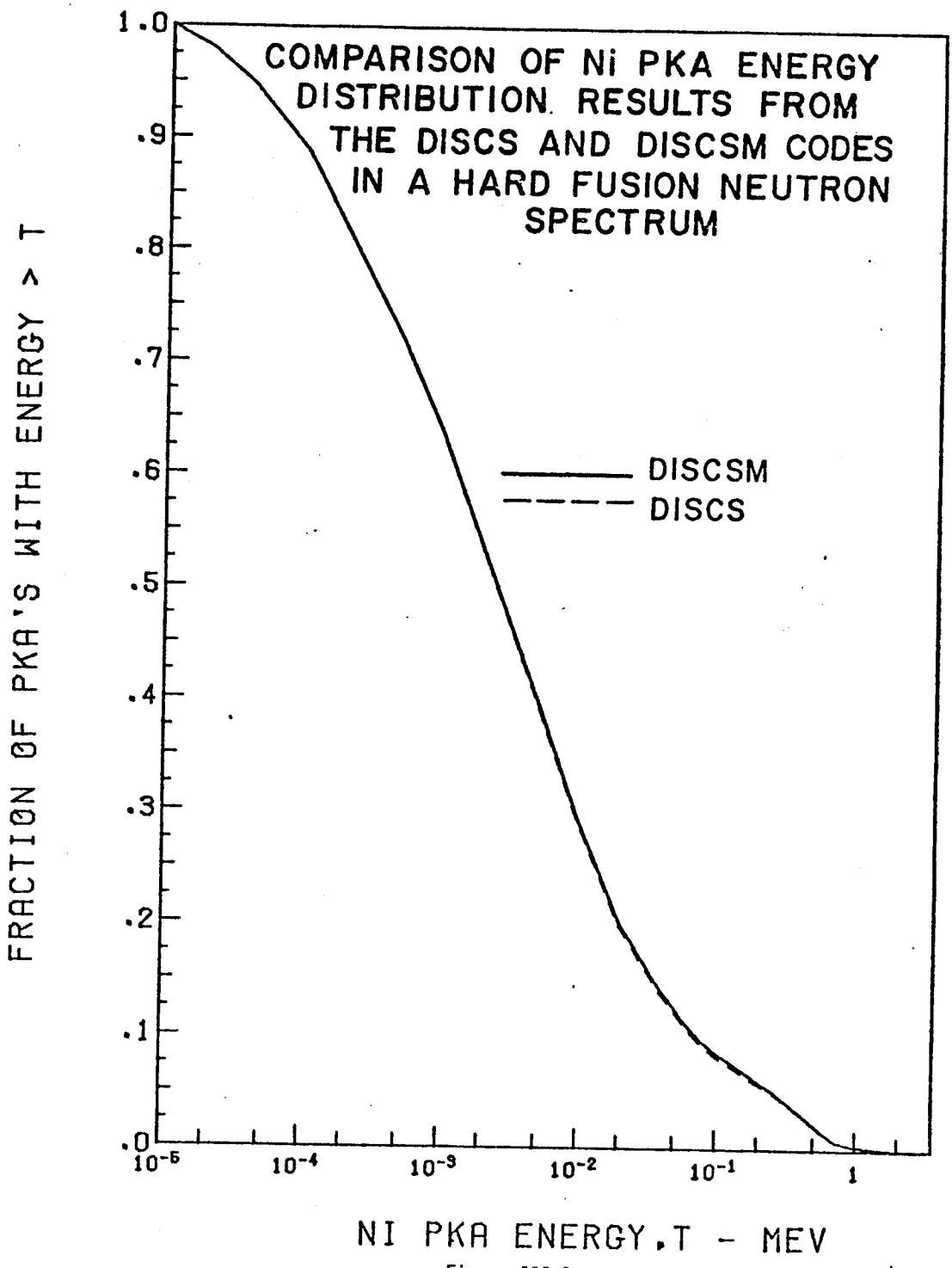
COMPARISON OF Ni PKA ENERGY DISTRIBUTION RESULTS FROM THE DISCS AND DISCSM CODES IN A HARD FUSION NEUTRON SPECTRUM
DISCSM
DISCS
FRACTION OF PKA'S WITH ENERGY > T
1.0
.9
.8
.7
.6
.5
.4
.3
.2
.1
.0
10⁻⁵
10⁻⁴
10⁻³
10⁻²
10⁻¹
1
NI PKA ENERGY, T - MEV

Figure III.1

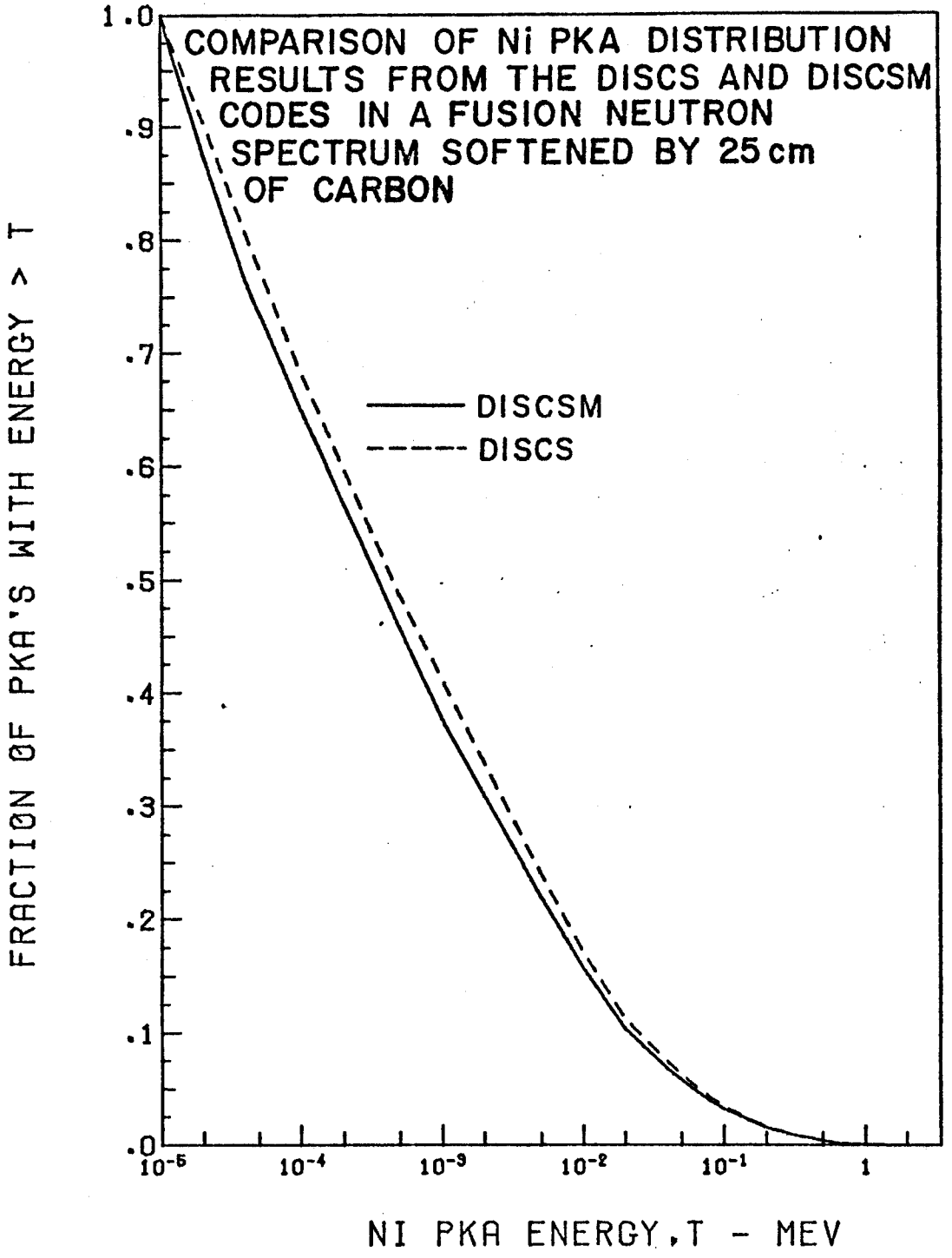
COMPARISON OF Ni PKA DISTRIBUTION RESULTS FROM THE DISCS AND DISCSM CODES IN A FUSION NEUTRON SPECTRUM SOFTENED BY 25 cm OF CARBON
DISCSM
DISCS
FRACTION OF PKA'S WITH ENERGY > T
1.0
.9
.8
.7
.6
.5
.4
.3
.2
.1
.0
10^{-5}
10^{-4}
10^{-3}
10^{-2}
10^{-1}
1
NI PKA ENERGY, T - MEV

Figure III.2

very strong in these calculations, but they might be very important in neutron spectra obtained in fusion reactor materials testing facilities utilizing deutron stripping reactions such as (D,Li) and (D,Be), where neutrons of energy up to 30-40 MeV can be found. Such charged particle out reactions will also be important in materials such as Al which has large (n,n'c) reactions cross sections below 15 MeV.

In summary, inclusion of low energy neutron capture reactions or high energy (n,n'c) reactions has a minimal effect on the spectral averaged displacement cross sections, but they do have an effect on the PKA spectra. We will use these new results to more accurately analyze the damage environment associated with the modified neutron spectra behind various ISSEC designs.

III.B.4. Discussion on Nuclear Model Validity

All nuclear reactions considered in the calculation of the total PKA differential cross section $\chi_t(E,T)$ are assumed to proceed through a compound nucleus formation and the secondary particles that come off are assumed to be emitted isotropically in the center-of-mass system. The only exception is the elastic scattering where the experimentally determined neutron energy dependent Legendre polynomial coefficients that result from the Legendre expansion of the scattered neutron angular distribution are used in the calculation of $\chi^{elas.}(E,T)$. The isotropic-emission and compound-nucleus

formation assumptions for the other nuclear reactions are reasonably valid at low neutron energies. However, at high neutron energies (14 MeV or higher) the direct interactions play an important role and the angular distribution of the emitted particles is peaked in the forward direction. The direct interactions become especially important for single charged particle emission reactions. For example, for (n,p) reactions at 14 MeV neutron energy, direct interactions can constitute as much as 20 to 60% of the reactions in light and medium mass nuclei (A = 25-70) to as much as 90% in heavy nuclei (A >90).[27] However, since these cross sections are generally small, one approximate way to treat the (n,p) reactions is to add the estimated compound nucleus contribution of such reactions to the continuum inelastic neutron scattering cross section and add the direct component to the elastic scattering cross section.

For the (n,α) reactions the isotropic-emission and compound-nucleus formation assumptions should be reasonably valid for medium mass nuclei. However, for heavy nuclei, the validity of these assumptions are not as warranted. It is reported that at 14 MeV, direct interactions contribute on the order of 55% of the total (n,α) reaction cross section in ^{93}Nb.[27] Figure III.3 compares the PKA energy probability distributions for (n,α) reactions from the isotropic-emission compound-nucleus model and calculations using experimentally measured angular emission distributions for

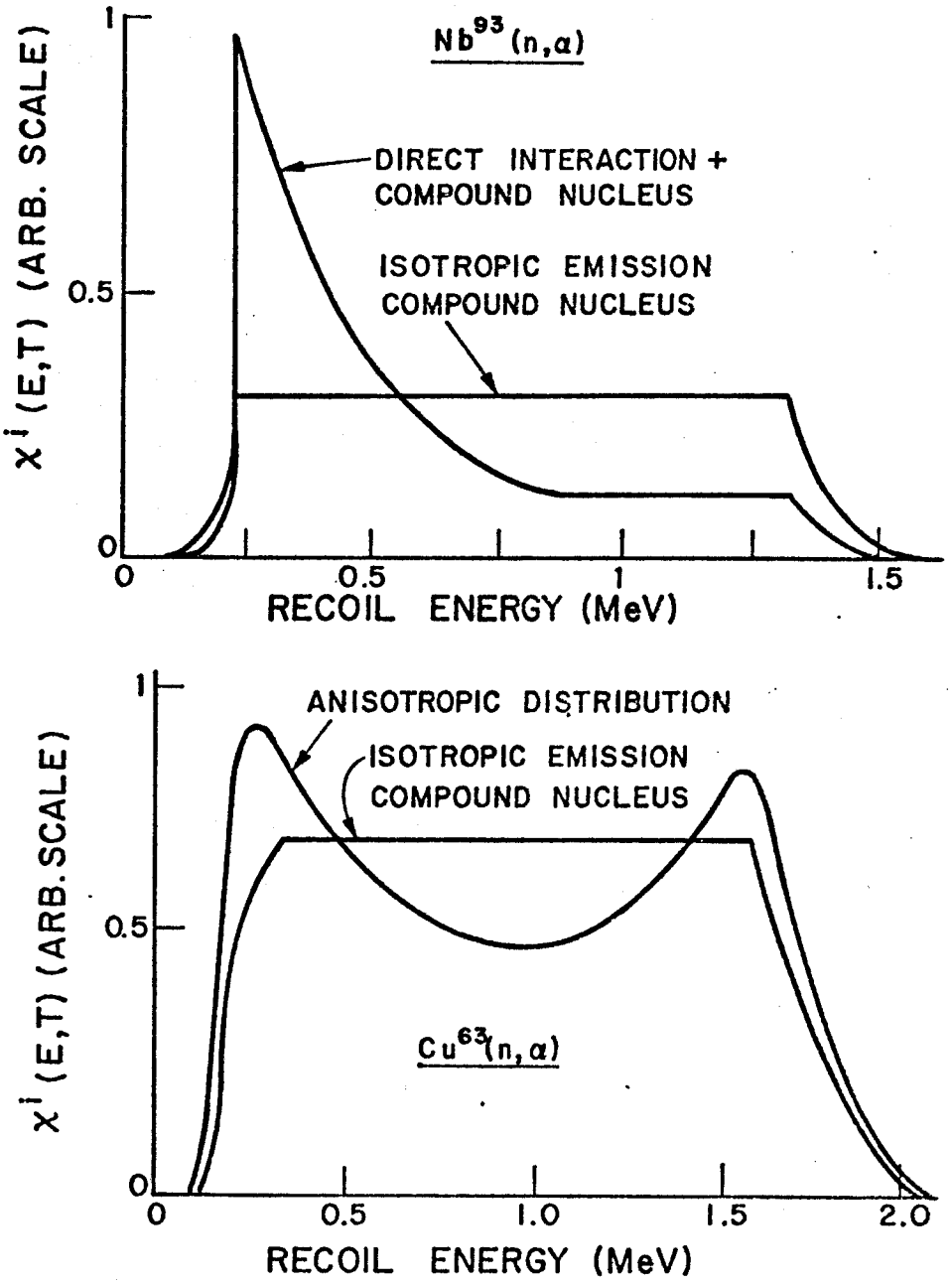

COMPARISON OF $\chi^{n,\alpha}(E,T)$ DISTRIBUTIONS FROM THE ISOTROPIC-EMISSION COMPOUND-NUCLEUS MODEL AND CALCULATIONS USING EXPERIMENTAL DATA FOR ^{63}Cu and ^{93}Nb AT 14 MeV (Ref. 27)

Figure III.3

^{63}Cu and ^{93}Nb at 14 MeV neutron energy. $\chi^{n,\alpha}(E,T)$ results for ^{63}Cu do not differ too much between the two sets of calculations, but for ^{93}Nb the recoil distribution is enhanced at low energies and diminished at high energies. Thus, in high Z elements direct reactions are generally less efficient in generating high energy PKA's than isotropic emission compound nucleus type reactions.

For neutron energies of up to 14 MeV, the charged particle emission nuclear reaction cross sections are still low so that the contribution of these reactions to total displacement cross sections are small. For example, at 14 MeV (n,p) and (n,α) reactions together make up only 5% and 7% of the total displacement cross sections, respectively in Nb and V.

For multiple particle emission reactions such as (n,2n), (n,n'p), (n,n'α) the isotropic-emission compound-nucleus model should be appropriate for medium mass nuclei at moderate energies (<20 MeV). One estimate of preequilibrium contribution to (n,2n) reactions in ^{93}Nb at 14 MeV is $\sim$10%.[27]

In fusion reactor applications, the displacement cross sections calculated by methods described in this chapter will probably overestimate the damage in first walls by about 10% or less. However, if one were to extend the models to higher energies and use these cross sections to estimate damage in materials to be tested in (D,Li) or (D,Be) source facilities where neutrons can have energies

up to 40 MeV the results would be overestimated by amounts much greater than 10%. The effects of direct interactions and anisotropic emission of secondary particles would have to be taken into account for the high energy spallation sources.

CHAPTER IV

CALCULATIONAL METHODS

To implement the calculations in this study, a computer package called MODISS for Modified Damage by ISSEC has been established. The flow diagram of MODISS is shown schematically in Figure IV.1. As can be seen the package consists of several programs each of which performs different functions. Some of the programs are directly taken from the literature without any modification. They are the neutronics code ANISN,[50] the radioactivity code DKR,[51] and the heat transfer codes HEAT[52] and FEM2D.[53] The damage analysis codes INPUTPM and DISCSM are modified versions of INPUTPP[40] and DISCS[27] as previously described in Chapter III. The other programs DPLOT, APLOT, XGRPAVE and most of NSPECAVE have been provided by the author for the purposes of this study. In the remainder of this Chapter the functions of the various programs in MODISS will be explained. The data requirements and the output of each code will also be shown.

IV.A. INPUTPM

Object: The object of the INPUTPM program is to collect nuclear data from various sources, process and output the data in a form that is compatible with the input requirements of the DISCSM program.

Input: An example of the card input data for the INPUTPM for the element niobium is shown in Table A.1 in Appendix A. The rest of the input comes from the ENDF-B/IV file which is assigned to the run

LAYOUT OF MODISS

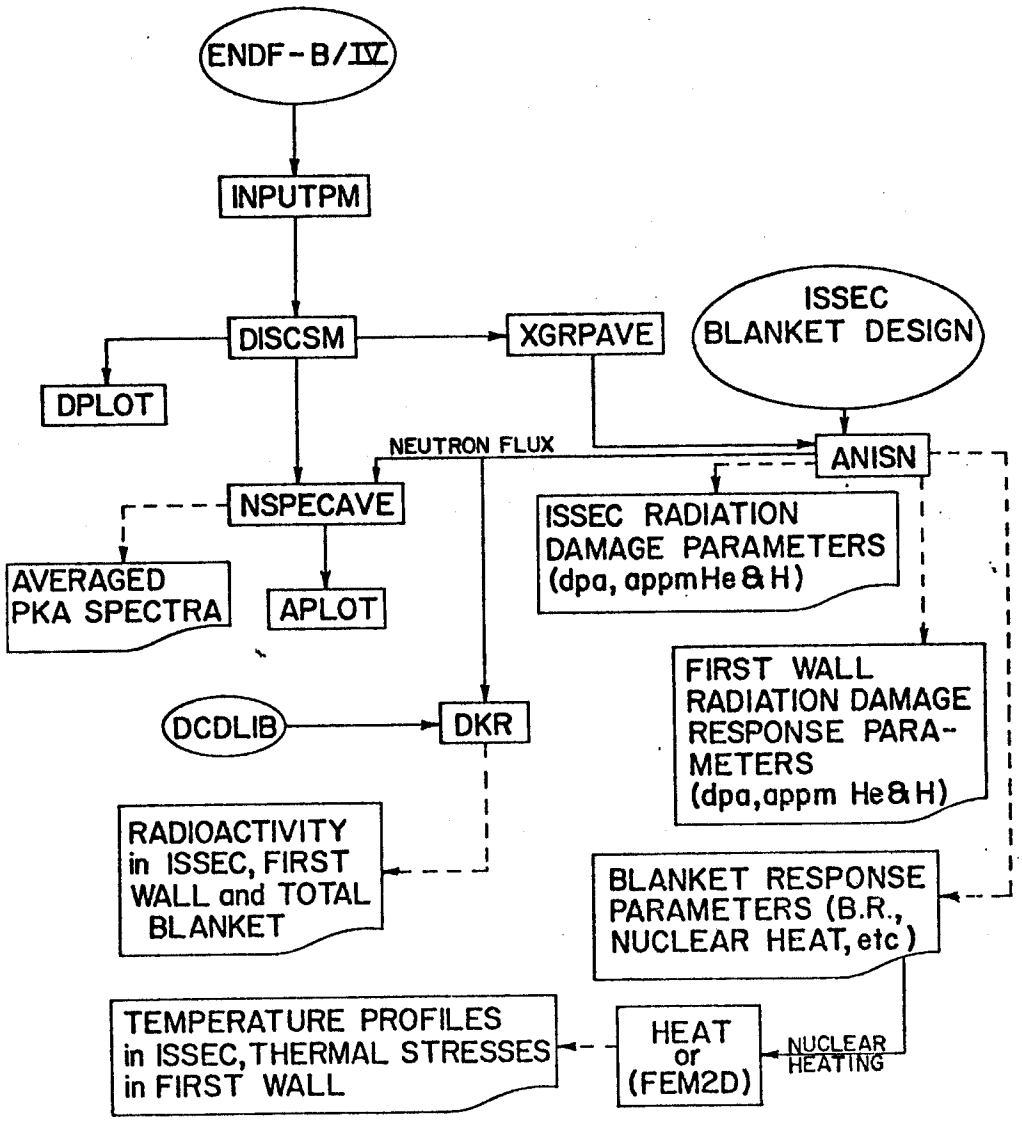

Figure IV.1

with a logical unit number 21 and contains the data for the element in question. The description of the input to be provided on cards is given in Table IV.1.

Structure and operation of the INPUTPM: Figure IV.2 shows the flow diagram of the INPUTPM code and the various functions of each program unit in the INPUTPM are briefly explained below.

MAIN

The function of the MAIN program is to set up the problem and to direct the flow of the runstream by calling various subroutines to obtain the necessary information from ENDF data files. Interpolation of the final reaction cross sections thus obtained from the fine input group structure mesh points to the 46 group structure end points is also done in MAIN. The last part of the MAIN program files all the data obtained in a format structure such that it can be read directly by the DISCSM program.

RESCAL

The subroutine RESCAL is used to read the resonance parameters from file 2 and the reaction cross sections from file 3 of the ENDF-B/IV. It calculates the total reaction cross sections in the input energy group structure and returns them to the MAIN program.

RESOLV

The subroutine RESOLV calculates the contributions to the elastic and (n,γ) reaction cross sections from resolved resonances using

Table IV.1

Card Input Data for INPUTPM

Card #	Format	List	Description
1	I5	NMAT	ENDF Mat number of the element to be analyzed
2	5A4	ELEM(5)	Name or identification of the element
3	Free	M2	Mass of target nucleus
		Z2	Atomic number of target nucleus
		EDK	Kinchin-Pease displacement energy (MeV)
		EDL	Lindhard displacement energy (MeV)
		TI	Kinchin-Pease ionization threshold (MeV)
		AA	Nuclear density parameter for nuclear temperature (AA=M2/10 or M2/20)
		EMAS	Maximum recoil energy for common integration (MeV)
4	Free	IT	Number of recoil energy grid points ($\leq$100)
		TMIN	Minimum cutoff energy (MeV)
5	Free	IELAS	= 0, No elastic analysis $\geq$ 1, Elastic reaction is done
		INELAS	= 0, No inelastic analysis $\geq$ 1, Inelastic reaction is done
		ICHAR	= 0, No (n,c) reactions are done = 1, 1 (n,c) reaction is done = 2, 2 (n,c) reactions are done
		IN2N	= 0, No (n,2n) reaction analysis $\geq$ 1, (n,2n) analysis is done
		IDSMOD	= 0, No secondary displacement model analysis = 1, Lindhard displ. model only = 2, Kinchin-Pease model only = 3, Lindhard and Kinchin-Pease models = 4, User supplied model only = 5, Lindhard, Kinchin-Pease, and User supplied models

Table IV.1 (cont.)

Card #	Format	List	Description
		NPLOT	= 0, No printer plots of PKA distributions given
		NPRKT	= 0, No printout of transfer kernel ≥ 1, Printout of transfer kernel given
		ITAVE	= 0, Average PKA energies not given ≥ 1, Average PKA energies per reaction are given
6	Free	INNC	= 0, No (n,n'c) reaction analysis = 1, 1 (n,n'c) reaction is done = 2, 2 (n,n'c) reactions are done
		INGAMA	= 0, No (n,γ) analysis ≥ 1, (n,γ) reaction is done
7	Free	NENG	Number of input energy group structure points
8*	Free	(E(M),M=1,NENG)	Input energy group structure
9	3I4	MAT1	ENDF Mat number of the element
		IT1	= 2 if resonance analysis wanted ≠ 2 if no resonance analysis
		IR1	= 151
10	3I4	MAT2	ENDF Mat number of the element
		IT2	= 3, ENDF cross section file
		IR2	Reaction number

Repeat card #10 for all (IR2) reactions considered including all resolved and unresolved inelastic levels. Reaction numbers have to be given in ascending order.

11	3I4	MAT2	= 0, Signals the end of type 10 cards
12	Free	IOUT	Number of output energy group structure points
13*	Free	(EOUT(I),I=1,IOUT)	Output energy group structure

If IN2N = 0, skip card #14.

Table IV.1 (cont.)

Card #	Format	List	Description
14	Free	NMC	Number of Monte Carlo experiments in (n,2n) analysis
		EB	Binding energy of the last neutron in the target nucleus (MeV)
		A2	Nuclear density parameter for second neutron
	If INNC = 0, skip cards #15 - 17.		
	Repeat cards #15 through 17 for each (n,n'c) reaction.		
15	5A4	(RNAME(L),L=1,5)	Name of the reaction
16	Free	M3NC	Mass of emitted charged particle
		Z3NC	Atomic number of emitted charged particle
		M4NC	Mass of recoil nucleus after (n,n'c) reaction
		Z4NC	Atomic number of recoil nucleus after (n,n'c) reaction
		CKNC	Coulomb barrier constant
		RCNC	Coulomb barrier constant
17	Free	NMCNC	Number of Monte Carlo experiments in the charged particle out part of (n,n'c) reaction
		SECP	Separation energy of the charged particle from the M2 nucleus
	If ICHAR = 0, skip cards #18 and 19.		
	Repeat cards #18 and 19 for each (n,c) reaction.		
18	Free	M3	Mass of emitted particle
		Z3	Atomic number of emitted particle
		M4	Mass of recoil nucleus
		Z4	Atomic number of recoil nucleus
		CK	Coulomb barrier constant
		RC	Coulomb barrier constant
19	5A4	(REAC(L),L=1,5)	Name of the reaction

(*) Energy group structures may actually fit on more than one card.

FLOW DIAGRAM OF INPUTPM

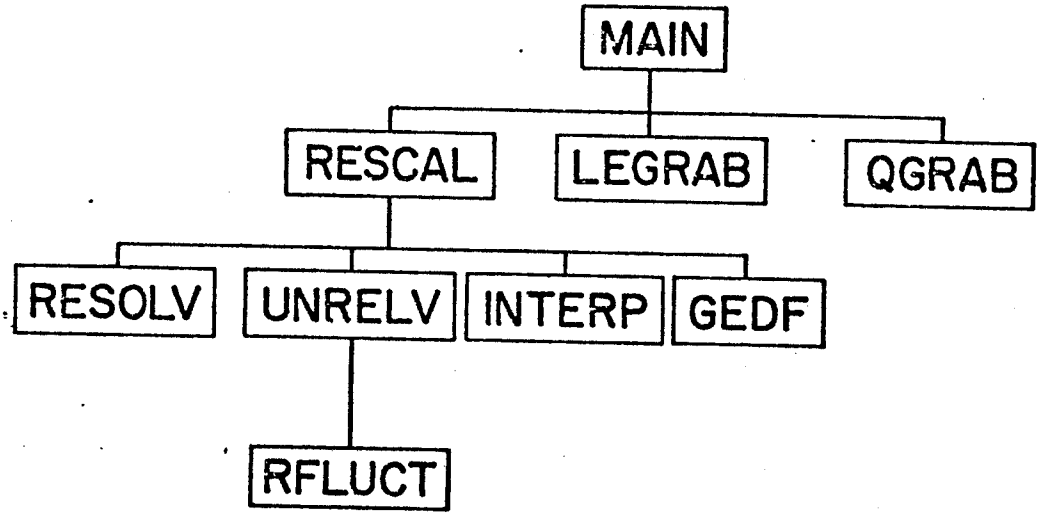

Figure IV.2

the formulas listed in the Appendix D of the ENDF manual.[49]

UNRELV

This subroutine calculates the contributions to the elastic and (n,γ) reaction cross sections from unresolved resonances. The formulas used are given in the Appendix D of reference 49.

RFLUCT

This subroutine is used to calculate the fluctuation integrals for the (n,γ), and elastic scattering reactions in the unresolved resonance region.

INTERP

The subroutine INTERP is used to interpolate, using the ENDF interpolation schemes, the total reaction cross sections obtained from ENDF to neutron energies corresponding to the energy point values of the input group structure.

GEDF

This subroutines reads, from file 15 of the ENDF, the normalized energy probability distributions of the secondary gammas from (n,γ) reactions at various neutron energies, and stores the information in the output file for use by the DISCSM.

LEGRAB

This subroutine is used to obtain the neutron energy dependent Legendre polynomial coefficients from the ENDF that result from the

Legendre expansion of the elastically scattered neutron angular distributions in the center of mass sytem.

QGRAB

The subroutine QGRAB obtains the Q values of the nuclear reactions involved from file 3 of the ENDF.

Output: The output of the INPUTPM program is in two parts. One part is intended for use as input for the DISCSM and is stored in a file which is assigned to the run with logical unit number of 15. Table A.2 of Appendix A shows a part of the filed output for the element niobium. The description of this output is given in the input description section of the DISCSM code. The second part of the output is the printed output and it consists of the total reaction cross sections in the fine input energy group structure, the list of Legendre polynomial coefficients at various neutron energies, and the Q values of the reactions involved.

IV.B. DISCSM

Object: The object of the DISCSM code is to calculate the displacement cross sections and the PKA probability distributions in an element which undergoes elastic, inelastic, (n,2n), (n,c) charged particle emission, (n,n'c) neutron-charged particle emission and (n,γ) capture reactions with neutrons of discrete energy.

Input: The input to the DISCSM code comes directly from the INPUTPM. A part of the input for a niobium run is given in Table A.2 of Appendix A and is described in Table IV.2.

Structure and operation: The layout of the DISCSM code is given in Figure IV.3 and the functions of each subroutine are briefly outlined below.

MAIN

The MAIN routine initially reads in the parameters that set up the problem, calculates the constant terms common to the whole program and depending on the needs of a specific problem calls various subroutines to perform different tasks.

GAMA

The first call to subroutine GAMA is to read the information on the normalized gamma energy distribution functions (records 6-23 in Table A.2 in Appendix A). Subsequent calls to GAMA through a second entry point is for calculating $\chi^{n,\gamma}(E,T)$ according to the outline given in Section III.B.2.a.

INTERP

INTERP is a Lagrangian interpolation routine.

ZERO

Subroutine ZERO is used to clear some of the arrays before the start of calculations at each neutron energy.

Table IV.2

Description of the Input to the DISCSM Code

Record #	Format	List	Description
1	2I5	NELEM NMAT	Number of elements to be analyzed ENDF material number of the first element to be analyzed
2,3	Record numbers 2 and 3 are the same as the card numbers 2 and 3 in the card input data for the INPUTPM code in Table IV.1.		
4,5	Record numbers 4 and 5 are the same as the card numbers 5 and 6 in the card input data for the INPUTPM and the variables have the same options.		
6	I10	NC	The number of partial distributions used to represent the normalized photon energy distribution $f(E_\gamma \leftarrow E)$ from (n,γ) reactions.
	Records 7 - 23 are repeated NC times.		
7	I10	NP	Number of energy points for the weight given to each partial distribution
8	6E11.5	(ENP(J),P(J), J=1,NP)	Neutron energy and the partial weight at that energy for each partial distribution
9	I10	NE	Number of neutron energies at which the normalized partial γ energy distributions are given
	Records 10-16 are repeated NE times.		
10	E11.5, I11	EN	Neutron energy
		INP	Number of points at which the normalized partial γ energy distribution for neutron energy EN are tabulated
11-16	6E11.5	(EG(K),G(K),K=1, INP)	Gamma energy and the value of the normalized partial distribution at that energy

Table IV.2 (cont.)

Record #	Format	List	Description
	Records 17-23 are a repeat of records 10-16 except for a different neutron energy.		
24	2I5	IT	Number of recoil energy grid points (≤100)
		NEN	Number of neutron energy group structure points - 1
25	2E10.5	E	Lowest neutron energy in the neutron group structure
26	E10.4, 2I5	CSE	Elastic reaction cross section at neutron energy E
		NLEG	Number of Legendre expansion coefficients given
		LTT	A flag in ENDF to specify the angular distribution of scattered neutrons
27	7E10.4	(F(L),L=1,NLEG)	Legendre polynomial coefficients
28	I5, E15.6	IEN	Number of resolved inelastic reaction levels
		EMIN	Minimum energy cutoff of continuum level
29,30	9F8.4	(Q(L),L=1,IEN)	The Q values of the resolved levels
31,32	10F7.4	CSINUR	Cross section of continuum level
		(CSINR(L), L=1, IEN)	Cross sections of resolved levels
33	I10, 2F10.4	NMC,EB,A2	See card #14 in input to INPUTPM
34	F10.4	CS	(n,2n) cross section
	See card numbers 15-19 in the card input data for the INPUTPM for the description of the unexplained variables in the records 35-42 below.		
35	4F10.3, 5A4	M3NC, Z3NC, M4NC, Z4NC, (RNAME(L), L=1.5)	

Table IV.2 (cont.)

Record #	Format	List	Description
36	2E10.4	CKNC,RCNC	
37	I10 2F10.4	NMCNC, SECP, EB	
38	E10.5	CSNC	(n,n'c) reaction cross section
	Records 35-38 are repeated for each (n,n'c) reaction.		
39	E10.5	CSNG	(n,γ) reaction cross section
40	4F10.3, 5A4	M3, Z3, M4, Z4, (REAC(L), L=1.5)	
41	3E10.4	CK,RC Q	 Reaction Q value
42	E10.5	CSC	(n,c) reaction cross section
	Records 39-42 are repeated for each (n,c) reaction		
46	2E10.5	E TMIN	Next neutron energy in the neutron energy group structure Minimum cutoff energy
47	same as record #26		
48	same as record #27		
49,50	same as record #'s 31,32		
51	same as record #34		
52	same as record #38		
53	same as record #39		
54,55	same as record $42		

Records 46-55 are repeated for each consecutive neutron energy point in the neutron group structure. Except when the (n,2n) reaction has a finite cross section, (n,n') inelastic continuum cross section is given right after the (n,2n) reaction cross section.

FLOW DIAGRAM OF DISCSM

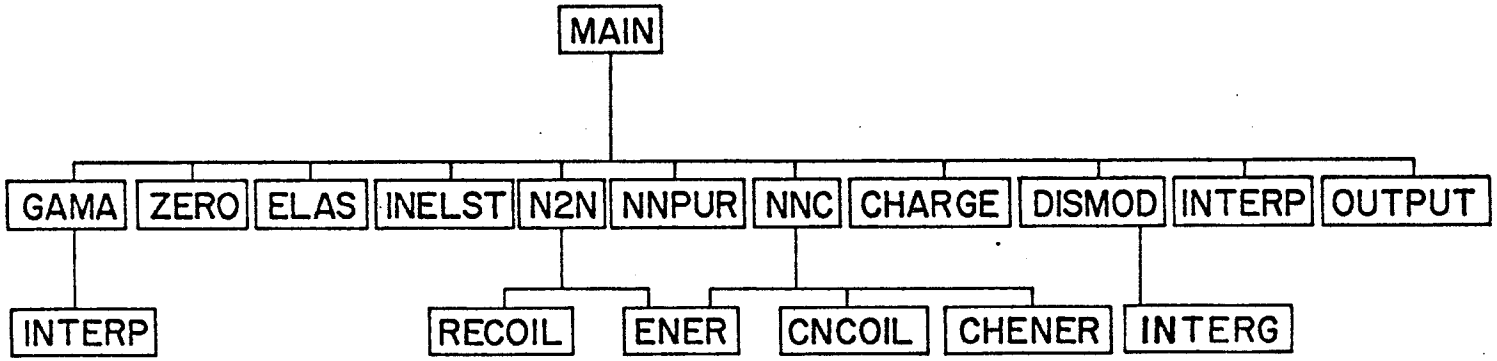

Figure IV.3

ELAS, INELST, N2N, NNPUR, NNC, CHARGE

Subroutines ELAS, INELST, N2N, NNC, CHARGE calculate the differential PKA production cross sections $\chi(E,T)$ from elastic, inelastic, (n,2n), (n,n'c) and (n,c) reactions according to the schemes outlined in Sections III.B.1.a., III.B.1.b., III.B.1.d., III.B.2.b., and III.B.1.c., respectively. The subroutine NNPUR is used to calculate $\chi(E,T)$ for the inelastic reaction when both the inelastic and (n,2n) reactions take place at the specified neutron energy.

RECOIL

The reaction kinematics to find the PKA energy after an (n,2n) reaction is performed in subroutine RECOIL.

ENER

Subroutine ENER does the evaporation model analysis when the emitted particle is a neutron. It is used to find the energy of the emitted neutron by methods described in Section III.B.1.d.

CNCOIL

Subroutine CNCOIL finds the energy of the PKA after an (n,n'c) reaction.

CHENER

When the emitted particle is a charged particle, the evaporation model analysis is done by CHENER. The energy of the emitted charged particle is found by methods described in Section III.B.2.b.

DISMOD

Secondary displacement model calculations are done in this subroutine.

INTERG

This subroutine does the integration over the PKA energy to find the total damage cross section per nuclear reaction per neutron energy.

OUTPUT

The outputting of the damage cross sections calculated is done by this subroutine.

Output: The printed output consists of three parts. The first part is just echo printing of the control parameters read in. In the second part a table of differential PKA production cross sections $\chi(E,T)$ vs. PKA energy T is given. The third part is a list of the damage production cross sections from Lindhard, and Kinchin and Pease displacement models, damage energy, nuclear reaction cross sections, and average PKA energy. The second and third parts are repeated for each neutron energy and the data in them are broken down to individual nuclear reaction contributions. Table A.3 in Appendix A shows a listing of the $\chi(E,T)$ and damage cross sections for Nb for a neutron energy of 14.92 MeV. $\chi(E,T)$ and the displacement cross section results from the Lindhard model are also stored in files for later use.

IV.C. DPLOT

Object: The purpose of the DPLOT program is to plot on a calcomp plotter the PKA probability distributions calculated by the DISCSM code as a function of PKA energy in different elements as a result of bombardment by neutrons of discrete energy and also to plot the resulting displacement cross sections as a function of neutron energy.

Input: The input to DPLOT comes from the filed output of the DISCSM. The file that contains PKA distributions is assigned to the run with a logical unit number 10, and that containing displacement cross sections with a logical unit number 15. For the execution of the program DPLOT the input from cards is minimal and is shown in Table IV.3.

Output: Examples of PKA distribution plots for Nb at 14.9 MeV neutron energy are given in Figures A.1, A.2, and A.3 of Appendix A. Figure A.1 shows the differential PKA probability distribution in units of barns/MeV as a function of PKA energy, T. Figure A.2 shows the normalized distribution of the fraction of PKAs with energy $T \pm dT$ as a function of T and shown in Figure A.3 is the fraction of PKAs with energy greater than T as a function of T. Similar plots can be generated for other neutron energies. Figure A.4 plots the displacement cross sections of Nb as a function of neutron energy. In Figures A.1 - A.4 the individual reaction contributions can be suppressed and only the total of all of them can be shown by setting the variable JUSTOT > 0 in the input.

Table IV.3

Input from Cards for the DPLOT Program

Card #	Format	Variable	Description
1	Free	IT NPTS	PKA energy grid points = 100 Neutron energy group structure points = 52
2	Free	JUSTOT	= 0 show on plots the individual reaction contributions as well as the total > 0 show only the total
3	Free	IDE	= 0/≠ 0 PKA probability distribution plots are not/are given
		IDEDF	= 0/≠ 0 Differential PKA probability distribution plots are not/are given
		IDEN1	= 0/≠ 0 Normalized PKA distribution plots are not/are given
		IDEGT	= 0/≠ 0 Fractional PKA distribution are not/are given
		IDC	= 0/≠ 0 Displacement cross sections as a function of neutron energy are not/are plotted
If IDE = 0, skip cards 4-17.			
4	Free	INS	Number of neutron energy points at which PKA distribution plots are given
5	Free	(NP(I),I=1,INS)	Energy point numbers in the neutron group structure for PKA plots
If IDEDF = 0, skip cards 6 to 9.			
6	Free	(LOG(M),M=1,4)	= 0 plot is linear-linear = 1 plot is linear-log = 2 plot is log-linear = 3 plot is log-log < 0 Flag indicating the end of scaling specifications for this plot type

Table IV.3 (cont.)

Card #	Format	Variable	Description
7*†	12A4	(XAXIS(I), I=1,12)	x-axis label for the plot
8*†	12A4	(YAXIS(I), I=1,12)	y-axis label for the plot
9*	15A4	(TITLE(I), I=1,14)	Title of the plot
	If IDEN1 = 0, skip cards 10-13.		
10	Free	(LOG(M), M=1,4)	same options as for card #6
11,12,13	x-axis, y-axis labels and title of normalized plots		
	If IDEGT = 0, skip cards 14-17.		
14	Free	(LOG(M), M=1,4)	same options as for card #6
15,16,17	x-axis, y-axis labels and title of fractional PKA distribution plots.		
	If IDC = 0, skip cards 18-21.		
18	Free	(LOG(M), M=1,4)	same options as for card #6
19,20,21	x-axis, y-axis labels and title of displacement cross-sections plots.		

(*) for the x-axis, y-axis and title cards the last two characters on the cards have to be $ signs.

(†) axis labels are put on two lines on the plots. On cards the lines are separated by set of characters, $/$.

IV.D. NSPECAVE

Object: The object of the NSPECAVE program is to take the PKA probability distributions and displacement cross sections calculated by the DISCSM code at discrete neutron energies and find the averaged PKA probability distributions and displacement cross sections in a spectrum of neutrons.

Input: The filed output of the DISCSM code constitutes the input to the NSPECAVE. The only input that is supplied on cards is the neutron energy spectrum and the flux of neutrons in that spectrum. The format of the card input for the NSPECAVE is given in Table IV.4.

Output: The printed output from the NSPECAVE program is as follows. It first gives the displacement cross sections in the energy group structure of the neutron flux. It then prints out the spectrum averaged displacement cross sections. Next, tables of differential, normalized, and fractional spectral average PKA recoil distributions are given. The spectrum averaged results are repeated for each neutron flux supplied.

Because of limitations on the available memory space with FORTRAN-V compiler in the Madison Academic Computing Center (MACC) Univac-1110 computer, the NSPECAVE program was run using the ASCII compiler, but the available graphics packages at the MACC are in FORTRAN. A subroutine in FORTRAN and an ASCII program can be interphased using some special library routines and functions at MACC but the total memory space used up by the whole program has to be less

Table IV.4

Description of the Card-Input to the NSPECAVE Program

Card #	Format	Variable	Description
1	Free	NEX	Number of energy points in the neutron energy spectrum
		ISAME	= 0/≠ 0, the end point energies of the group structure in which the neutron fluxes are given are/are not the same as the neutron energies at which the displacement cross sections are calculated by the DISCSM code
2*	Free	(EF(M), M=1,NEX)	The group structure for the neutron flux
3	15A4	(TITLE(M),M=1,15)	Title of the neutron flux
4*	Free	(FX(M),M=1,NEX-1)	Neutron flux

(*) The information on cards 2 and 4 may actually fit on more than one card.

Repeat cards 3 and 4 as many times as there are different neutron fluxes in which PKA probability distribution and displacement cross sections averaging is needed.

than that allowed for FORTRAN programs alone. Therefore, the graphics routines could not be called directly from the NSPECAVE but the spectral averaged PKA distributions results had to be filed and reread by another ASCII program, the memory size of which did not exceed 65.000 word locations. That program is APLOT and is described below.

IV.E. APLOT

Object: The object of the APLOT program is to plot on a Calcomp plotter the neutron spectrum averaged PKA recoil distributions calculated by the NSEPCAVE program.

Input: As has been mentioned already, the input to the APLOT program comes from the filed output of the NSPECAVE. This file is assigned to the run with a logical unit number of 20 and could be a temporary file if both NSPECAVE and APLOT are executed in the same run. The input to APLOT from cards is intended to set up the problem to what kind of plots are needed and to give the axis labels and titles to be printed on the plots. The description of the card input to APLOT is given in Table IV.5.

Output: Plots can be generated showing the averaged differential, normalized and fractional PKA energy distributions in desired neutron flux spectra. The individual nuclear reaction contributions can be shown on the plots by setting the variable JUSTOT equal to zero in the input or they can be suppressed. Plots comparing the total PKA distributions in selected neutron spectra can also be

Table IV.5

Description of the Card Input to APLOT

Card #	Format	Variable	Description
1	Free	JUSTOT	= 0/≠ 0 The individual reaction contributions on neutron spectrum averaged PKA distribution plots will/will not be shown
2	Free	IDIF	= 0/≠ 0 Differential PKA probability distribution plots will not/will be given
		INOR	= 0/≠ 0 Normalized PKA probability distribution plots will not/will be given
		IFRAC	= 0/≠ 0 Fractional PKA probability distribution plots will not/will be given
3	10I5	(ILESS(I),I=1,10)	Negative of the sequence numbers of the neutron fluxes, in the order they are supplied to the NSPECAVE program, for which the averaged PKA probability distributions will not be plotted
4	Free	ICOMD	= 0/≠ 0 Comparison total differential PKA distributions in selected neutron spectra will not/will be plotted
		ICOMN	= 0/≠ 0 Comparison total normalized PKA distributions in selected neutron spectra will not/will be plotted
		ICOMF	= 0/≠ 0 Comparison total fractional PKA distributions in selected neutron spectra will not/will be plotted
5	10I5	(ICLESS(I),I=1,10)	Negative sequence numbers of the neutron fluxes, in the order they are supplied to the NSPECAVE program, for which the total averaged PKA probability distributions will not be included in the comparison plots

Table IV.5 (cont.)

Card #	Format	Variable	Description
	If IDIF = 0, skip cards 6,7, and 8.		
6	Free	(LOG(M),M=1,4)	= 0 linear-linear scaling = 1 linear-log scaling = 2 log-linear scaling = 3 log-log scaling < 0 shows the end of scaling specifications for this plot type
7*†	12A4	(IX(I),I=1,12)	x-axis label for the differential PKA distributions plots
8*†	12A4	(IY(I),I=1,12)	y-axis label for the differential PKA distributions plots
	If INOR = 0, skip cards 9, 10, and 11.		
9	Free	(LOG(M),M=1,4)	Same options as for card #6
10	12A4	(IX(I),I=1,12)	x-axis label for the normalized PKA distributions plots
11	12A4	(IY(I),I=1,12)	y-axis label for the normalized PKA distributions plots
	If IFRAC = 0, skip cards 12, 13, and 14.		
12	Free	(LOG(M),M=1,4)	Same options as for card #6
13	12A4	(IX(I),I=1,12)	x-axis label for the fractional PKA distributions plots
14	12A4	(IY(I),I+1,12)	y-axis label for the fractional PKA distributions plots
	If ICOMD = 0, skip cards 15 - 18.		
15	Free	(LOG(M),M=1,4)	Same options as for card #6
16	12A4	(IX(I),I=1,12)	x-axis label for the comparison total differential PKA distributions plot
17	12A4	(IY(I),I=1,12)	y-axis label

Table IV.5 (cont.)

Card #	Format	Variable	Description
18*	15A4	(IT(I),I=1,15)	Plot title
If ICOMN = 0, skip cards 19 - 22.			
19	Free	(LOG(M),M=1,4)	Same options as for card #6
20	12A4	(IX(I),I=1,12)	x-axis label for the comparison total normalized PKA distributions plot
21	12A4	(IY(I),I=1,12)	y-axis label
22	15A4	(IT(I),I=1,15)	Plot title
If ICOMF = 0, skip cards 23 - 26.			
23	Free	(LOG(M),M=1,4)	Same options as for card #6
24	12A4	(IX(I),I=1,12)	x-axis label for the comparison total fractional PKA distributions plot
25	12A4	(IY(I),I=1,12)	y-axis label
26	15A4	(IT(I),I=1,15)	Plot title

(*) The last two characters in all the x-axis, y-axis label and plot title strings have to be $ signs.

(†) axis labels are put on two lines on the plots. On cards the lines are separated by set of characters, $/$.

shown. Figures A.5 and A.6 of Appendix A show the differential and fractional Nb PKA energy distributions in an unsoftened fusion neutron spectrum, respectively. Figure A.7 shows a comparison of fractional total Nb PKA probability distributions in three different neutron spectra; hard fusion, fusion softened by 25 cm of solid carbon, and in EBR-II.

IV.F. XGRPAVE

Object: The displacement cross sections calculated by the DISCSM code are point values. They are calculated at discrete neutron energies, whereas the neutron fluxes calculated by the ANISN program are group values. In order to be able to calculate displacements per atom in various locations in the blanket using the fluxes from the ANISN program, the pointwise displacement cross sections calculated by the DISCSM code have to be group averaged. That is the purpose of the XGRPAVE program.

Description: The program uses the following formula to calculate the group averaged displacement cross sections,

$$\bar{\sigma}_{i,x} = \frac{\int_{E_{li}}^{E_{hi}} W(E)\, \sigma_{i,x}(E)dE}{\int_{E_{li}}^{E_{hi}} W(E)\, dE} \qquad 4.1$$

where E_{li} and E_{hi} are the lower and upper energy boundary values of the i^{th} group,

$W(E)$ is a weighting function, taken to be $\frac{1}{E}$,

x denotes the reaction,

$\sigma_{i,x}(E)$ for each x is taken to be

$$\sigma_i(E) = \sigma_{li} + \frac{\frac{1}{E} - \frac{1}{E_{li}}}{\frac{1}{E_{hi}} - \frac{1}{E_{li}}} (\sigma_{hi} - \sigma_{li}) \quad \text{for } E < E_c \qquad 4.2$$

and

$$\sigma_i(E) = \sigma_{li} + \frac{E - E_{li}}{E_{hi} - E_{li}} (\sigma_{hi} - \sigma_{li}) \quad \text{for } E > E_c \qquad 4.3$$

where σ_{li} and σ_{hi} are the cross sections at the lower and upper end point energies of the i^{th} group, and

E_c is the energy where the total displacement cross sections for the element in question go through a minimum. E_c is usually <1 keV.

Input: The displacement cross sections are read from the output file of the DISCSM code which is assigned to the run with a logical unit number of 15. The only information from cards is the 46 group energy structure shown in Table B.1 in Appendix B, and it is read from cards with a free format.

Output: The output is a list of group averaged displacement cross sections in units of barns. Tables A.4 and A.5 in Appendix A show the pointwise displacement cross sections for Nb as calculated by the DISCSM code and the group averaged displacement cross sections in the 46 group energy structure as calculated by the XGRPAVE program, respectively.

IV.G. ANISN[50]

ANISN is a one-dimensional discrete ordinates transport code with anisotropic scattering. It is a well-known code in the neutronics and photonics area. In this work it is also used to study the nuclear performance of fusion reactor blanket designs with ISSECs. One such blanket design that has been used extensively in this study is shown in Figure V.11 of Chapter V. The thickness of the ISSEC zone between the plasma and the first wall was taken as variable and all the other dimensions were kept constant. The composition of each zone as well as the thicknesses used are shown in Figure V.11. A density factor of 0.5 for the first wall and 1.0 for the ISSEC, breeding and reflector zones were used, although in practice a density factor of less than 1.0 would be more appropriate in the breeding and reflector zones to take into account the coolant passages and in the ISSEC zone to take into account the porosity of the ISSEC material. This would result in thicker zones. However, the neutron "optical" thickness would be the same in both cases. To simulate the final shield and structures that would be present in an actual design albedos of 0.05, 0.10, 0.15, 0.20, 0.25 were used for neutron groups 1 through 5 (9 to 14.9 MeV) of the 46 group energy structure shown in Table B.1, respectively. An albedo of 0.3 was used for neutrons of lower energy groups.

In all cases the ANISN program was run with a S_4-P_3 approximation. It has been shown elsewhere[54] that this approximation is adequate to predict integral parameters such as tritium breeding and

gas production rates to within approximately 2% of a higher order calculation like S_{16}-P_5.

Since this study has been in progress over a period of more than 4 years, some of the earlier results from the ANISN program were obtained using the nuclear cross section data from ENDF-B/III files and the rest from ENDF-B/IV. The ENDF-B/III data were processed by the SUPERTOG[55] code and the ENDF-B/IV data were processed by the AMPX[56] modular code system. The only exception is Nb. The evaluation of the Nb cross sections was always based on ENDF-B/III data. The two sets of data from ENDF-B/III and ENDF-B/IV show some differences. For example, it is shown that for a standard bench mark blanket[57] the use of ENDF-B/IV data gives about a 4% higher breeding ratio than if the ENDF-B/III data are used.[58] However, the conclusions obtained in this study are not greatly affected by this change-over in data from ENDF-B/III to ENDF-B/IV because most of the earlier studies in this work that used the ENDF-B/III data were carried out with the slab geometry blanket model shown in Figure V.1 of Chapter V. The ISSEC material was kept the same, namely carbon, and the first wall material, was varied to show and compare the effects of the softened neutron spectrum on the damage state of the different potential first wall materials. Later studies that utilized the ENDF-B/IV data were done with the cylindrical geometry blanket model of Figure V.11 with one fixed first wall material, 316 SS, and different ISSEC materials, C, V, Nb, Mo and W for tokamak applications

and liquid Li, Pb and Pb_4Li-eutectic for laser fusion applications. The idea here was to show and compare the effects of the various ISSEC materials on the 316 SS first wall radiation damage, and the blanket parameters. Therefore comparisons were made within each data set and switching from ENDF-B/III to ENDF-B/IV does not significantly affect the conclusions of this study.

Input and Output: There is a comprehensive users manual that explains the input and output of the ANISN program in detail.[50] Due to the space limitations only the important considerations in the input and the output of the ANISN program will be mentioned here. For more information the reader is urged to consult reference 50.

The main points in the ANISN input include a geometric description of the blanket design, the nuclear performance of which is to be studied, boundary conditions, neutron source conditions, materials composition and density in each zone, and the activity cross sections and the kerma factors for each element present in the design. The activity cross sections are processed from nuclear data in ENDF-B files. The neutron and gamma kerma factors used in this study were calculated using the MACK[59] and MUG[60] codes, respectively.

The main output for the purposes of this study from the ANISN program consists of the total flux (neutrons (or photons) $-cm^{-2}-sec^{-1}$) by energy group and by interval midpoint, and a list of selected activities for all elements by interval in units of reactions $-cm^{-3}-sec^{-1}$. Activities are also integrated over all intervals

in each zone and listed in units of reactions per second per zone. Activities are normalized to a unit source neutron/sec whereas the total flux is normalized to a large number such as 10^{15} source neutrons/sec.

IV.H. DKR[51]

Object: The purpose of the DKR code in the MODISS package is to find the radioactivity, biological hazard potential and afterheat of the total blanket and its individual components such as the first structural wall and the ISSEC for various operating and aftershutdown times.

Description: DKR is a radioactivity calculation code for fusion reactors. It was prepared at the University of Wisconsin-Madison as part of a Ph.D. thesis.[61] It is also documented in references 51 and 62.

DKR takes as its main input the neutron flux from the output of the ANISN program and the data in the Decay Chain Data Library (DCDLIB).[62] The DCDLIB is a concise library containing necessary nuclear data information for use in the fusion activity studies. The data in the DCDLIB include for the stable and radioactive nuclides, the reaction cross sections, reaction products and branching ratios to isomeric states, and for the radioactive nuclides it also includes the decay constants, the decay modes and decay products, average energies of the emitted particles and the Maximum Permissible Concen-

tration (MPC) values.[63] The reaction cross sections in the DCDLIB are taken from ENDF-B/IV and complemented from BNL-325[64] whenever necessary. The radioactive decay data are either from ENDF-B/IV, or from the table of isotopes[65] for isotopes not in the ENDF-B/IV library.

Using the data in the DCDLIB and the neutron flux from the ANISN program, the DKR code constructs linear decay chains for all nuclides present in the system and calculates the radioactivity, biological hazard potential (BHP), and afterheat due to β- and γ-rays, and that due to β-rays only. The calculations are done for a number of operating and aftershutdown times. The results can be obtained for just one part of the blanket, such as the first structural wall or the ISSEC, or they can be integrated over the total blanket.

IV.I. Heat Transfer Analysis Codes HEAT[52] and FEM2D[53]

Object: The object of these codes in the MODISS package is to calculate the temperature profiles in ISSECs and heat fluxes from the ISSEC to the first structural wall.

IV.I.1. HEAT

HEAT is a very general heat transfer analysis code. It uses the finite difference technique as its method of solution. The primary purpose of HEAT is to obtain numerical solutions of steady state, general transient or steady-periodic heat transfer problems. The program solves for either temperatures or heat fluxes for problems

that can be formulated in the form

$$mc_p \frac{dT}{dt} = Q_{conduction} + Q_{convection} + Q_{infrared\ radiation} + Q_{solar\ radiation} + Q_{generated} \quad 4.4$$

The program is also capable of performing parameter uncertainty analysis on temperatures and heat fluxes.

The method of solution of Eq.(4.4) is explained in references 52 and 66 and the code is documented in reference 52.

In solving the ISSEC problems, Eq. (4.4) reduces to

$$mc_p \frac{dT}{dt} = Q_{conduction} + Q_{infrared\ rad.} + Q_{generated} \quad 4.5$$

where m is the mass of the nodal region,

c_p is the heat capacity of the material,

T is the temperature, and

t is time.

The net energy conducted into node i is calculated by

$$Q_{conducted} = \sum_{j=1}^{n} C_{ji}(T_j - T_i) \quad 4.6$$

where n is the number of neighboring nodes to node i, and

C_{ji} is the conductance between nodes j and i and is given as

$$C_{ji} = \frac{kA}{\Delta x} \quad 4.7$$

where k is the thermal conductivity,

A is the conduction area between nodes i and j, and

Δx is the conduction distance between i and j.

The radiation term in Eq. (4.5) is given as

$$Q_{\text{infrared radiation}} = \sum_{j=1}^{N} \varepsilon_i \varepsilon_j A_i \hat{F}_{ij} \sigma (T_j^4 - T_i^4) \qquad 4.8$$

where Q is the net radiation heat transfer to node i,

N is the number of radiating nodes,

ε_i, ε_j are the emissivities of nodes i and j,

A_i is the radiation area of node i,

$\hat{F}_{ij}$ is the infrared exchange factor between nodes i and j. If surfaces are diffuse reflectors of radiation then $\hat{F}_{ij}$ is the view factor looking from node i to node j, and

σ is the Stefan-Boltzmann constant.

The last term in Eq. (4.5) is the nodal heat generation term. It is the sum of neutron plus gamma heating in each nodal zone and is taken directly from the output of the ANISN program.

IV.I.2. FEM2D

The program FEM2D[53] uses a finite-element technique to solve two-dimensional, steady-state or transient, conduction problems. It is much easier and less expensive to use than the program HEAT. Its one disadvantage is that it does not have provisions for thermal

radiative heat transfer. Therefore, in cases where radiation is important, the program HEAT is used. Otherwise FEM2D is used. More detailed information on the program FEM2D can be obtained from reference 53.

Having obtained the temperature profiles in the ISSEC and the heat fluxes to the first structural wall, the thermal stresses associated with rigid first structural walls are calculated by a thin plate approximation using the formula

$$\sigma_{th} = \pm \frac{\alpha}{2} \frac{E}{k(1-\nu)} \left(W_s t + \frac{W_n}{2} t^2\right) \qquad 4.9$$

where σ_{th} is the thermal stress in the first wall,

α is the coefficient of expansion of the first wall,

E is the modulus of elasticity of the first wall,

ν is the Poisson's ratio at the average temperature of the wall,

W_s is the heat flux incident on the first wall,

W_n is the average nuclear heating in the first wall, and

t is the thickness of the first wall.

CHAPTER V

RESULTS AND ANALYSIS

Three of the five blanket concepts in Chapter II have been studied in great detail. They are the class 1, 4 and 5 blankets. The results from these studies are presented in this chapter. First, in Section V.A., the effects of a variable thickness carbon ISSEC in a burner blanket system (class 4 in Chapter II) on the radiation damage parameters of potential fusion reactor first wall materials is discussed. The results are given for systems operating on both D-T and D-D plasma cycles. Section V.B. outlines the studies carried out using an externally breeding, lithium cooled type blanket system (class 1 in Chapter II) with 316 SS structure and different ISSECs with varying thicknesses. The results are presented with respect to the normal radiation damage functions in the 316 SS first structural wall. Also included are the total blanket parameters such as energy multiplication, breeding ratio and radioactivity, radiation damage inside ISSECs, mechanical design and heat transfer considerations of ISSECs, and other factors affecting the choice of one ISSEC material over the other such as cost, vacuum properties, sputtering, blistering, and thermal shock resistance.

The blanket systems employing liquid metals Li or Pb, or Pb_4Li eutectic as ISSECs (class 5 in Chapter II) for laser fusion applications are studied in Section V.C. The effect of the liquid ISSECs

on the displacement and gas production rates in the first structural wall, the breeding ratio, energy multiplication, and the spatial distribution of the energy deposition in the blanket is shown as the thickness of the ISSEC is varied. The displacement cross sections used in obtaining the dpa results given in this Chapter and in Chapter II were previously calculated by Doran et al.[43,67] However, we do compare these results to those which would have been obtained if the new displacement cross sections, (from the MODISS package) had been employed. This comparison is made for Nb and 316 SS in Section V.C. Finally, a discussion on the results presented in this Chapter is given in Section V.E.

V.A. The Response of the Anticipated First Wall Materials to Fusion Neutron Spectra Degraded by a Carbon ISSEC

V.A.1. Introduction

The one dimensional-homogeneous blanket design used for obtaining the results in this section is shown in Figure V.1. A variable thickness carbon zone was placed between the plasma and the first wall. A density factor (D.F.) of 1.0 was used for the neutronic calculations although in practice a D.F. of $\sim$0.7 would be more reasonable and would result in a thicker ISSEC region. However, the neutron "optical" thickness would be the same in both cases. The first wall thickness of 1 cm at a D.F. of 1.0 is intended to cover most reactor design cases. Again, lower D.F.s and increased thickness would be used in practice to include coolant (which we assumed to be

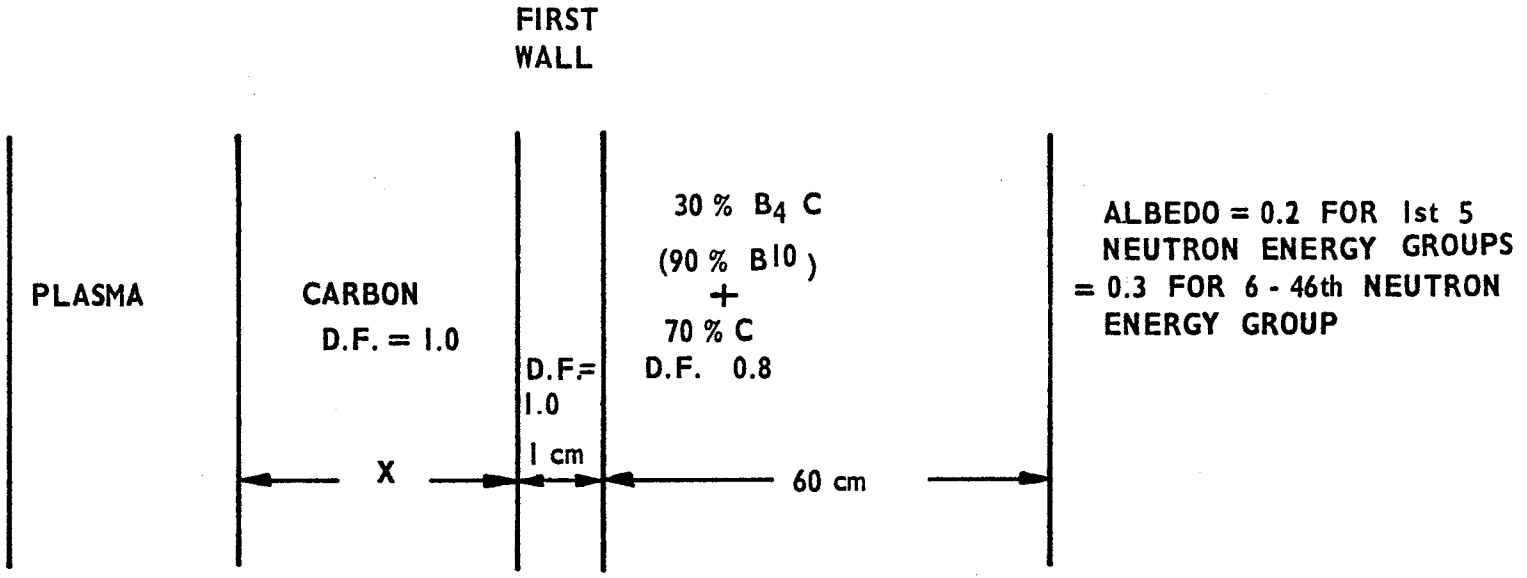

D.F. = DENSITY FACTOR.

MODEL BLANKET DESIGN USED TO STUDY THE EFFECT OF GRAPHITE SPECTRAL SHIFTER ON THE RADIATION DAMAGE PARAMETERS IN THE FIRST WALL.

Figure V.1

helium gas) and void spaces. The first wall materials considered were Al, V, 316 SS, Nb, Mo and Ta. The first wall is followed by a 60 cm thick reflector-shield region composed of 30% B_4C (enriched to 90% B-10) and 70% carbon. An albedo of 0.2 was used to simulate the final shield for the first five neutron energy groups (9 to 14.9 MeV) and an albedo of 0.3 was used for neutrons of lower energy. Obviously, no attempt was made to breed tritium in this reactor design but only to highlight the anticipated first wall structural materials responses to the degraded neutron spectra.

The nuclear performance of this type of reactor design was studied by solving the discrete ordinates form of the neutron transport equation for a slab using the ANISN[50] program with a S_4-P_3 approximation. The neutron multigroup cross sections (except for gas production in molybdenum) were processed using the program SUPERTOG[55] from nuclear data in ENDF/B3.[49] Gas production cross sections for Mo were calculated by Pearlstein.[68] The displacement cross sections were calculated from a computer code developed by Doran[67,69] and the values used in these calculations are given in references 9 and 10. All calculations were performed using 46 neutron energy groups shown in Appendix B.

The reactions considered for the radioactivity calculations, along with appropriate branching ratios and half lifes are given in reference 9. The radioactivity and appropriate decay factors for 316 SS were calculated using the DKR program.[51] The composition

of 316 SS was assumed to be 70% Fe, 18% Cr and 12% Ni for all calculations except radioactivities. The composition of the 316 SS for the radioactivity calculations is given in reference 9.

All the calculations are done for two different reactors operating with deuterium-tritium (D-T) and deuterium-deuterium (D-D) plasma cycles. The blanket structure shown on Figure V.1 was used for both calculations. All the results are normalized to 1 MW/m^2 of neutrons passing through the first wall (or inner ISSEC surface). In D-D case, it is assumed that all the tritium that is produced through one branch of the D-D fusion reaction is consumed in the reactor. As a result, the energy of 50% of the neutrons generated in D-D plasma is 14.1 MeV and the energy of the other half is 2.45 MeV. In the D-T case, all neutrons are of 14.1 MeV energy. With this assumption in mind, we can calculate the incident neutron fluxes corresponding to the 1 MW/m^2 neutronic wall loading in the two cases. In the D-T case,

$$(14.1\ \frac{MeV}{n})(1.602\times10^{-19}\ \frac{MW\text{-}sec}{MeV})(4.43\times10^{13}\ \frac{n}{cm^2\text{-}sec})(10^4\ \frac{cm^2}{m^2}) = 1\ \frac{MW}{m^2}$$

(neutronic)

In the D-D case,

$$(\frac{14.1+2.45}{2}\ \frac{MeV}{n})(1.602\times10^{-19}\ \frac{MW\text{-}sec}{MeV})(7.56\times10^{13}\ \frac{n}{cm^2\text{-}sec})(10^4\ \frac{cm^2}{m^2})$$

$$= 1\ \frac{MW}{m^2}(\text{neutronic})$$

The incident flux required to give a 1 MW/m^2 neutronic wall loading is 4.43×10^{13} n/cm^2-sec for the D-T reaction and in the D-D case, it is 7.56×10^{13} n/cm^2-sec (3.78×10^{13} n/cm^2-sec of 14.1 MeV and 3.78×10^{13} n/cm^2-sec of 2.45 MeV neutrons).

V.A.2. Results and Analysis

V.A.2.a. Reduction of Displacement Damage

The displacement rates in the Al, V, 316 SS, Nb, Mo and Ta first walls are listed in Table V.1 and displayed in Figures V.2 to V.4 as functions of carbon ISSEC thickness.

The reader should be cautioned that it is the relative and not absolute rates of damage which are important. This is because one cannot accurately compare one element with another on dpa values alone; the homologous temperature of irradiation has as much or more influence on the final damage state as does the total damage level.

A few interesting observations can be made from Table V.1. For the same neutron wall loading, even though the number of 14.1 MeV neutrons incident on the first wall from the D-D plasma is approximately 85% as much as from a D-T plasma, the displacement rates are higher in D-D systems by 20-35%. The reason for this is that (1) the 2.45 MeV neutrons will cause considerable displacement damage compared to 14.1 MeV neutrons ($\sim$80% as much despite the factor of 6 difference in energy) and (2) more total neutrons ($\sim$70% are required to achieve a neutronic wall loading of 1 MW/m^2. However, the rela-

Table V.1

Factors of ISSEC Produced Reduction in Displacement Damage in Various CTR First Wall Materials in D-T and D-D Fusion Environments

	dpa/year[(a)]			
		D-D Fusion		
Material	No ISSEC	12.5 cm C	12.5 cm C Damage Ratio	25 cm C
Al	19.8	4.8	0.24	1.32
V	18.4	5.8	0.32	2.22
316 SS	16.8	3.2	0.19	0.86
Nb	10.8	2.14	0.20	0.54
Mo	12.2	2.34	0.19	0.6
Ta	10.5	2.08	0.20	0.52
		D-T Fusion		
Al	12.7	3.4	0.27	
V	12.9	3.8	0.29	
316 SS	11.3	2.50	0.22	
Nb	8.48	1.64	0.19	
Mo	9.47	1.77	0.19	
Ta	8.42	1.60	0.19	

(a) 1 MW/m^2 neutron wall loading and 100% Duty Factor

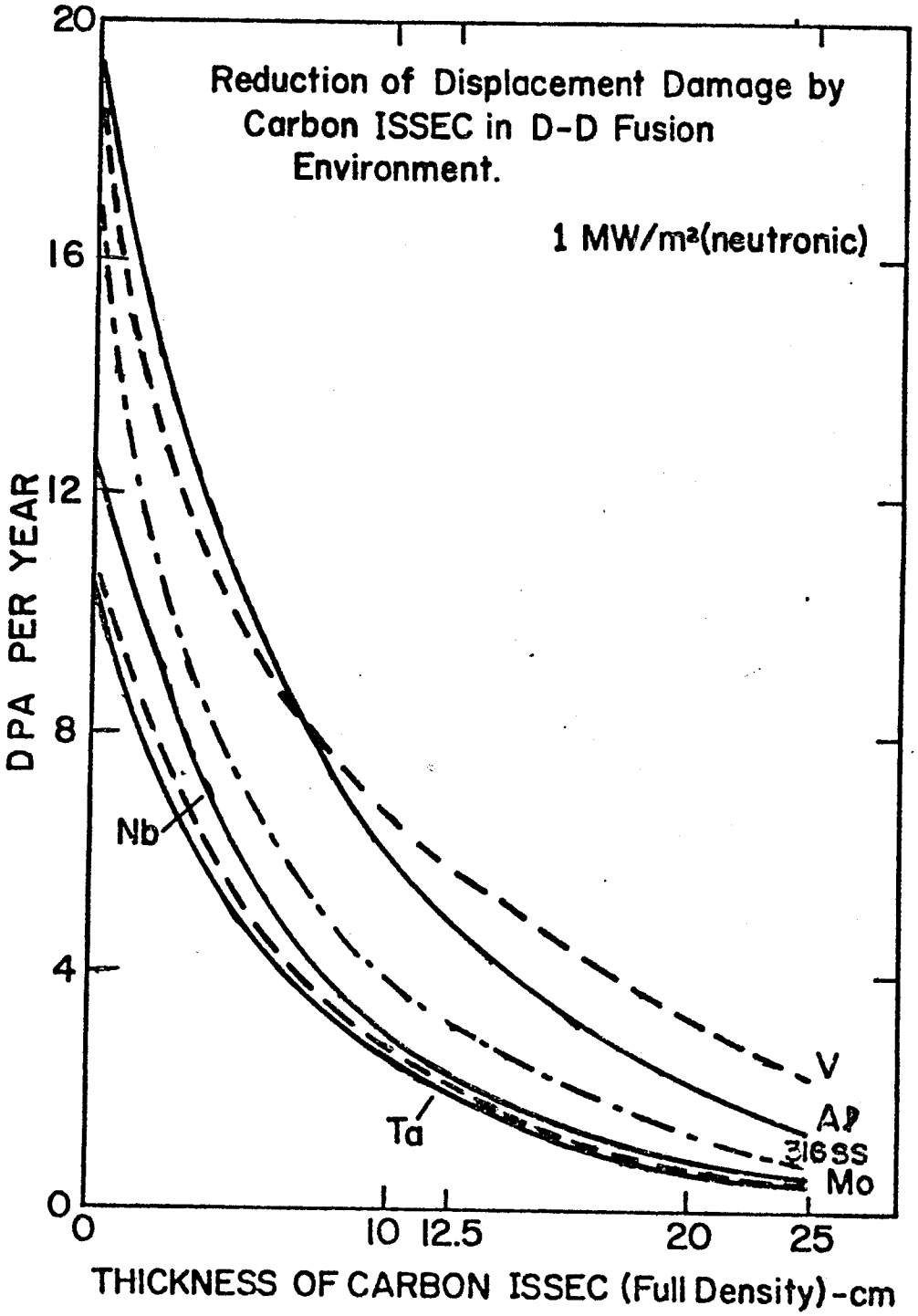
Reduction of Displacement Damage by
Carbon ISSEC in D-D Fusion
Environment.
1 MW/m²(neutronic)
DPA PER YEAR
20
16
12
8
4
0
0
10
12.5
20
25
THICKNESS OF CARBON ISSEC (Full Density)-cm
Nb
Ta
V
Al
316SS
Mo

Figure V.2

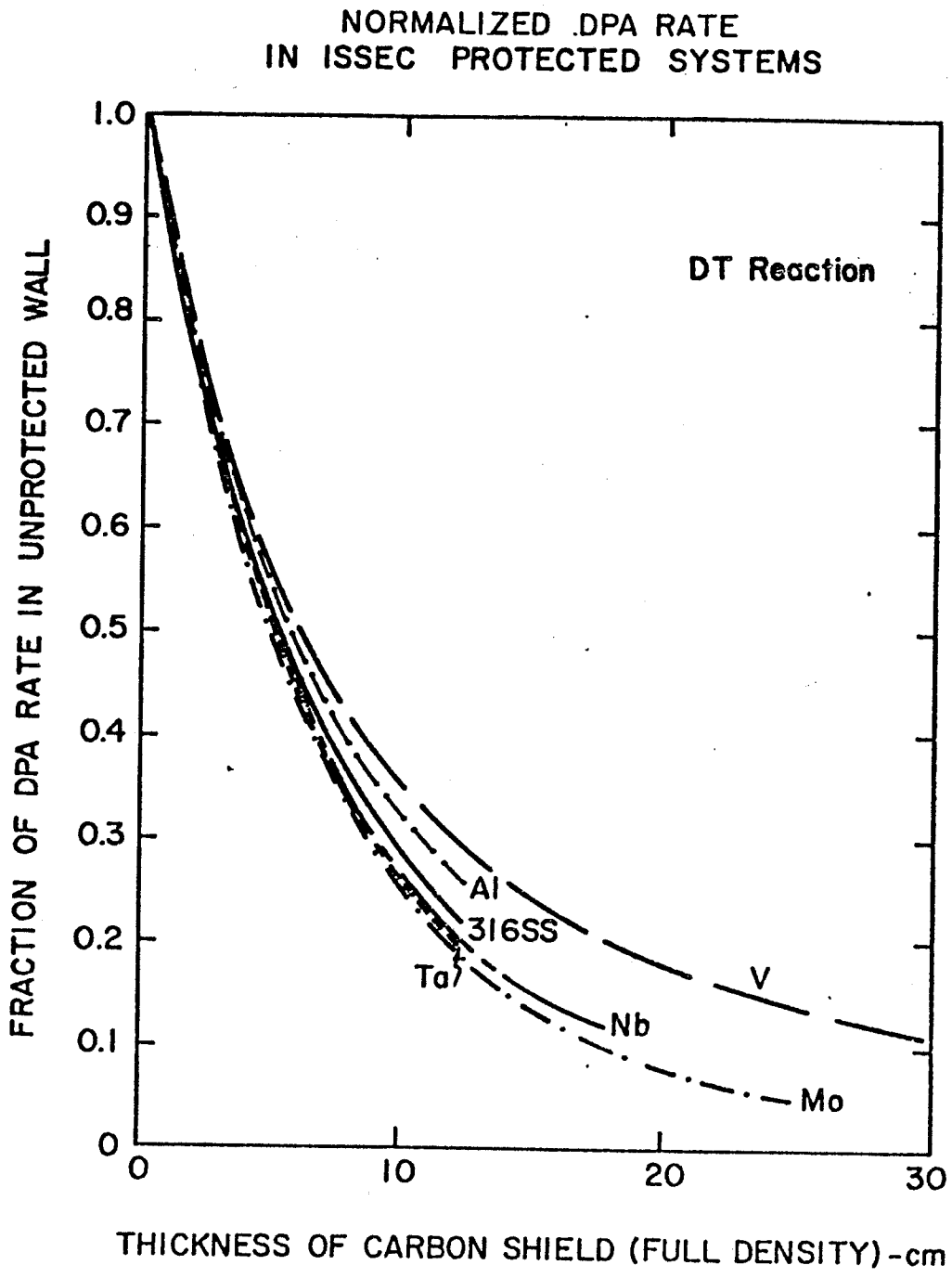
NORMALIZED DPA RATE
IN ISSEC PROTECTED SYSTEMS
DT Reaction
FRACTION OF DPA RATE IN UNPROTECTED WALL
1.0
0.9
0.8
0.7
0.6
0.5
0.4
0.3
0.2
0.1
0
0
10
20
30
Al
316SS
Ta
V
Nb
Mo
THICKNESS OF CARBON SHIELD (FULL DENSITY)-cm

Figure V.3

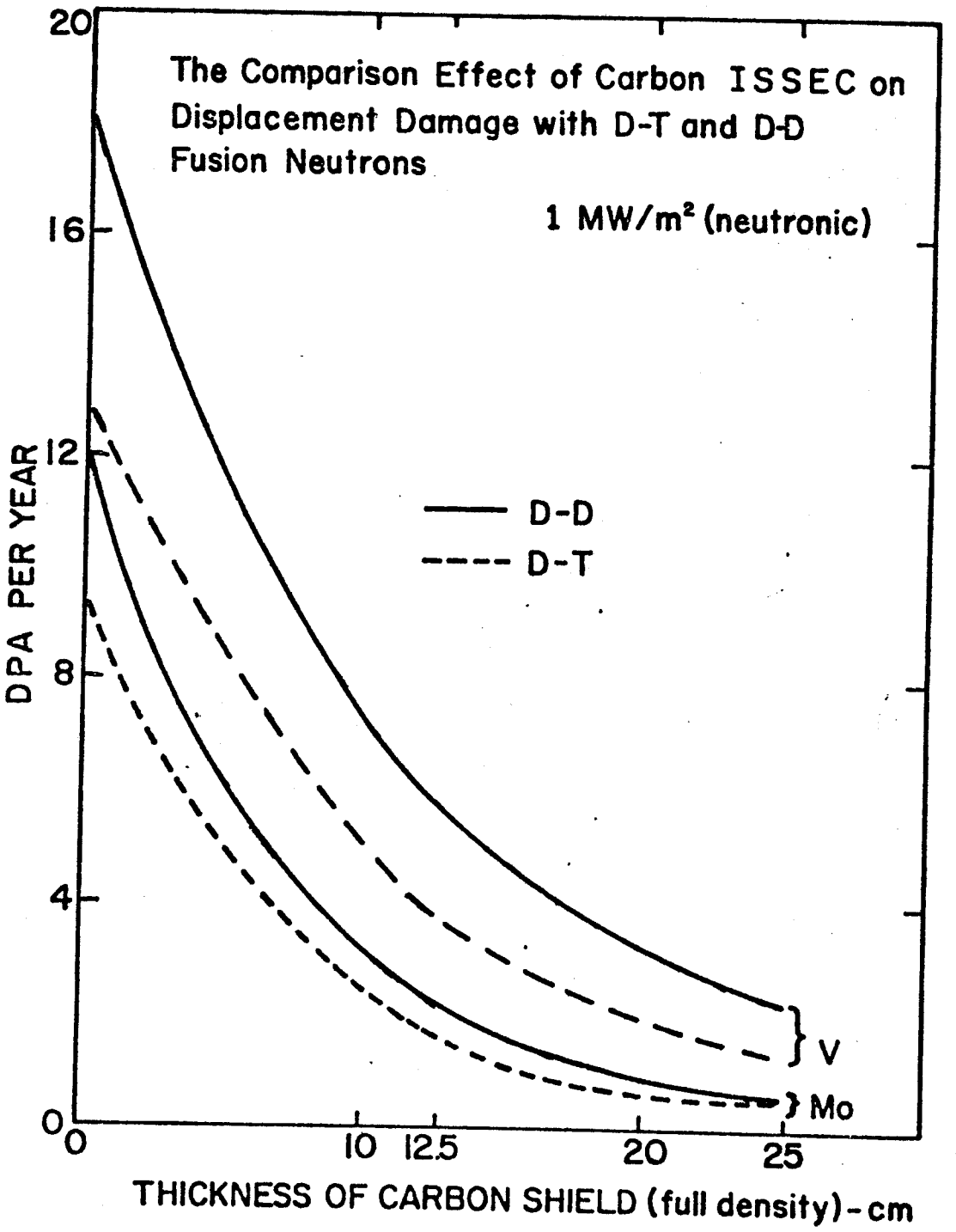
The Comparison Effect of Carbon ISSEC on Displacement Damage with D-T and D-D Fusion Neutrons
1 MW/m² (neutronic)
D-D
D-T
V
Mo
DPA PER YEAR
THICKNESS OF CARBON SHIELD (full density) - cm
0
4
8
12
16
20
0
10
12.5
20
25

Figure .V.4

tive effect of the ISSEC in reducing displacement damage is about the same.

It is also observed that the ISSEC has a greater effect in reducing the displacement damage in high Z elements as compared to low Z elements. The reason is complex but can be roughly explained by the low ionization threshold in low Z elements.[69a] This means that the primary knock on atoms in Al lose much less energy in elastic (displacement) collisions than do the PKAs in Nb. For example, in Al, 107 keV is lost to displaced atoms per PKA produced by 14 MeV neutrons and 51 keV from 1 MeV neutrons (a ratio of 2.1). The elastic energy lost by an average PKA in Nb is 213 keV from 14 MeV neutrons and 56 keV from 1 MeV neutrons (a ratio of 3.8). Hence, the reduction in neutron energy by the ISSEC is more effective in Nb than in Al.

Turning to relative reduction in displacement damage as a function of carbon thickness, we see in Figure V.3 that a reduction of 3-5 can be achieved using 12.5 cm of carbon while reductions by a factor of 20 can be accomplished by using 25 cm of carbon ISSEC in front of Mo. The significance of this observation is that if the wall life is predominantly determined by the level of the total displacement damage (without regard to the spatial configuration of defects) then one might extend the wall life due to radiation damage alone by factors of 5-20 in Mo and similar values in other systems. The relative reduction in dpa rate achieved with the D-D system are within 10-30% of the D-T case and are not presented graphically here.

V.A.2.b. Reduction of He and H Production Rates

Table V.2 lists the effect of carbon ISSEC on He gas generation rates in potential CTR first wall materials subjected to neutrons from D-D plasma and Table V.3 gives the results for hydrogen production. The same results for the D-T plasma are shown in Table V.4. Analysis of the cross section data reveals that almost all the helium and hydrogen production reactions in the materials considered for this study have thresholds over 2.5 MeV. This means that the helium and hydrogen production rates in the D-D plasma case are lower than in the D-T case by a factor almost identical to the reduction in the 14.1 MeV component of the incident flux per 1 MW/m^2 neutronic wall loading; namely by the factor of 4.43/3.78 (1.17).

The absolute effect of carbon ISSEC on helium generation in metals for the D-T case is shown on Figure V.5. The same general behavior holds true for the D-D neutrons. The absolute effect here is much more pronounced than in the case of displacement damage. Reductions in helium gas productions range from 7 to 14 for 12.5 cm carbon and from 7 to 11 for hydrogen production with the same carbon thickness. The factors of reduction are 27-80 and 17-55, respectively for a 25 cm carbon ISSEC. Except for V and Al, the reduction in He production is always greater than that for the reduction in hydrogen production. The reduction in helium gas production in Ta is a factor of 2 more than the reduction in V. This is due to the lower threshold for (n,α) reactions in V ($\sim$7 MeV) than for Ta (11 MeV).

Table V.2

Effect of Carbon ISSEC on the Helium Gas Production Rate in Potential CTR Materials in D-D Fusion Environment

Appm He/Year[a]

Material	No ISSEC	12.5 cm C	25 cm C
Al	405	42.8	8.90
V	67.0	9.72	2.46
316 SS[b]	239	22.8	4.6
Nb	27.8	2.82	0.58
Mo	62.0	5.94	1.2
Ta	6.42	0.46	0.08

(a) 1 MW/m^2 neutron wall loading, 100% Duty Factor

(b) Neglecting helium from Ni^{59}

Table V.3

Effect of Carbon ISSEC on the Hydrogen Gas Production Rate in Potential CTR First Wall Materials in D-D Fusion Environment

Appm H/Year[a]

Material	No ISSEC	12.5 cm C	25 cm C
Al	944	92.5	20.0
V	122	24.4	7.32
316 SS	675	88.4	20.6
Nb	93.6	10.7	2.32
Mo	127	11.7	2.32
Ta	0	0	0

(a) 1 MW/m^2 neutron wall loading, 100% Duty Factor

Table V.4

Effect of Carbon ISSEC Thickness on the Gas Production Rates in Potential CTR Materials[a]

	D-T Plasma					
	appm He/yr			appm H/year		
Material	No ISSEC	12.5 cm ISSEC	Damage Ratio	No ISSEC	12.5 cm ISSEC	Damage Ratio
Al	476	50.1	0.11	1110	111	0.10
V	78.6	11.4	0.15	143	28.6	0.20
316 SS	280	26.8	0.10	736	100	0.14
Nb	32.7	3.32	0.10	110	12.6	0.11
Mo	72.6	6.95	0.10	149	13.7	0.09
Ta	7.52	0.55	0.07	0	0	-

(a) 1 MW/m^2 neutronic wall loading, 100% Duty Factor

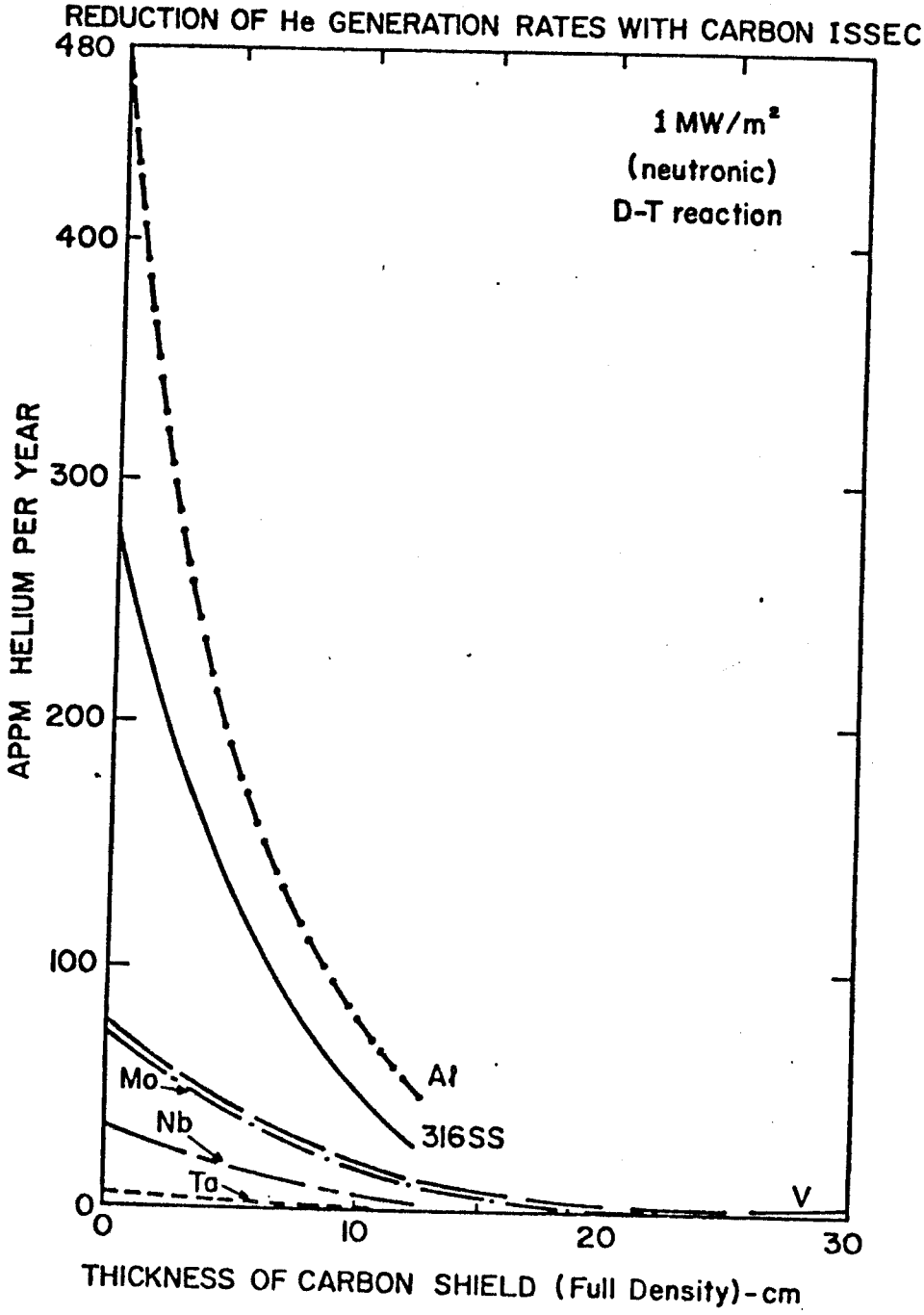
REDUCTION OF He GENERATION RATES WITH CARBON ISSEC
1 MW/m²
(neutronic)
D-T reaction
APPM HELIUM PER YEAR
480
400
300
200
100
0
0
10
20
30
Al
316SS
Mo
Nb
Ta
V
THICKNESS OF CARBON SHIELD (Full Density)-cm

Figure V.5

The relative reduction values are plotted in Figure V.6 and it is to be noted that on a linear scale, there is little difference between the elements. If there is a discernable trend, it is that the relative reduction is greater for high Z elements than for low Z elements. This is undoubtedly due to the high coulomb barrier (and therefore higher threshold energies) for (n,α) reactions in the high Z elements.

There is one major thing missing in the data we have presented so far as the helium generation in 316 SS is concerned. As we increase the thermal components of the flux in the first wall by putting carbon in front of it, the $Ni^{58}(n,\gamma)$ $Ni^{59}(n,\alpha)$ reaction sequence plays an important role and the helium generation in 316 SS increases dramatically. We have calculated this effect and the results are given in Table V.5 for various plant operating times, with 100% duty factor, and for different ISSEC thicknesses. The calculational procedure for this is given in reference 10. Table V.6 lists the total amount (due to thermal and high energy neutron reactions) of He generated in 316 SS first wall. The results are also plotted in Figure V.7. It is apparent that while this thermal neutron induced helium generation is negligible when we have no ISSEC in both D-D and D-T cases, it becomes increasingly important as the carbon thickness and the first wall lifetime increases. This is especially true in D-D because of the larger number of neutrons and the softer spectrum.

For the D-T case with 12.5 cm of ISSEC, the amount of helium generated from $Ni^{58}(n,\gamma)$, $Ni^{59}(n,\alpha)$ reactions never quite catches up

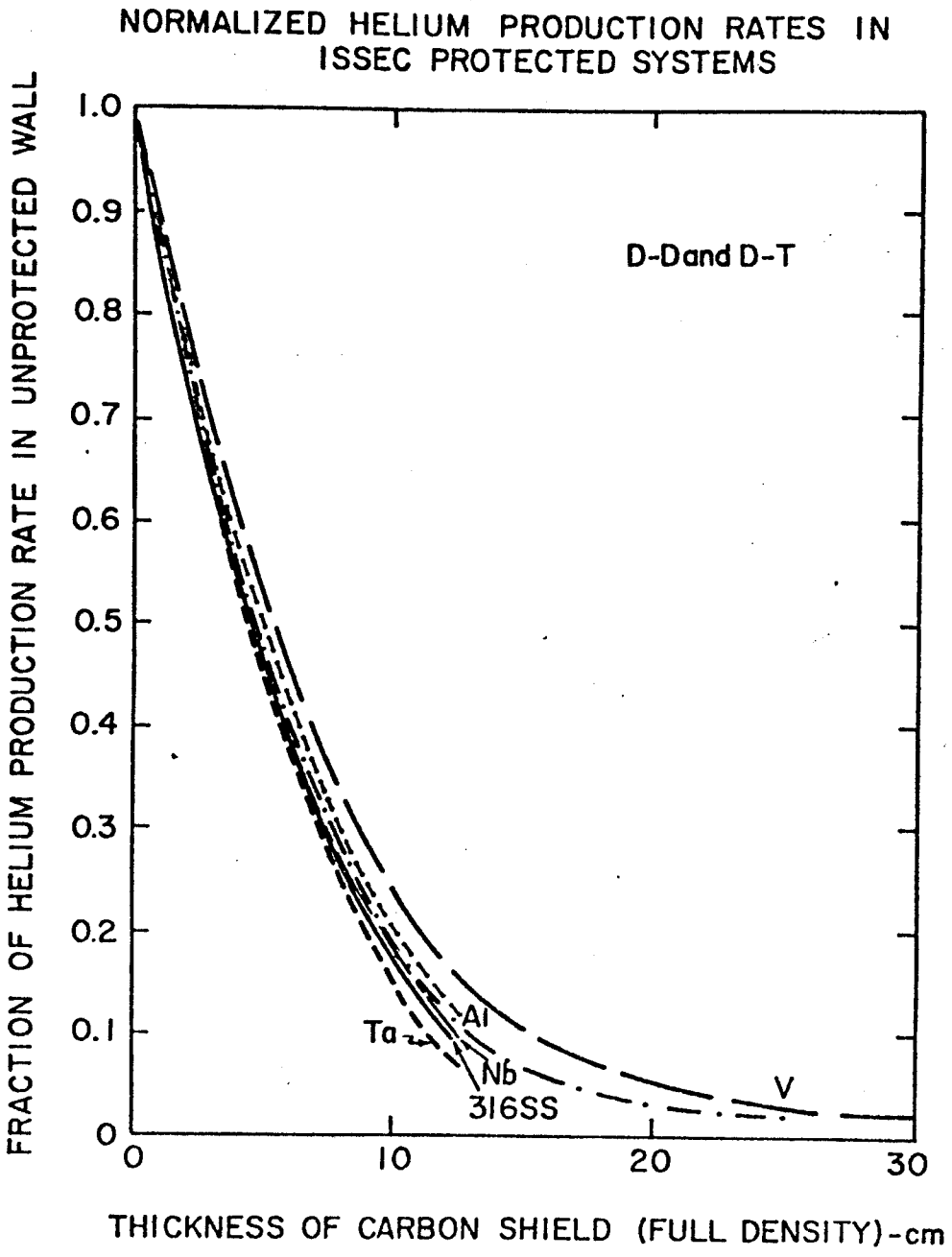
NORMALIZED HELIUM PRODUCTION RATES IN ISSEC PROTECTED SYSTEMS
FRACTION OF HELIUM PRODUCTION RATE IN UNPROTECTED WALL
1.0
0.9
0.8
0.7
0.6
0.5
0.4
0.3
0.2
0.1
0
D-Dand D-T
Ta
Al
Nb
316SS
V
0
10
20
30
THICKNESS OF CARBON SHIELD (FULL DENSITY)-cm

Figure V.6

Table V.5

Appm He* Generated in 316 SS from $Ni^{58}(n,\gamma)$, $Ni^{59}(n,\alpha)$ Reaction Sequence Only

D-D

Operation Time (years)	No ISSEC	12.5 cm C	25 cm C
1	0.0052	5.65	28.2
2	0.0212	22.6	113
5	0.133	141	704
10	0.531	565	2820
20	2.12	2260	11260

D-T

	No ISSEC	12.5 cm ISSEC
1	0.0023	1.14
2	0.0093	4.55
5	0.059	28.5
10	0.23	114
20	0.94	455

* Per 1 MW/m^2 neutron wall loading, 100% Duty Factor

Table V.6

Total Appm He Generated in 316 SS*

D-D

Operation Time (Year)	No ISSEC	12.5 cm ISSEC	25 cm ISSEC
1	239	28.5	32.8
2	477	68.2	122
5	1190	255	727
10	2390	793	2861
20	4770	2720	11400

D-T

	No ISSEC	12.5 cm ISSEC
1	280	27.9
2	560	58.2
5	1400	163
10	2800	382
20	5600	991

* Per 1 MW/m^2 neutron wall loading, 100% Duty Factor and includes threshold and thermally produced gas.

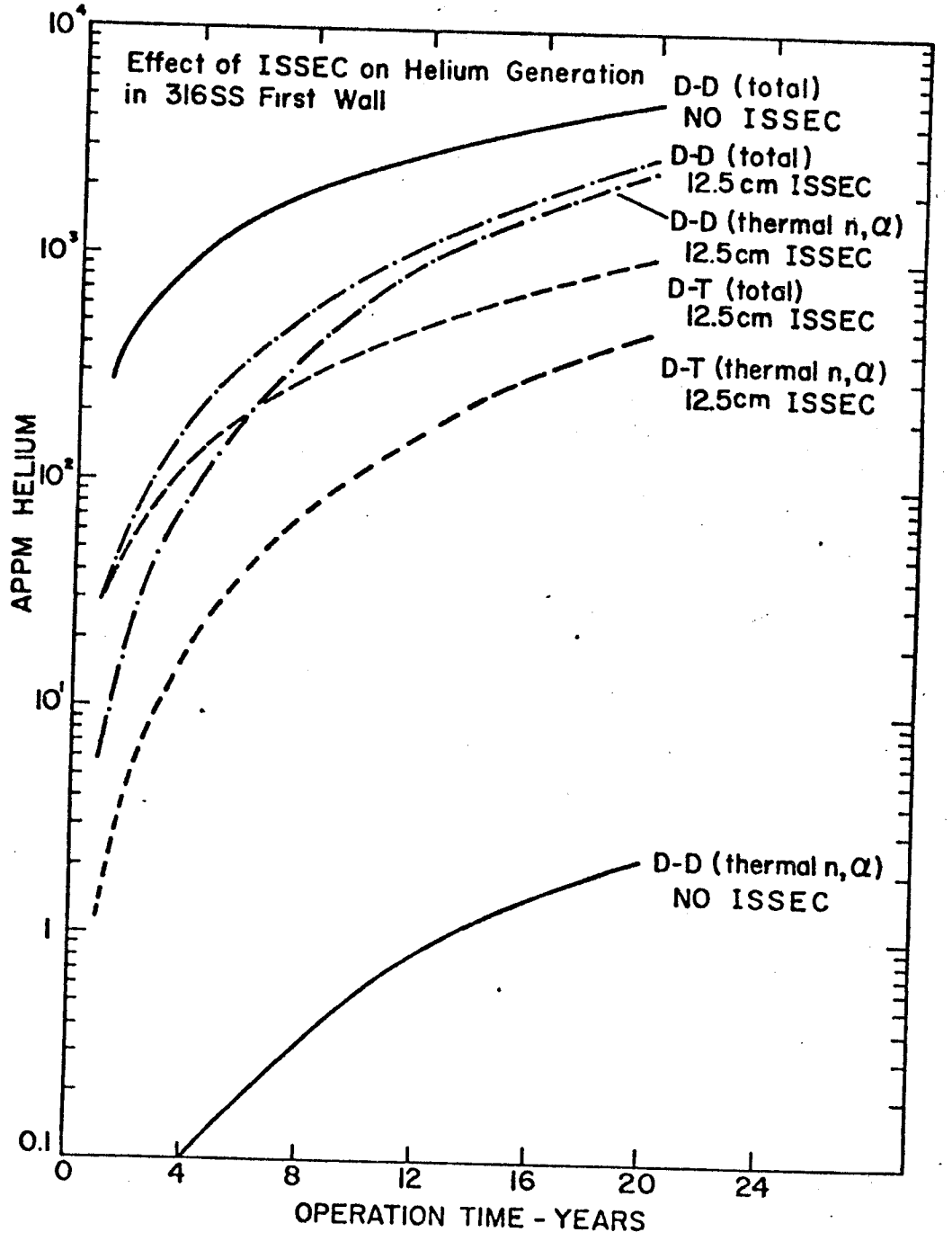
Effect of ISSEC on Helium Generation
in 316SS First Wall
D-D (total)
NO ISSEC
D-D (total)
12.5 cm ISSEC
D-D (thermal n,α)
12.5cm ISSEC
D-T (total)
12.5cm ISSEC
D-T (thermal n,α)
12.5cm ISSEC
D-D (thermal n,α)
NO ISSEC
APPM HELIUM
10⁴
10³
10²
10¹
1
0.1
0
4
8
12
16
20
24
OPERATION TIME - YEARS

Figure V.7

with the amount of helium generated from (n,α) reaction with fast neutrons even after 20 years of operation. But in the D-D case, the thermally produced α's override the fast neutron produced α's after about 4 years with 12.5 cm ISSEC, and after about 6 months with 25 cm of ISSEC.

V.A.2.c. Effect of an ISSEC on the Neutron Induced Radioactivity

The effect of ISSECs on the neutron induced radioactivity depends on whether the isotopes causing the most radioactivity are produced as a result of fast neutron or thermal neutron activation. One may even get reversal of the trends depending on the half lives of the isotopes.

Table V.7 lists the levels of neutron induced radioactivity in potential CTR first wall materials at various times after shutdown for a two year operating time in a D-D system. The results are tabulated for bare wall and two different ISSEC thicknesses. Table V.8 lists the radioactivity after 20 years of irradiation time. Two year irradiation results are plotted in Figures V.8, 9 and 10 at shutdown, 1 year after shutdown and 100 years after shutdown, respectively. At shutdown and 100 years after shutdown, results for D-T plasma case are given in Tables V.9 and V.10 along with the D-D results for comparison. The D-T neutronic calculations were done for only 0 and 12.5 cm ISSEC thicknesses. For both D-D and D-T cases the trends are the same. The short term radioactivity decreases for Nb,

Table V.7

Level of Neutron Induced Radioactivity at Various Times After Shutdown in the First Wall of a Carbon ISSEC Protected System After 2 Years of Operation/D-D Plasma

		Curies/cm^3 (a)					
		Shutdown	1 Day	1 Week	1 Year	20 Years	100 Years
Al	No ISSEC	39.8	6.84	8.8×10^{-3}	1.3×10^{-5}	1.3×10^{-5}	1.3×10^{-5}
	12.5 cm ISSEC	11.2	0.72	9.4×10^{-4}	7.7×10^{-7}	7.7×10^{-7}	7.7×10^{-7}
	25 cm ISSEC	17.9	0.15	1.9×10^{-4}	1.3×10^{-7}	1.3×10^{-7}	1.3×10^{-7}
V	No ISSEC	27.2	5.52	.56	~ 0	~ 0	~ 0
	12.5 cm ISSEC	95.4	.4	.04	~ 0	~ 0	~ 0
	25 cm ISSEC	345.4	.1	1.3×10^{-2}	~ 0	~ 0	~ 0
Nb	No ISSEC	183.4	146.4	96.6	1.9×10^{-3}	1.9×10^{-3}	1.9×10^{-3}
	12.5 cm	122.2	12.9	8.5	8.4×10^{-3}	8.4×10^{-3}	8.4×10^{-3}
	25 cm ISSEC	126.2	2.5	1.64	9.6×10^{-3}	9.6×10^{-3}	9.6×10^{-3}
Ta	No ISSEC	497	164.8	120.8	13.9	9.0×10^{-18}	~ 0
	12.5 cm ISSEC	1951	1270	1221	140.6	9.2×10^{-17}	~ 0
	25 cm ISSEC	2478	1632	1573	181	1.2×10^{-16}	~ 0
316 SS	No ISSEC	83.5	58.1	--(b)	23.5	2.1(c)	2.1×10^{-3}
	12.5 cm ISSEC	26.3	23.0	--(b)	4.9	0.42(c)	1.81×10^{-4}
	25 cm ISSEC	47.0	45.2	--(b)	7.9	0.71(c)	3.45×10^{-5}

(a) Per 1 MW/m^2 neutronic wall loading, 100% Duty Factor

(b) Not calculated

(c) Values at 10 years after shutdown

Table V.8

Level[a] of Neutron Induced Radioactivity at Various After Shutdown Times in the First Wall of an ISSEC Protected System After 20 Years of Operation/D-D Plasma

		Curies/cm^3 (a)					
		Shutdown	1 Day	1 Week	1 Year	20 Years	100 Years
Al	No ISSEC	39.8	6.84	9.0×10^{-3}	1.3×10^{-4}	1.3×10^{-4}	1.3×10^{-4}
	12.5 ISSEC	11.8	0.72	9.4×10^{-4}	7.8×10^{-6}	7.8×10^{-6}	7.8×10^{-6}
	25 cm ISSEC	17.9	0.15	2.0×10^{-4}	1.3×10^{-6}	1.3×10^{-6}	1.3×10^{-6}
V	No ISSEC	27.2	5.52	.56	~ 0	~ 0	~ 0
	12.5 cm ISSEC	95.4	.4	.04	~ 0	~ 0	~ 0
	25 cm ISSEC	345.4	.1	1.3×10^{-2}	~ 0	~ 0	~ 0
Nb	No ISSEC	183.4	146.4	96.6	.019	.019	.019
	12.5 cm ISSEC	122.2	12.9	8.58	.084	.084	.084
	25 cm ISSEC	126.4	2.58	1.74	.096	.096	.096
Ta	No ISSEC	498.4	166.4	122.2	14.1	9.2×10^{-18}	0
	12.5 cm ISSEC	1966	1286	1236	142.4	9.2×10^{-17}	0
	25 cm ISSEC	2498	1651	1592	183.2	1.2×10^{-16}	0
316 SS	No ISSEC	125.5	99.6	--[b]	57.2	5.2[c]	0.019
	12.5 cm ISSEC	32.1	28.8	--[b]	11.3	1.02[c]	1.67×10^{-3}
	25 cm ISSEC	46.6	45.1	--[b]	17.8	1.6[c]	3.14×10^{-4}

(a) units are curies/cm^3 per 1 MW/m^2 neutron wall loading at 100% duty factor

(b) Not calculated

(c) values at 10 years after shutdown

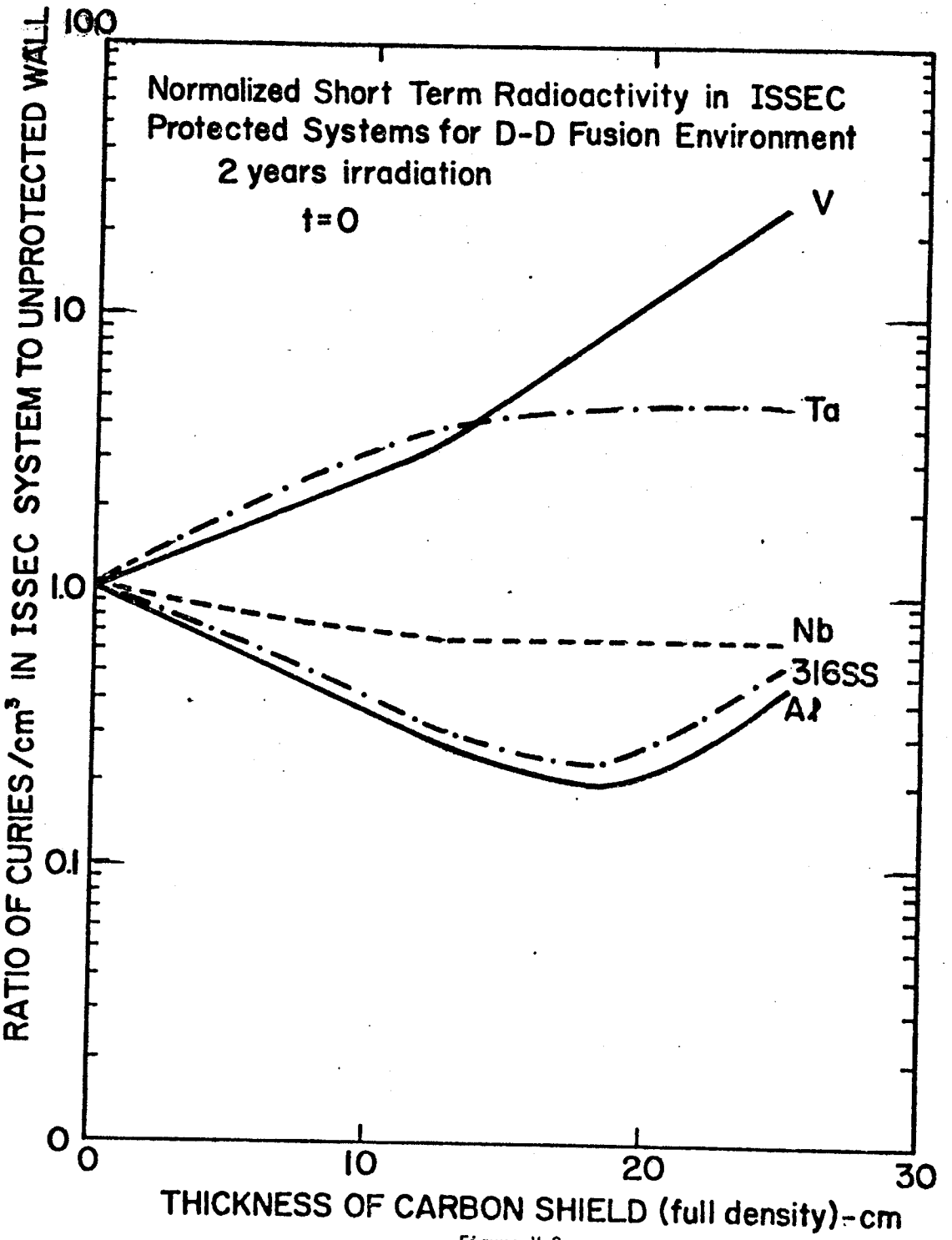
Normalized Short Term Radioactivity in ISSEC
Protected Systems for D-D Fusion Environment
2 years irradiation
t=0
V
Ta
Nb
316SS
Al
RATIO OF CURIES/cm³ IN ISSEC SYSTEM TO UNPROTECTED WALL
100
10
1.0
0.1
0
0
10
20
30
THICKNESS OF CARBON SHIELD (full density)-cm

Figure V.8

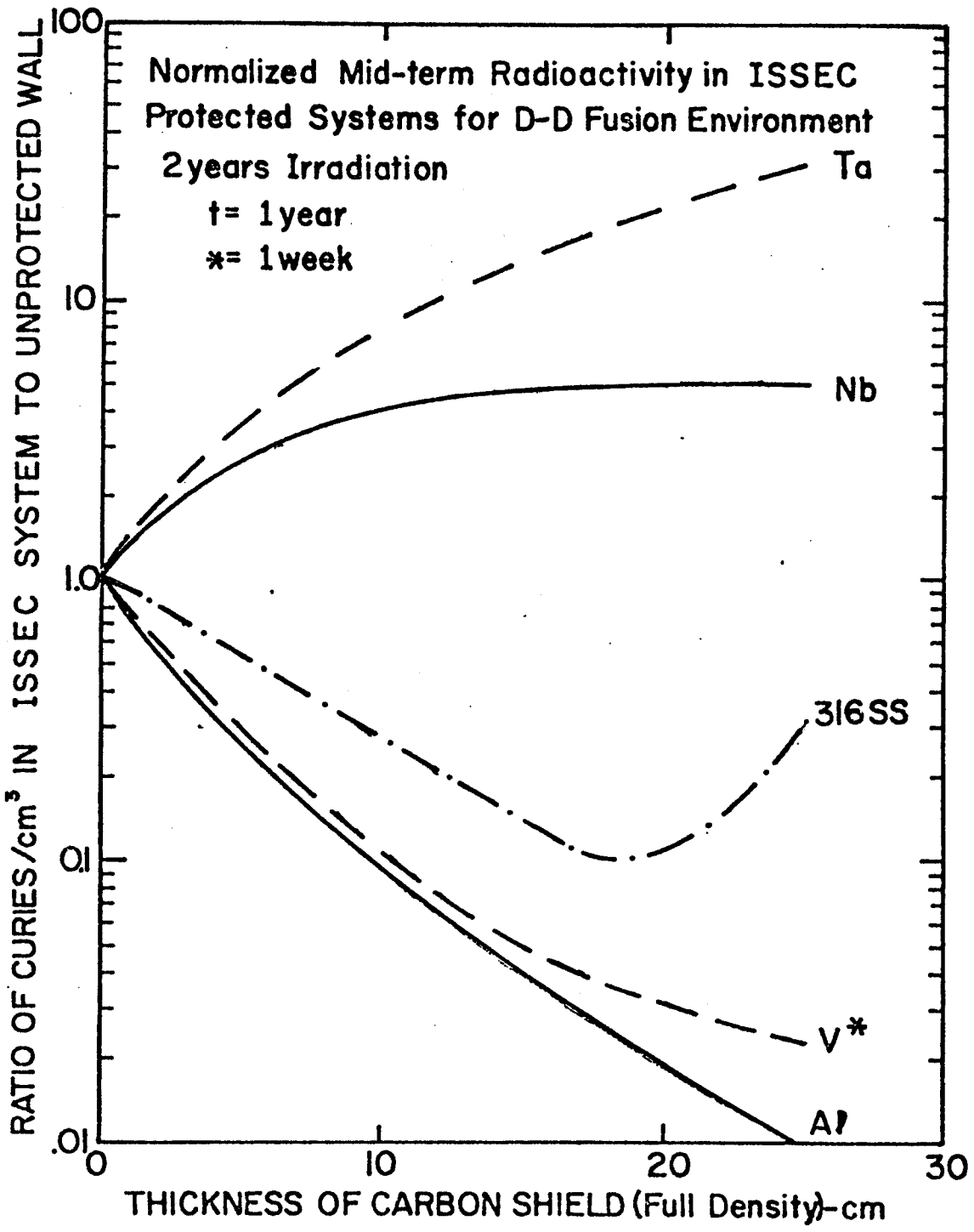
Normalized Mid-term Radioactivity in ISSEC
Protected Systems for D-D Fusion Environment
2years Irradiation
t= 1year
*= 1week
Ta
Nb
316SS
V*
Al
RATIO OF CURIES/cm³ IN ISSEC SYSTEM TO UNPROTECTED WALL
100
10
1.0
.1
.01
0
10
20
30
THICKNESS OF CARBON SHIELD (Full Density)-cm

Figure V.9

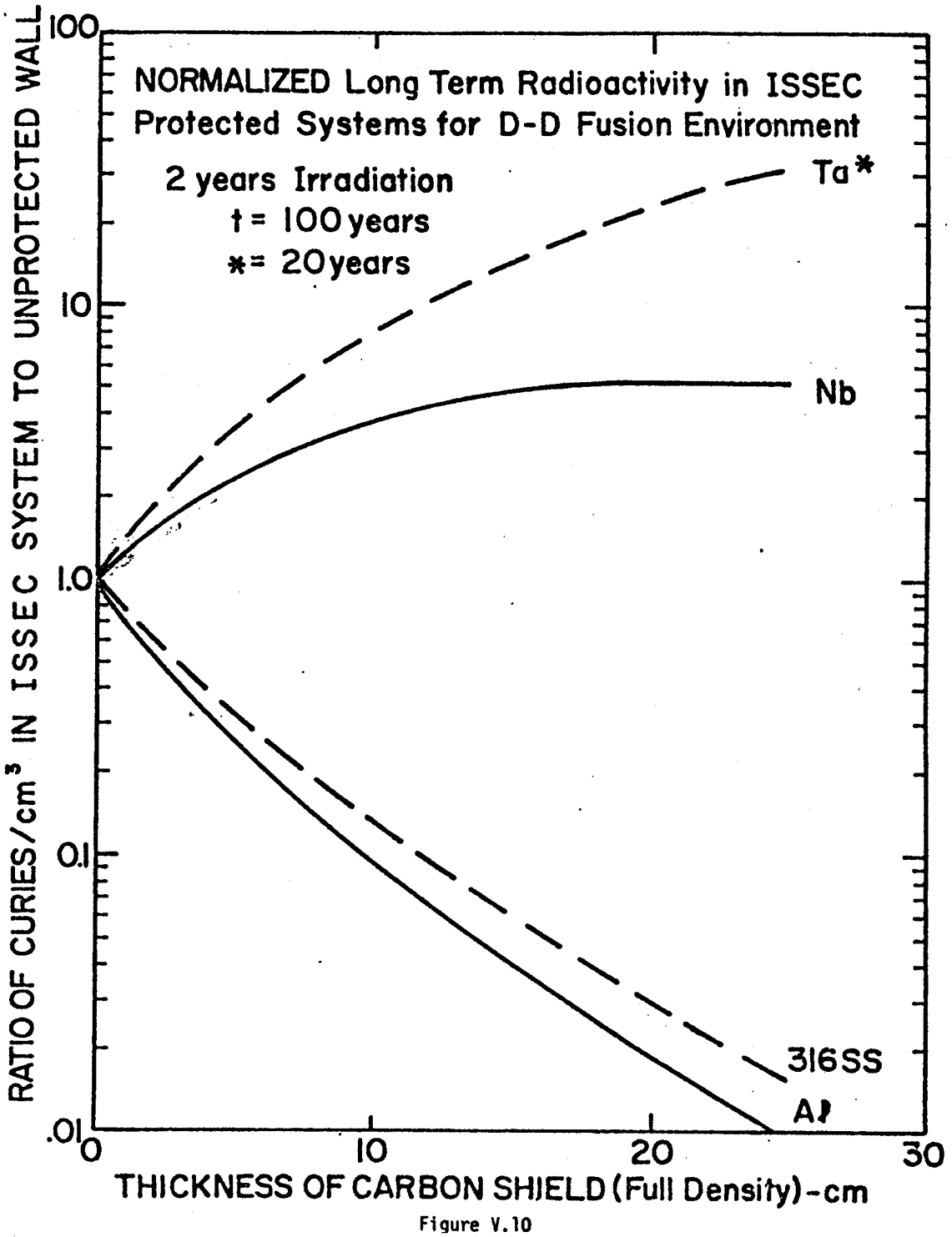
NORMALIZED Long Term Radioactivity in ISSEC
Protected Systems for D-D Fusion Environment
2 years Irradiation
t = 100 years
* = 20 years
Ta*
Nb
316SS
Al
RATIO OF CURIES/cm³ IN ISSEC SYSTEM TO UNPROTECTED WALL
100
10
1.0
0.1
.01
0
10
20
30
THICKNESS OF CARBON SHIELD (Full Density)-cm

Figure V.10

Table V.9

Level of Neutron Induced Radioactivity at Shutdown in First Wall in an ISSEC Protected System After 2 Years of Irradiation

D-T Plasma[(a)]

Material	No ISSEC	12.5 cm ISSEC	Fraction of Unprotected First Wall Values
Al	47.4	20.4	0.43 (decrease)
V	13.3	32.8	2.44 (increase)
316 SS	91.2	15.3	0.17 (decrease)
Nb	138	60.4	0.43 (decrease)
Mo	NA	NA	---
Ta	471	925	1.96 (increase)

D-D Plasma[(a)]

Material	No ISSEC	12.5 cm ISSEC	Fraction of Unprotected First Wall Values
Al	39.8	11.2	.28 (decrease)
V	27.2	95.4	3.51 (increase)
316 SS	83.5	26.3	.32 (decrease)
Nb	183	122	.67 (decrease)
Mo	NA	NA	---
Ta	497	1950	3.93 (increase)

(a) curies/cm^3 per 1 MW/m^2 neutron wall loading at 100% duty factor

NA - Not Available

Table V.10

Level of Neutron Induced Radioactivity 100 Years After Shutdown in the First Wall of ISSEC Protected System After 2 Years of Irradiation

Material	No ISSEC	D-T Plasma[a] 12.5 cm of ISSEC	Fraction of Unprotected First Wall Values
Al	1.49×10^{-5}	9.14×10^{-7}	0.06 (decrease)
V	$<10^{-15}$	$<10^{-15}$	0.15[b] (decrease)
316 SS	3.42×10^{-3}	2.05×10^{-4}	0.06 (decrease)
Nb	0.001	0.0038	3.85 (increase)
Mo	NA	NA	----
Ta	$<10^{-15}$	$<10^{-15}$	8[c] (increase)

Material	No ISSEC	D-D Plasma[a] 12.5 cm of ISSEC	Fraction of Unprotected First Wall Values
Al	1.3×10^{-5}	7.7×10^{-7}	0.06 (decrease)
V	$<10^{-15}$	$<10^{-15}$	0.07[b] (decrease)
316 SS	2.1×10^{-3}	1.81×10^{-4}	0.09 (decrease)
Nb	1.9×10^{-3}	8.4×10^{-3}	4.42 (increase)
Mo	NA	NA	----
Ta	$<10^{-15}$	$<10^{-15}$	10.2[c] (increase)

(a) curies/cm^3 per 1 MW/m^2 neutronic wall loading, 100% duty factor
(b) value 1 week after shutdown
NA - Not Available
(c) values 20 years after shutdown

316 SS and Al, but it increases for V and Ta as the thickness of the carbon shield is increased to 12.5 cm. When one considers the long term radioactivity, V and Nb switch places and Ta and Nb have higher radioactivities while 316 SS, V and Al have lower radioactivities than with 12.5 cm of ISSEC than they do with no ISSEC.

As the thickness of the ISSEC is increased over 12.5 cm, some interesting things start to happen. In Al and 316 SS those isotopes produced as a result of thermal neutron activation gain importance and the radioactivity curves start to rise. Nb and Ta total activities saturate but V keeps increasing. At 1 year after shutdown, 316 SS curve still has the same shape but Al radioactivity keeps decreasing because of the short half lives of those isotopes thermally produced. The Nb and Ta activities again tend to saturate. At 100 years after shutdown in 316 SS, the thermally activated radioisotopes have decayed away and the total radioactivity continues to decrease with increasing carbon thickness.

It should also be noted in Tables V.9 and V.10 that the ISSEC is more effective in reducing neutron induced radioactivity at shutdown in 316 SS and Nb for D-T than for D-D. It is also apparent that the ISSEC is more effective for Al in the D-D case than for the D-T case. At 100 years after shutdown, the reduction in radioactivity in 316 SS is less in the D-D system. The reduction factor is about the same in Al for both cases. At long times after shutdown radioactivity in V decays to insignificant levels. However, at 1 week

after shutdown, it is reduced more in D-D system than in D-T. Long term radioactivities in Nb and Ta increase more for the D-D than the D-T case because long lived radioisotopes in Nb and Ta are produced as a result of thermal (n,γ) reactions.

V.A.3. Discussion on Normalization

All the resulted presented here so far and elsewhere[8,9] have been normalized to 1 MW/m^2 neutronic wall loading. When one considers only one type of reactor with a certain plasma cycle, this way of normalizing the radiation damage results is quite convenient. The response of different materials to neutron spectral shifting, provided the same blanket structure is used in all cases, is also straightforward. However, when one considers two different plasma reactions as we have, another way of comparing the radiation damage results might be to normalize on the basis of MW of power. In the real case, the difficulty is that one needs to breed tritium for the D-T cycle whereas in the D-D cycle, this is not required. Therefore, it is quite probable that two completely different blanket structures would be used and the neutron energy multiplication, as well as γ heating, can be much different for the two cases. All the present calculations were done with the same non-breeding blanket scheme shown in Figure V.1, so any comparison made on the basis of total power generation would not be meaningful.

Another way of quoting the damage would be to normalize it on the basis of a megawatt of power generated in the plasma. Such a

comparison requires a knowledge of the burnup of tritium and He-3 atoms produced by the D-D reactions. Miley[70] has shown that at 30 keV, essentially all the tritium produced is consumed and approximately 20% of the He-3 is "burned".

The reactions taking place and the energies of various products (MeV) in a D-D plasma are given below.

$$D + D \rightarrow T(1.01) + p(3.03)$$

$$D + D \rightarrow He^3(0.82) + n(2.45)$$

$$D + T \rightarrow He^4(3.52) + n(14.06)$$

$$D + He^3 \rightarrow He^4(3.67) + p(14.67)$$

If we use the results of Miley, we can calculate the neutron flux associated with a 1 MW/m^2 wall loading based on the thermal power produced in the D-D plasma.

$$1\ MW/m^2(\text{plasma thermal}) = (\text{const.}) \times \left(\frac{4.04+3.27+17.60+0.2\times18.3}{2}\right) \frac{MeV}{n} \times (4.34 \times 10^{13}\ n/(cm^2\text{-sec})$$

In the D-T case,

$$1\ \frac{MW}{m^2}\ (\text{plasma thermal}) = (\text{const.}) \times 17.6\ \frac{MeV}{n} \times 3.55 \times 10^{13}\ \frac{n}{cm^2\text{-sec}}$$

where the conversion factor (const.) has a value of 1.602×10^{-15}. It appears that if we wanted to normalize our results to 1 MW/m^2 (plasma thermal), the D-T results (dpa, gas production, activation, etc.) would be approximately 20% less than presented here and the D-D

results would be 43% less. These reductions tend to make the displacement rate equal in both systems and increase the advantage of the D-D spectrum with respect to helium and hydrogen production.

For illustration, results for 316 SS are reproduced in Table V.11 for the two normalizations. In this table, dpa and hydrogen production results are lower when they are normalized on the basis of plasma thermal by the factors given above; namely 20% in D-T and 43% in D-D cases. The same conclusions can be drawn about the other materials considered here.

Analysis of this work leads us to the observation that the radiation damage incurred in protected or unprotected D-D systems is almost the same as for the D-T systems. For example, as we see in Table V.11 the displacement damage is higher in D-D systems when neutronic wall loading normalization is used, but this becomes about the same in the two systems when plasma thermal normalization is used.

Gas production results are 10 to 15% lower in D-D with 1 MW/m^2 (neutronic) normalization in an unprotected system. This difference in gas production rates goes to 30-40% for the plasma thermal normalization but when the effect of the ISSEC is considered, the helium production rate can actually increase over that in the D-T system.

V.A.4. Conclusions for This Section

V.A.4.a. General Conclusions about Both D-T and D-D Carbon ISSEC Systems

. Reduction in displacement rates in the metals considered

Table V.11

A Comparison of Possible Normalization Procedures
for D-D and D-T Fusion Systems - 316 SS First Wall

		1 MW/m^2 Neutronic			1 MW/m^2 Plasma Thermal		
		D-D	D-T	D-D/D-T	D-D	D-T	D-D/D-T
dpa/yr	No C	16.8	11.3	1.49	9.64	9.06	1.06
	12.5 cm C	3.2	2.5	1.28	1.97	2.0	0.99
	25 cm C	0.86		-	0.49		
Appm He	No C	2387	2800	0.85	1370	2240	.61
10 yrs	12.5 cm C	793	381	2.08	317	305	1.04
	25 cm C	2861			956		
Appm	No C	675	736	0.92	388	590	.66
H/yr	12.5 cm C	88.4	100	0.88	50.8	80.1	.63
	25 cm C	20.6	-	-	11.8	-	-

of 3-5 can be obtained with 12.5 cm of carbon. Twenty-five (25) cm of carbon can reduce displacement damage by a factor of 8 to 20.

- With the exception of 316 SS (or any nickel containing material) helium production can be reduced by factors of 7 to 14 with 12.5 cm of carbon and by factor of 27 to 80 with 25 cm of carbon.
- The use of a carbon ISSEC to soften the neutron spectrum incident on the 316 SS initially decreases the helium production rates by a factor of 8-10 for 12.5 cm (1 year). However, due to build-up of Ni-59 which has a high thermal (n,α) cross section, the total amount of helium generated after 10 years of operation is actually greater in D-D ISSEC system than that in an unprotected first wall.
- Depending on the mode of activation and time after shutdown the ISSEC systems can increase or decrease the induced radioactivity. In general, it decreases the short term radioactivity of Al, 316 SS, and Nb. It actually increases the activity in V and Ta. The behavior is somewhat different for long term activities in that the activity of V is decreased and that of Nb is increased over the unprotected case. (The rest of the values stay the same.)

There are also several conclusions we can state for D-D versus D-T ISSEC protected systems that produce the same neutron power and have it passing through the same wall area.

V.A.4.b. Advantages of a D-D ISSEC

- The helium production rates are approximately 15% lower for all elements except those containing Ni regardless of the ISSEC thickness.
- The short lived radioactivity is reduced without an ISSEC in Al (16%) and 316 SS (9%). Behind a 12.5 cm ISSEC this reduction is 45% for Al.
- The long lived radioactivity is reduced without an ISSEC in Al (13%) and 316 SS (39%). Behind a 12.5 cm ISSEC, it is reduced by 16% in Al and 12% in 316 SS.

V.A.4.c. Disadvantages of a D-D ISSEC

- The displacement damage is increased, without an ISSEC, in Al (56%), V(43%), 316 SS (49%), Nb (27%), Mo (29%), and Ta (25%). Behind 12.5 cm ISSEC the rates are still higher than in a D-T system for Al (41%), V (53%), 316 SS (28%), Nb (30%), Mo (32%), and Ta (30%).
- The helium production from Ni^{59} is increased by a factor of 5 behind a carbon ISSEC.
- The total helium production is 2% greater after one MW-year of D-D neutron irradiation and 175% greater after 20 years of irradiation for 12.5 cm ISSEC.
- The short lived radioactivity without an ISSEC is increased in V (105%), Nb (33%), and Ta (1%). Behind a 12.5 cm ISSEC, the radioactivity is increased in V (188%), Nb (103%), Ta (111%) and 316 SS (72%) over the similar D-T case.

. The long lived radioactivity is increased in the unprotected wall for Nb (90%) and Ta (61%). Behind a 12.5 cm ISSEC it is also increased for Nb (121%) and Ta (115%).

The above conclusions for the displacement rates will be altered by ∿29% if the results are calculated on the basis of total power generated in the plasma. In general, this will tend to make the displacement rates about the same for both D-T and D-D systems and make the D-D system more advantageous from the standpoint of helium and hydrogen production by high energy reactions. The exception is that the total amount of helium produced in Ni containing alloys will still be greater in D-D as compared to D-T systems.

The conclusions about the short and long lived activity will be the same except for one exception, the short lived activity of Ta without an ISSEC will be decreased, not increased.

An overall conclusion is that a D-D system does not represent a significant advantage over a D-T system unless relative difference of 20% in the amount of He produced in non-Ni containing alloys is a critical feature. Certainly a D-D system represents no significant advantage over the D-T case with respect to dpa, He and induced radioactivity in 316 SS.

V.B. A Comprehensive Study of Graphite and Metal ISSECs in Tokamak Fusion Reactors

V.B.1. Introduction

The one-dimensional, homogeneous, cylindrical geometry, model blanket design used in studies in this section is shown in Figure V.11.

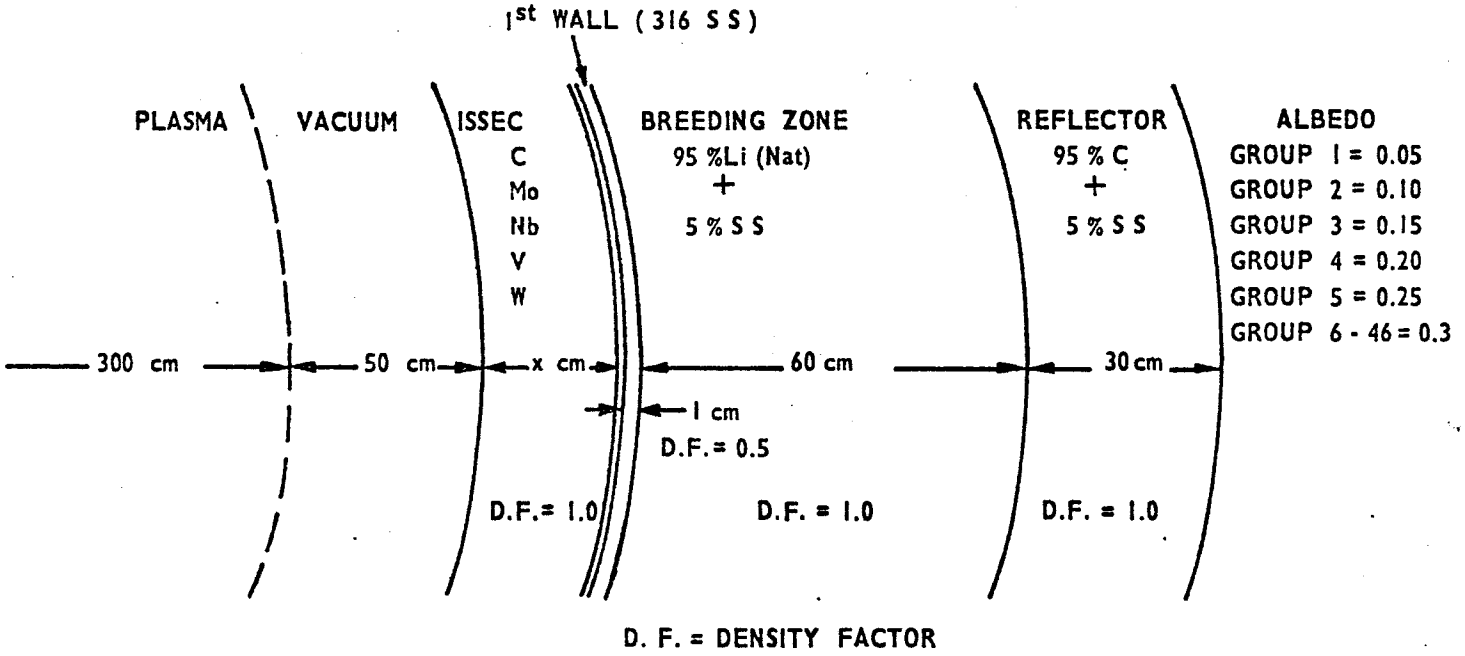

1 - DIMENSIONAL CYLINDRICAL BLANKET MODEL USED IN THIS STUDY

Figure V.11

A variable thickness ISSEC zone was placed between the plasma and a 316 SS first structural wall. The materials studied for an ISSEC were carbon, molybdenum, niobium, vanadium and tungsten. (Many of the details of this work are given in reference 11.) The first wall material used in all cases was 316 SS with 1 cm thickness at a D.F. of 0.5 and it was followed by a 60 cm thick breeding zone composed of 95% natural lithium and 5% 316 SS for structural material. Behind the breeding zone is a 30 cm thick reflector zone with a composition of 95% C and 5% SS. Both the breeding zone and the reflector zone have a D.F. of 1.0 although in reality in the reflector zone a D.F. of less than 1.0 would be more appropriate to take into account the coolant passages. To simulate the final shield albedos of 0.05, 0.10, 0.15, 0.20, 0.25 were used for neutron groups 1 through 5 (9 to 14.9 MeV) of the 46 group energy structure shown in Appendix B. An albedo of 0.3 was used for neutrons of lower energy.

The nuclear performance of this type of reactor design was studied by solving the discrete ordinates form of the neutron transport equation for a cylinder using the ANISN[50] program with a S_4-P_3 approximation.

The neutron and gamma production cross sections were obtained as a coupled set of 100 neutron groups and 21 gamma groups produced for EPR calculations.[71] This data set was generated with the AMPX modular code system[56] from nuclear data in ENDF/B-IV. The only exception is Nb where evaluation of the cross sections is based on

ENDF/B-III data. (Previous calculations in Section V.A. and in references 8 to 10 were all based on ENDF/B-III data.)

Due to the costs and computer memory limitations, the 100 neutron group cross sections were collapsed to 46 groups keeping the same fine group structure above 2 MeV as in the original set. The 46 group neutron and 21 group gamma interaction cross sections group structures used in these calculations are given in Appendix B.

Neutron kerma factors were generated using the MACK program[59] and the gamma kerma factors were calculated using the MUG[60] code. The displacement cross sections were calculated from a computer code developed by Doran[43,67,69] except the displacement cross sections for carbon were from Morgan.[72] The values used in these calculations are given in references 8 and 9.

Radioactivity calculations have been performed with the DKR[51] code using the fluxes calculated by ANISN and nuclear data from Decay Chain Data Library (DCDLIB).[62]

The heat transfer problems involving thermal radiation were solved using the program HEAT.[52] A simpler finite element code FEM2D[53] was used for problems involving conduction only. For radiation problems, all radiative surfaces were assigned emissivities of 0.9 keeping in mind that metal surfaces would have to be painted black or carbon coated to achieve an emissivity that high. In all cases, a first structural wall temperature of 500°C was assumed.

All results are normalized to 1 MW/m^2 neutronic wall loading, i.e., 1 MW of neutron energy passing through the first wall (or inner ISSEC surface) per m^2 of area. A surface heat load of 4 W/cm^2 was taken assuming there would be a divertor to reduce the charged particle flux incident on the first wall or inner ISSEC surface. The heat flux number is consistent with calculations reported for UWMAK-II[5] and UWMAK-III.[73]

V.B.2. Effects of ISSEC on the 316 SS Structural First Wall

V.B.2.a. Reduction of Displacement Damage in the First Wall

The first wall neutron spectra obtained using the ANISN[50] program in the cylindrical geometry of the model blanket shown in Figure V.11 are combined with the 316 SS displacement cross sections, to yield the displacement rates shown in Figure V.12. The absolute values of the displacement rates, in units of dpa per 1 MW/m^2 neutronic wall loading per year, are plotted as a function of increasing ISSEC thickness for five different ISSEC materials. As can be seen in Figure V.12, W is most effective in reducing the displacement damage in the first wall while C is least effective. In fact, we can see from the figure that the higher the atomic number of the ISSEC material, the more effective it is. This is mainly due to the higher neutron inelastic cross sections of higher Z metals at high neutron energies.

Factors of reduction in the displacement rates in the 316 SS first wall vary between 2 for C and approximately 5 for W for a 10 cm

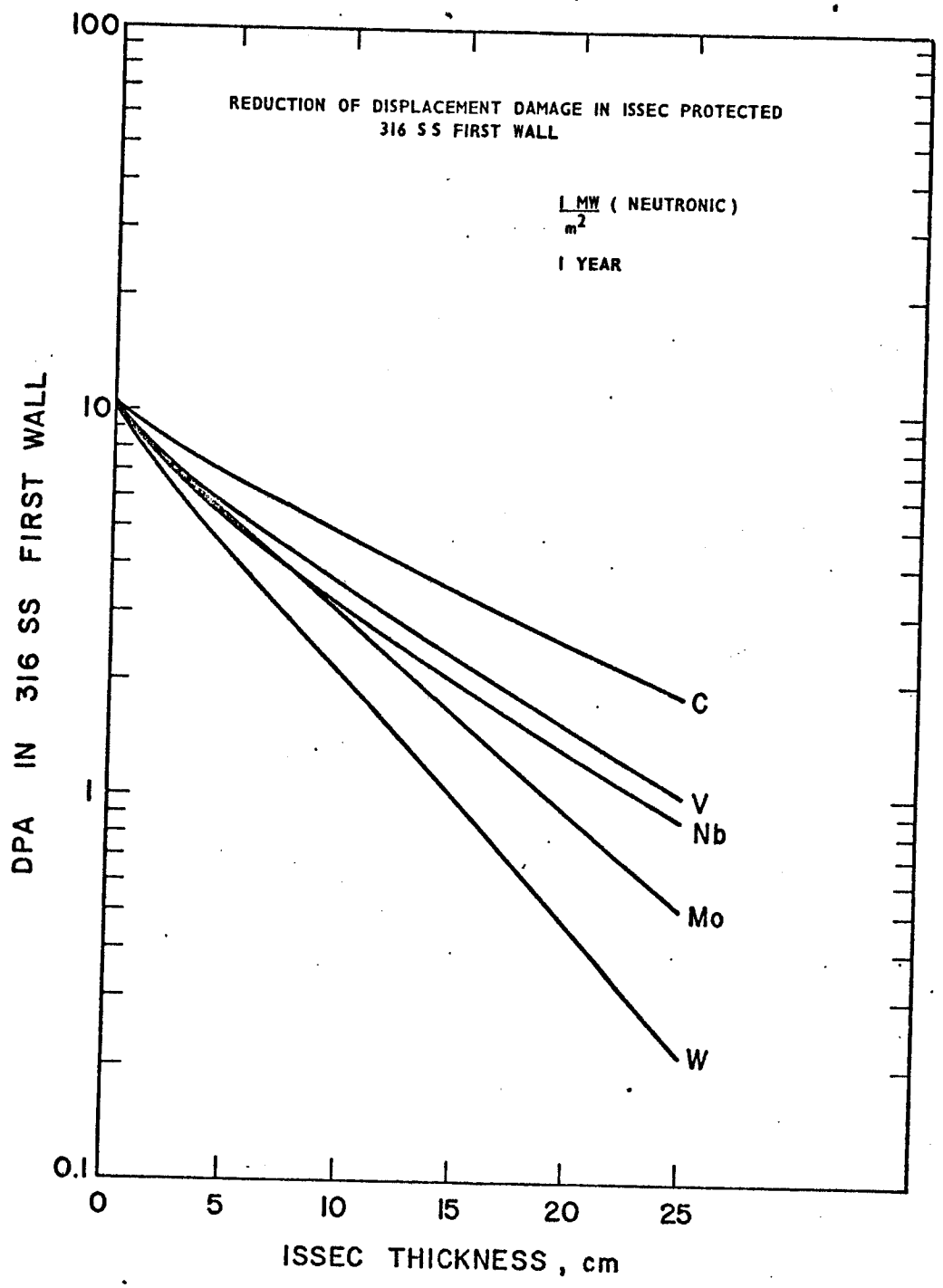
REDUCTION OF DISPLACEMENT DAMAGE IN ISSEC PROTECTED
316 S S FIRST WALL
1 MW (NEUTRONIC)
m²
1 YEAR
DPA IN 316 SS FIRST WALL
100
10
1
0.1
0
5
10
15
20
25
ISSEC THICKNESS , cm
C
V
Nb
Mo
W

Figure V.12

thick spectral shifter. These reductions are much higher for a 25 cm ISSEC varying between approximately 5 for C and approximately 50 for W. The significance of this observation is that if the wall life is predominantly determined by the level of the total displacement damage, then one might extend the wall lifetime due to radiation damage alone by factors of 2-50.

V.B.2.b. Reductions in He and H Production Rates

The effects of 5 different ISSEC materials on the helium and hydrogen production rates in the 316 SS first wall are shown in Figures V.13 and V.14, respectively. The gas production rates are given in terms of appm per 1 MW/m^2 neutronic wall loading per year. The absolute effect here is more pronounced than in the case of displacement damage. This is due to the fact that gas production cross sections have the threshold reactions which occur above $\sim$2 MeV whereas the displacement cross sections are continuous from thermal energies.

The factors of reduction in helium production rates in the first wall vary between 3.2 for C and 12 for W for 10 cm thickness and between 12 and 275 for a 25 cm ISSEC of the respective materials. Similar reductions are seen in the hydrogen production rates. The helium production rates shown in 316 SS do not include thermally produced α's from the $Ni^{58}(n,\gamma)Ni^{59}(n,\alpha)$ reaction sequence, but as was shown earlier in the case of a D-T plasma[10] thermally produced

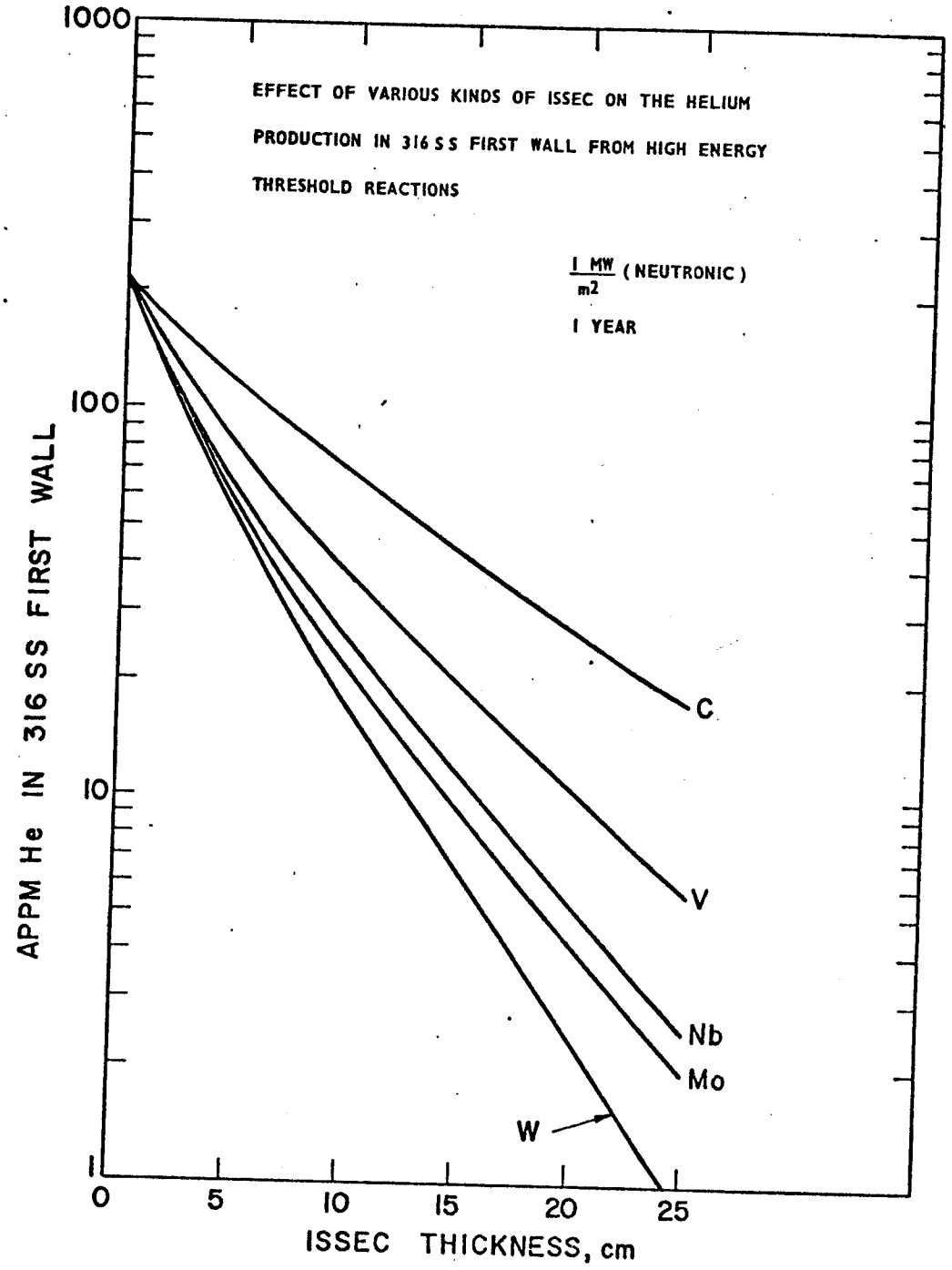
EFFECT OF VARIOUS KINDS OF ISSEC ON THE HELIUM
PRODUCTION IN 316 S S FIRST WALL FROM HIGH ENERGY
THRESHOLD REACTIONS
1 MW / m2 (NEUTRONIC)
1 YEAR
APPM He IN 316 SS FIRST WALL
1000
100
10
1
0
5
10
15
20
25
ISSEC THICKNESS, cm
C
V
Nb
Mo
W

Figure V.13

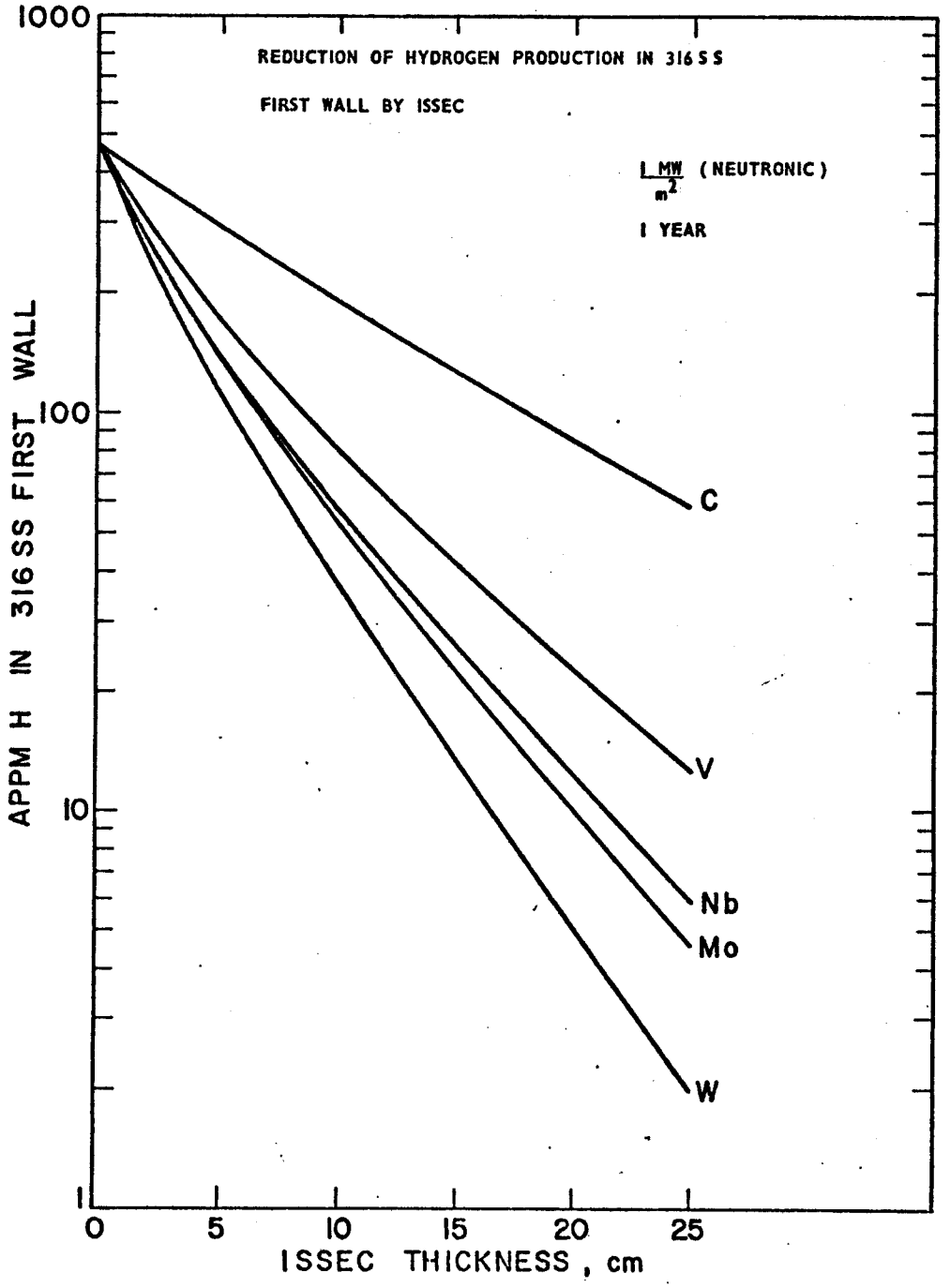
REDUCTION OF HYDROGEN PRODUCTION IN 316 S S
FIRST WALL BY ISSEC
1 MW/m² (NEUTRONIC)
1 YEAR
APPM H IN 316 SS FIRST WALL
1000
100
10
1
C
V
Nb
Mo
W
0
5
10
15
20
25
ISSEC THICKNESS, cm

Figure V.14

helium constituted less than 18% of total helium production in a 316 SS first wall protected by a 12.5 cm carbon ISSEC after 5 years of operation time.

V.B.2.c. Radioactivity and Afterheat

The ISSECs can change the neutron induced radioactivity in the first structural wall. Since most of the activity of 316 SS is the result of transmutations due to high energy neutrons, the presence of an ISSEC reduces, to varying degrees, the activity of the first wall. However, at long times after shutdown when only a few nuclides dominate the radioactivity, the activation due to thermal neutrons may cause a deviation from this trend.

At shutdown, the major contributors to the radioactivity of the 316 SS first wall are $^{55}Fe(t_{1/2} = 2.6\ yr)$, $^{56}Mn(t_{1/2} = 2.6\ hr)$, $^{51}Cr(t_{1/2} = 27.8\ days)$, $^{58}Co(t_{1/2} = 71.3\ days)$, $^{54}Mn(t_{1/2} = 303\ days)$; these isotopes contribute more than 85% of the total activity in the case of an unprotected wall. After one year of decay, ^{55}Fe alone contributes more than 80% of the radioactivity. Other radioisotopes such as ^{54}Mn, $^{57}Co(t_{1/2} = 270\ days)$, $^{60}Co(t_{1/2} = 5.26\ yrs)$ and ^{58}Co contribute 18% of the radioactivity. The major contributors to 316 SS at 100 years after shutdown are long half-life radioisotopes; $^{93}Mo(t_{1/2} = 1000\ yrs)$, $^{93m}Nb(t_{1/2} = 13.6\ yrs$, from β^+ decay of $^{93}Mo)$ and $^{63}Ni(t_{1/2} = 92\ yrs)$.

Tables V.12, V.13 and V.14 show the changes in the first wall radioactivity, biological hazard potential (BHP) in air, and afterheat

Table V.12 Specific Radioactivity of First Wall* (Ci/cm^3)

ISSEC Material	ISSEC Thickness	Time After Shutdown 0	1 h	1 d	1 Mo	1 y	100 y
No ISSEC		75.89	66.12	52.59	42.25	22.47	3.37×10^{-3}
C	5 cm	43.41	37.44	28.29	22.61	11.54	2.72×10^{-3}
	10 cm	29.99	25.77	18.28	14.08	6.79	6.64×10^{-3}
Mo	5 cm	23.14	19.85	15.57	12.16	6.40	2.27×10^{-3}
	10 cm	9.71	8.30	6.31	4.63	2.40	1.55×10^{-3}
W	5 cm	19.91	17.10	13.47	10.56	5.60	1.95×10^{-3}
	10 cm	7.20	6.17	4.74	3.53	1.85	1.08×10^{-3}
Nb	5 cm	24.02	20.65	16.39	12.96	6.87	2.21×10^{-3}
	10 cm	10.14	8.70	6.78	5.14	2.70	1.72×10^{-3}
V	5 cm	31.83	27.52	20.85	16.40	8.68	2.34×10^{-3}
	10 cm	18.00	15.27	10.20	7.59	3.97	1.89×10^{-3}

* 2 years operation, 1 MW/m^2 neutron wall loading

Table V.13 Specific BHP of First Wall* (km^3 of air/W-cm^3)

ISSEC Material	ISSEC Thickness	Time After Shutdown 0	1 h	1 d	1 Mo	1 y	100 y
No ISSEC		67.80	66.53	58.45	42.33	18.36	3.66×10^{-3}
C	5 cm	38.39	37.61	33.14	24.44	10.19	3.18×10^{-3}
	10 cm	23.43	22.92	20.05	14.95	6.06	1.02×10^{-2}
Mo	5 cm	17.87	17.49	15.29	10.96	4.76	1.42×10^{-3}
	10 cm	6.45	6.30	5.47	3.88	1.67	7.27×10^{-4}
W	5 cm	16.14	15.79	13.79	9.87	4.32	1.28×10^{-3}
	10 cm	5.29	5.16	4.49	3.18	1.39	5.68×10^{-4}
Nb	5 cm	20.31	19.89	17.41	12.48	5.45	1.54×10^{-3}
	10 cm	7.92	7.75	6.75	4.81	2.09	9.02×10^{-4}
V	5 cm	26.99	28.59	24.84	17.83	7.78	2.11×10^{-3}
	10 cm	14.44	14.01	11.86	8.44	3.67	1.57×10^{-3}

* 2 years operation, 1 MW/m^2 neutron wall loading

Table V.14 First Wall Afterheat Density* (Watt/cm^3)

ISSEC Material	ISSEC Thickness	Time After Shutdown: 0	1 h	1 d	1 Mo	1 y	100 y
No ISSEC		0.419	0.299	0.107	0.85×10^{-1}	0.30×10^{-1}	0.42×10^{-6}
C	5 cm	0.269	0.193	0.62×10^{-1}	0.49×10^{-1}	0.16×10^{-1}	0.33×10^{-6}
	10 cm	0.206	0.147	0.39×10^{-1}	0.31×10^{-1}	0.95×10^{-2}	0.80×10^{-6}
Mo	5 cm	0.133	0.906×10^{-1}	0.31×10^{-1}	0.24×10^{-1}	0.84×10^{-2}	0.26×10^{-6}
	10 cm	0.574×10^{-1}	0.395×10^{-1}	0.13×10^{-1}	0.92×10^{-2}	0.32×10^{-2}	0.17×10^{-6}
W	5 cm	0.113	0.770×10^{-1}	0.26×10^{-1}	0.21×10^{-1}	0.73×10^{-2}	0.22×10^{-6}
	10 cm	0.417×10^{-1}	0.266×10^{-1}	0.92×10^{-2}	0.68×10^{-2}	0.24×10^{-3}	0.19×10^{-6}
Nb	5 cm	0.135	0.921×10^{-1}	0.32×10^{-1}	0.25×10^{-1}	0.90×10^{-2}	0.25×10^{-6}
	10 cm	0.580×10^{-1}	0.398×10^{-1}	0.13×10^{-1}	0.10×10^{-1}	0.35×10^{-2}	0.19×10^{-6}
V	5 cm	0.189	0.136	0.42×10^{-1}	0.32×10^{-1}	0.11×10^{-1}	0.27×10^{-6}
	10 cm	0.127	0.917×10^{-1}	0.20×10^{-1}	0.15×10^{-1}	0.52×10^{-2}	0.21×10^{-6}

*2 years operation, 1 MW/m^2 neutron wall loading

respectively, at various times after shutdown for different ISSEC materials and thicknesses.

At shutdown and until 1 year after shutdown, W is the most effective ISSEC material to reduce the first wall radioactivity, mainly because of its absorption and inelastic scattering properties. A factor of 10 reduction of the activity in the first wall can be achieved by W of 10 cm thickness.

W is followed by Mo and Nb which are nearly the same in reducing the radioactivity; a factor of 3 for an ISSEC of 5 cm thickness and by a factor of 7 for 10 cm of material. The V ISSECs of 5 cm and 10 cm thickness reduce the activity by factors of 2 and 4 respectively. Carbon is the least effective material for reducing the activity among these materials; a factor of 1.8 for 5 cm thick case and a factor of 2.5 for 10 cm thickness. For decay times of 100 years, the activity reduction due to ISSECs is not as great as at shutdown and the differences among these materials become smaller. One interesting fact about the long term radioactivity of the first wall is that it actually increases as the carbon thickness increases because of ^{63}Ni and ^{93}Mo which are both produced from (n,γ) reactions.

By the same token, the BHP and the afterheat of the first wall decreases in roughly the same proportion as the radioactivity decreases.

V.B.3. Effects of ISSEC on the Total Blanket

We will be concerned here with only three parameters out of the

many that characterize a certain type of blanket. These parameters are the tritium breeding ratio, energy multiplication (total energy available per fusion event) and radioactivity.

V.B.3.a. Tritium Breeding Ratio

In Figure V.15 the total breeding ratio in the model blanket of Figure V.11 is plotted as a function of increasing ISSEC thickness for five different ISSEC materials. Other dimensions and compositions of each region in Figure V.11 were kept constant. We see from Figure V.15 that the breeding ratio is always less in an ISSEC protected system than in systems with no ISSEC. The reason for this is that when an ISSEC is placed between the plasma and the first structural wall, the lower energy spectrum reduces the Li-7 (n,n'T) reaction rate and there are generally fewer neutrons available in the breeding zone to breed tritium by Li-6 (n,T). Some neutrons interact in the ISSEC either through high energy or low energy reactions and also the amount of thermal neutron capture increases in the first wall and the structure as the ISSEC thickness increases. If an ISSEC material has a high (n,2n) reaction cross section (e.g., V or Mo), that tends to help the neutron inventory in the breeding zone and the breeding ratio does not drop as fast as it would just due to the neutron energy degradation. Even though C is the material with the lowest parasitic absorption cross section, V and Mo ISSEC systems have a higher breeding ratio in the 8 to 20 cm region respectively, because of this (n,2n) effect.

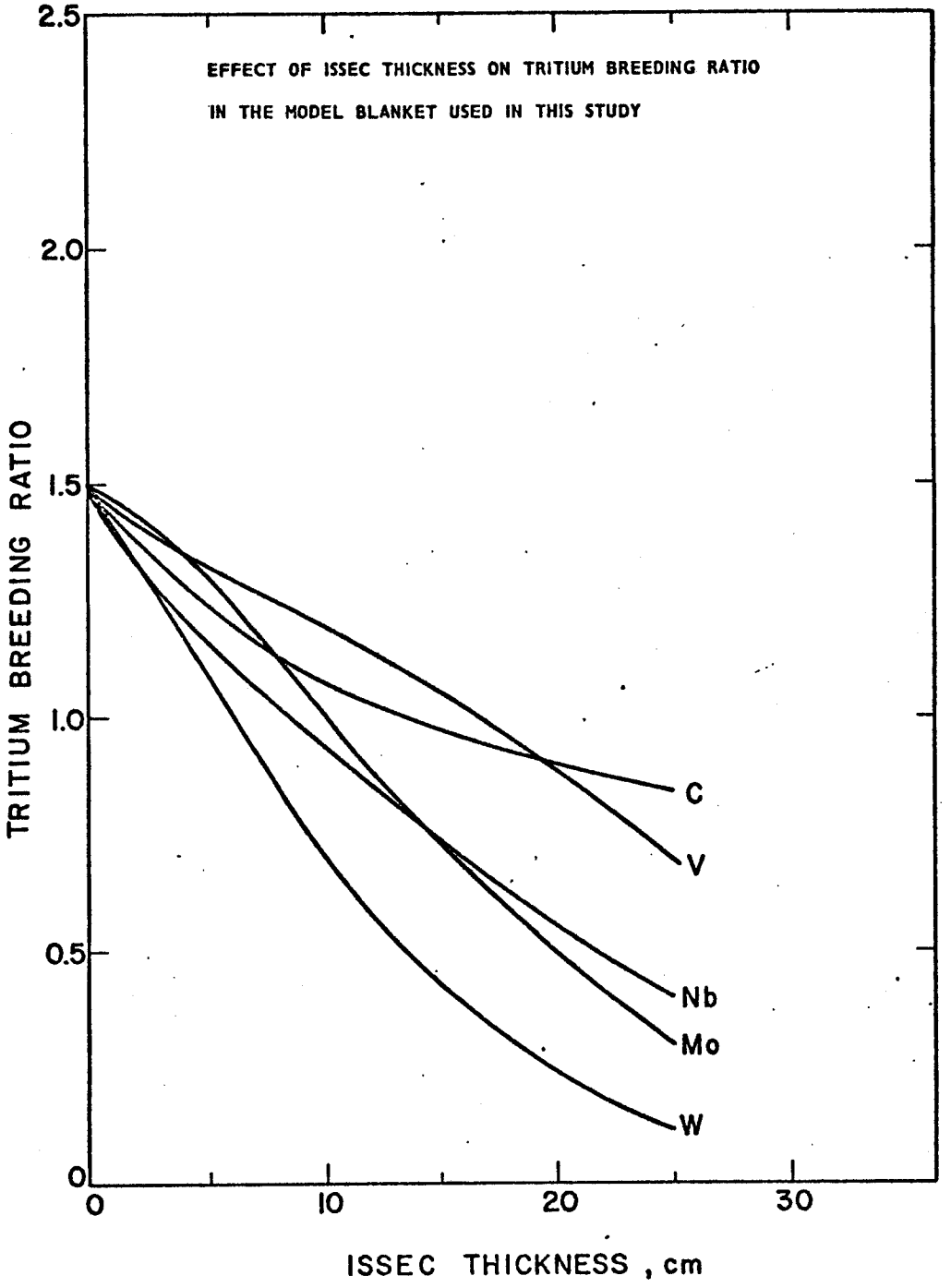
EFFECT OF ISSEC THICKNESS ON TRITIUM BREEDING RATIO
IN THE MODEL BLANKET USED IN THIS STUDY
TRITIUM BREEDING RATIO
2.5
2.0
1.5
1.0
0.5
0
0
10
20
30
ISSEC THICKNESS , cm
C
V
Nb
Mo
W

Figure V.15

The maximum useful thickness of an ISSEC in a certain blanket might be limited by the amount of breeding required. For example, if we require a minimum breeding ratio of 1.0 in our model blanket, the maximum thickness of a C or V ISSEC is limited to ∿18.5 cm, Mo to 10 cm, Nb to 8.5 cm and W to about 6 cm.

V.B.3.b. Energy Multiplication in the Blanket

Table V.15 lists the heating rates by neutrons and gammas and also gives the total energy deposited in the blanket (including the 3.52 MeV α energy) per fusion event in the various designs studied.

It is seen from this table that a C ISSEC reduces the total energy deposited in the reactor per fusion event by 3-4%. Neutron heating is somewhat reduced (fewer exothermic Li-6 (n,T) reactions and more endothermic reactions in C) and the gamma heating is increased compared to the no ISSEC case. This reduction in neutron heating and increase in gamma heating is more apparent in metal ISSEC cases. Vanadium ISSECs also reduce the total energy output of the blanket per fusion event. It is also evident from the results in Table V.15 that for the same neutronic wall loading, a reactor with a Mo ISSEC will have a higher thermal power output than reactors either with no ISSEC or C, Nb, V or W ISSECs. A V ISSEC system will have the least output power. The significance of this is that if all the results in this paper were to be normalized per megawatt of thermal power (MW_{th}) output, a Mo ISSEC system would have the additional advantage of running

Table V.15

Nuclear Heating in the Model Blanket and ISSEC Used in this Study

ISSEC Material	ISSEC Thickness (cm)	Neutron Heating (MeV)(a)	Gamma Heating (MeV)(a)	Total Energy (a,b) Per Fusion (MeV)
No ISSEC		12.9	3.2	19.6
C	5	12.4	3.2	19.1
	10	12.1	3.3	18.9
	25	11.8	3.6	18.9
Mo	5	9.4	8.5	21.4
	10	6.9	12.6	23.0
	25	2.6	20.3	26.4
Nb	5	8.8	7.6	19.9
	10	6.7	10.3	20.5
	25	3.2	15.3	22.0
V	5	10.2	3.9	17.6
	10	8.8	4.8	17.1
	25	6.2	8.8	18.5
W	5	7.7	9.2	20.4
	10	4.6	13.0	21.1

(a) Per neutron born in plasma

(b) Includes 3.52 MeV α energy

at a lower neutronic wall loading, and consequently a higher ISSEC thickness would be allowed.

V.B.3.c. Radioactivity of Blanket

Total radioactivity of the blanket (including the ISSEC) strongly depends on the choice of ISSEC material, because the ISSEC, which protects the first wall from high energy neutrons, is itself subject to the neutron activation and may show high or low activity.

Total blanket activities are shown in Figure V.16. Compared to the no ISSEC case, the amount of total radioactivity at shutdown is slightly decreased in a C and V ISSEC protected blanket while in the W, Mo and Nb ISSEC cases it increases.

After 10 years of decay, the radioactivity for all cases falls to about the same level. However, after a 1000 years the activity of Mo protected system is over a hundred times the base case while the radioactivity of the Nb system is almost 10 times higher. The rest of the systems are the same order of magnitude of the base case.

V.B.4. Radiation Damage in ISSEC

V.B.4.a. Displacement Damage and Gas Production

While the radiation damage in the first structural wall is being reduced to levels discussed in Section V.B.2. the ISSEC itself encounters the same sort of high energy neutron fluxes that the first wall would without an ISSEC. That gives rise to the dpa rates on the order of 8-13 dpa/yr and helium production rates on the order of

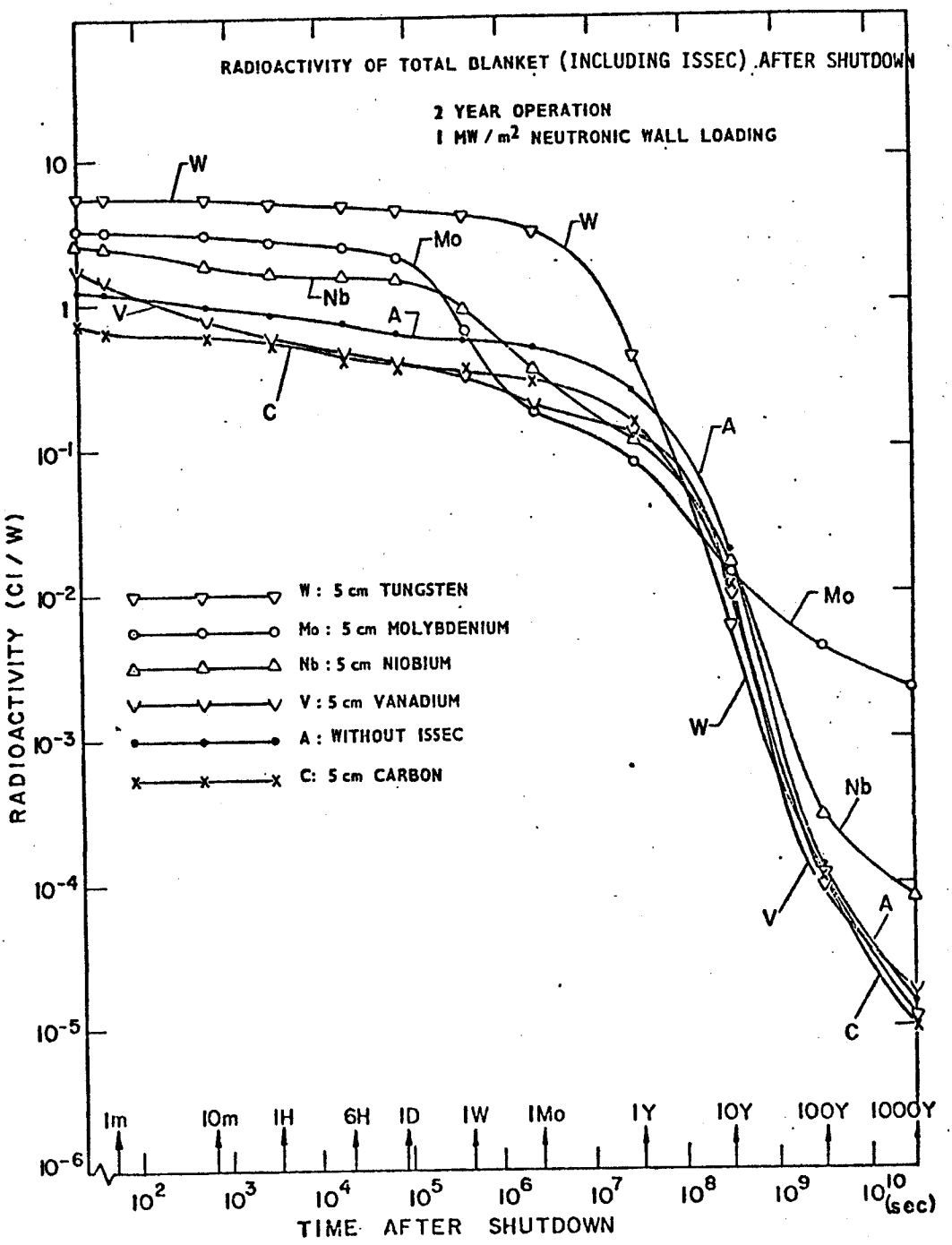
RADIOACTIVITY OF TOTAL BLANKET (INCLUDING ISSEC) AFTER SHUTDOWN
2 YEAR OPERATION
1 MW / m2 NEUTRONIC WALL LOADING
RADIOACTIVITY (CI / W)
TIME AFTER SHUTDOWN
W : 5 cm TUNGSTEN
Mo : 5 cm MOLYBDENIUM
Nb : 5 cm NIOBIUM
V : 5 cm VANADIUM
A : WITHOUT ISSEC
C: 5 cm CARBON
1m
10m
1H
6H
1D
1W
1Mo
1Y
10Y
100Y
1000Y
(sec)

Figure V.16

20-2400 Appm He/yr (the high number being for C) per 1 MW/m^2 neutronic wall loading in the front few layers of an ISSEC.

Dpa rates as a function of distance into the ISSEC are shown in Figure V.17 and helium and hydrogen production rates in the five ISSEC materials are tabulated in Table V.16.

The bulk radiation effects in carbon and graphite have been reviewed elsewhere[74-83] and will not be covered in detail here. Basically, carbon or graphite goes through two stages during bombardment with neutrons. The first stage is shrinkage by different amounts in volume and the second stage is expansion. In most data reported to date on the dimensional changes in carbon and graphite with neutron irradiation, the reversal from shrinkage to expansion takes place at fluences of about 1-2 x 10^{22} n/cm^2 (5-10 dpa) at temperatures of 800-1400°C. Above 1400°C, the fluence required for runaway swelling is not certain at this time,[84,85] but the bulk of the data predicts a lower damage rate at the higher temperatures.[85] It was originally thought that the high amount of helium generated in C could coalesce to form large bubbles and cause considerable dimensional changes and tearing. However some recent experiments tend to show that helium generated in carbon may in fact diffuse out at T > 800°C with almost 100% efficiency without any build-up inside.[86-88] The surface effects regarding carbon and graphite will be examined in Section V.B.6.

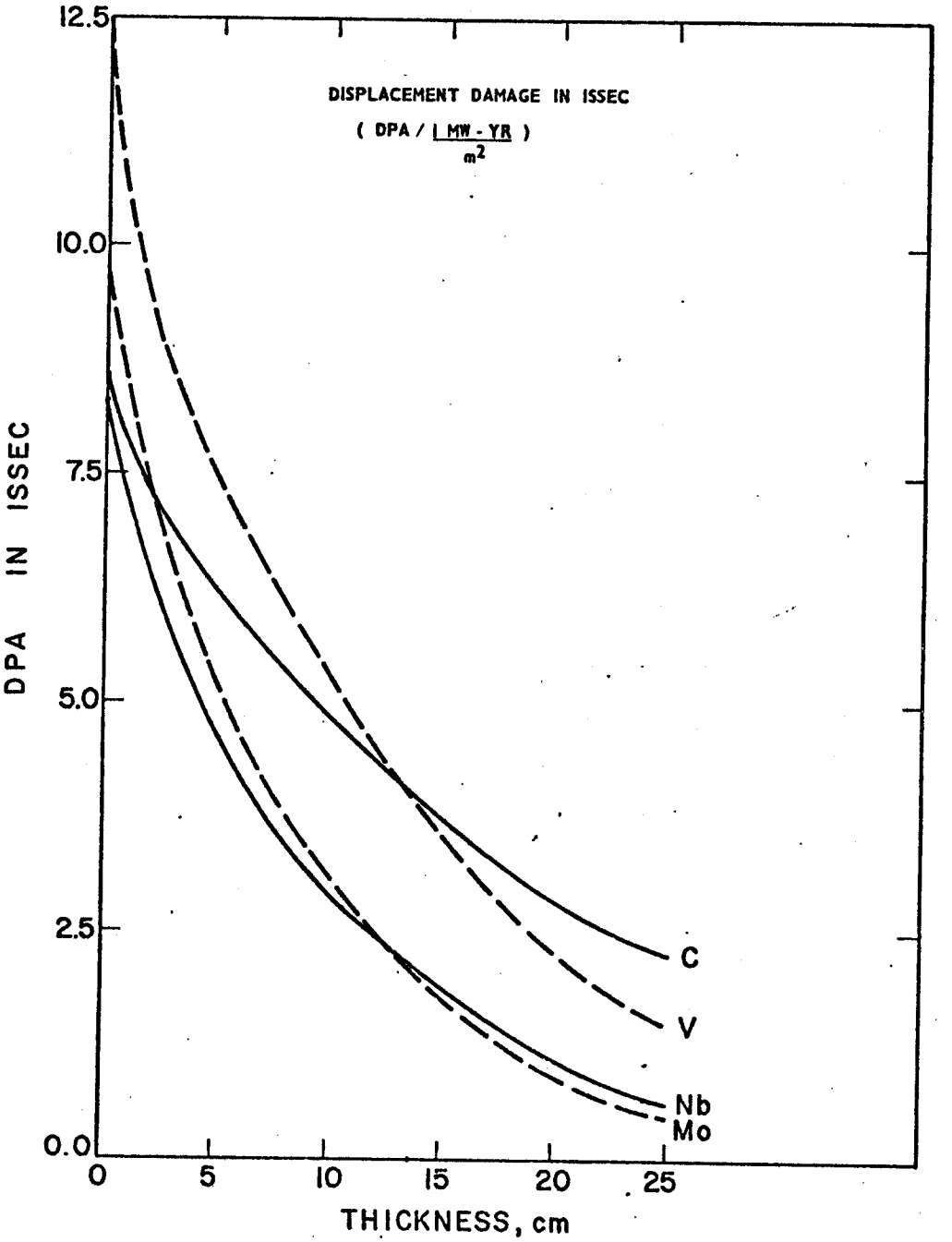
DISPLACEMENT DAMAGE IN ISSEC
(DPA / 1 MW - YR / m2)
DPA IN ISSEC
12.5
10.0
7.5
5.0
2.5
0.0
0
5
10
15
20
25
THICKNESS, cm
C
V
Nb
Mo

Figure V.17

Table V.16

Helium and Hydrogen Production in Various ISSEC Materials

Distance From Front Surface (cm)	C	Appm He per 1 $\frac{\text{MW-Yr(neutronic)}}{m^2}$ Mo	Nb	V	W
0	2340	43.0	21.8	54.5	3.71
5	1245	12.7	6.9	21.4	0.91
10	715	4.84	2.75	9.83	0.30
15	435	2.06	1.23	4.98	0.11
20	275	0.91	0.58	2.65	0.04
25	190	0.49	0.33	1.63	0.02
		Appm H per 1 $\frac{\text{MW-Yr(neutronic)}}{m^2}$			
0	none	70.5	71.3	91.3	7.98
5	none	20.9	22.7	36.4	1.95
10	none	7.96	9.05	16.9	0.65
15	none	3.39	4.06	8.66	0.23
20	none	1.50	1.93	4.69	0.08
25	none	0.80	1.12	3.02	0.04

The effect of the displacement rates and gas production rates as shown in Figure V.17 and Table V.16 on the metal ISSECs are not known, especially at temperatures of 1500-2000^{o}C. It is expected that at such high temperatures point defects such as vacancies and interstitials may anneal out or recombine quickly, and insoluble gas atoms will form bubbles. The lack of void swelling will be countered by the swelling due to gas bubbles and the net effect is also unknown at this time. However, an ISSEC, being a non-structural non-load bearing member, could operate with some deformations and cracks. As will be discussed in Section V.B.5, if the ISSEC could be constructed in such a fashion that it is free to expand in all directions, tolerance limits might be quite liberal.

V.B.4.b. Radioactivity, Biological Hazard Potential and Afterheat of ISSEC

As discussed earlier, the ISSECs generally reduce the first wall activity while they themselves become active. The amount of activity induced in the ISSEC varies greatly depending on the ISSEC material. The activities of different materials for 5 cm ISSECs are shown in Figures V.18, V.19 and V.20 with those for the first wall without an ISSEC.

One observation is that the activity of C, mainly from ^{6}He ($t_{1/2}$ = 0.8 sec), is three orders of magnitude lower than that of the others at shutdown. After one minute, the activity is dominated by ^{14}C($t_{1/2}$ = 5730 yr) whose magnitude is six orders lower than the shutdown of C.

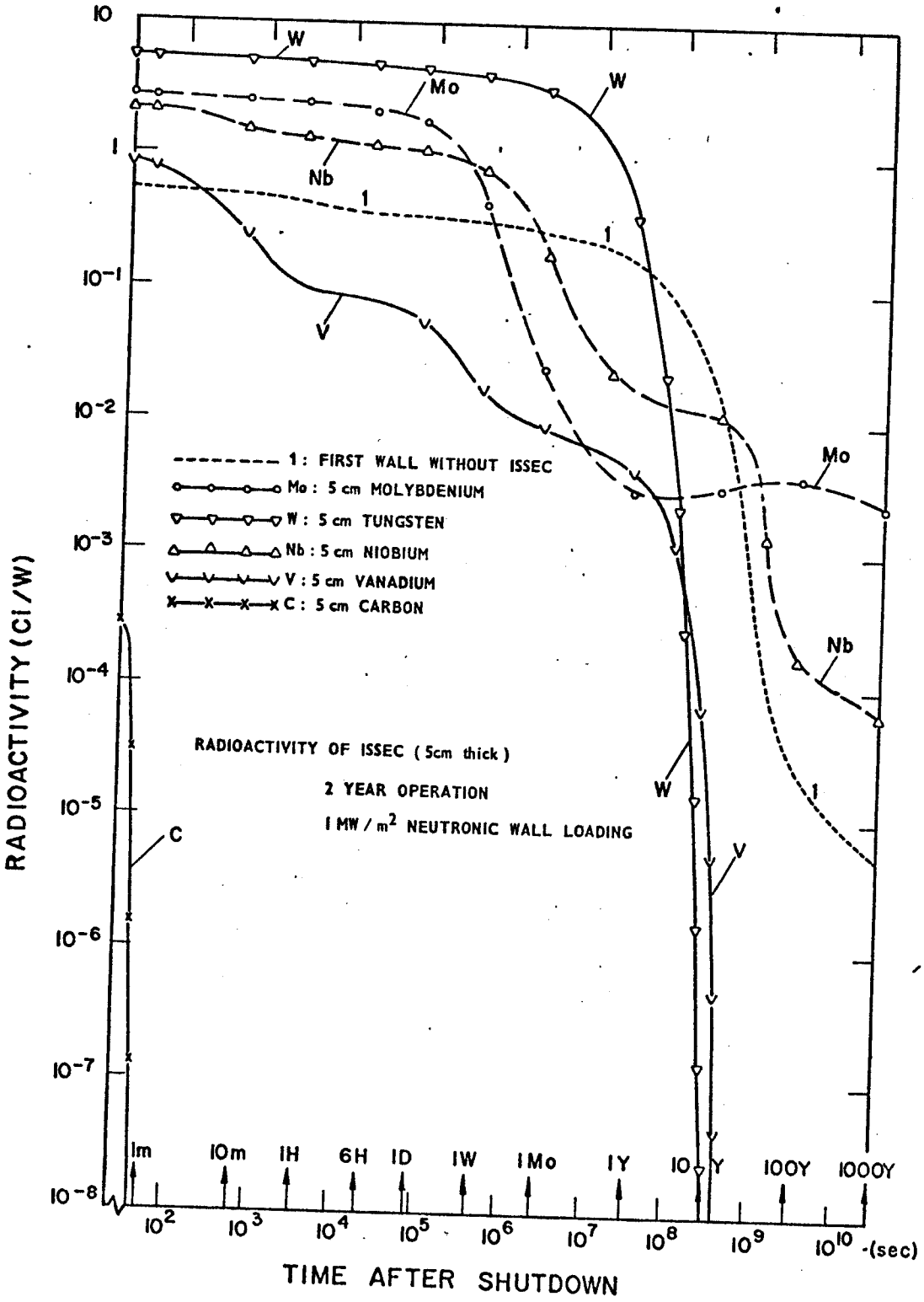
RADIOACTIVITY (CI/W)
TIME AFTER SHUTDOWN
1 : FIRST WALL WITHOUT ISSEC
Mo : 5 cm MOLYBDENIUM
W : 5 cm TUNGSTEN
Nb : 5 cm NIOBIUM
V : 5 cm VANADIUM
C : 5 cm CARBON
RADIOACTIVITY OF ISSEC (5cm thick)
2 YEAR OPERATION
1 MW / m2 NEUTRONIC WALL LOADING
1m
10m
1H
6H
1D
1W
1Mo
1Y
10Y
100Y
1000Y
(sec)

Figure V.18

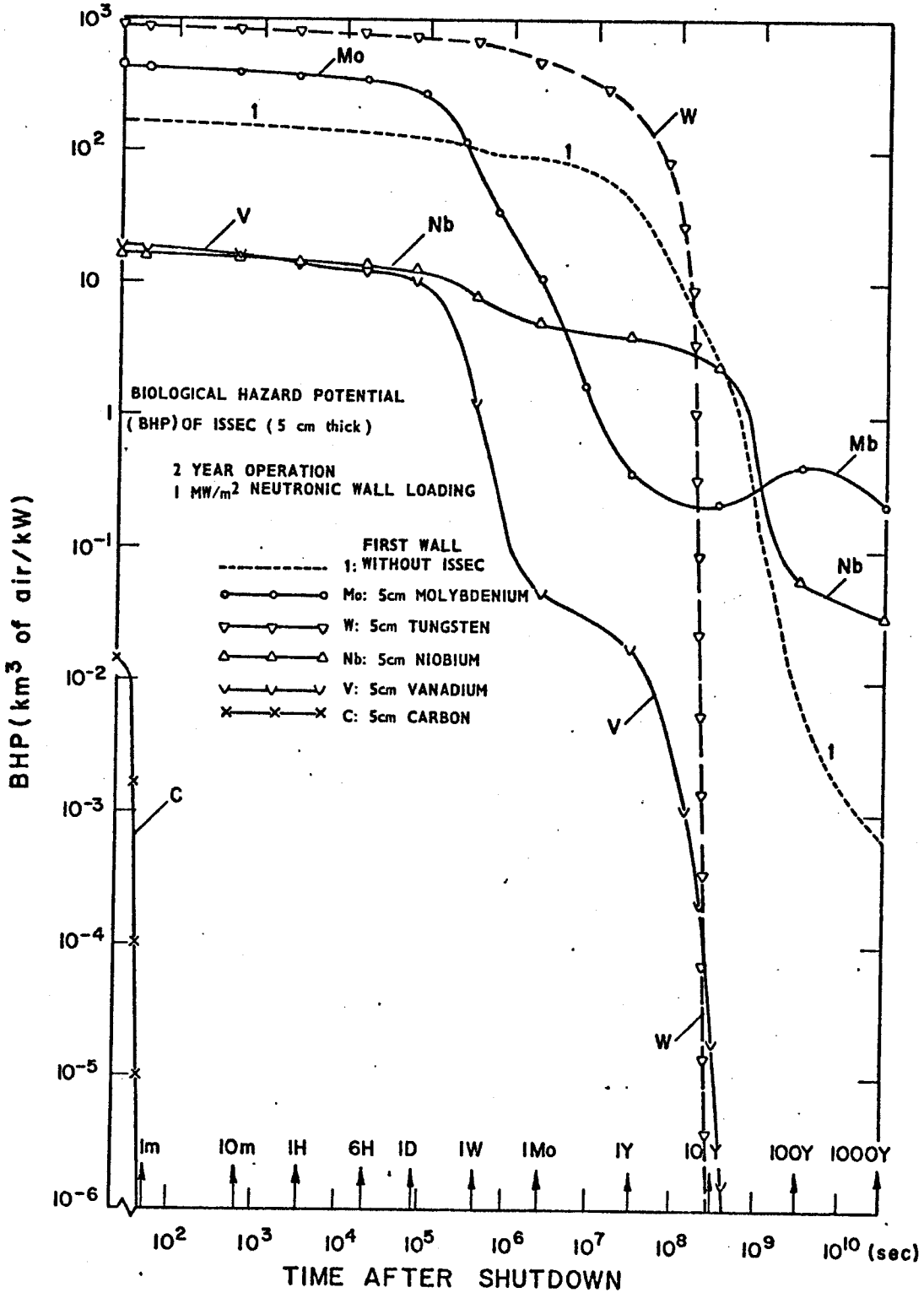
BIOLOGICAL HAZARD POTENTIAL
(BHP) OF ISSEC (5 cm thick)
2 YEAR OPERATION
1 MW/m2 NEUTRONIC WALL LOADING
FIRST WALL
1: WITHOUT ISSEC
Mo: 5cm MOLYBDENIUM
W: 5cm TUNGSTEN
Nb: 5cm NIOBIUM
V: 5cm VANADIUM
C: 5cm CARBON
BHP (km3 of air/kW)
TIME AFTER SHUTDOWN
(sec)
Im
10m
1H
6H
1D
1W
1Mo
1Y
10Y
100Y
1000Y

Figure V.19

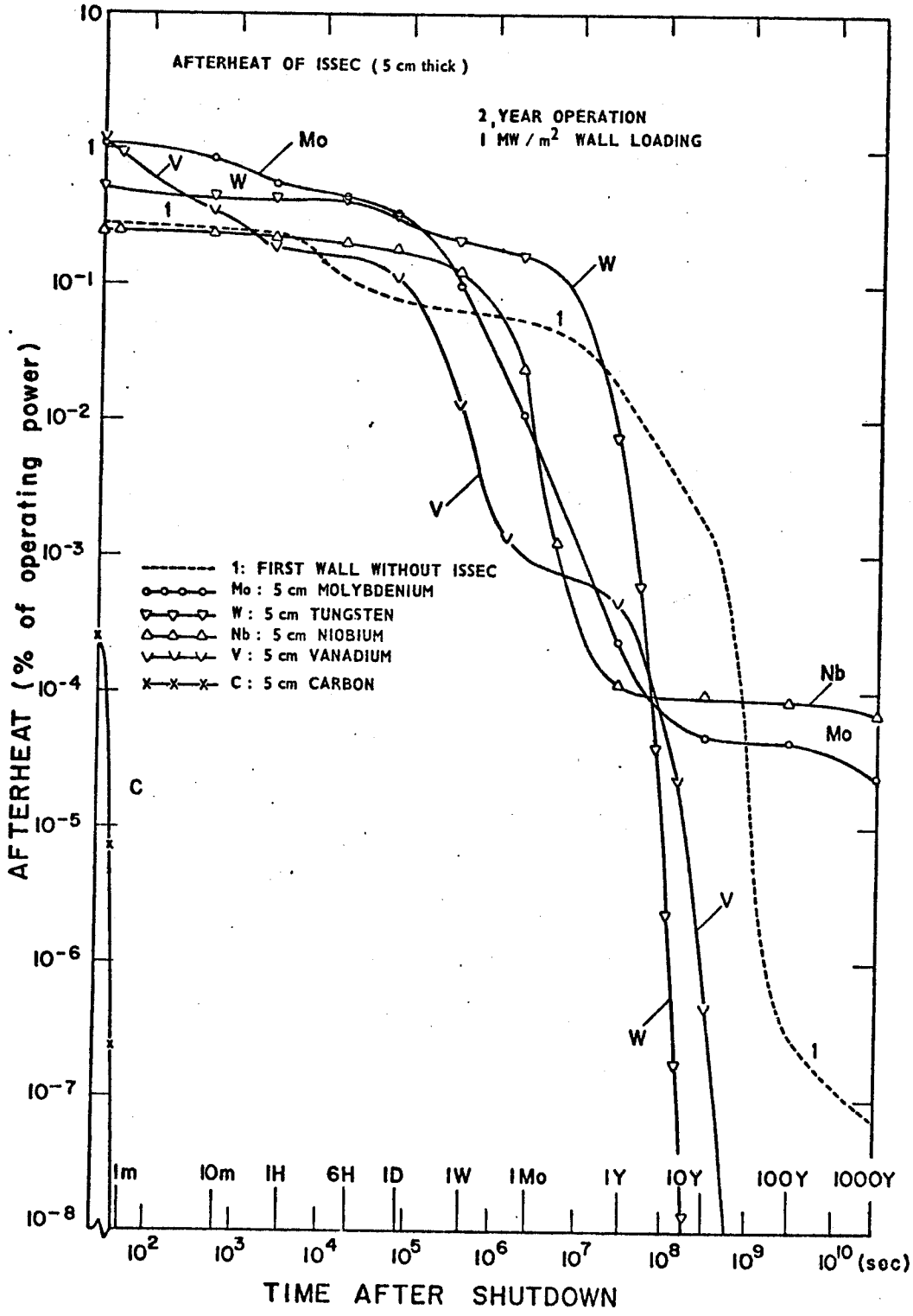
AFTERHEAT OF ISSEC (5 cm thick)
2 YEAR OPERATION
1 MW / m2 WALL LOADING
1: FIRST WALL WITHOUT ISSEC
Mo : 5 cm MOLYBDENIUM
W : 5 cm TUNGSTEN
Nb : 5 cm NIOBIUM
V : 5 cm VANADIUM
C : 5 cm CARBON
AFTERHEAT (% of operating power)
TIME AFTER SHUTDOWN
1m
10m
1H
6H
1D
1W
1Mo
1Y
10Y
100Y
1000Y
(sec)

Figure V.20

The level of radioactivity at shutdown is highest for W with Mo, Nb and V following in decreasing order. This order changes to W, Nb, V and Mo after 1 year of decay. After 100 years, both Mo and Nb show the long-term activities, and with the Mo level only three orders of magnitude lower than that at shutdown.

The biological hazard potential (BHP) of the ISSEC generally follows the behavior of radioactivity. BHP is another measure of radiological hazard obtained by dividing the amount of radioactivity with the maximum permissible concentration of each radioisotope. The long-term BHP is governed by ^{93}Mo in the molybedenum ISSEC, and ^{93m}Nb in the niobium ISSEC.

The afterheat of the various ISSECs at shutdown varies among V, Mo, W, and Nb in decreasing order, and after 1 year of decay the order changes to W, V, Mo and Nb. Beyond 100 years, only Nb and Mo show any afterheat, but at relatively minor levels.

V.B.5. Mechanical Design and Heat Transfer of ISSECs

An ISSEC (Internal Spectrum Shifter and Energy Converter) is envisioned as a passive non-structural member placed between the plasma and the first structural vacuum wall. In the process of softening the neutron spectrum, a considerable amount of heat will be generated inside an ISSEC. This heat, plus the heat incident on the front surface of an ISSEC due to ions and electromagnetic radiation originating in the plasma, will have to be transferred to the blanket behind. We considered two processes by which heat could be

transferred from an ISSEC to the first wall. They are thermal radiation and simple conduction mechanisms. For the present we have excluded any active cooling schemes for ISSECs.

For reasons of simplicity in design radiation cooled ISSECs made of a high temperature material like graphite or a refractory metal have received the most attention. Table V.17 lists the front and back surface temperatures of the five ISSEC materials considered at 5, 10 and 25 cm thicknesses subject to the boundary conditions stated earlier.

We see from Table V.17 that beyond some certain thickness the front surface temperature of the spectral shifter exceeds the melting point of the material. Obviously one cannot allow the ISSEC to melt during operation. If the absolute maximum temperature the front wall of the ISSEC can attain is taken to be the melting point of the respective material, it is found that with radiation cooling only, ISSEC's cannot have a thickness any greater than 20.5 cm for C and 13 cm, 11.5 cm, 10 cm and 18.5 cm for Mo, Nb, V and W respectively.* In actual practice the limits would be set much lower than these given here.

In a tokamak reactor the pressure inside the plasma chamber is envisioned to be $\sim 10^{-5}$ torr. Another important thickness criteria then is that the vapor pressure of any material enclosed in the

---

*For 1 MW/m^2 neutron wall loading and 4 $watts/cm^2$ of surface heat load.

Table V.17

Front and Back Surface Temperatures in the Radiation Cooled 5, 10 and 25 cm ISSECs*

(°C)

	5 cm ISSEC		10 cm ISSEC		25 cm ISSEC	
Material	T_{Front} (a)	T_{Back} (b)	T_{Front}	T_{Back}	T_{Front}	T_{Back}
C	1480	1290	2085	1465	(**)	(1680)
Mo	1670	1545	2265	1810	(**)	(2110)
Nb	1630	1485	2210	1710	(**)	(1960)
V	1370	1215	(**)	(1400)	(**)	(1755)
W	1790	1630	2350	1850	(**)	(2060)

*For 1 MW/m^2 neutronic and 4 W/cm^2 surface heat loading

**Exeeeds melting point

a)Front means facing plasma

b)Back means facing first wall

vacuum chamber be kept below that value. Figure V.21 plots the vapor pressure of the five ISSEC materials considered in this study versus temperature. If we assume that 10^{-5} torr is the maximum vapor pressure allowed then the maximum ISSEC temperature is 2000°C for C, ~1950°C for Mo, 2100°C for Nb, 1300°C for V, and 2600°C for W. These temperatures, under the conditions stated previously, translate into maximum allowable thicknesses of 9.5 cm for C, 7.5 cm for Mo, 9 cm for Nb, and 4.5 cm for V and 12.5 cm for W as shown in Table V.18.

It is important that a radiation cooled ISSEC be an unrestricted body, free to move. Otherwise the kind of thermal stresses set up inside an ISSEC of any appreciable thickness will far exceed the yield strength of the material at such elevated temperatures. One such scheme where the ISSEC could expand freely in all directions could be an ISSEC made up of a series of square plates. Each square plate could be attached to the first wall through its center by a non-conducting ceramic stud. Because of the type of temperature profile in a radiation cooled ISSEC, the front wall of the ISSEC will expand more than the back surface and the square plate would tend to bow outwards (towards the first wall). A maximum temperature limit would be reached when the inside corners of the plate touch the 316 SS first structural wall to cause partial meltdown of the first wall. Calculations show that with proper choice of the size of the plates and the length of the connecting studs, both carbon and metal ISSECs can run safely without ever touching the first wall.

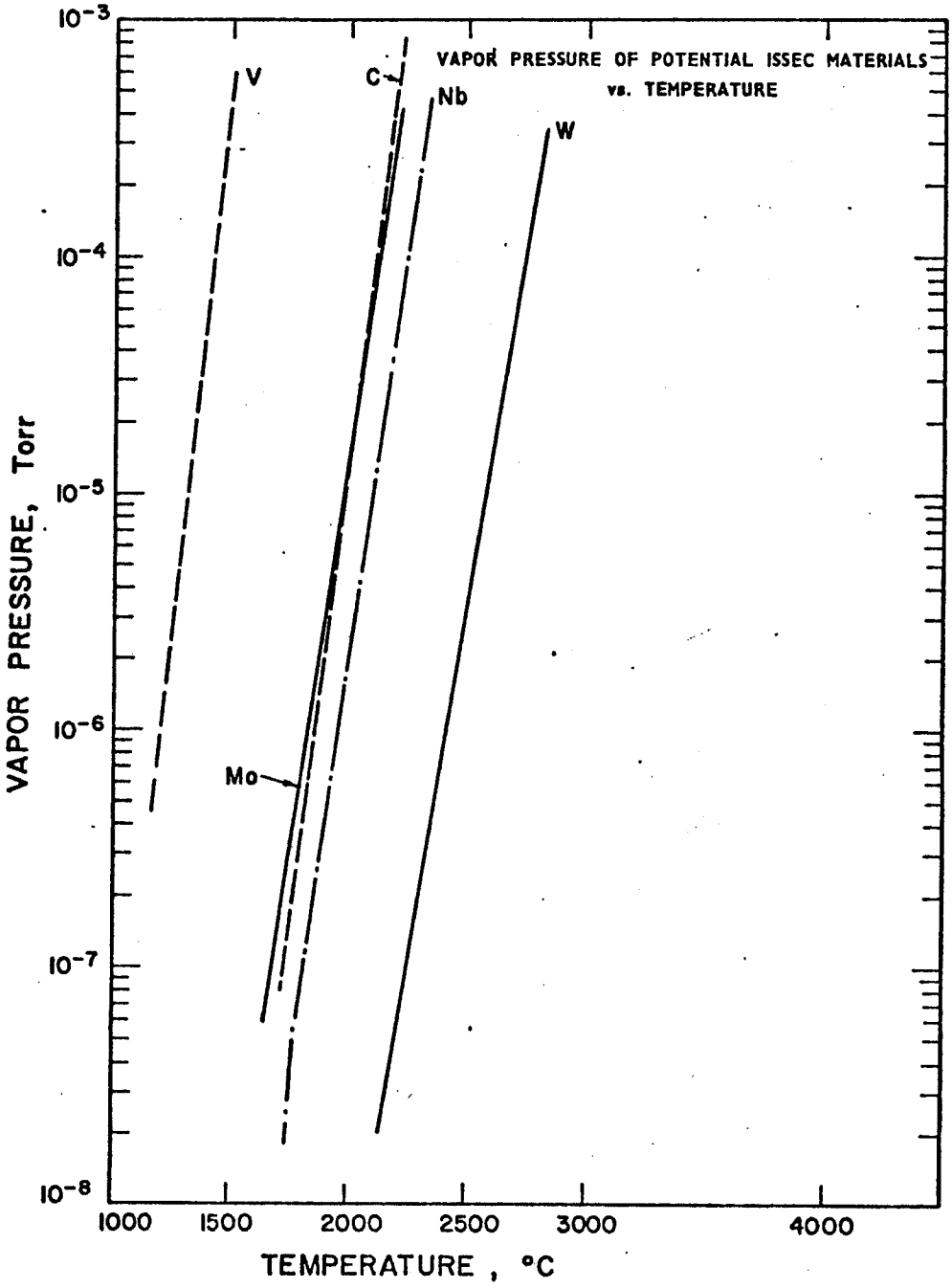
VAPOR PRESSURE OF POTENTIAL ISSEC MATERIALS
vs. TEMPERATURE
V
C
Nb
W
Mo
VAPOR PRESSURE, Torr
10^{-3}
10^{-4}
10^{-5}
10^{-6}
10^{-7}
10^{-8}
1000
1500
2000
2500
3000
4000
TEMPERATURE , °C

Figure V.21

Table V.18

Maximum Allowable ISSEC Thicknesses[a] in Three Limiting Cases With Radiation Cooling Only

ISSEC Material	Maximum Temperature Limit[b] (cm)	Maximum Vapor Pressure Limit (cm)	Breeding Ratio[c] Limit (cm)
C	20.5	9.5	13
Mo	13	7.5	10
Nb	11.5	9	8.5
V	10	4.5	18.5
W	18.5	12.5	6

(a) 1 MW/m^2 neutronic and 4 W/cm^2 surface heat load.
(b) For melting.
(c) For the model blanket used in this study and a breeding ratio of 1.0.

If an ISSEC could be designed in such a way that it can still expand freely in all directions to minimize thermal stresses, but cooled by conduction plus radiation, thicker ISSECs could be used in actual designs. One such design will be described below but it should be emphasized that this is an example and not the only way an ISSEC can be supported from and conduct its heat to the first wall.

Assume the ISSEC is made up of an array of rectangular plates with each plate having its longer dimension along the toroidal axis of a tokamak reactor plasma chamber. Behind each plate there is the structure shown in Figure V.22. The attachment of the plates to the first wall is also illustrated in Figure V.22. The stem connecting the ISSEC to the first wall may or may not be of the same material as the ISSEC. If it would be necessary to change the ISSEC during the lifetime of the plant, plates could be moved in and out of each module along the tracks in the first wall. If the ISSEC is stuck to the first wall, it could be cutoff from the stem, and the other two spare slots in the first wall under each plate, shown in Figure VI-22, can be used. If the diamond shaped blanket concept of I. Sviatoslavsky[91] (Figure V.23), the rectangular shaped blanket model of R. Benenati et al.[92] or the cassette blanket concept of D. Steiner et al.[93] with sliding first walls is adopted, changing the ISSEC should be fast and easy.

Because of symmetry, the heating rates and temperature should not vary along the toroidal length of the plates. The variation in

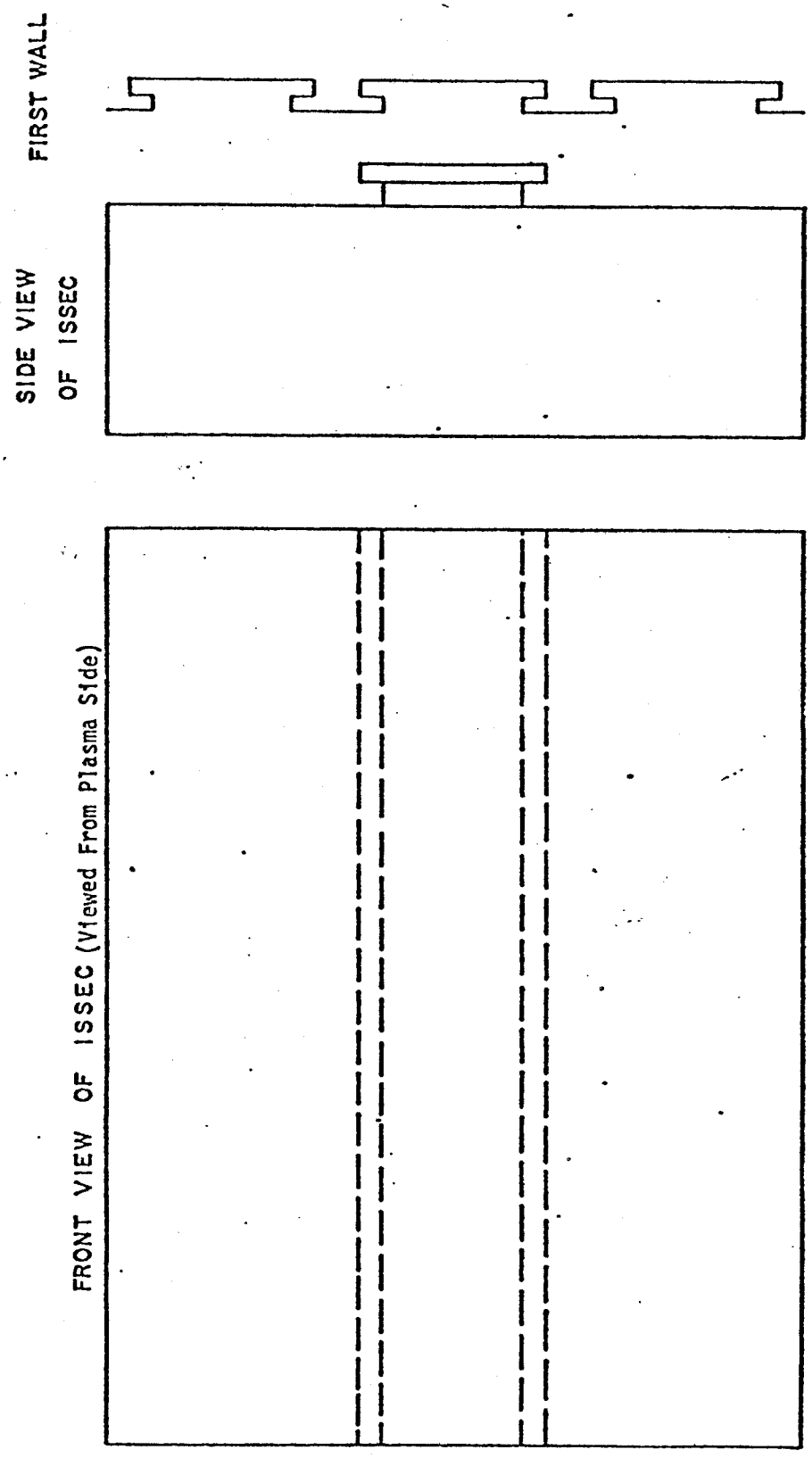

A Radiation Plus Conduction Cooled ISSEC Plate and Its Attachment to the First Wall

Figure V-22

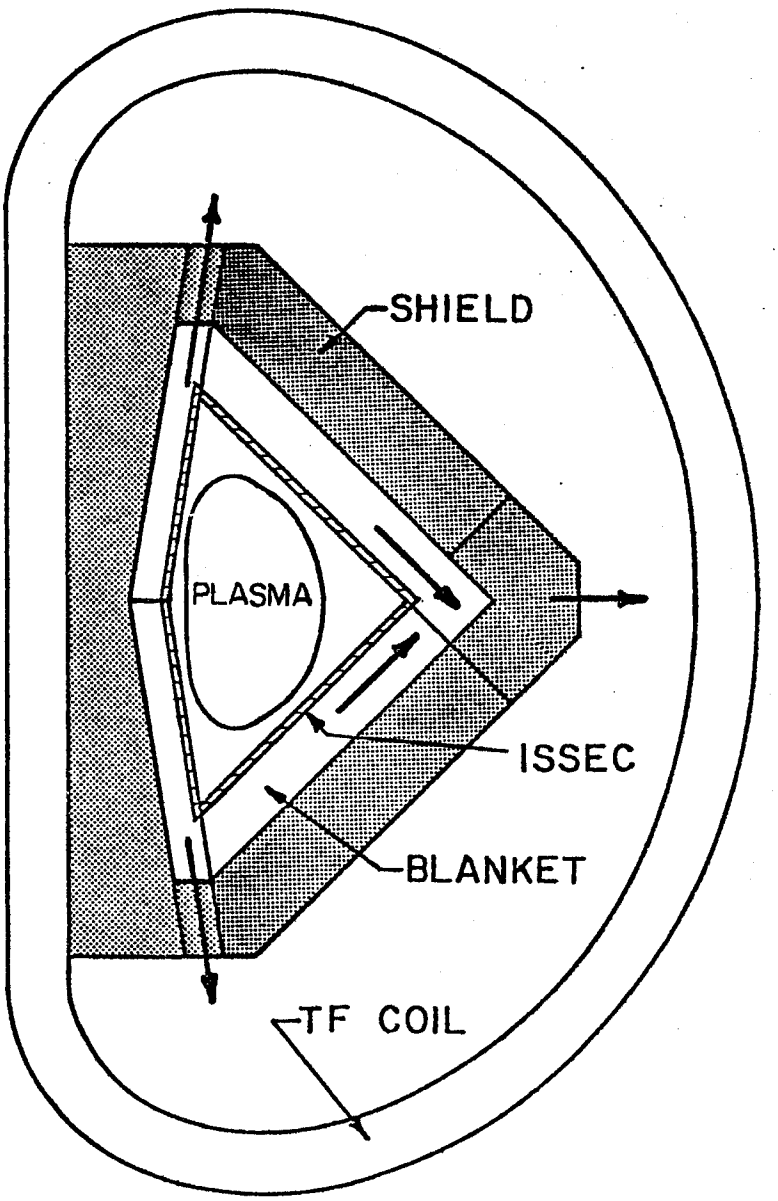

Incorporation of ISSEC into Moveable Blanket Concept[91]

Figure V.23

temperature is only along the width (poloidal direction) and thickness of each plate. Along the poloidal direction the temperature can be taken as symmetrical with respect to the centerline of the ISSEC. Figure V.24 shows the bottom half of a side view for a 5 cm thick 15 cm wide ISSEC plate. On Figure V.24 shown are the nodal point temperatures for the five ISSEC materials; Mo, Nb, V. W, and C. The nodal points 14 and 15 were assumed at 500^{o}C constant temperature. The connecting stem, 0.5 cm long, was also taken tobe the same material as the ISSEC and good contact was assumed between the ISSEC and the 316 SS first wall. The heat was assumed to be transferred through the throat (points 14-15) by conduction only. It was found that in this case more than 90% of heat transfer was by conduction and inclusion of radiative heat transfer did not change nodal point temperatures by more than 5%. Figure V.25 shows the temperatures for 10 cm thick ISSEC cases. For both Figures V.24 and V.25 the connecting stem was taken as 0.5 cm long and the same material as the ISSEC.

For the 5 cm thick ISSEC cases, a contact area equivalent to 20% of ISSEC back surface (3.0 cm^2 per cm of length of rectangular slab of 15 cm width) was assumed. Contact area was 22.5% for 10 cm cases. Actually the above assumptions are for the cross sectional area of the throat between the ISSEC and the first wall. As can be seen from Figure V.22, the actual heat transfer area between the ISSEC and the first wall will be higher than just the area of the

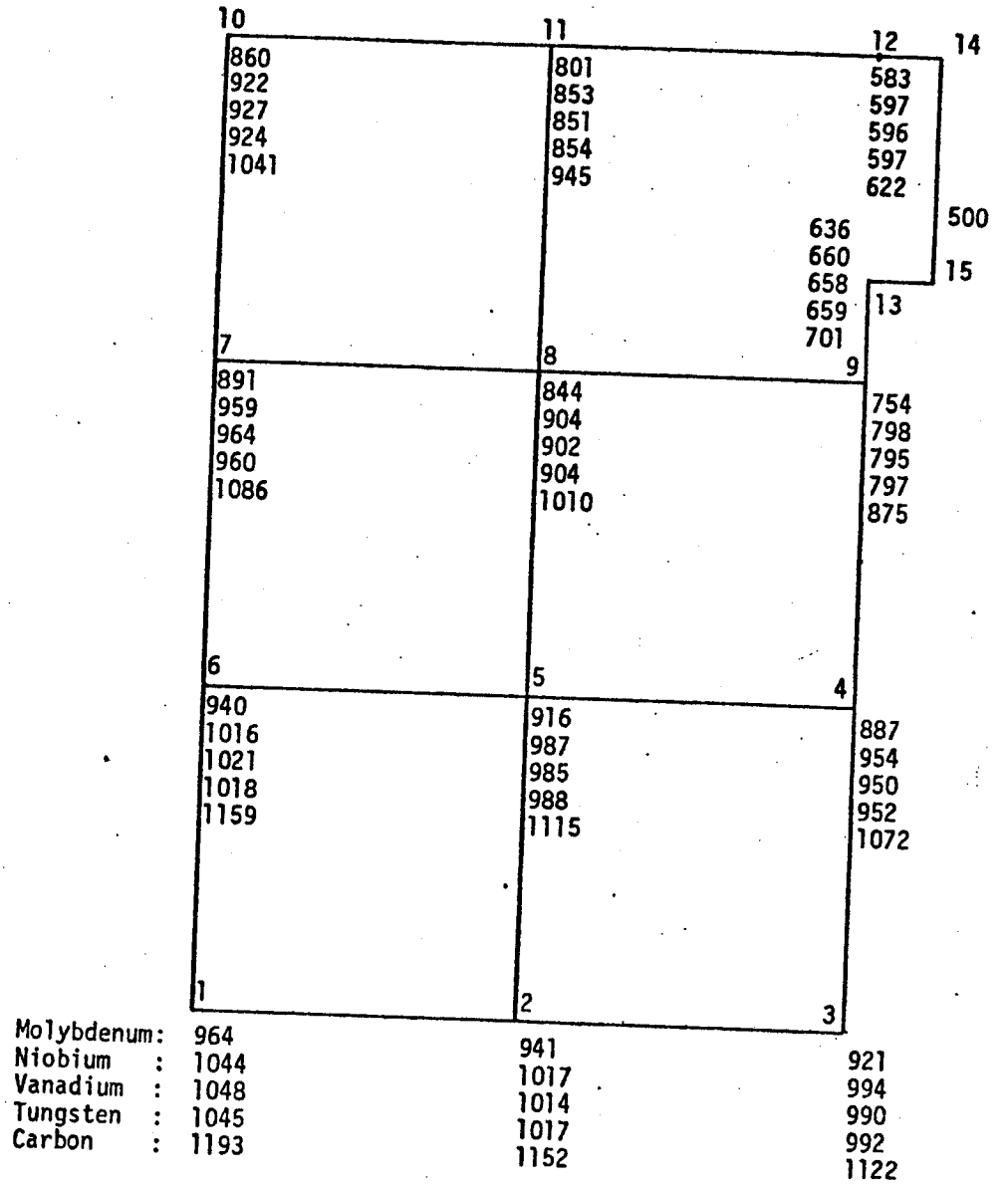

Nodal point temperatures (^{o}C) in 5 cm thick, 15 cm wide ISSECs cooled by conduction only. (Contact area is 20% of ISSEC back surface area.)

Figure V.24

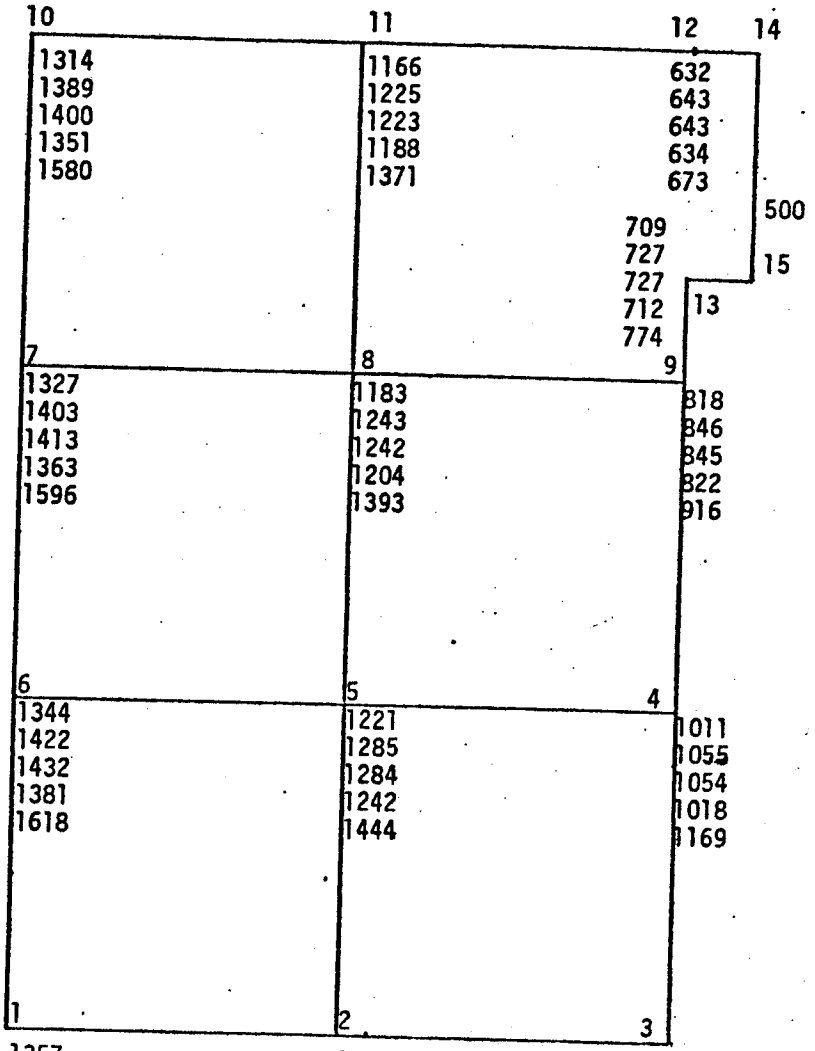

Molybdenum:	1357	1236	1064
Niobium :	1435	1300	1113
Vanadium :	1445	1300	1112
Tungsten :	1393	1255	1073
Carbon :	1634	1463	1239

Nodal point temperatures (^{o}C) in 10 cm thick, 15 cm wide ISSECs cooled by conduction only. (Contact area is 22.5% of ISSEC back surface area.)

Figure V.25

throat, especially if the material making up the ISSEC and the connecting stem has a much higher thermal conductivity than the first wall material, which is the case with 316 SS and materials considered for an ISSEC in this study. The significance of this increase in contact area is not only that the temperatures shown in Figures V.24, 25 will be lower than shown but also the flux of heat conducted to the first wall will be less. Table V.19 lists the total heat generated in 5 and 10 cm thick ISSECs per cm of length and 15 cm of width. It also gives the amount of heat conducted to the first wall, conduction heat flux, temperature drop across 316 SS first wall and the thermal stresses generated in it for the given heat fluxes. The unirradiated yield strength of 316 SS is 475 Mpa at 500^{o}C and higher at lower temperatures. The thermal stresses listed in Table V.19 are lower than 475 Mpa by 12-75%. If another material with a higher thermal conductivity were to be used for the first wall, the temperature gradients and thermal stresses listed in Table V.19 could be much lower.

Even though the ISSEC design presented here is probably not the ultimate, it can be seen from calculations that a 1 MW/m^2 neutronic and 4 W/cm^2 surface heat loading would allow either a graphite or a metal ISSEC with thicknesses of at least 15 cm to be employed in a tokamak reactor of dimensions similar to the UWMAK class [4,5,73] without exceeding the stress limitations of a 316 SS first wall.

Table V.19

Generation and Conduction of Heat From ISSECs to 316 SS First Wall and the Thermal Stress Generated in the First Wall

ISSEC Thickness (cm)	ISSEC Material	Total[1,2] Nuclear Heat Generated (W)	Total Heat Conducted (W)	Conduction[5] Heat Flux to First Wall (W/cm^2)	Temp.[6] Drop Across First Wall (°C)	Thermal[6] Stresses in First Wall (Mpa)
5	C	330	352[3]	65.2	74.1	144
	Mo	688	674	125	142	275
	Nb	592	586	109	124	240
	V	262	290	53.7	61.0	119
	W	844	814	151	172	332
10	C	550	488[4]	84.1	95.6	185
	Mo	1254	1052	181	206	397
	Nb	1002	850	147	167	323
	V	470	414	73.1	83.1	161
	W	1320	1104	190	216	417

(1) For 15 cm width and unit length plates.

(2) Nuclear heating per 1 MW/m^2 neutronic wall load. Does not include 4 W/cm^2 surface heat.

(3) For 5 cm cases 90% of heat transfer was assumed by conduction and 10% by thermal radiation.

(4) For 10 cm cases, 80% of heat transfer was assumed by conduction and the rest by radiation.

(5) Conduction areas of 5.4 and 5.9 cm^2 per unit length of slab was assumed for 5 and 10 cm thick cases, respectively.

(6) A thickness of 0.25 cm was assumed between coolant and the front surface of the first wall.

V.B.6. Other Considerations Affecting ISSECs

V.B.6.a. Cost

Table V.20 lists the current raw and the fabricated material costs of the various ISSEC materials considered in this study.[94] Among the five materials listed in Table V.20, the most available[94-96] from the standpoint of resources and the least expensive one is C (which is also the easiest to fabricate). Mo, Nb and W cost about the same but W is the hardest to fabricate followed by Mo and Nb. The thickest W plate that could be fabricated by forging at the present time is about 2-3 cm x 10 cm x 30 cm dimensions at 92% theoretical density.[94] The dimensions of Mo, Nb and V plates that can be fabricated by forging at present are about 5 cm x 15 cm x length, 5 cm x 30 cm x length, and 5 cm x 30 cm x length respectively with desired length up to 150 cm.[94]

V.B.6.b. Vacuum Properties and Vapor Pressure

Vapor pressures of the five ISSEC materials considered in this study were given in Figures V.21. The free vaporization rates of these materials as a function of temperature are presented in Table V.21. Values for carbon are taken from reference 90 and the free vaporization rates of the other four materials are calculated using the formula[97]

$$\dot{n}(T) \cong \frac{3.5 \times 10^{22}}{\sqrt{M}} \frac{P(T)}{\sqrt{T}}$$

Table V.20

Current Materials Costs for ISSECs[94]

Material	$/kg Raw	Fabricated
Carbon	3	10
Molybdenum	55	110
Niobium	65	100
Vanadium	100	200
Tungsten	35	70

Table V.21

Free Vaporization Rate of Various ISSEC Materials (atoms/cm^2 sec)

Temperature (^oC)	C	Mo	Nb	V	W
1000	$5.5x10^2$	$3.0x10^4$	$2.4x10^1$	$2.4x10^{11}$	$4.0x10^{-5}$
1500	$9.8x10^{10}$	$1.0x10^{11}$	$4.7x10^9$	$5.8x10^{16}$	$2.3x10^5$
2000	$4.0x10^{15}$	$3.0x10^{13}$	$1.9x10^{14}$	-	$6.5x10^{10}$
2500	$4.4x10^{18}$	$5.8x10^{17}$	-	-	$2.0x10^{14}$
3000	$1.0x10^{21}$	-	-	-	$5.4x10^{16}$

where $\dot{n}(T)$ is the free vaporization rate in units of atoms/cm^2-sec at temperature T,

P(T) is the vapor pressure in torr,

M is the atomic weight of material, and

T is the temperature in °K.

We see from Table V.21 and Figure V.21 that W is the best of the five materials from a vacuum properties standpoint. It is followed by Nb while Mo and C have somewhat higher vapor pressures. V is the least suitable of these five materials for vacuum applications.

Other criteria that affect the use of materials in vacuum environments are the gas content, and absorption of gases on the material. The gas content of metals is not expected to present a problem. Carbon, which may have a high gas content before baking, was originally thought by many to be unsuitable for hard vacuum applications. However, several experiments have shown that with proper outgassing and baking at high temperatures, the residual gas content in carbon could be lowered drastically.[98-100]
G. A. Beitel[99] measured the quantity and composition of gases retained in several graphites and tungsten. After a 300°C and 24 hour bake out, he found that the results were quite similar for graphite and tungsten.

More recently G. P. Lang and V. L. Holmes[100] measured the gas content of WCA and Thornel 50 S graphite fibers. They found

that relatively large amounts of gas (0.40-0.1 torr liters/gram for WCA and 0.2-0.5 torr liters/gram for Thornel 50 S at 1500-2000°C) are removed from the fibers during an initial desorption. But after the first desorption the amount of gas removed from the samples was very small (0.001-0.01 torr liters/gram for WCA and 0.01-0.03 torr liters/gram for Thornel 50 S at 1500-2000°C).

Lang and Holmes[100] also measured the sticking probability of hydrogen and air on WCA and Thornel 50 S fibers at simulated tokamak fusion reactor operating conditions. They showed that the sticking probability of both hydrogen and air on these fibers was very low on the order of 10^{-8} - 10^{-10}, which should present no problem during refueling operations between burns.

V.B.6.c. Surface Effects

The side of the ISSEC facing the plasma in a tokamak fusion reactor will be subjected to high fluxes of high energy atomic D^+, T^+ and He^+ ions, 14.1 MeV neutrons as well as lower energy back scattered neutrons and impurity ions present in the plasma. All of these particles to some degree will cause sputtering of atoms off the surface of an ISSEC. Deuterium (D^+), and T^+ ions could react chemically with carbon and add to removal rate of surface atoms through formation of some volatile hydrocarbons. Helium and D^+ ions could also cause blisters in metals. The surface effects problem cannot be covered in any detail here and we will only mention some

of the more important experiments in this area and briefly comment on their results.

V.B.6.c.1. Sputtering

Behrish has recently summarized the light ion sputtering values for Mo[101] and Nb[97] and his results for Mo are given in Figure V.26. Results from references 101 and 97 indicate that sputtering yields of Mo and Nb are very similar with the maximum in the sputtering curves occurring at 3-5 keV for D and T and at approximately 5 keV for He. The maximum sputtering coefficients are:

for Mo: 0.008 for D^+, 0.02 for T^+ and 0.05 for He, and

for Nb: 0.012 for D^+, 0.018 for T^+ and 0.1 for He.

There isn't much information on the ion sputtering of V and W, but Behrish[97] reports that the sputtering yield of V might be about a factor of 2-3 higher than for Nb, and W might be a factor of 2-3 lower than Nb.

The ion sputtering of carbon deserves special attention in that it is reported to react chemically with atomic hydrogen and its isotopes at certain temperatures.[86,102-111] The difficulty, however, is finding the experimental values of the sputtering coefficient for D^+, T^+ and He^{++} at appropriate energies characteristic of a tokamak fusion reactor. A few recent studies,[102-105] utilizing hydrogen isotopes to measure the sputtering behavior of carbon, have been made at appropriate energies and some results are summarized in

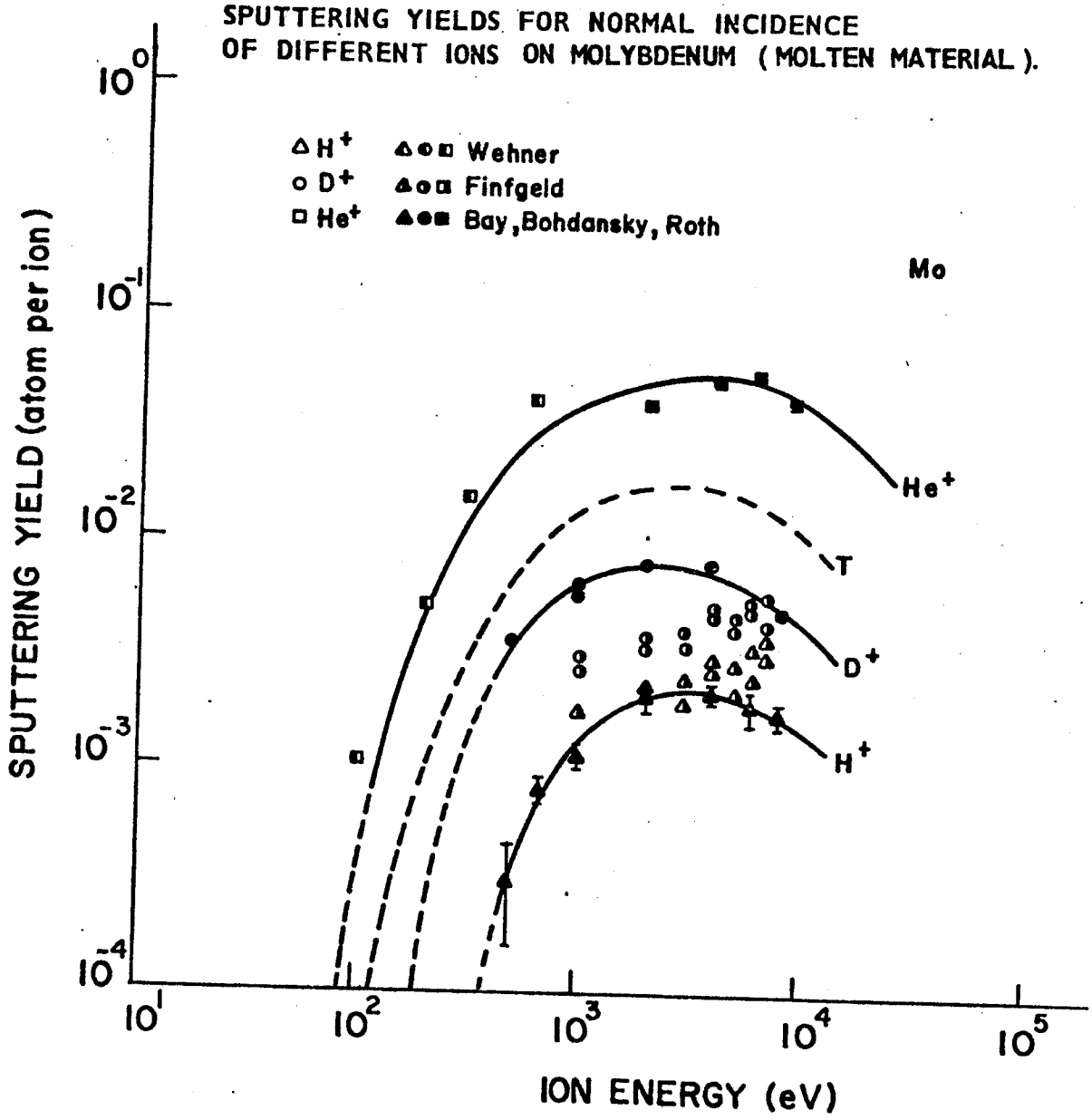
SPUTTERING YIELDS FOR NORMAL INCIDENCE
OF DIFFERENT IONS ON MOLYBDENUM (MOLTEN MATERIAL).
△ H+ ▲●■ Wehner
○ D+ ▲●□ Finfgeld
□ He+ ▲●■ Bay, Bohdansky, Roth
Mo
He+
T
D+
H+
SPUTTERING YIELD (atom per ion)
ION ENERGY (eV)
10^0
10^-1
10^-2
10^-3
10^-4
10^1
10^2
10^3
10^4
10^5

Figure V.26

Figures V.27[102,105] and V.28.[104] The basic difference between these studies is that the data in Figure V.27 comes from 2-20 keV H, D and T ions on carbon which was heated to 1400°C while that in Figure V.28 comes from carbon bombarded at 1900°C with very low energy (0.2 eV) hydrogen. Some general observations about Figures V.27 and 28 are:

1) The sputtering coefficients rise from a value of 10^{-2} atom/atom at room temperature to a maximum of $\sim 8 \times 10^{-2}$ at 600°C. This peak has been found to be associated with methane formation.

2) As the temperature is increased above 600°C, the sputtering values start to return to their low initial values. This is accompanied by a reduced methane formation.

3) The sputtering coefficient from tritium is reduced as its energy is increased from 2 to 6 keV. However, 6 keV tritium is more effective in producing methane than is the same energy deuterium.

4) The low energy hydrogen bombardment depicted in Figure V.28 shows smaller absolute levels of methane formation than for higher energy hydrogen. Furthermore, the low energy sputtering is quite sensitive to crystal orientation.

5) Above 1000°C, the formation of acetylene takes place although the absolute values are still low ($<<10^{-2}$ atom/atom).

6) There appears to be a region between 800 and 1200°C where little gasification occurs.

The peak in the sputtering yield vs. temperature curve around 600°C was also observed by other investigators.[103,106,107,110]

Figure V.27

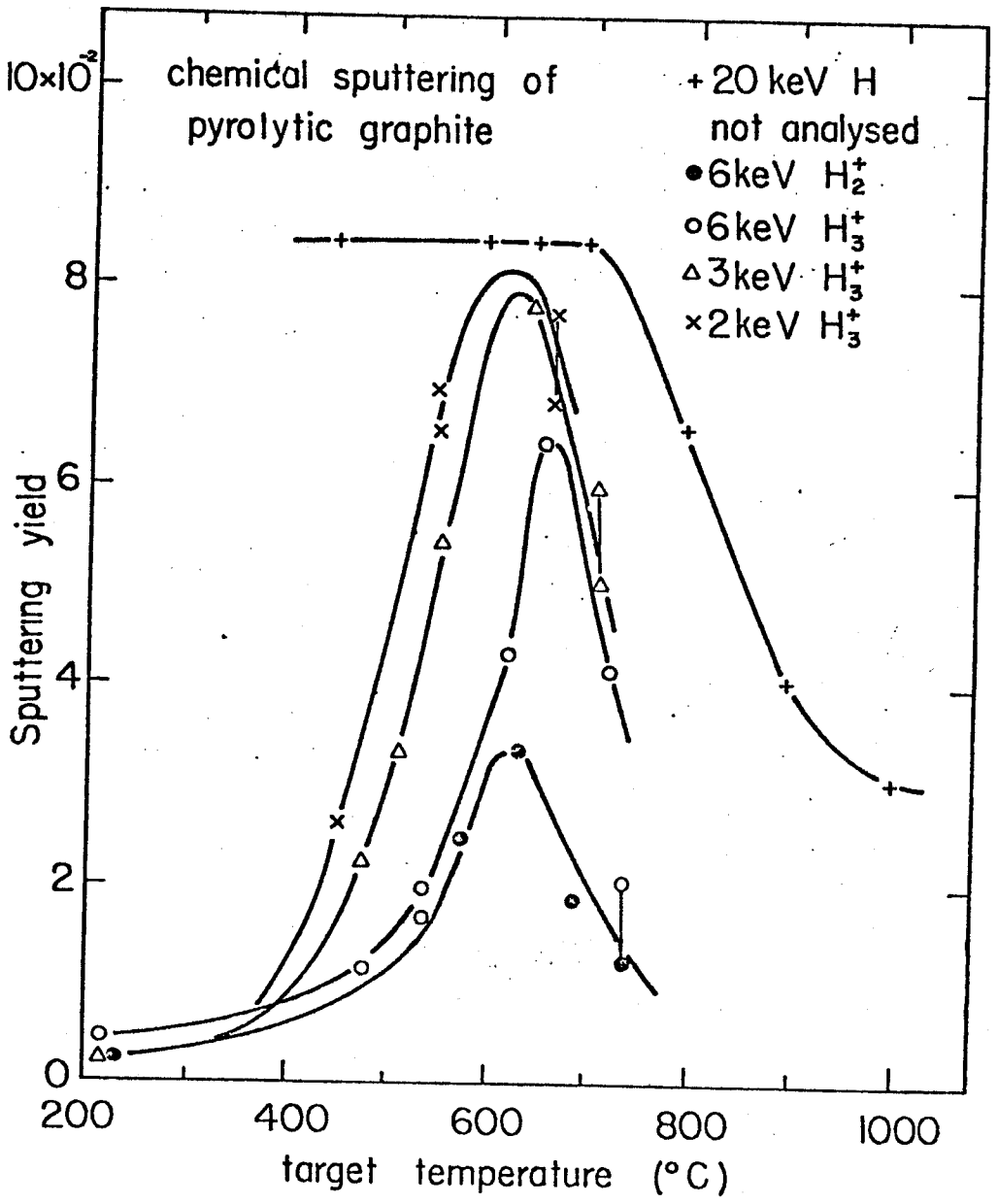
chemical sputtering of
pyrolytic graphite
+ 20 keV H
not analysed
●6keV H_2^+
○6keV H_3^+
△3keV H_3^+
×2keV H_3^+
10×10⁻²
8
6
4
2
0
Sputtering yield
200
400
600
800
1000
target temperature (°C)

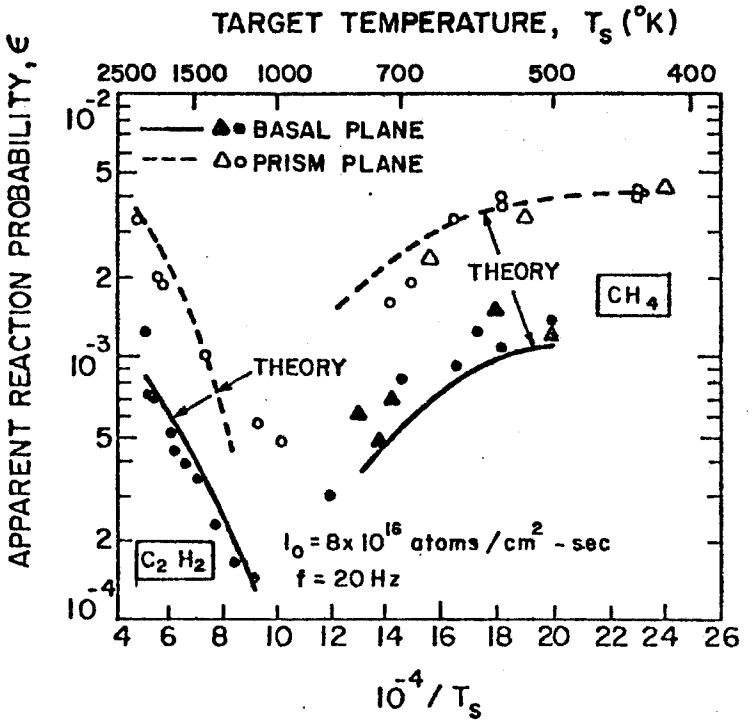

Figure V.28

Effect of Temperature and Crystal Orientation on the Reaction Probability of Carbon (104)

R. Ekern, et al.[109] irradiated rayon based WCA graphite cloth at room temperature, 400°C and 800°C with deuterons and $^4He^+$ ions at 100 and 250 keV energy. They observed considerable flaking of individual fibers at room temperature irradiations but at 400°C and 800°C irradiation surface damage was greatly reduced. In fact, in high temperature irradiations with $^4He^+$ they did not observe any flaking or other surface damage.

Physical sputtering of graphite by helium ions is thought to be practically independent of temperature.[111] Two independent measurements give the sputtering ratio as 0.06 for 0.4 keV He ions[112] and 0.07 for 0.5 keV He ions.[113]

The sputtering yield results for carbon on carbon are even more scarce than hydrogen and helium bombardment results. One value quoted in the literature is 0.4 for 45 keV C on C.[114] Assuming that this value is correct, the self sputtering yield of carbon under tokamak operating conditions (1-20 keV C on C) may be expected to be around 0.5-0.6.

The incident 14.1 MeV and lower energy back scattered neutrons will also cause atoms to be sputtered from the front surface of ISSEC. Unfortunately, there have been no 14 MeV neutron studies on Mo, W or carbon. Most studies have been carried out on Nb[115-119] and very little on V.[119] However, fission neutron sputtering results of Garber, et al.[120] show the neutron sputtering rates of Mo, Nb, V, and W within a factor of 2 of each other. The current 14 MeV neutron

sputtering values on Nb range from approximately 10^{-4} to 10^{-3} on the high side[115] to 10^{-5} - 10^{-4} on the low side.[116-118] Lacking any specific data and using Nb as a model for Mo, V, W and carbon, it appears to be reasonable to choose a value of 10^{-4} atom/neutron for the 14 MeV neutron sputtering of all five ISSEC materials considered in this study.

In order to determine the erosion of the ISSEC surface as a result of sputtering, one needs to know the current of charged particles incident on the surface from the plasma, the energy of these incident particles and the sputtering coefficient at that energy. Using the values calculated for UWMAK-III[73] for the charged particle fluxes incident on the ISSEC, and the sputtering coefficients given in this section, we can calculate the flux of particles leaving the ISSEC surface by

$$\phi = \sum_i S_i(E)\ \phi_i(E)$$

where $S_i(E)$ is the sputtering ratio (atoms per particle) for the i'th particle with energy E incident on the ISSEC.

$\phi_i(E)$ is current of i'th particles at energy E on the ISSEC surface.

Table V.22 gives the energy and the current of charged particles and neutrons incident on the ISSEC surface per 1 MW/m^2 neutronic wall loading under UWMAK-III[73] conditions (1% plasma burnup and 99.9% efficient divertor). Also listed in Table V.22 are the sputtering

Table V.22

Summary of Particles Striking the ISSEC Surface for UWMAK-III[73] Conditions

Particle	Mean Energy-keV	(2) Current-$cm^2 s^{-1}$	Physical Sputtering Coefficient Atoms/Particle[1] C	Mo	Nb	V	W
D^+	3	5.8×10^{12}	0.01	0.008	0.01	0.02	0.005
T^+	3	5.8×10^{12}	0.01	0.02	0.02	0.04	0.01
He^{++}	3	6.8×10^{11}	0.1	0.06	0.09	0.18	0.05
He^{++}	100	6.8×10^{10}	0.05	0.007	0.02	0.04	0.01
n	14.1×10^3	4.43×10^{13}	10^{-4}	10^{-4}	10^{-4}	10^{-4}	10^{-4}

(1) Assume constant with temperature

(2) Adjusted to 1 MW/m^2 average neutronic wall loading.

Table V.23

Flux of Sputtered Atoms From Various ISSEC Surfaces

Particle	Mean Energy-keV	Atoms/cm^2 sec C	Mo	Nb	V	W
D^+	3	5.8×10^{10}	4.6×10^{10}	5.8×10^{10}	1.2×10^{11}	2.9×10^{10}
T^+	3	5.8×10^{10}	1.2×10^{11}	1.2×10^{11}	2.3×10^{11}	5.8×10^{10}
He^{++}	3	6.8×10^{10}	4.1×10^{10}	6.1×10^{10}	1.2×10^{11}	3.4×10^{10}
He^{++}	100	3.4×10^{9}	4.8×10^{8}	1.4×10^{9}	2.7×10^{9}	6.8×10^{8}
n	14.1×10^3	4.4×10^{9}	4.4×10^{9}	4.4×10^{9}	4.4×10^{9}	4.4×10^{9}
Total	-	1.9×10^{11}	2.1×10^{11}	2.5×10^{11}	4.8×10^{11}	1.3×10^{11}

coefficients for the various incident particle-target combinations at the incident particle energy shown. Table V.23 gives the flux of sputtered atoms from various ISSEC surfaces due to D^+, T^+, He^{++} ions and 14.1 MeV neutrons. Comparing the values for the total flux of sputtered atoms from the surfaces of the five ISSEC materials from Table V.23 with those given in Table V.21 for vaporization, we see that the rate of vaporization is about the same as the rate of sputtering at about 1550°C for carbon, 1600°C for Mo, 1650°C for Nb, 1050°C for V and 2100°C for W. When the surface temperature of each material is below the value given above, the sputtering rate is higher than the vaporization rate, otherwise the vaporization rate is higher.

V.B.6.c.2. Blistering

Blisters have been observed in Mo,[121-125] Nb,[126-128] V[129-131] and W[121] with He^+ irradiations. In some instances they have also been observed with D^+ and H^+ irradiations on Mo.[122,123,125] In general, the blister skin thickness is about the same as the depth at which range probability distribution of incident particles peaks. The minimum fluence for blisters to form and exfoliate decreases with increasing temperature and particle current, increases with increasing ion energy.

To the author's knowledge, there has been no experimental data reported to show blisters forming in graphite with helium ion bombardment.[103,108,109,132,133]

It is not certain at this time whether blisters in metals keep reforming after every exfoliation or that they will stop forming after the first few exfoliations. Some recent results by Roth, et al.[134] show that if the ions have a spread in energies or if they strike the wall with varying angles of incidence, after the first few exfoliations, the surface becomes so porous that the bombarding particles diffuse out as fast as they are injected. If this happens to be true at high fluences, or if it turns out that no blisters form in carbon, metal surfaces could be carbon coated to avoid serious problems with blisters.

V.B.6.d. Thermal Shock Resistance

Resistance to thermal shock is a measure of the ability of a material to resist crack formation and fracture when subjected to sudden heating or cooling. No standard tests exist which will accurately evaluate the property since shape is an important factor. A figure of merit number is obtained when the parameters k (thermal conductivity), S (tensile strength), α (coefficient of thermal expansion), and E (modulus of elasticity) are combined as $\frac{kS}{\alpha E}$. The higher this number, the better the ability of the material to resist thermal shock.

Table V.24 gives $\frac{kS}{\alpha E}$ values for the five ISSEC materials investigated at two temperatures. We see from the table that W has the best resistance to thermal shock followed by C, Nb, Mo and V in decreasing order at 1600°C. At 1200°C Nb is next to W, C is third,

Table V.24

Relative Figure of Merit for Thermal Shock Resistance of Potential ISSEC Materials*

Material	Temperature 1200°C	1600°C
C	51.	40.
Mo	47.	15.
Nb	70.	39.
V	0.35	0.35
W	200.	100.

* $\frac{kS}{\alpha E}$ Watts/cm - high numbers are desired

and then Mo and V.

There are two important things to note about Table V.24. One is that C, a non-metal, has as good or better thermal shock resistance than metals at high temperatures. The other is that V, because of its very low strength at high temperatures, is at the bottom of thermal shock resistance scale.

V.B.7. Discussion on Results Presented in Sections V.B.1 through V.B.6

A comparison of the five ISSEC materials considered in this study is made in Table V.25 on the basis of how much they reduce the displacement and gas production rates in the 316 SS first wall, and how they change the total blanket (including ISSEC) radioactivity and the energy multiplication when they are used at maximum allowable thicknesses, respectively, for pure radiation and radiation plus conduction cooling schemes. We also list the fabricated materials costs of the five ISSECs if they were to be used in a UWMAK-type reactor with a 13 m major and 5 m minor radius and the thickness shown. Factors that limit the maximum thickness of each ISSEC material are shown in parentheses by the thickness values. The maximum ISSEC temperatures are also shown.

It is interesting to note that all five materials reduce the displacement damage by $\sim$1/2 (to within 25%) and the helium production is reduced by a factor of 2 to 6. The only ISSEC material to result in an overall reduction in blanket radioactivity at shutdown

Table V.25

Comparison of the Five ISSEC Materials Considered in This Study

Material	Maximum Thickness(cm)	Maximum Temp. (°C)	Reduction Factors in 316SS First Wall(1)		Total Blanket Radioactivity(1)			Increase in Energy Production(4)	Relative Fabricated Cost
			dpa	Appm He	Shutdown	1 Yr.	1000 Yr.		
				(a) Radiation Cooling Only					
C	9.5(V.P.)	2000	0.49	0.34	0.46	0.37	0.60	0.96	1(2)
Mo	7.5(V.P.)	1950	0.4	0.16	3.78	0.23	267	1.15	55
Nb	8.5(B.R.)	2050	0.36	0.15	3.83	0.34	9.87	1.04	48
V	4.5(V.P.)	1300	0.59	0.41	1.19	0.52	1.07	0.90	36
W	6(B.R.)	1900	0.37	0.19	5.11	1.66	0.77	1.05	53
				(b) Radiation Plus Conduction Cooling					
C	13(B.R.)	1900	0.4	0.24	0.33	0.22	0.48	0.96	1(3)
Mo	10(B.R.)	1350	0.30	0.10	4.72	0.15	365	1.17	54
Nb	8.5(B.R.)	1300	0.36	0.15	3.83	0.34	9.87	1.04	35
V	8(V.P.)	1300	0.43	0.23	1.95	0.35	1.01	0.88	53
W	6(B.R.)	1150	0.37	0.19	5.11	1.66	0.77	1.05	39

V.P. = Vapor Pressure
B.R. = Breeding Ratio
(1) Values normalized to 1.0 in blanket with no ISSEC
(2) Normalized cost 3.94×10^6 $
(3) Normalized cost 5.4×10^6 $
(4) Using standard blanket as 1.0

is carbon while all of the metallic ISSECs increase the activity. After 1 year of decay the total radioactivity of the ISSEC and blanket is reduced for all the materials except W. On the other hand, the long term activity (at 1000 years after shutdown) is increased for Mo, Nb, and V ISSECs while it is reduced by 23% with W and almost 50% with C. The carbon and V ISSECs reduce the energy production per fusion while the Nb and W slightly increase it and Mo results in a 15-17% energy production increase. Finally, the relative cost of the metal ISSECs to produce the above results is a factor of 30-55 higher than the cost of a carbon ISSEC. The advantages and disadvantages of each ISSEC material as compared to others considered in this study are summarized in Table V.26.

Examination of Tables V.25 and V.26 show that because of its various disadvantages such as high vapor pressure, low melting point, reduction in nuclear heating in the blanket, high cost, etc., V would probably not make a good ISSEC material. Comparing Mo and Nb one can see that Mo in every respect is as good or better than Nb. Therefore, Mo would be considered to be a better ISSEC material than both V and Nb. A comparison between Mo and W is difficult in that W has the most desirable advantages from the point of view of reducing radiation damage in the first structural wall, low vapor pressure, high melting point, and low long term radioactivity, but it is much harder to fabricate and it is also hard to breed tritium. In fact, as we see in Table V.25, a breeding ratio limited 6 cm thick W

Table V.26

Comparison of Various ISSEC Materials Considered in this Study

	Carbon	Molybdenum	Niobium	Vanadium	Tungsten
Major Advantages:	. Low radioactivity	. Effective in reducing radiation damage to first wall	. Low vapor pressure	. High (n,2n) cross section	. Most effective in reducing the dpa and gas production rates in the first wall
	. Low afterheat	. Increases nuclear heating in blanket	. Increases nuclear heating in blanket	. Low long term radioactivity	. Low vapor pressure
	. Low cost	. High (n,2n) cross section	. High thermal conductivity		. High thermal conductivity
	. Easily fabricated	. High thermal conductivity	. Low vapor pressure		. High thermal shock resistance
	. Good vacuum properties	. High melting point			. High melting point
	. Low vapor pressure	. Low vapor pressure			. Low long term radioactivity
	. Low blistering rate				. Increases nuclear heating in blanket
	. High temperature strength				
	. Good thermal shock resistance				
Major Disadvantages:	. Less effective in reducing dpa and gas production rates in the first structural wall	. High short and long term radioactivity	. Embrittled by small amounts of C, O, N	. High vapor pressure	. Hard to fabricate
	. Reduces nuclear heating in the blanket	. Hard to fabricate	. High cost and U.S. resource problem	. Availability and high cost	. Availability
	. Chemical sputtering CH_4 at < 800°C C_2H_2 at > 1200°C (?)	. High cost	. High long term radioactivity	. Blistering	. High cost
		. Blistering	. Blistering	. Low thermal shock resistance	. Hard to breed tritium
				. Low melting point	. High radioactivity at shutdown
				. Reduces nuclear heating in blanket	. Blistering

ISSEC is less effective than 10 cm thick Mo ISSEC (also limited by breeding ratio) in reducing the dpa and helium production rates in the first wall. Based on these considerations at the present time Mo would be the best of the four metals studied for use as an ISSEC material.

A definitive choice between a graphite ISSEC and a Mo ISSEC is also not clear. From radioactivity, afterheat, cost, and fabricability standpoint, graphite is clearly superior to Mo, but Mo reduces the radiation damage in the first structural wall more (by 20% in dpa and ∿100% in He production) and increases the energy multiplication in the blanket (by as much as 15-17%). If indeed the question of C_2H_2 formation between hydrogen ions and C at high temperatures is resolved, the choice might become clearer, but at this time neither C nor Mo has a clear superiority over the other.

V.B.8. Conclusions

A few general conclusions can be gathered from these studies about both graphite and metal ISSEC cases.

- ISSECs reduce the displacement damage in the first structural wall. Reduction factors vary between 2-5 for a 10 cm thick ISSEC, between 5-50 for a 25 cm thick spectral shifter.
- The gas production rates in the first structural wall are also reduced by ISSECs. Helium production rates are reduced by factors of 3.2-12 with a 10 cm thick ISSEC and by factors

of 12 to 275 with a 25 cm thick ISSEC. The reductions in hydrogen production rates are 2.5 to 12.7 and 8 to 235 respectively with 10 cm and 25 cm shield thickness.

. The short and intermediate term radioactivity, Biological Hazard Potential (BHP) and afterheat of the 316 SS first wall are reduced by all ISSECs, and the long term activities are actually increased by a 10 cm or thicker carbon ISSEC.

. All five ISSECs reduce the breeding ratio in the model blanket used in this study. Reduction factors vary between 1.25 and 2.1 for a 10 cm thick ISSEC and between 2.1 and 13.6 for a 25 cm thick ISSEC.

. Mo, Nb, and W ISSECs increase the total energy available per fusion in the model blanket of this study while C and V ISSECs decrease it.

. The radioactivity of the total blanket (including the ISSEC) a short time after shutdown is higher than the unprotected case for W, Mo and Nb ISSECs but it is lower with C and V ISSECs. At 1-10 years after shutdown the blanket has about the same radioactivity with and without an ISSEC. But a long time after shutdown (longer than 100 years) a Mo ISSEC system has the most radioactivity followed by the Nb ISSEC system. Carbon, W, and V ISSEC protected designs have about the same radioactivity as unprotected blankets.

- Maximum displacement rates in the ISSECs themselves per 1 MW/m^2 neutron wall loading per year vary between 8.4 for Nb and 12.5 dpa/yr for V. Maximum helium production rates vary between 3.7 for W and 2300 appm/yr for C.
- The radioactivity at shutdown of all metal ISSECs is about the same order of magnitude (1-10 Ci/W), and is higher than that of C ISSEC by a factor of about 10^4. At long times after shutdown (longer than 100 years) radioactivity in C, W and V ISSEC has decayed away while in Mo it is $\sim$0.001 times its value at shutdown and in Nb about 10^{-4} times its shutdown value.
- Most ISSECs cooled only by thermal radiation are limited by their vapor pressure and the maximum allowable thicknesses are 9.5 cm for C, 7.5 cm for Mo, and 4.5 cm for V for a 1 MW/m^2 neutronic and 4 W/cm^2 surface heat loading. Niobium and tungsten are limited to 9 and 12.5 cm by vapor pressure and 8.5 and 6 cm by breeding ratio considerations, respectively.
- A conduction plus radiation cooled ISSEC can have greater thickness up to 15 cm or higher depending on the specific design.
- Molybdenum appears to be the best overall choice for a metal ISSEC (compared to W, Nb, V).

. A definitive choice between a carbon and molybdenum ISSEC cannot be made at this time as both materials have strong positive features but in different areas.

V.C. The Effects of Liquid ISSECs; Li, Pb, and Pb_4Li Eutectic in Inertial Confinement Fusion Reactors

V.C.1. Introduction

The use of a liquid Li ISSEC to protect the first walls of laser fusion reactors has been proposed by scientists at Lawrence Livermore Laboratory.[7] The initial concept involves a 'waterfall' of liquid lithium ranging in thickness from 10-50 cm dropping from the top of a laser fusion reactor to be collected at the bottom of the reaction chamber. The purpose of the waterfall is many fold, and a few of the most obvious reasons are listed below.

. To collect and absorb all photons emitted or reflected from the D-T containing fuel pellet.

. To collect all charged particles (unburnt fuel, reaction products and tamper material).

. To moderate the neutrons in order to reduce the damage in the first wall.

. To breed tritium.

. To absorb any shock wave generated in the reaction chamber by the microexplosion.

In this study in addition to Li, two other materials, Pb and a Pb-Li eutectic (Figure V.29)[135] with a composition of roughly 4 lead atoms to every lithium atom and a melting point of 325°C are con-

sidered as liquid ISSECs and the thickness of the ISSEC is varied up to 100 cm. The Pb-Li eutectic alloy, even though it is not a compound, is represented as Pb_4Li in this study.

In a laser fusion reactor reaction chamber the maximum pressure allowed for laser beam propagation is on the order of 0.1 torr.[136] Figure V.30 shows the vapor pressures of liquid Li and Pb as a function of temperature. The vapor pressure of the Pb-Li eutectic used will probably be between the values for pure Li and Pb. We see from

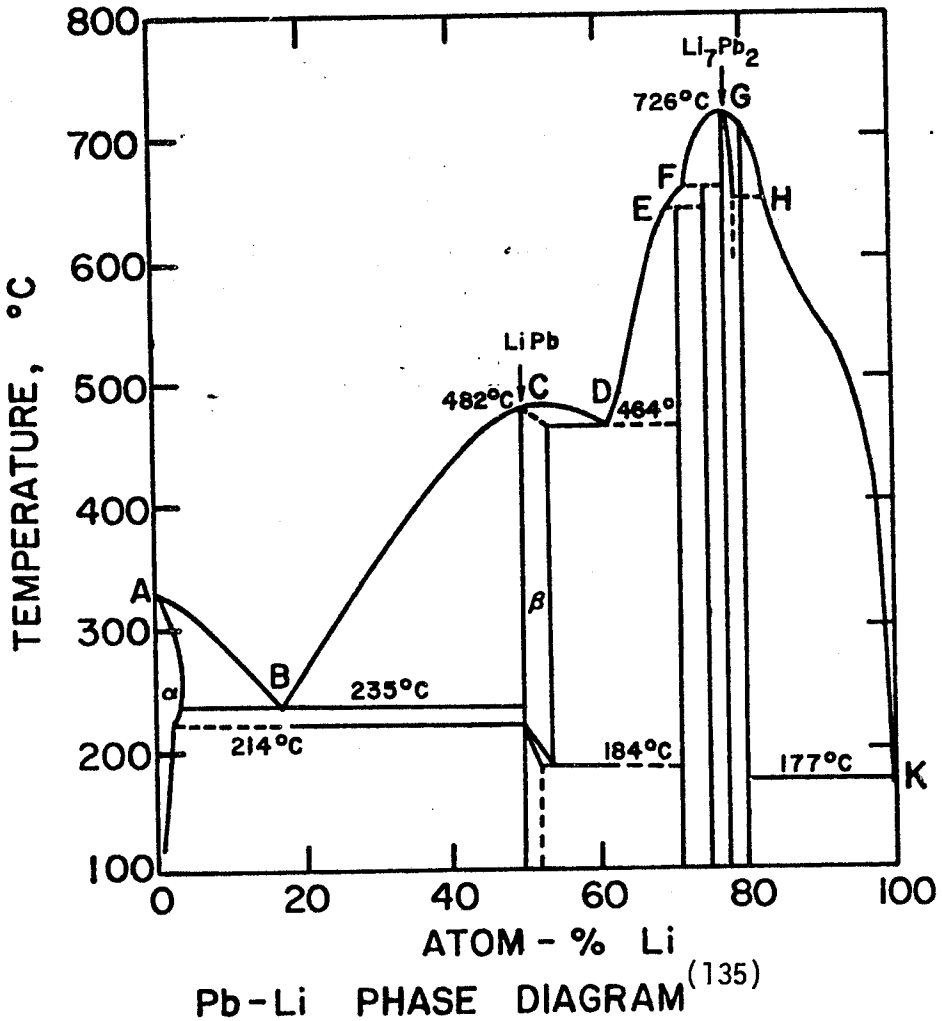

Pb-Li PHASE DIAGRAM[135]

Figure V.29

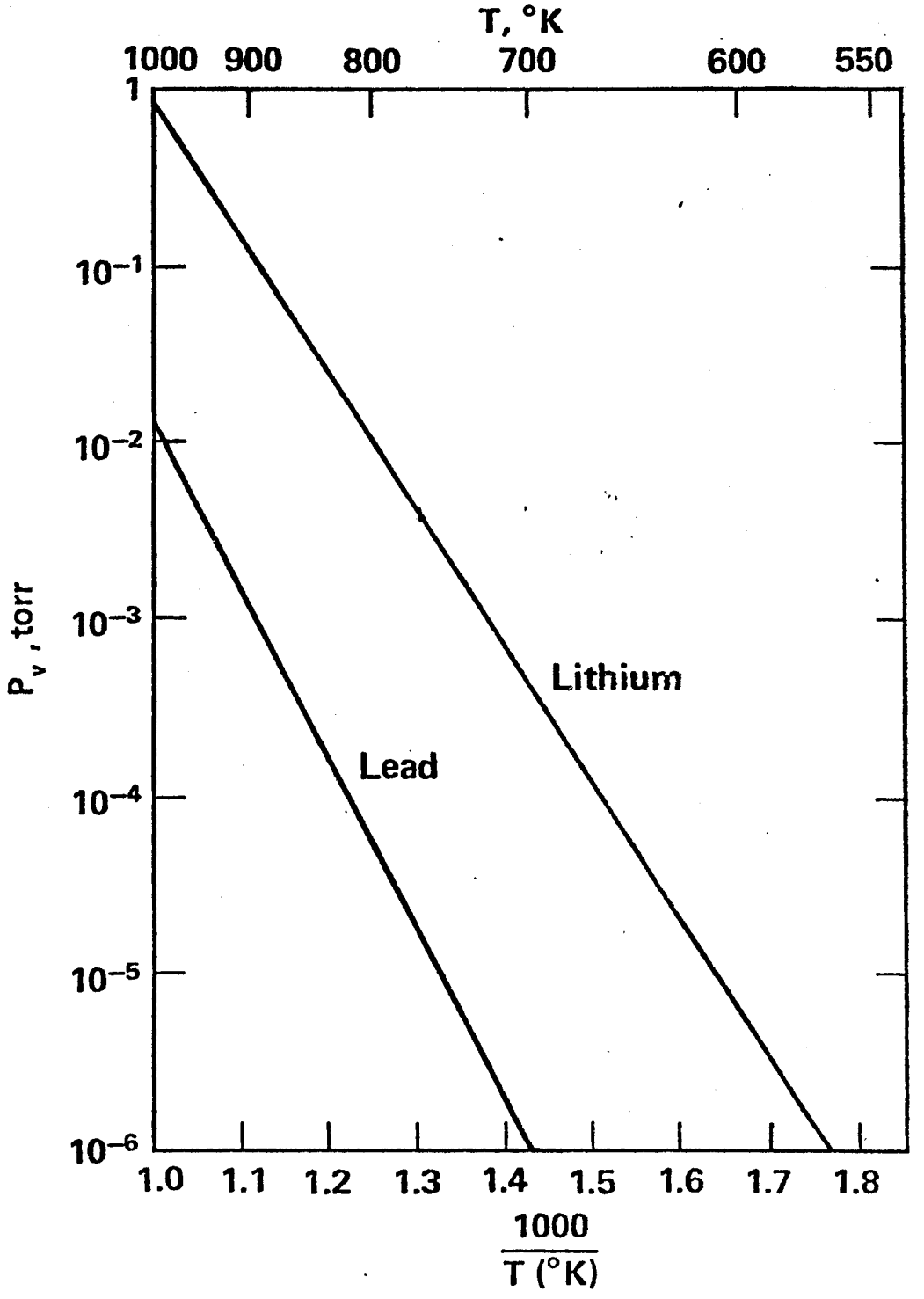

VAPOR PRESSURE VS. TEMPERATURE FOR LIQUID LITHIUM AND LEAD (Ref. 7)

Figure V.30

Figure V.30 that the vapor pressure of liquid Li does not reach 0.1 torr until about 600°C. Liquid Pb has a vapor pressure that is about two orders of magnitude less than that of liquid Li at the same temperature. At such high temperatures corrosion considerations will probably be more restrictive than vapor pressure and depending on the structural material employed a lower maximum temperature limit might be set by those considerations rather than the vapor pressure.

While there are many other questions about the exact mechanism by which this liquid metal 'waterfall' will be formed, and about the rapidity with which the proper geometry can be re-established after the microexplosion, the radiation protection feature of this concept can be estimated at this time.

The blanket geometry used in these calculations is shown in Figure V.11 and the calculational procedures are the same as described in Section V.B.1. The only difference is the ISSEC material and the thickness of it.

V.C.2. Results and Analysis

The information obtained in this part of the study is analyzed with respect to three general categories: a) Damage parameters in the first 316 SS wall, b) Breeding ratio, and c) Heat deposition profiles. Each of these parameters will be considered in turn.

V.C.2.a. Damage Parameters

V.C.2.a.1. Displacement Damage

The effect of the various ISSEC thicknesses on the reduction in displacement damage in the 316 SS first structural wall is listed in

Table V.27 and plotted in Fig. V.31.

The displacement damage after equal thicknesses of Li and Pb are roughly the same but for different reasons. The low moderating power of Li for high energy neutrons tends to maintain a rather hard neutron spectrum. Lead, on the other hand, is much more effective than Li in moderating high energy neutrons but its high (n,2n) and low absorption cross sections result in rather high flux of high energy (> 1 MeV) neutrons to the first wall. The net result is a coincidentally similar effect on the dpa rate with increasing ISSEC thickness. The addition of Li-6 to Pb counters the low absorption characteristics and hence the Pb_4Li alloy is even more effective than either Pb or Li by itself.

V.C.2.a.2. Gas Production

The reduction in the helium and hydrogen production rates with varying thicknesses of ISSEC are also given in Table V.27 and plotted for helium in Figure V.32.

Comparing Figures V.31 and V.32, one can see that the relative effectiveness of all three ISSECs is greater for reducing the helium generation rates in the first wall than it is for reducing displacements. The second thing to notice is that while both Pb and Li are essentially the same in reducing the displacement damage in the first wall, a Pb ISSEC reduces the helium production in 316 SS much more than does a Li ISSEC of the same thickness. The reason for this is that energies of most of the neutrons coming from the (n,2n) reactions of Pb are below the threshold values for the (n,α) reactions

Table V.27

Summary of Radiation Damage in 316 SS First Wall Behind Various ISSECs

ISSEC Material	dpa/yr ($1\ MW/m^2$)	Appm He/yr ($1\ MW/m^2$)	Appm H/yr ($1\ MW/m^2$)
None	10.1	218	470
	20 cm		
Li	5.4	82	210
Pb	4.8	14	37
Pb_4Li	4.0	13	35
	40 cm		
Li	2.8	32	96
Pb	2.6	1.8	5.4
Pb_4Li	1.6	1.5	4.4
	100 cm		
Li	0.5	2.0	10.5
Pb	0.4	0.004	0.4
Pb_4Li	0.1	0.002	0.012

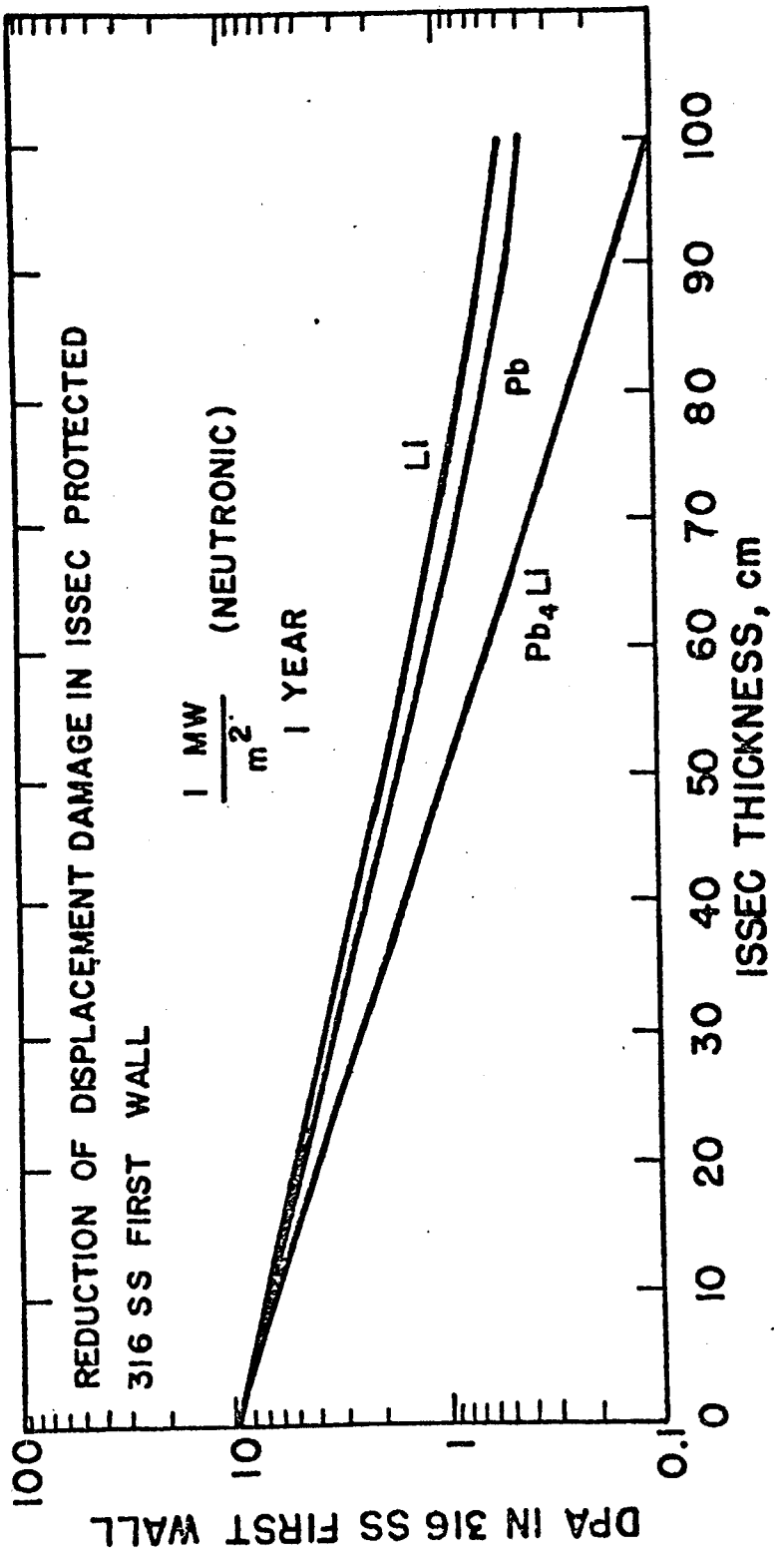
REDUCTION OF DISPLACEMENT DAMAGE IN ISSEC PROTECTED
316 SS FIRST WALL
1 MW/m² (NEUTRONIC)
1 YEAR
Li
Pb
Pb4Li
DPA IN 316 SS FIRST WALL
ISSEC THICKNESS, cm
100
10
1
0.1
0
10
20
30
40
50
60
70
80
90
100

Figure V.31

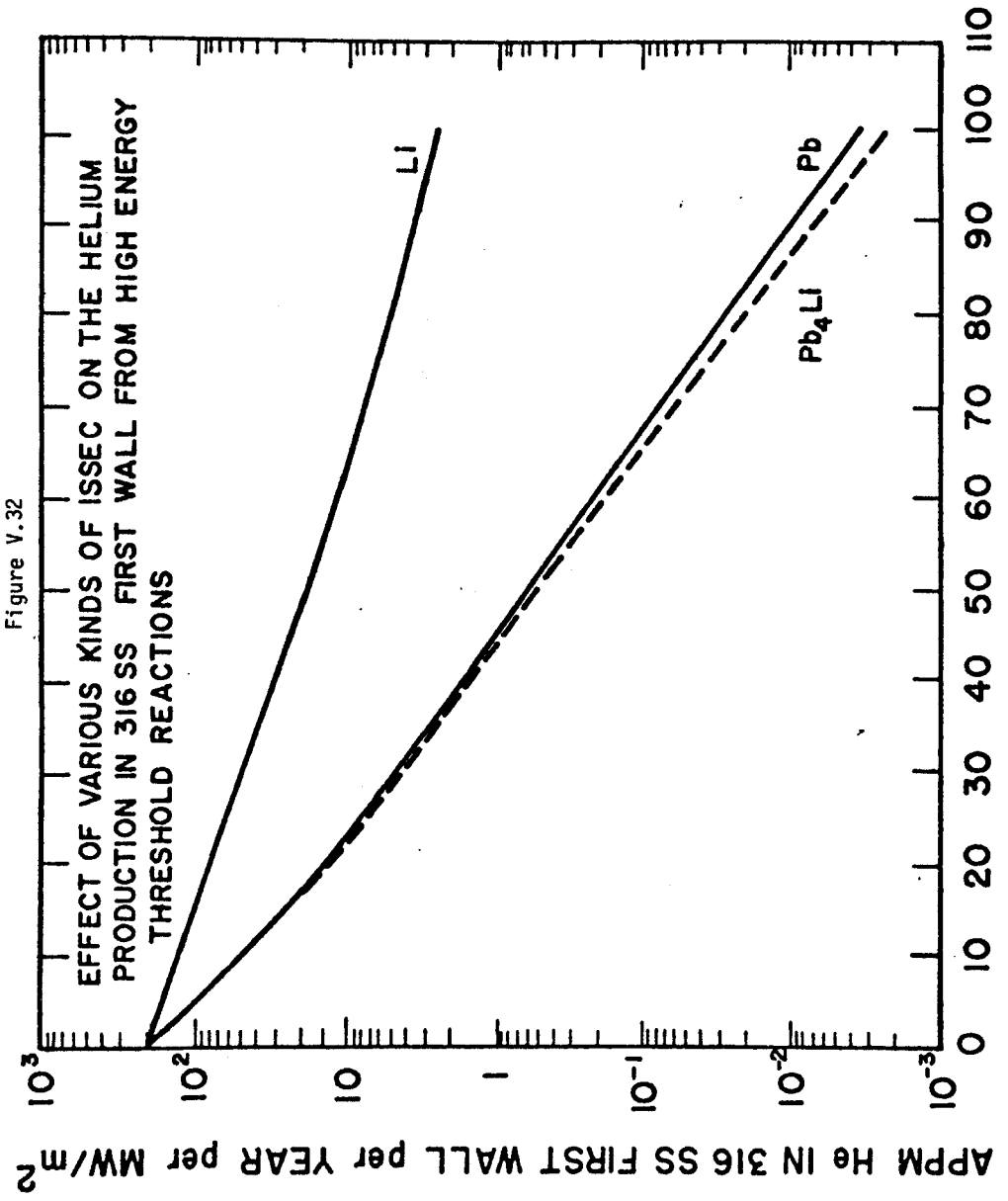
EFFECT OF VARIOUS KINDS OF ISSEC ON THE HELIUM PRODUCTION IN 316 SS FIRST WALL FROM HIGH ENERGY THRESHOLD REACTIONS
Li
Pb
Pb4Li
APPM He IN 316 SS FIRST WALL per YEAR per MW/m2
ISSEC THICKNESS, cm
10^3
10^2
10
1
10^-1
10^-2
10^-3
0
10
20
30
40
50
60
70
80
90
100
110

Figure V.32

in steel. The effectiveness of the liquid Pb_4Li ISSEC in reducing the helium production in the 316 SS first wall is a little higher than that of a pure Pb.

V.C.2.b. Breeding Ratio

Figure V.33 shows the total breeding ratio in the system as a function of ISSEC thickness. Also shown in Figure V.33 is the breeding in just the ISSEC for Li and Pb_4Li ISSEC cases. It can be seen from that figure that the overall breeding ratio initially increases in all three cases. It saturates in Li and Pb_4Li cases after about 30 cm of ISSEC thickness but it starts to decrease after about 30 cm of thickness in the case of Pb. The breeding ratio in just the ISSEC itself exceeds 1.0 in Li and Pb_4Li ISSECs after about 30 and 50 cm thicknesses, respectively. The significance of this is that one can do all the breeding inside the reaction chamber with Li and Pb_4Li ISSECs and there is no need to breed tritium behind the first solid wall.

V.C.2.c. Energy Extraction

Total energy absorbed in the ISSEC plus the blanket per neutron born in D-T is plotted in Figure V.34 as a function of ISSEC thickness. The total heating in the blanket without any ISSEC protection is 19.6 MeV/n, and it stays surprisingly constant as the thickness of the Li ISSEC is increased. On the other hand, the total heating in the Pb_4Li ISSEC system initially shows a large increase, but after

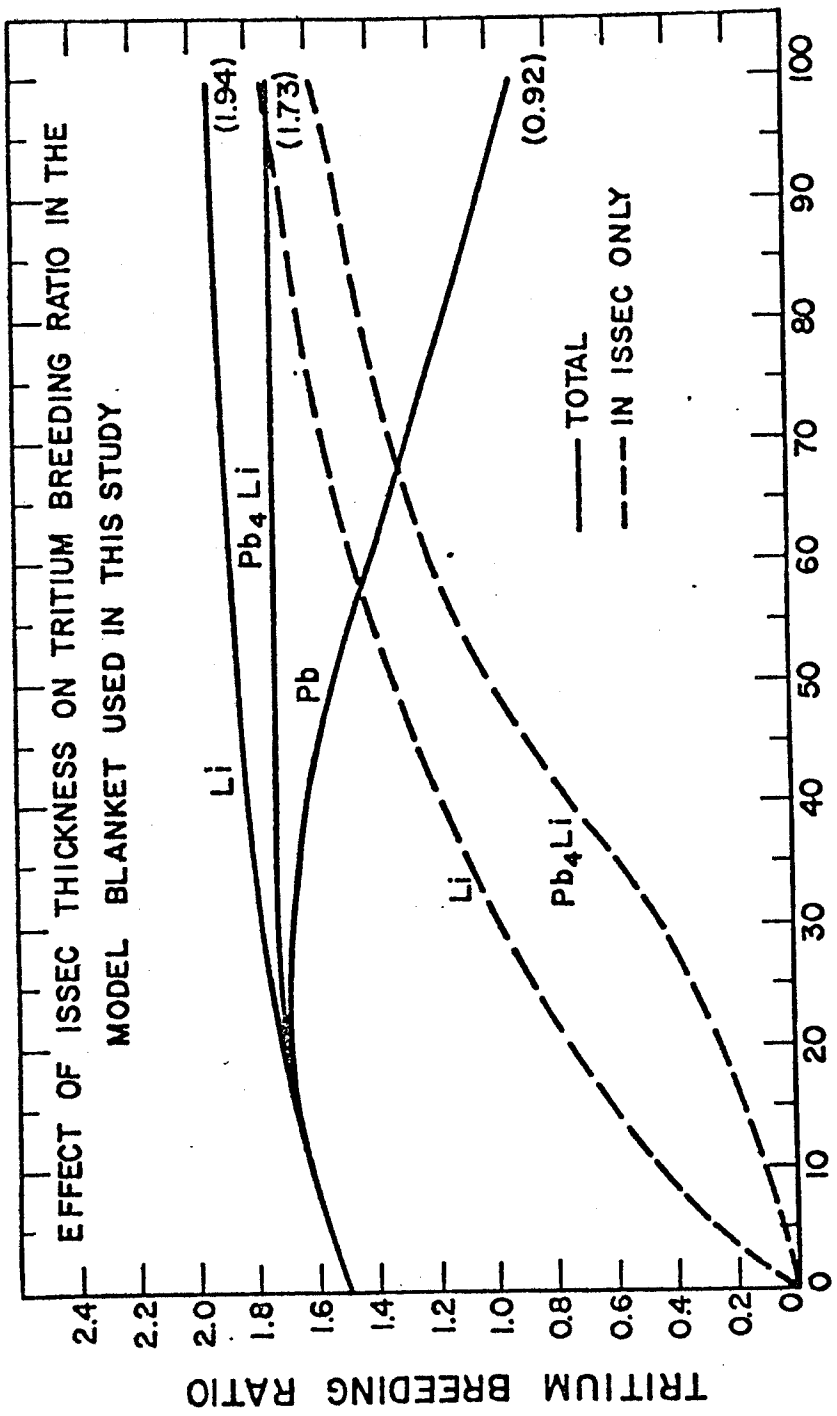
EFFECT OF ISSEC THICKNESS ON TRITIUM BREEDING RATIO IN THE MODEL BLANKET USED IN THIS STUDY
TRITIUM BREEDING RATIO
ISSEC THICKNESS, cm
TOTAL
IN ISSEC ONLY
Li
Pb4 Li
Pb
(1.94)
(1.73)
(0.92)
Li
Pb4Li
0
0.2
0.4
0.6
0.8
1.0
1.2
1.4
1.6
1.8
2.0
2.2
2.4
0
10
20
30
40
50
60
70
80
90
100

Figure V.33

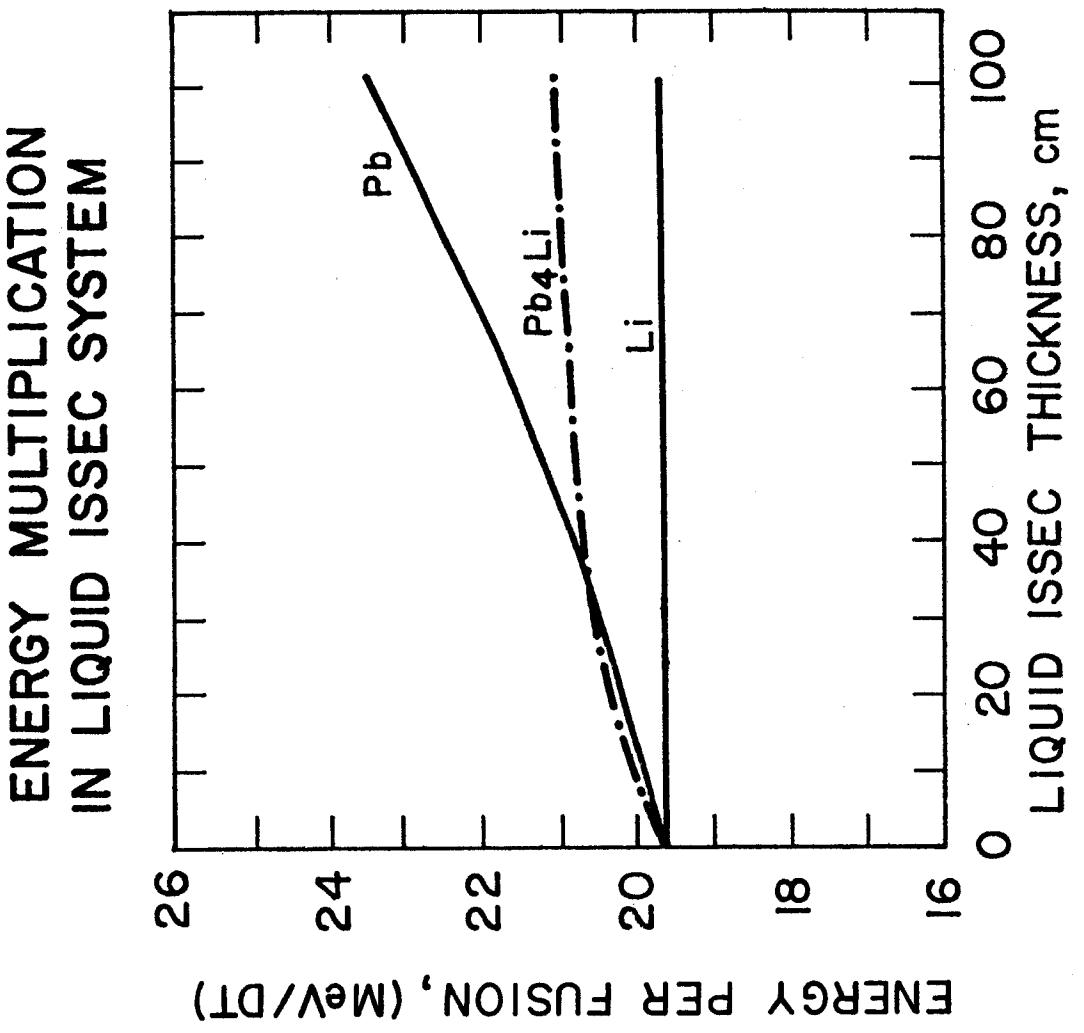
ENERGY MULTIPLICATION
IN LIQUID ISSEC SYSTEM
ENERGY PER FUSION, (MeV/DT)
26
24
22
20
18
16
0
20
40
60
80
100
LIQUID ISSEC THICKNESS, cm
Pb
Pb4Li
Li

Figure V.34

about 30 cm thickness, it levels off at ∿21.0 MeV/n, a value in between that of pure Li and Pb.

The fraction of energy absorbed in the liquid ISSEC (including charge particles) is plotted in Figure V.35, and it shows that for thickness of 20-30 cm, the ISSEC zone will generate >50% of the energy. The fraction of heat collected in ISSEC is always greater with Pb_4Li ISSEC than with pure Li and Pb. Ninety (90) percent of heat in a liquid Pb_4Li ISSEC system is deposited in about 77 cm of ISSEC and only 2% of the total heat is left for the blanket behind a 100 cm liquid Pb_4Li zone. Proportionately less energy is absorbed in the Pb ISSEC because of the breeding behind the first wall. About 20% of the total heat generated in that system remains to be collected in the blanket even after a 100 cm thick ISSEC zone.

The absolute amount of heat deposited in Pb_4Li ISSEC is also always greater than both in Pb and Li. At 50 cm thickness, for example, the amount of heat absorbed in the ISSEC is 16.0 MeV/n for Pb_4Li, 15.2 MeV/n for Li, and 12.8 MeV/n for Pb. At 90 cm ISSEC thickness 17.6 MeV/n is deposited in both Li and Pb ISSECs but the amount of heat absorbed in Pb_4Li ISSEC is 19.8 MeV/n. At 100 cm thickness the amount of energy deposited in ISSEC per neutron born in D-T plasma is 20.6 MeV for Pb_4Li, 18.8 MeV for Pb and 18.1 MeV for Li.

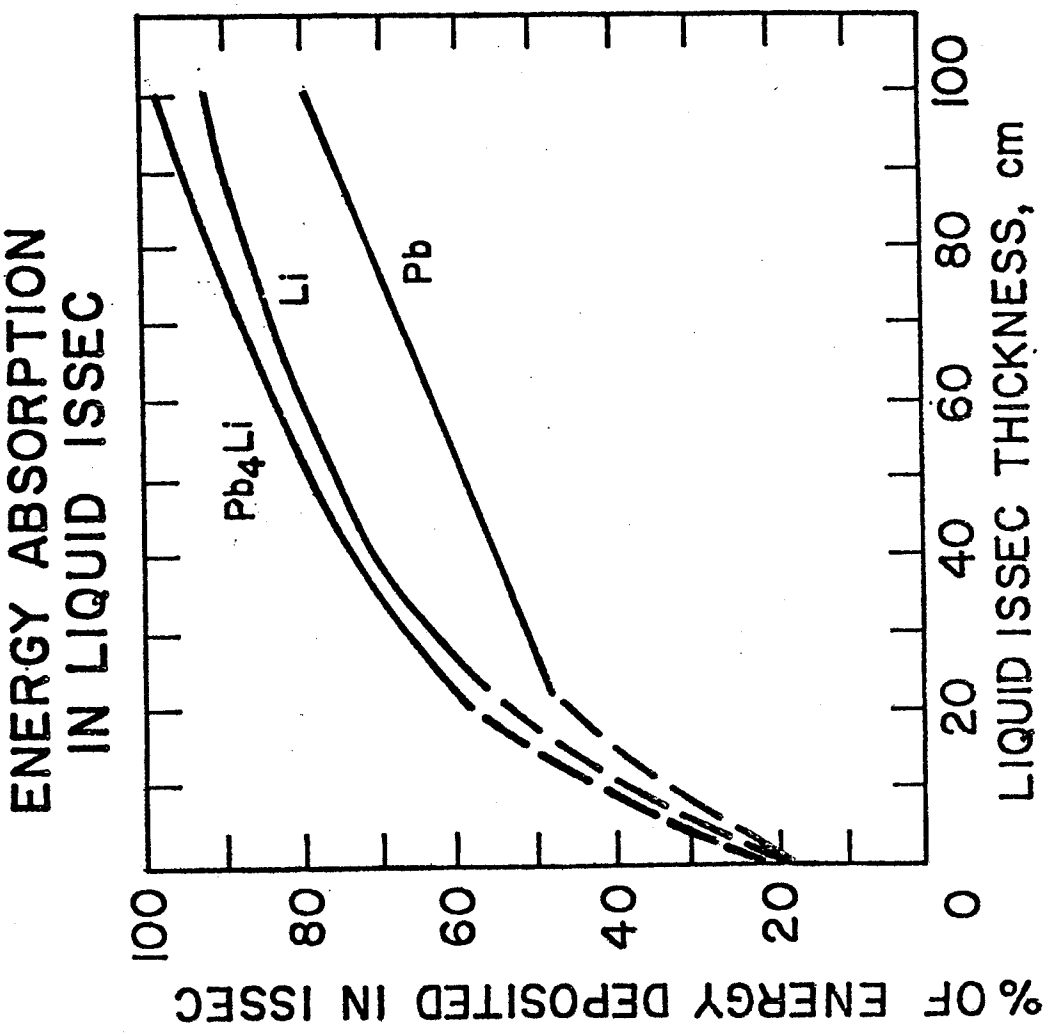
ENERGY ABSORPTION
IN LIQUID ISSEC
Pb4Li
Li
Pb
% OF ENERGY DEPOSITED IN ISSEC
LIQUID ISSEC THICKNESS, cm
0
20
40
60
80
100

Figure V.35

V.C.3. Discussion on Results Obtained in This Section

Aside from protecting the first walls of a laser fusion reactor against high fluxes of photons and charged particles (which could be done by a relatively thin stream of liquid) it is important to see what beneficial effect the concept can have on extending the useful first wall lifetime.

For an illustrative example let us consider 316 SS at three different temperatures; 600°C, 500°C, and 300°C. The criteria for failure is different in each of these temperature ranges. Helium embrittlement is the limiting feature of 600°C, void swelling is the problem at 500°C, and crack propagation and helium gas bubble swelling is critical at 300°C. While the exact dpa and helium concentration limits are not known for these regimes, a conservative estimate on the basis of past experience leads to the projections shown in Table V.28. Assuming that we desire to have "permanent" first wall for 30 years of operation at a nominal wall loading of 5 MW/m^2 and a plant factor of 70%, we can use the information in Tables V.28 and V.27, and Figures V.31 and V.32 to estimate the required ISSEC thickness. The necessary ISSEC thickness is given in Table V.29. Taking the higher value of the two thicknesses associated with each ISSEC material at each first wall temperature in Table V.29 as the design limit, we list in Table V.30 what the other system parameters would be for that thickness of an ISSEC.

Table V.28

Estimate of Damage Limitations in 316 SS Irradiated in a Fusion Neutron Spectrum

	Design Limit	
Temperature °C	dpa	appm He
300	200*	4000
500	150*	500
600	100	10*

*Limiting Parameter

Table V.29

Summary of Liquid Metal ISSEC Thickness Required to Extend 316 SS First Wall Life to Reactor Life[a]

	Require ISSEC Thickness-cm					
Temperature °C	Li		Pb		Pb_4Li	
	dpa	He	dpa	He	dpa	He
300	52	37	47	12	37	12
500	58	~85	52	30	41	30
600	74	~200	67	67	50	65

(a) 5 MW/m^2 at 70% P.F. for 30 years. (1060 dpa, 22,900 appm He accumulated for an unprotected wall.)

Table V.30

Summary of Necessary Liquid ISSEC Thicknesses Required to Extend Useful Lifetime of 316 SS to 30 Years at 70% P.F. and 5 MW/m^2 Wall Loading

System Parameters

Temperature °C	Thickness cm	dpa/yr	Appm He/yr	B.R.^{T}	B.R.^{I}	MeV n	% Energy in ISSEC
		Lithium					
300	52	6.67*	63	1.9	1.36	19.7	77
500	85	2.4	16.7*	1.9	1.66	19.7	89
600	~200	~0.02	~0.33*	~2	~2	19.7	~100
		Lead					
300	47	6.67*	2.8	1.58	---	21.0	59
500	52	5.0*	1.8	1.50	---	21.3	61
600	67	3.3*	0.33*	1.34	---	22.2	67
		Pb_4Li					
300	37	6.67*	7.0	1.73	0.62	20.6	71
500	41	5.0*	4.55	1.73	0.68	20.7	73
600	65	1.85	0.33*	1.73	1.24	20.8	85

*Design Limit

B.R.^{T} --- Total Breeding ratio in system

B.R.^{I} --- Breeding ratio in ISSEC only

The required ISSEC thickness to reduce the dpa level to value desired at end of life (Table V.28) falls in the general range of 45-75 cm for Li and Pb and 35-50 cm for Pb_4Li. The requirements from the helium generation levels are generally more severe for Li and it is found that the ISSEC thickness must be much greater than 1 meter and probably on the order of 2 meters for 600°C operation. At all three first wall temperatures and from both the dpa and appm He considerations, the required ISSEC thickness to extend the first wall lifetime to 30 years at 5 MW/m^2 wall loading at 70% plant factor is <u>less</u> for a Pb_4Li ISSEC than it is for Li ISSEC. From the displacement damage point of view less thickness of Pb_4Li is required for full lifetime operation than for pure Pb, but from the helium production point of view the required ISSEC thickness is about the same for both materials.

It appears from Tables V.29 and V.30 that the main advantage of a pure Li ISSEC system is its high breeding ratio. Although all three systems have quite adequate overall breeding, only Li ISSEC shows an internal breeding ratio greater than one at ISSEC thicknesses less than 50 cm. If an ISSEC thickness of more than 50 cm is required, Pb_4Li is clearly superior to both Li and Pb in that it has higher percentage of energy deposited in ISSEC, it can breed internal to the first structural wall and with 65 cm thickness the first wall can run at any temperature less than 600°C and still meet its design criteria for a full lifetime operation.

There is an ISSEC thickness above which it probably makes no sense to run the first wall hot because there is very little heat to collect. For example it is entirely conceivable that one could collect the last 10% of the energy at 300°C and not suffer very greatly on overall efficiency. This could especially be true if the ISSEC increased the overall heating rate in the system as does Pb and Pb_4Li ISSECs. The limit at which 90% of total heat is deposited inside ISSEC is ∿90 cm for Li, ∿120 cm for Pb and ∿77 cm for Pb_4Li.

The concept of 'cold' first walls and blankets has a great attractiveness because it would significantly reduce the complexity of the reactor design and perhaps even the tritium leakage.

V.C.4. Conclusions of this Section

It has been shown that either a 45-75 cm thick liquid, Li or Pb ISSEC or a 35-50 cm Pb_4Li ISSEC can reduce the displacement damage in the 316 SS first structural wall to such levels as to allow it to achieve a 'permanent' lifetime (∿100 MW-yr/m^2) in a laser fusion reactor. Pb and Pb_4Li ISSECs are much more effective in reducing the helium production in the first wall than Li. The Pb ISSEC is the most effective in increasing the energy multiplication in the blanket, but Pb_4Li ISSEC has the highest percentage of energy deposited in the liquid ISSEC region.

Conclusions regarding each of the ISSEC materials considered are listed below separately:

Li:

- High breeding ratio, both overall and internal,
- Least effective in reducing the helium production rates in the 316 SS first wall; therefore suitable for low temperature operation only.

Pb:

- Increases the thermal output of the system by increased energy multiplication,
- Effective in reducing the helium production in the 316 SS first wall,
- Does not allow breeding internal to the first structural wall,
- Double heat extraction scheme is required; both from the ISSEC and from the blanket behind the first wall.

Pb_4Li:

- Increases the thermal output,
- Effective in reducing the helium generation in the 316 SS first wall,
- Most effective in reducing the displacement damage in the first wall,
- For thicknesses greater than 50 cm breeding internal to the first wall is possible,
- For the same thickness both the percentage and the absolute amount of energy deposited in ISSEC is highest.

An overall conclusion to be obtained from this study is that the liquid ISSEC material that has the best overall characteristics is Pb_4Li and the thickness to be used is 50 to 75 cm.

V.D. The Effect of Displacement Cross Sections Calculated by the DISCSM Code on the Reduction of Displacement Damage in Various First Wall Materials by ISSECs

The displacement cross sections for various elements have recently been recalculated by the author using the DISCSM code with proper inclusion of charged particle-out [(n,p), (n,α), (n,n'p), (n,n'α), etc.], and (n,γ) reactions, and using the ENDF-IV data rather than ENDF-III as in previous calculations.[43,67] The DISCSM calculations show the displacement cross sections to be higher than the old ones at high neutron energies. These newer cross sections were available after the bulk of calculations for this thesis had been completed. How the displacement rates listed in Tables V.1, and V.27 and displayed in Figure V.12 would have differed if these new cross sections had been used is illustrated below for Nb and 316 SS first walls.

As an example, to show the difference between the old and newer set of cross sections we plot in Figure V.36 for 316 SS the older cross sections of D.G. Doran[43,67] and the newer set of cross sections calculated using the DISCSM code.

The newer cross sections would increase the effectiveness of the ISSEC in reducing the displacement damage in the first wall,

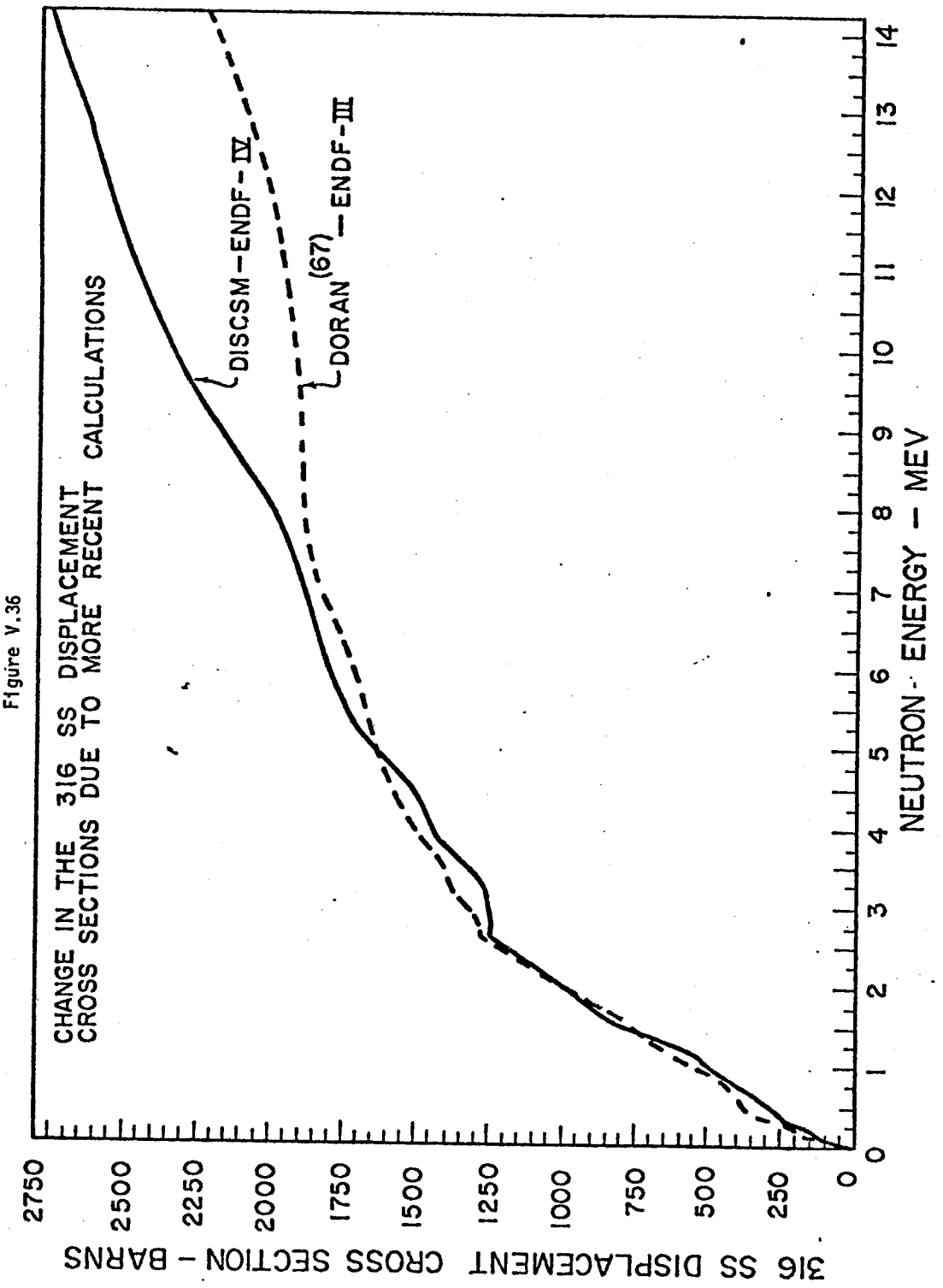
CHANGE IN THE 316 SS DISPLACEMENT CROSS SECTIONS DUE TO MORE RECENT CALCULATIONS
DISCSM-ENDF-IV
DORAN(67)-ENDF-III
316 SS DISPLACEMENT CROSS SECTION - BARNS
NEUTRON ENERGY - MEV
0
250
500
750
1000
1250
1500
1750
2000
2250
2500
2750
1
2
3
4
5
6
7
8
9
10
11
12
13
14

Figure V.36

because the dpa rates in the unprotected first wall would go up more than in the protected wall where the average neutron energy is lower. This is shown in Tables V.31, V.32, and V.33 where factors of reduction in the displacement rates in Nb, and 316 SS first walls are higher when the newer set of displacement cross sections are used. The results are similar for the other first wall materials.

V.E. Discussion on Results Presented in Sections V.A., V.B., and V.C.

It is seen that all ISSECs, solid or liquid, reduce the displacement and gas production rates in the first structural wall of a fusion reactor. Reduction factors in the displacement damage vary between 0 (which corresponds to the case of a very thin curtain) and 100 depending on the first structural wall material, the particular type of ISSEC, and the thickness of the ISSEC. Helium and hydrogen production rates are reduced by factors of 0 to about 10^5. If the first wall lifetime is determined by the displacement rate alone, it will increase by factors of up to 100. If the helium production is the sole determining factor the first wall life will increase up to 10^5 times over the lifetime of an unprotected wall. Actually the first wall lifetime will be determined by a combined effect of displacement damage and the gas production rates along with others such as the temperature, microstructure and the amount of cold work put in. Therefore, the actual realizable benefit from the point of view of an increase in the first structural wall lifetime due to an ISSEC,

Table V.31

Effect of the Displacement Cross Sections Calculated by the DISCSM Code on the Reduction of Displacement Damage in Nb and 316 SS First Walls by a Carbon ISSEC (slab geometry blanket model)

First Wall Material	Carbon ISSEC Thickness-cm	Doran-(67) ENDF-III dpa/yr	Doran-(67) ENDF-III Reduction Factor	DISCSM-ENDF-IV dpa/yr	DISCSM-ENDF-IV Reduction Factor
		(a) D-D Plasma			
Nb	0	10.8	-	11.3	-
	12.5	2.14	0.20	2.14	0.19
	25	0.54	0.05	0.54	0.048
316 SS	0	16.8	-	18.1	-
	12.5	3.2	0.19	3.31	0.18
	25	0.86	0.051	0.84	0.046
		(b) D-T Plasma			
Nb	0	8.48	-	9.09	-
	12.5	1.64	0.19	1.67	0.18
316 SS	0	11.3	-	13.1	-
	12.5	2.50	0.22	2.61	0.20

Table V.32

Effect of Displacement Cross Sections Calculated by the DISCSM Code on the Reduction of D-T Displacement Damage in 316 SS First Wall by Carbon and Metallic ISSECs

		Doran-(67) ENDF-III		DISCSM-ENDF-IV	
	ISSEC thickness-cm	dpa/yr	Reduction Factor	dpa/yr	Reduction Factor
No ISSEC		10.1		11.4	
C ISSEC	5	6.79	0.67	7.48	0.66
	10	4.78	0.47	5.15	0.45
Mo ISSEC	5	5.26	0.52	5.29	0.46
	10	3.01	0.30	2.84	0.25
Nb ISSEC	5	5.14	0.51	5.22	0.46
	10	3.14	0.31	2.98	0.26
V ISSEC	5	6.61	0.56	5.88	0.52
	10	3.59	0.36	3.57	0.31
W ISSEC	5	4.33	0.43	4.36	0.38
	10	2.07	0.20	1.97	0.17

Table V.33

Effect of Displacement Cross Sections Calculated by the DISCSM Code on the Reduction of Displacement Damage in 316 SS First Wall by Liquid ISSECs

First Wall Material	ISSEC thickness-cm	Doran-(67) ENDF-III dpa/yr	Doran-(67) ENDF-III Reduction Factor	DISCSM-ENDF-IV dpa/yr	DISCSM-ENDF-IV Reduction Factor
None		10.1	-	11.4	-
Li	40	2.8	0.28	2.6	0.23
	100	0.5	0.05	0.35	0.03
Pb	40	2.6	0.26	2.4	0.21
	100	0.4	0.04	0.28	0.025
Pb_4Li	40	1.6	0.16	1.4	0.12
	100	0.1	0.01	0.06	0.005

which translates into a net economic benefit from the operation, maintenance and materials cost of the power plant, might be somewhat different than what is implied by the numbers given above. However, the economic gains due to an increase in the lifetime of the first structural wall are still expected to be high. This would especially be true if the ISSEC also happens to increase the energy multiplication in the blanket as in the case of Mo, Nb, W, Pb, and Pb_4Li ISSECs.

As can be seen from the results in Sections V.A. and V.B., the blanket geometry employed has a sizeable effect on the calculated effectiveness of the ISSEC in reducing the radiation damage parameters in the first structural wall. For example, for a carbon ISSEC and the 316 SS first wall combination the results in Figures V.3 and V.6 of Section V.A., indicate that a 10 cm carbon ISSEC reduces the displacement damage and the helium production in the first wall by factors of 3.5 and 5.7 respectively. On the other hand, results in Figures V.12 and V.13 of Section V.B. give reduction factors of 2.2 and 3.1 for the displacement and helium gas production rates in the 316 SS first wall for the same thickness of a carbon ISSEC. The discrepancy comes from several causes such as 1) slab versus cylindrical geometry calculations, 2) the difference in the thickness and the composition of the blanket regions behind the first wall, and 3) a shift from ENDF-B/III to ENDF-B/IV in nuclear data input for the ANISN program. The neutron source conditions were the same in calculations both in Sections V.A. and V.B. It was a uniform isotropic source.

Of the three reasons given above the first one is believed to be the overriding one. In comparing the slab geometry to cylindrical geometry the calculated effectiveness of an ISSEC is reduced because of two factors; a) in the case of an unprotected wall, neutrons spend more time slowing down and therefore cause more reactions in the first wall for the slab geometry case. As a result, both the displacement and gas production rates are higher (11.3 dpa/yr versus 10.1 dpa/yr in displacement damage and 280 appm/yr versus 218 appm/yr in helium gas production). b) In the case of an ISSEC protected wall, because the neutrons spend more time slowing down in the ISSEC and causing more reactions, the current of neutrons that are passing through the first wall is softer in the slab geometry case than for cylindrical geometries. This gives rise to lower displacement and gas production rates in the first structural wall in slab geometry than in cylindrical geometry calculations. The net effect of a) and b) is that the reduction factors are lower in cylindrical geometry calculations.

The reason number 3, given above, might also be important in the case of a carbon ISSEC because the gas production cross sections of C^{12} were lower in ENDF-B/IV than they were in ENDF-B/III. This would mean more of neutrons would be reaching the first structural wall, causing more reactions when ENDF-B/IV data are employed.

In Section V.C. in studying the effects of liquid metal ISSECs on the 316 SS first wall and blanket response functions the cylindrical model blanket of Figure V.11 was used with a 350 cm radius

uniform neutron source. However, in laser fusion reactors, which are more likely candidates than tokamaks to employ liquid ISSECs, the neutron source will be approximately a point source, the size of a micropellet. The reaction chamber is also expected to be more spherical than cylindrical. How these gemoetrical changes might affect the results and conclusions of Section V.C. has been studied and the findings of this search is given in Figure V.37 with respect to displacement damage in the first wall. It is seen in Figure V.37 that changing from a uniform source in cylindrical geometry blanket to a point source in spherical geometry blanket, without changing any of the thicknesses has a large effect on the displacement rate in the first wall when there is no ISSEC protection. However, as the thickness of the ISSEC is increased, this difference becomes small and at liquid Pb_4Li ISSEC thicknesses of 40 cm or larger the absolute amount of displacement damage is essentially the same in the two cases. The 100 cm thick liquid Pb_4Li ISSEC case was rerun again in cylindrical geometry with the same thicknesses as before except a line source was used instead of a uniform source. The result of this calculation is also shown in Figure V.37, and it is almost the same as the result obtained from uniform source calculations. The results with the helium production in the 316 SS first wall are about the same as the displacement damage results presented in Figure V.37.

Therefore it is seen that even though the factors of reduction in the displacement and gas production rates in the first wall by ISSECs are slightly changed when a more appropriate point source

EFFECT OF NEUTRON SOURCE AND GEOMETRY ON THE DISPLACEMENT DAMAGE IN 316 SS FIRST WALL

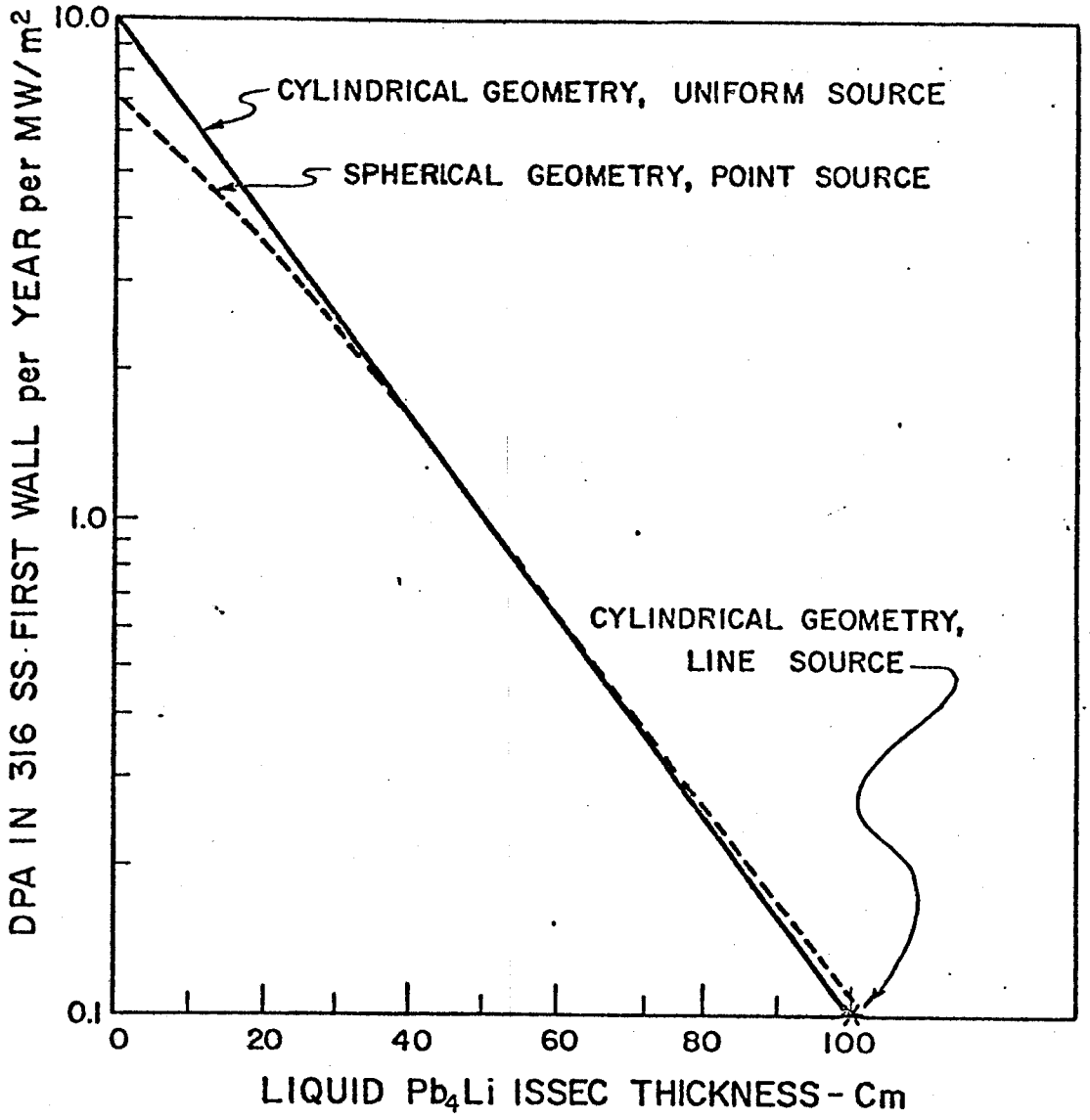

Figure V.37

condition is used, the absolute amount of damage is approximately the same in the two cases when the liquid Pb_4Li ISSEC thickness exceeds ∿40 cm. The conclusions in Section V.C. were mainly based on absolute damage rates in the first wall. Therefore the thicknesses given in Table V.30 for lifetime operation of the first wall will probably not change by more than 10%.

As is apparent from Sections V.A.2.c., V.B.2.c., and V.C.3.c., the ISSECs can either increase or decrease the specific radioactivity in the first structural wall and in the total blanket system (including the ISSEC). However, even when the specific radioactivity in terms of curies/cm^3 or curies/KW of thermal power is increased, the total mass of radioactive structure that will need to be disposed of at the end of the plant life is expected to be reduced because of the longer wall life.

As a general rule the ISSECs reduce the radioactivity that is produced by high energy neutron activations. If, in those systems where the radioactivity increases with the increasing ISSEC thickness, one could separate those isotopes that have high either short or long term radioactivity as a result of thermal neutron activation, (e.g. by isotope separation schemes[137]) one will have reduced the radioactivity in the system every time. Thus with a combination of neutron spectrum and isotopic tailoring one can produce the ultimate minimum environmental impact reactor.

From the calculations in this study it is apparent that there is a great economic incentive for employing ISSECs in either magnetic confinement or inertially confined fusion reactor systems. However, there are still some questions that need to be answered before ISSECs can be used in a practical sense. Most of these questions are experimental in nature. The reason they have not been worked on thus far is either due to the lack of facilities to do the experiments or that the ideas are still new and there had not been any need for the information previously.

For the carbon ISSEC - metallic first structural wall combination the major remaining question is the plasma-carbon interactions over 1400°C temperature, whether or if it does, how much acetylene formation takes place. For the metallic ISSECs, the question is what the effects of radiation might be at such high temperatures of 1000-2000°C and maximum dpa and helium production rates of 8-13 dpa/yr/MW/m^2 and 4-55 appm He/yr/MW/m^2, respectively. For the solid ISSECs, carbon and metallic, it would also be helpful to design a more efficient scheme than the one presented in Section V.B.5. for the attachment of the ISSEC to the first wall. The transfer of heat from the ISSEC to the first wall by conduction or by actively cooling allowing a thicker ISSEC to be used would also be of great benefit.

The major remaining questions for the liquid metal ISSECs are 1) corrosion by the liquid metals Pb, Li and Pb_4Li alloy at tempera-

tures around 400-600°C, 2) the pumping power requirements for the Pb and Pb_4Li systems, 3) transmission of the laser light through the vapor generated right after the pellet microexplosion, and 4) the formation and the stability of 50-70 cm thick liquid metal waterfalls.

CHAPTER VI

DISCUSSION ON THE POSSIBILITY OF FUSION REACTOR MATERIALS TESTING IN FISSION REACTORS

The MODISS computer package, given in Chapter IV, was used to generate the Primary Knock on Atom (PKA) spectra curves for iron, chromium, nickel, niobium and vanadium. All the results are obtained from the neutron flux spectrum in the 316 SS first structural wall of the model blanket design, shown in Figure V.11 of Chapter V. The PKA distributions without an ISSEC, and behind varying thicknesses of different ISSECs are compared to those obtained in a fast, EBR-II, and a thermal, HFIR fission reactor neutron spectra in Figures VI.1 through VI.14.

Figure VI.1 shows the differential PKA spectrum for Fe in EBR-II, HFIR and 5 different first wall fusion neutron spectra; no ISSEC (hard fusion), behind 25 cm of solid carbon and molybdenum ISSECs and behind 115 cm of liquid Li and 91 cm of liquid Pb_4Li ISSECs. Figure IV.2 shows the same type of curves except for cases behind 46 cm of liquid Li, 45 cm liquid Pb and 37 cm of liquid Pb_4Li ISSECs along with EBR-II and HFIR results.

The parameters plotted in Figures VI.1 and VI.2 are the total flux averaged PKA production cross sections, $\bar{\chi}_t$ vs. the PKA energy, T. $\bar{\chi}_t$ is given as:

$$\bar{\chi}_t = \Sigma_i \ \bar{\chi}_i \qquad 6.1$$

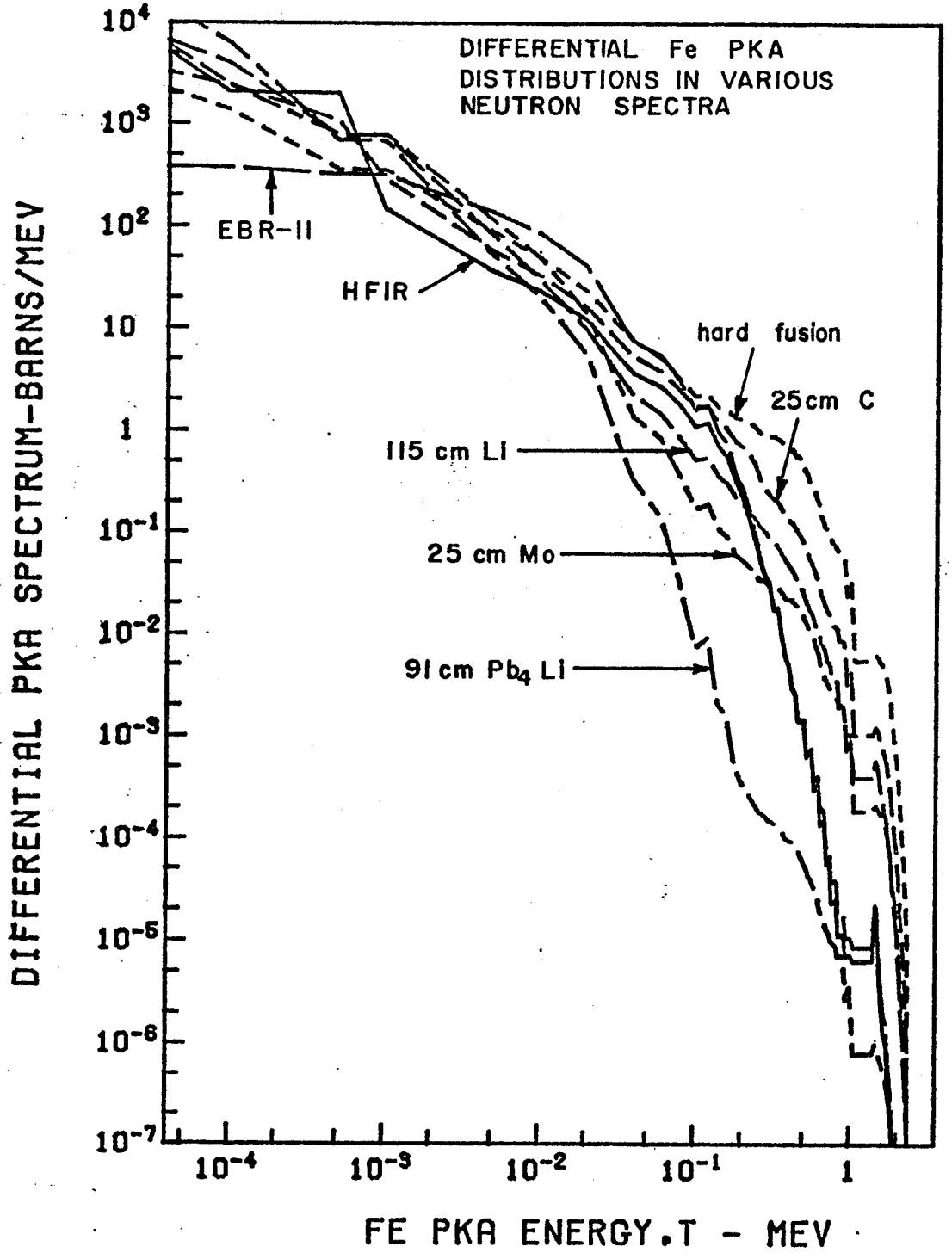
DIFFERENTIAL Fe PKA
DISTRIBUTIONS IN VARIOUS
NEUTRON SPECTRA
EBR-II
HFIR
hard fusion
25cm C
115 cm Li
25 cm Mo
91 cm Pb4 Li
DIFFERENTIAL PKA SPECTRUM-BARNS/MEV
FE PKA ENERGY.T - MEV
10^4
10^3
10^2
10
1
10^-1
10^-2
10^-3
10^-4
10^-5
10^-6
10^-7
10^-4
10^-3
10^-2
10^-1
1

Figure VI.1

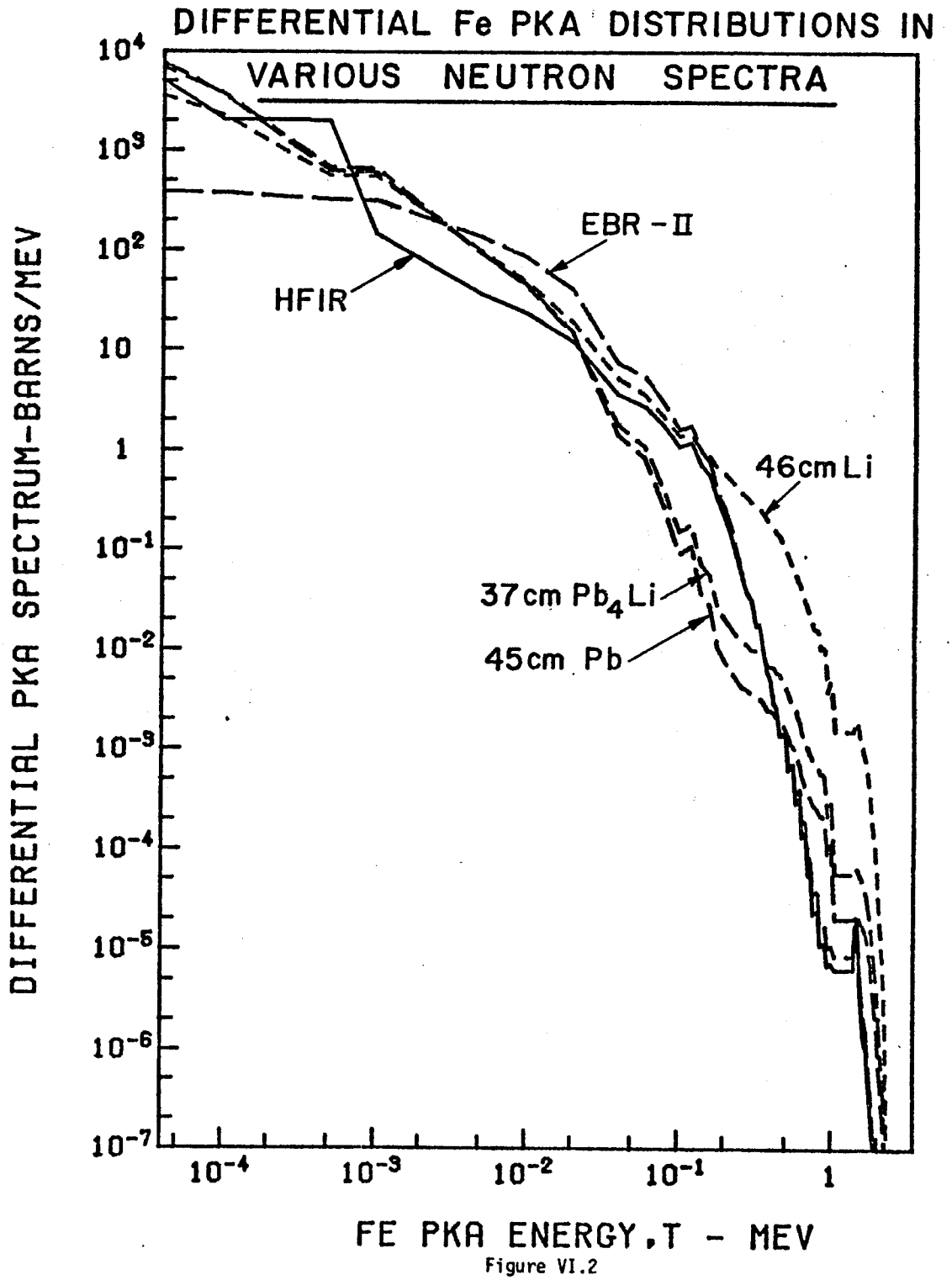
DIFFERENTIAL Fe PKA DISTRIBUTIONS IN
VARIOUS NEUTRON SPECTRA
EBR - II
HFIR
46cm Li
37cm Pb4Li
45cm Pb
DIFFERENTIAL PKA SPECTRUM-BARNS/MEV
FE PKA ENERGY, T - MEV
10^4
10^3
10^2
10
1
10^-1
10^-2
10^-3
10^-4
10^-5
10^-6
10^-7
10^-4
10^-3
10^-2
10^-1
1

Figure VI.2

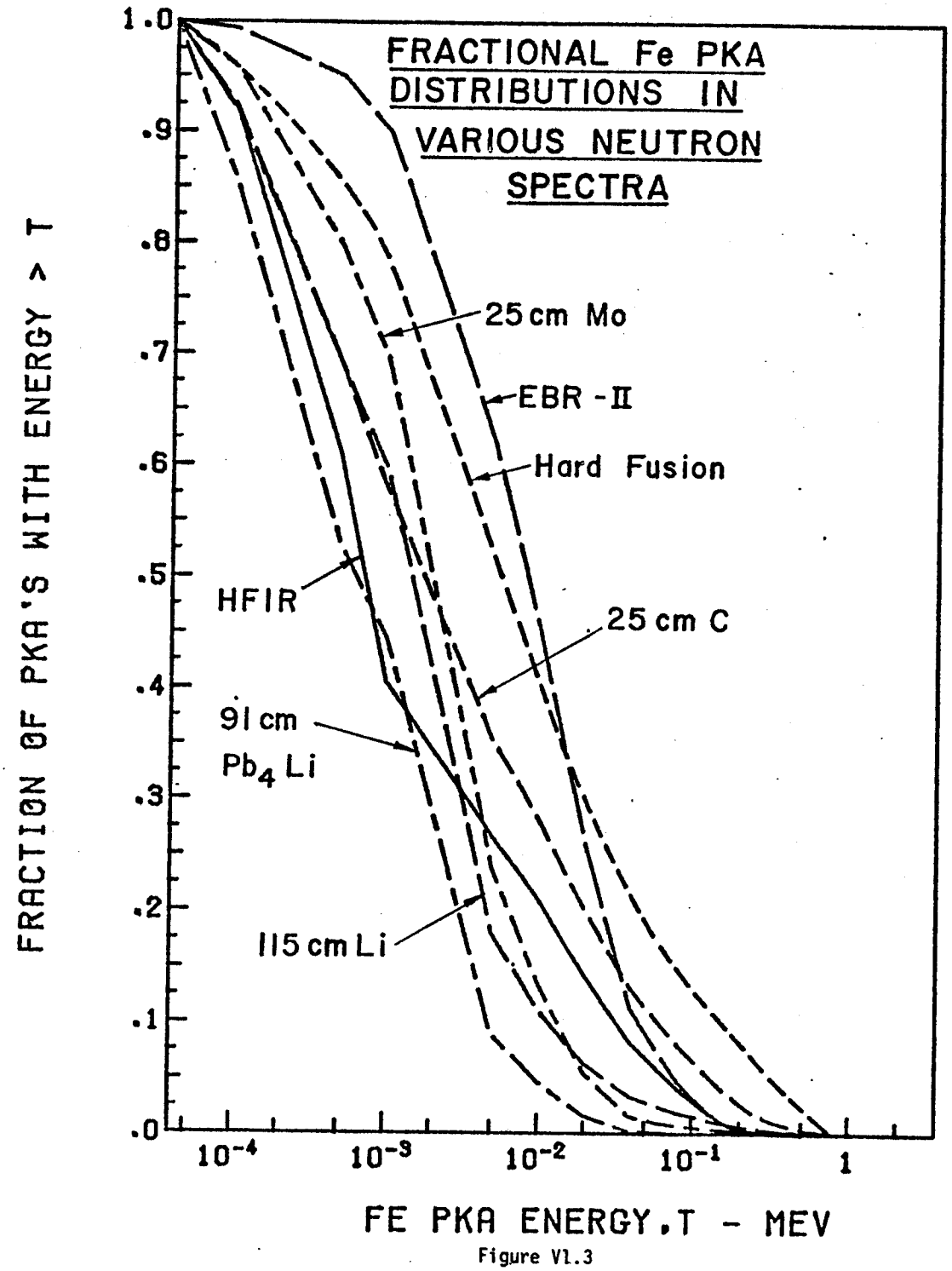
FRACTIONAL Fe PKA DISTRIBUTIONS IN VARIOUS NEUTRON SPECTRA
25 cm Mo
EBR - II
Hard Fusion
HFIR
25 cm C
91 cm Pb4 Li
115 cm Li
FRACTION OF PKA'S WITH ENERGY > T
FE PKA ENERGY, T - MEV
1.0
.9
.8
.7
.6
.5
.4
.3
.2
.1
.0
10-4
10-3
10-2
10-1
1

Figure VI.3

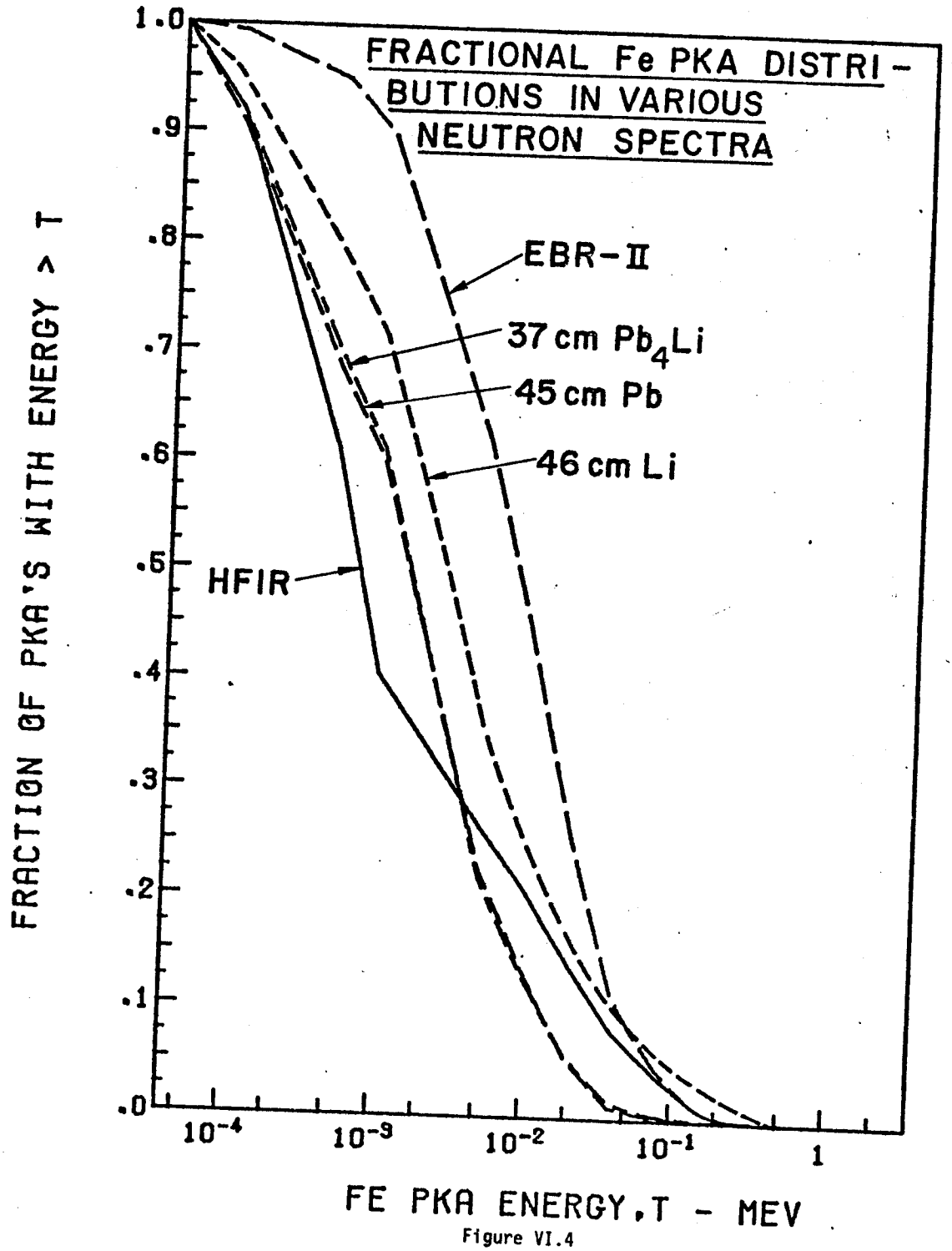
FRACTIONAL Fe PKA DISTRI-
BUTIONS IN VARIOUS
NEUTRON SPECTRA
EBR-II
37 cm Pb4Li
45 cm Pb
46 cm Li
HFIR
FRACTION OF PKA'S WITH ENERGY > T
1.0
.9
.8
.7
.6
.5
.4
.3
.2
.1
.0
10-4
10-3
10-2
10-1
1
FE PKA ENERGY, T - MEV

Figure VI.4

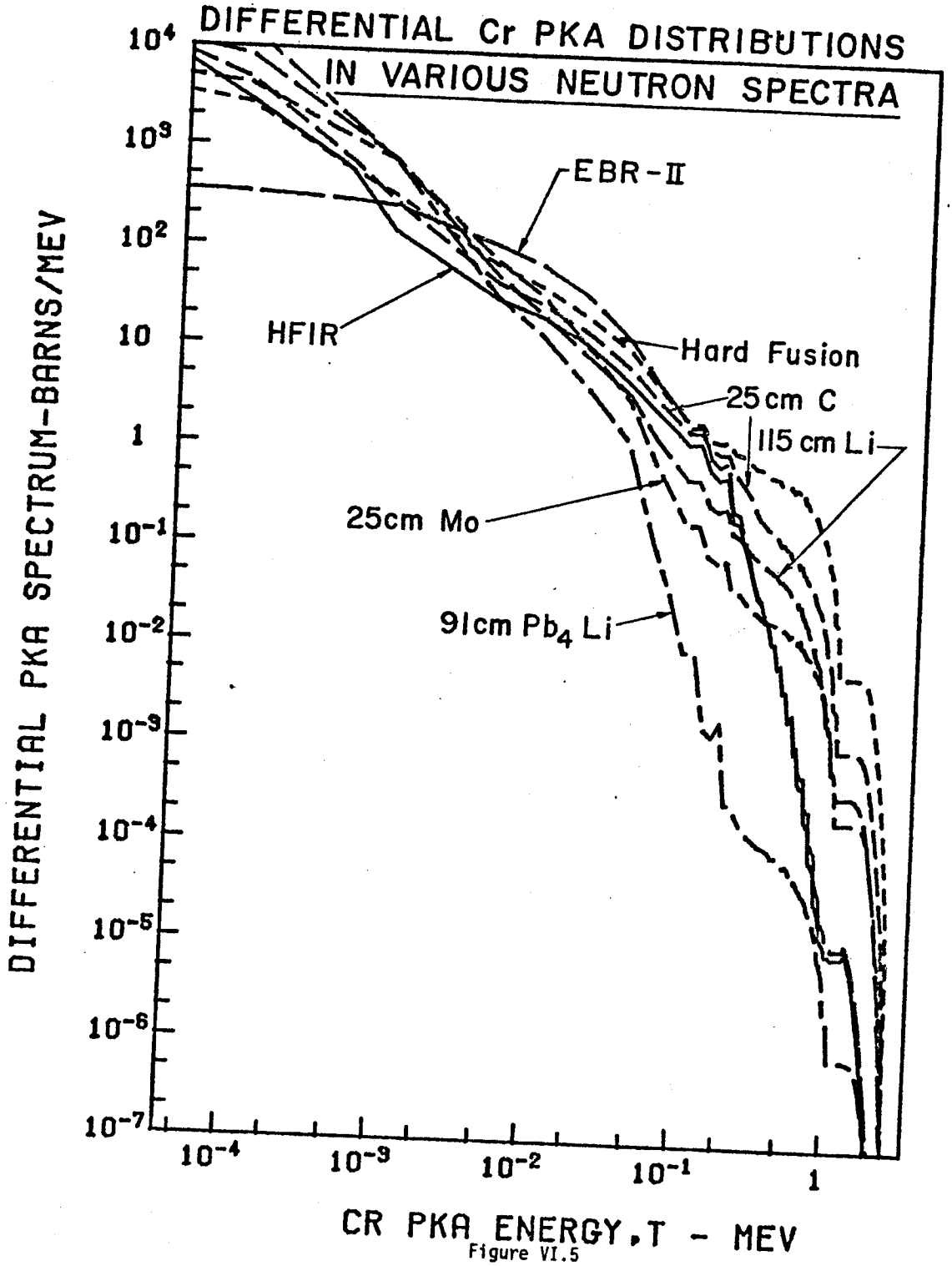
DIFFERENTIAL Cr PKA DISTRIBUTIONS
IN VARIOUS NEUTRON SPECTRA
EBR-II
HFIR
Hard Fusion
25cm C
115 cm Li
25cm Mo
91cm Pb4 Li
DIFFERENTIAL PKA SPECTRUM-BARNS/MEV
CR PKA ENERGY, T - MEV
10^4
10^3
10^2
10
1
10^-1
10^-2
10^-3
10^-4
10^-5
10^-6
10^-7
10^-4
10^-3
10^-2
10^-1
1

Figure VI.5

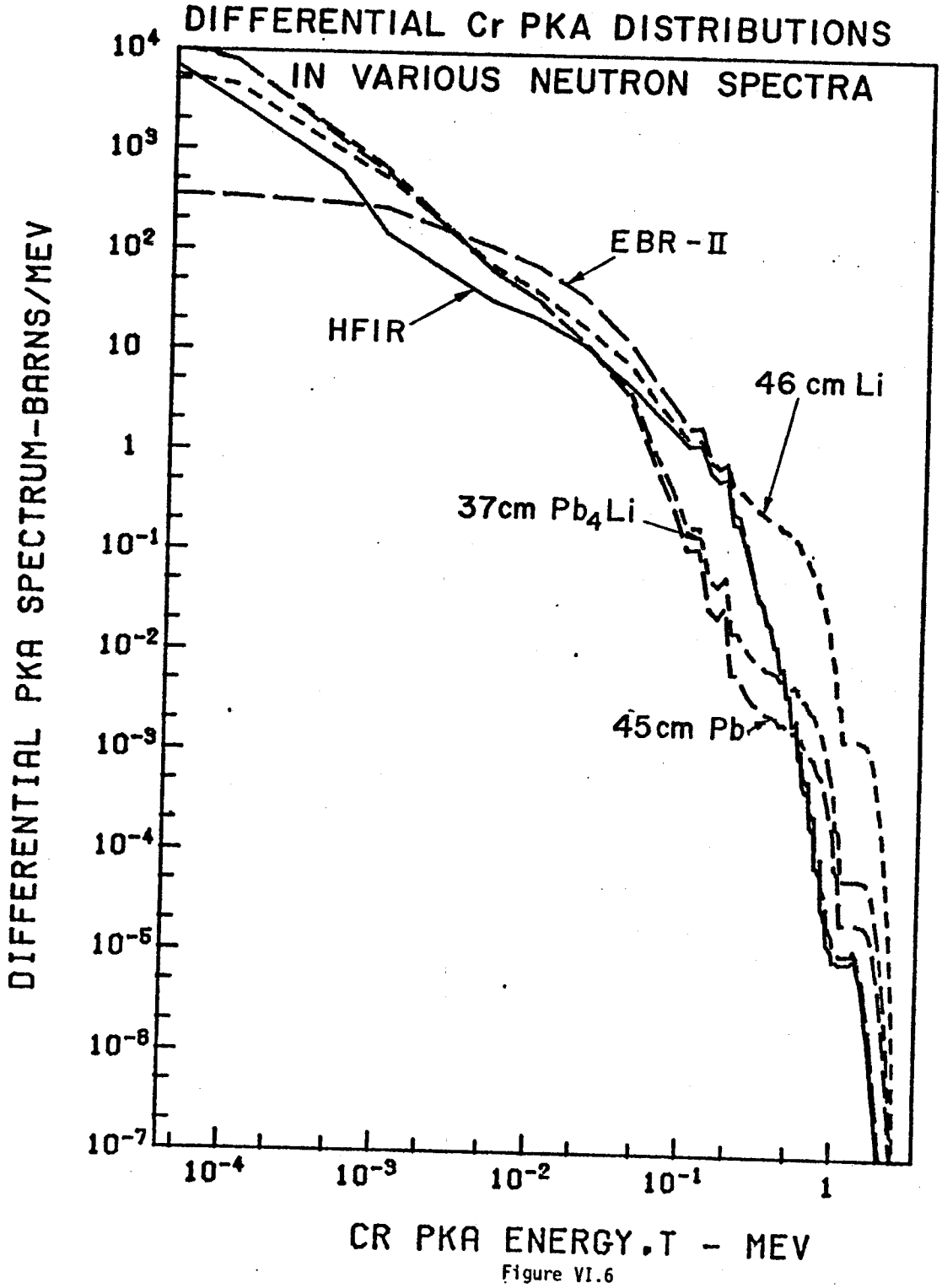
DIFFERENTIAL Cr PKA DISTRIBUTIONS
IN VARIOUS NEUTRON SPECTRA
DIFFERENTIAL PKA SPECTRUM-BARNS/MEV
CR PKA ENERGY, T - MEV
EBR-II
HFIR
46 cm Li
37cm Pb4Li
45cm Pb
10^4
10^3
10^2
10
1
10^-1
10^-2
10^-3
10^-4
10^-5
10^-6
10^-7
10^-4
10^-3
10^-2
10^-1
1

Figure VI.6

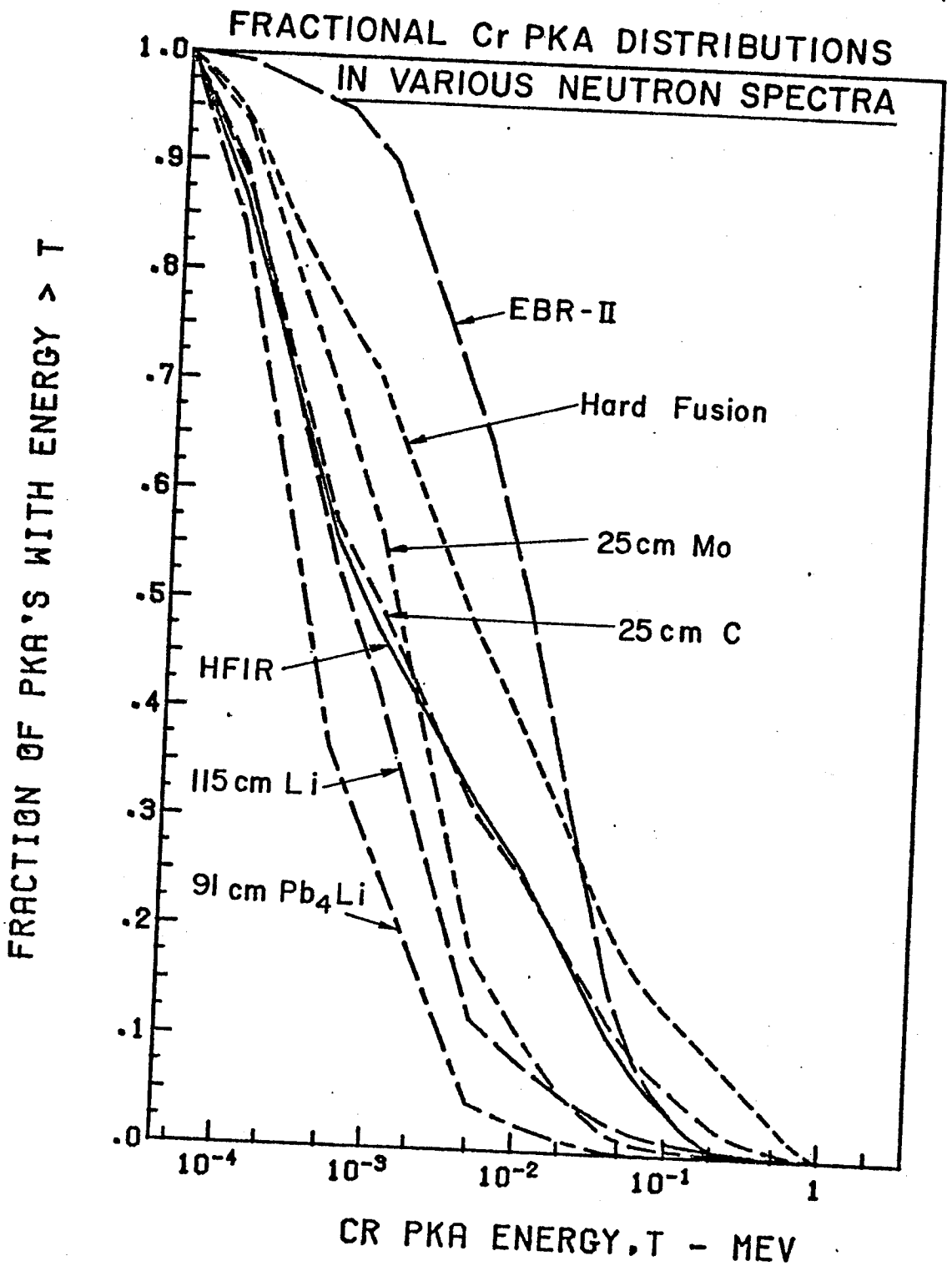
FRACTIONAL Cr PKA DISTRIBUTIONS
IN VARIOUS NEUTRON SPECTRA
FRACTION OF PKA'S WITH ENERGY > T
1.0
.9
.8
.7
.6
.5
.4
.3
.2
.1
.0
EBR-II
Hard Fusion
25cm Mo
25cm C
HFIR
115cm Li
91cm Pb4Li
10-4
10-3
10-2
10-1
1
CR PKA ENERGY, T - MEV

Figure VI.7

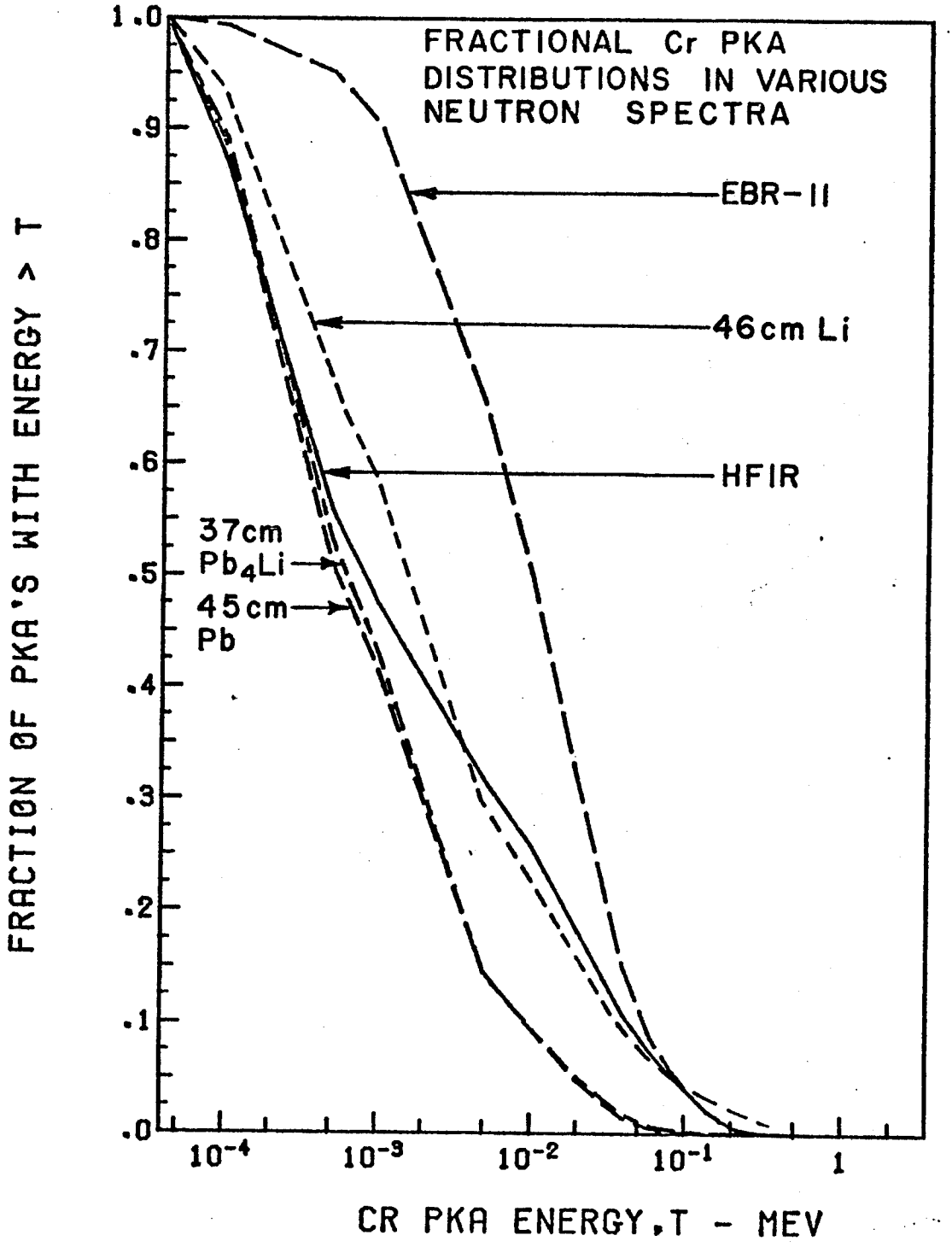
FRACTIONAL Cr PKA
DISTRIBUTIONS IN VARIOUS
NEUTRON SPECTRA
EBR-II
46cm Li
HFIR
37cm
Pb4Li
45cm
Pb
1.0
.9
.8
.7
.6
.5
.4
.3
.2
.1
.0
10-4
10-3
10-2
10-1
1
FRACTION OF PKA'S WITH ENERGY > T
CR PKA ENERGY, T - MEV

Figure VI.8

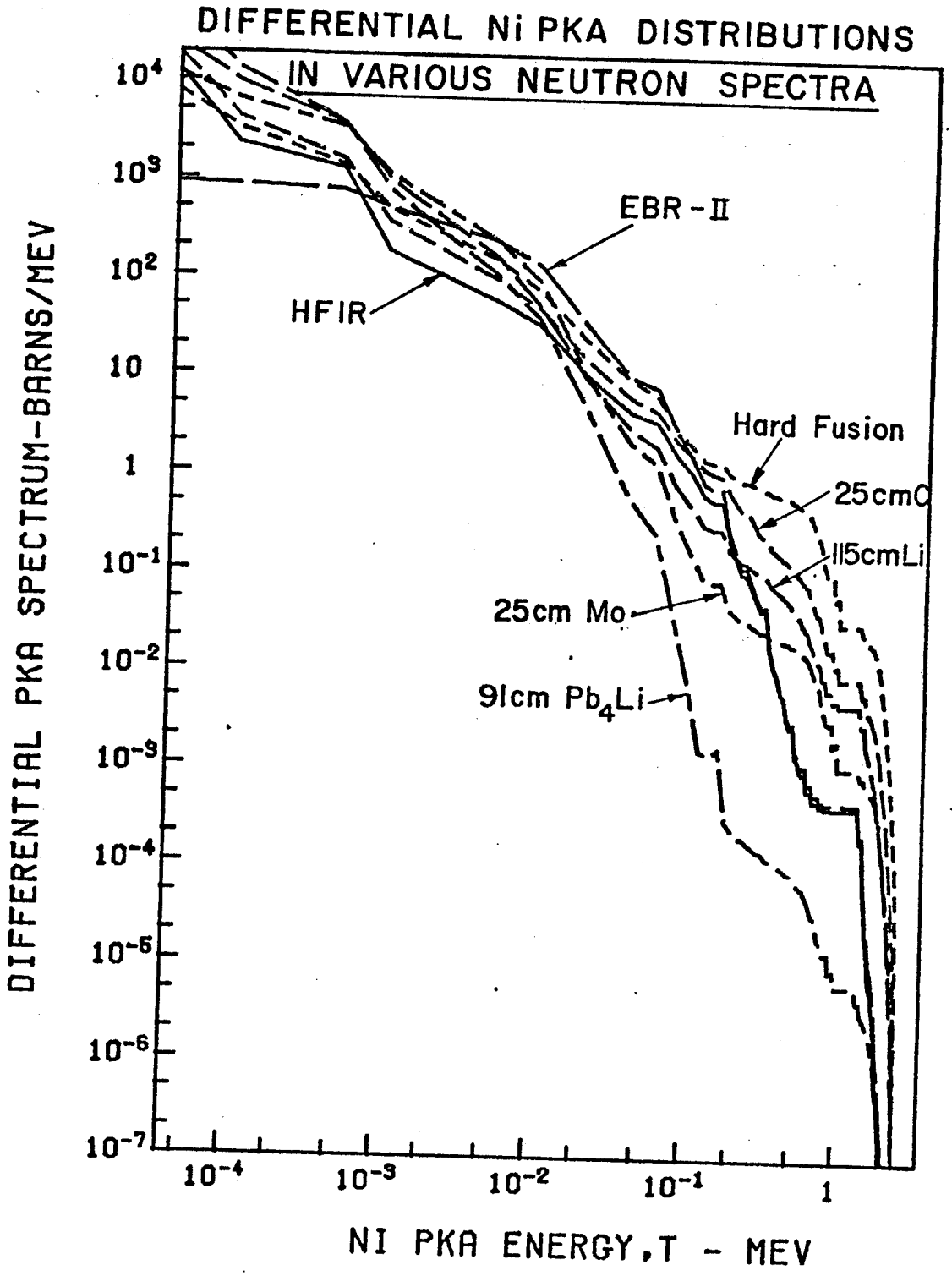
DIFFERENTIAL Ni PKA DISTRIBUTIONS
IN VARIOUS NEUTRON SPECTRA
DIFFERENTIAL PKA SPECTRUM-BARNS/MEV
NI PKA ENERGY, T - MEV
EBR-II
HFIR
Hard Fusion
25cmC
115cmLi
25cm Mo
91cm Pb4Li
10^4
10^3
10^2
10
1
10^-1
10^-2
10^-3
10^-4
10^-5
10^-6
10^-7
10^-4
10^-3
10^-2
10^-1
1

Figure VI.9

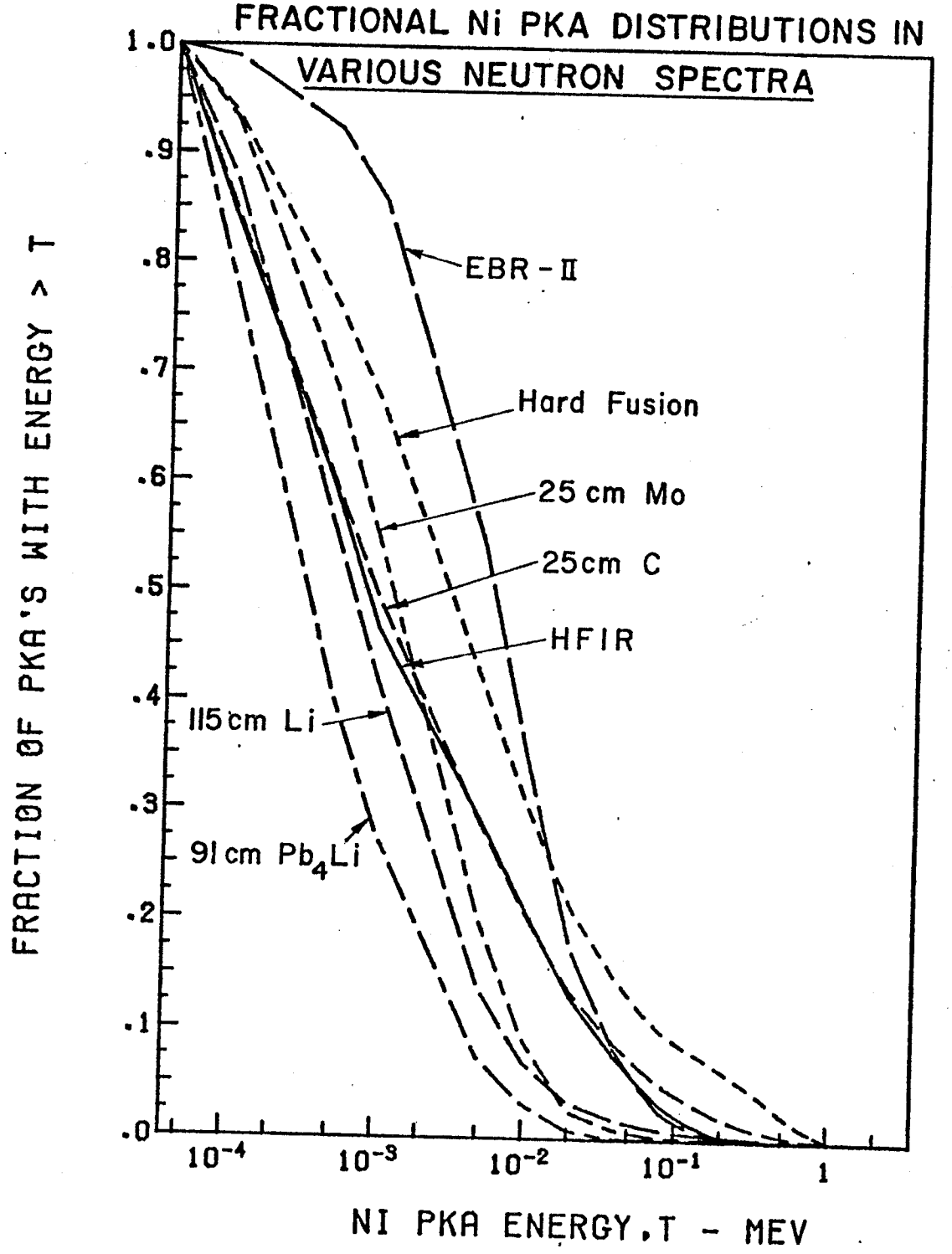
FRACTIONAL Ni PKA DISTRIBUTIONS IN
VARIOUS NEUTRON SPECTRA
FRACTION OF PKA'S WITH ENERGY > T
1.0
.9
.8
.7
.6
.5
.4
.3
.2
.1
.0
EBR-II
Hard Fusion
25 cm Mo
25cm C
HFIR
115cm Li
91cm Pb4Li
10-4
10-3
10-2
10-1
1
NI PKA ENERGY, T - MEV

Figure VI.10

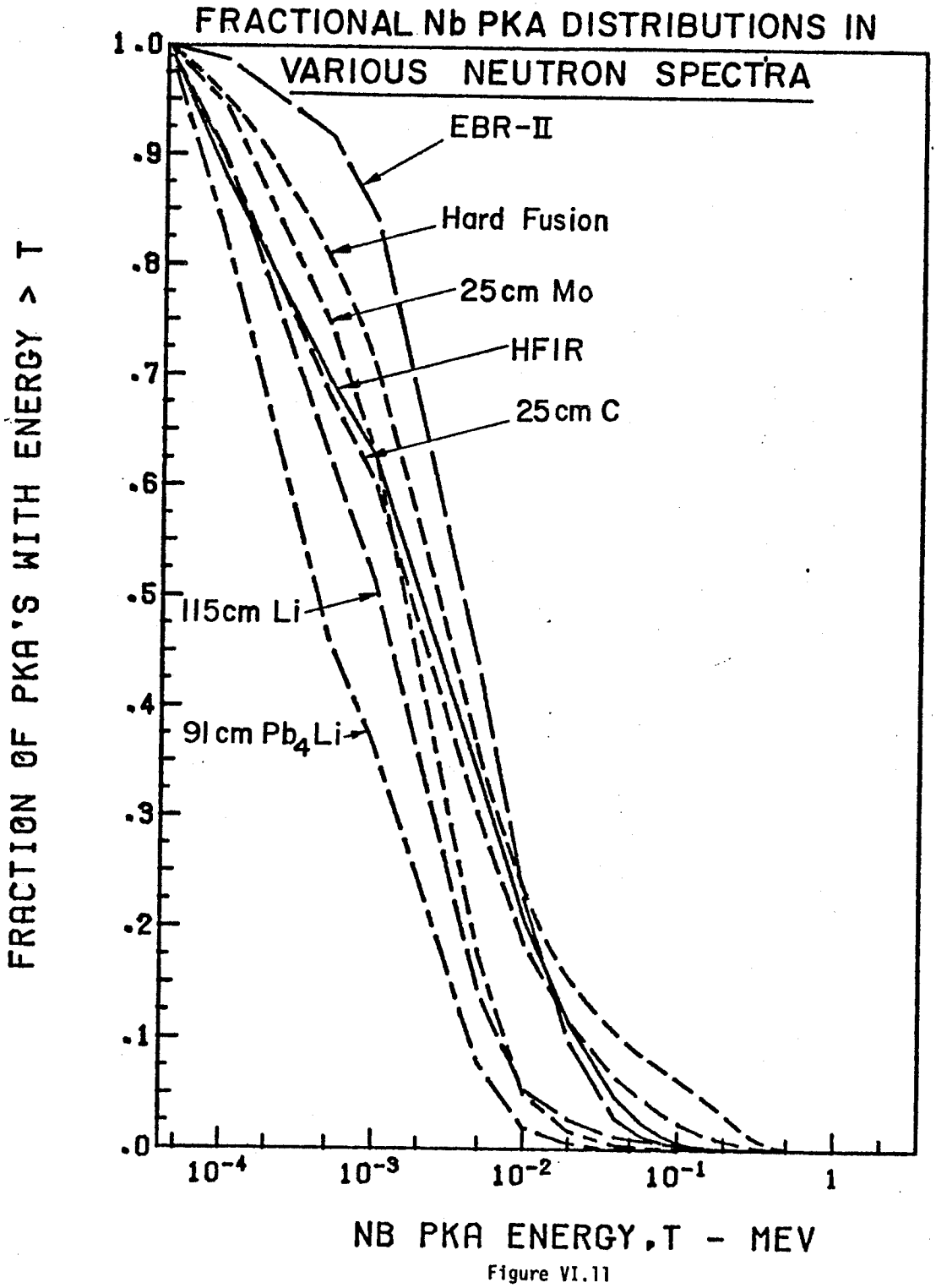
FRACTIONAL Nb PKA DISTRIBUTIONS IN
VARIOUS NEUTRON SPECTRA
EBR-II
Hard Fusion
25cm Mo
HFIR
25cm C
115cm Li
91cm Pb4Li
FRACTION OF PKA'S WITH ENERGY > T
1.0
.9
.8
.7
.6
.5
.4
.3
.2
.1
.0
10-4
10-3
10-2
10-1
1
NB PKA ENERGY, T - MEV

Figure VI.11

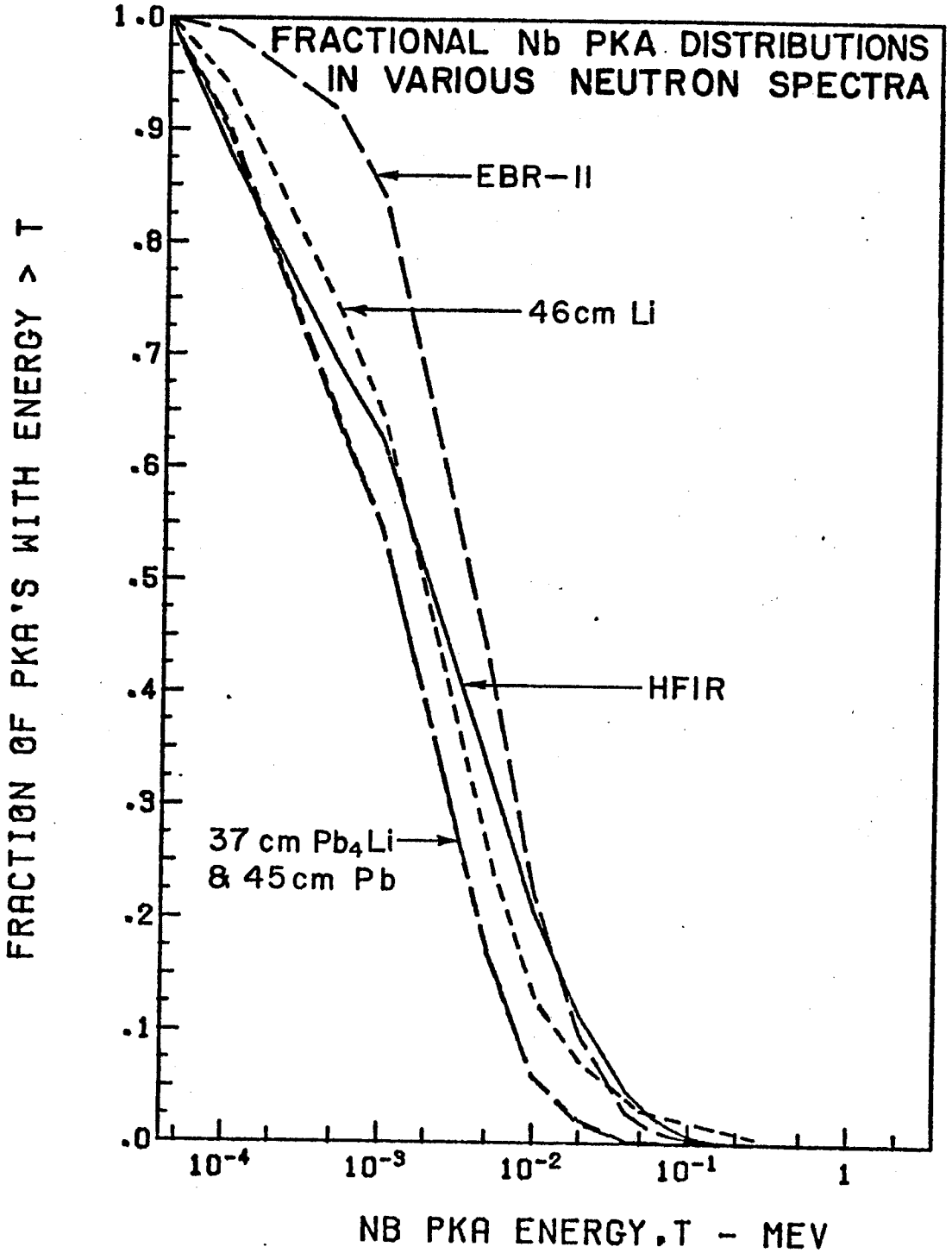
FRACTIONAL Nb PKA DISTRIBUTIONS
IN VARIOUS NEUTRON SPECTRA
EBR-II
46cm Li
HFIR
37 cm Pb4Li
& 45cm Pb
FRACTION OF PKA'S WITH ENERGY > T
1.0
.9
.8
.7
.6
.5
.4
.3
.2
.1
.0
10-4
10-3
10-2
10-1
1
NB PKA ENERGY, T - MEV

Figure VI.12

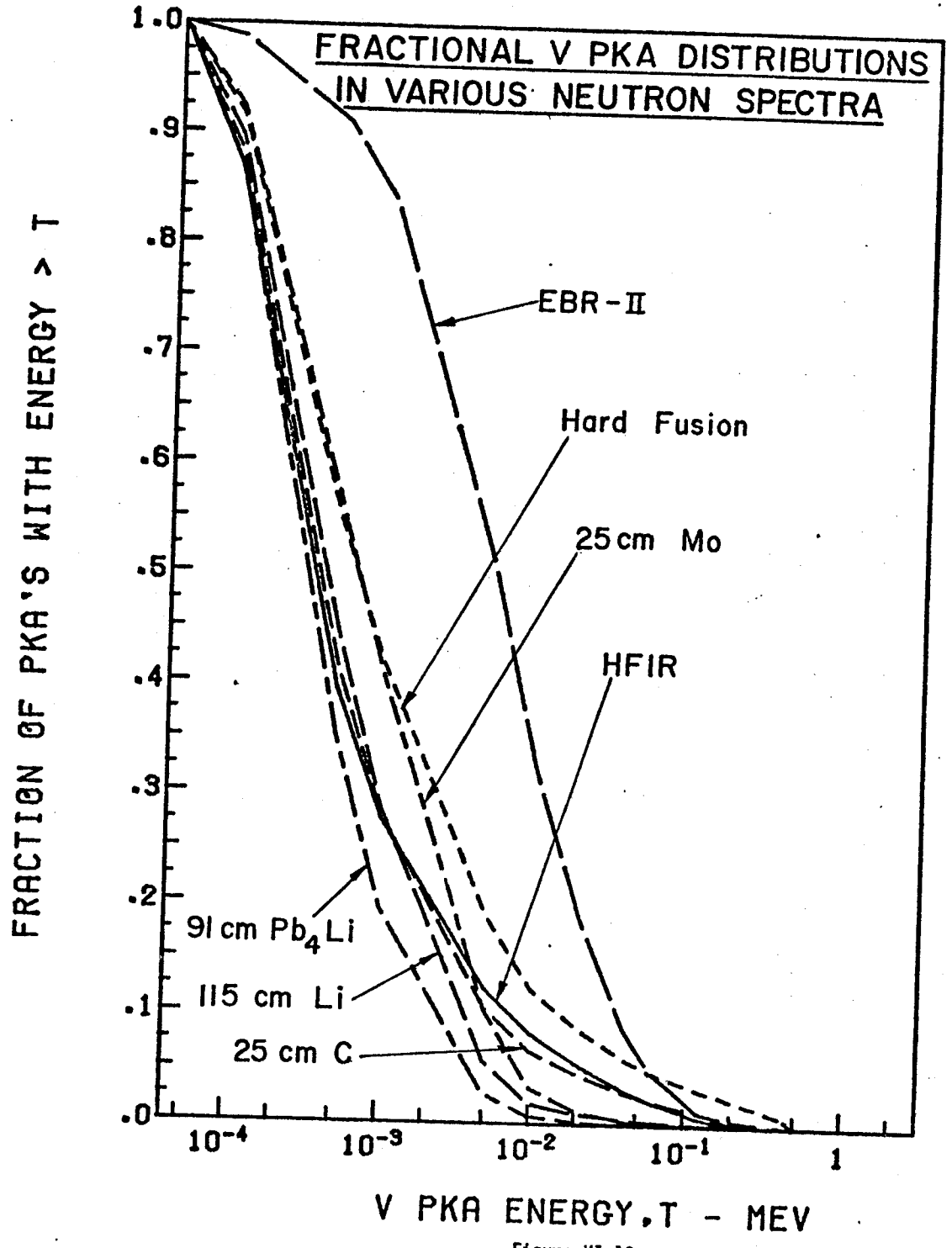
FRACTIONAL V PKA DISTRIBUTIONS
IN VARIOUS NEUTRON SPECTRA
FRACTION OF PKA'S WITH ENERGY > T
1.0
.9
.8
.7
.6
.5
.4
.3
.2
.1
.0
EBR-II
Hard Fusion
25 cm Mo
HFIR
91 cm Pb4Li
115 cm Li
25 cm C
10-4
10-3
10-2
10-1
1
V PKA ENERGY, T - MEV

Figure VI.13

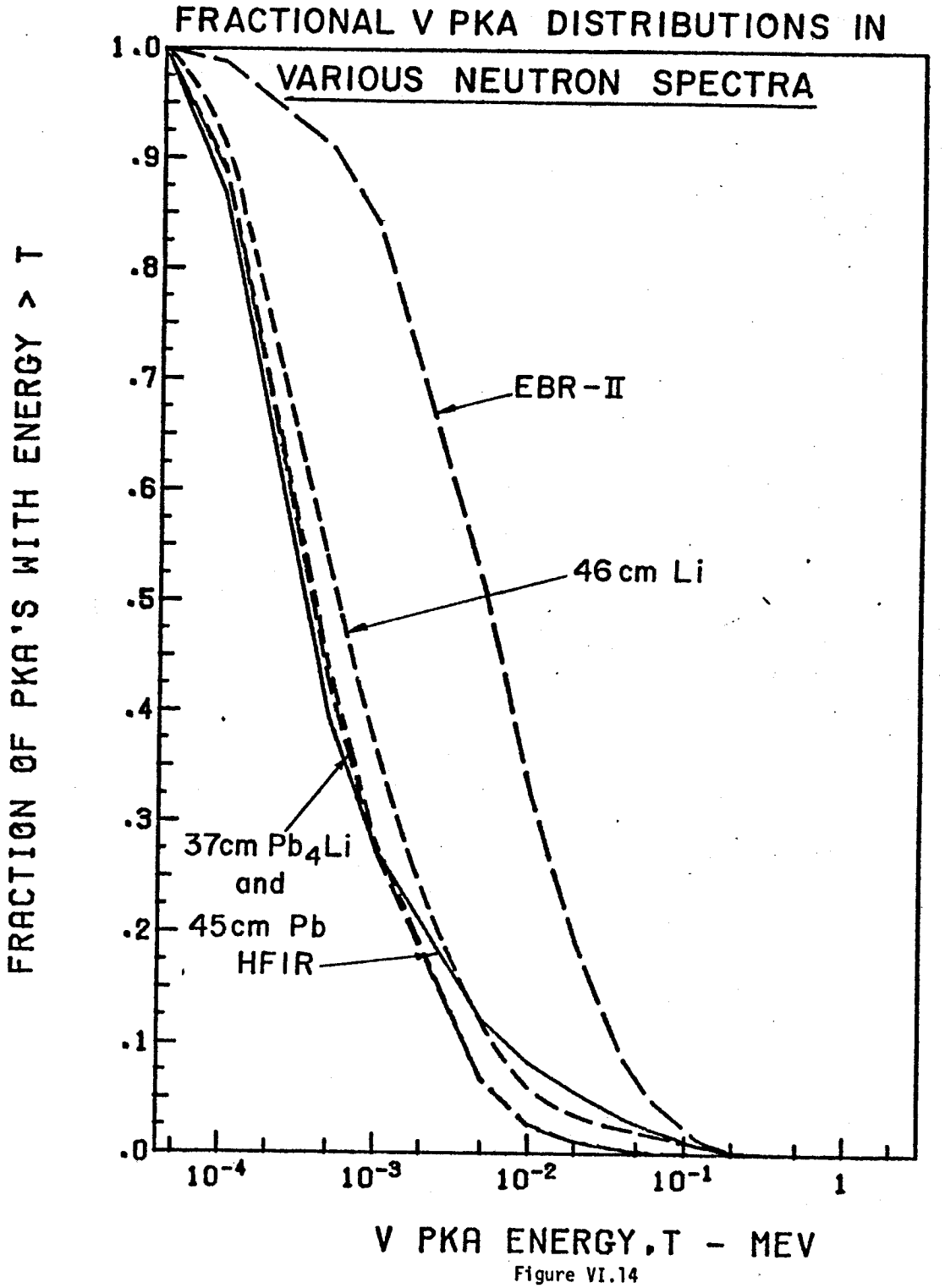
FRACTIONAL V PKA DISTRIBUTIONS IN
VARIOUS NEUTRON SPECTRA
FRACTION OF PKA'S WITH ENERGY > T
1.0
.9
.8
.7
.6
.5
.4
.3
.2
.1
.0
EBR-II
46 cm Li
37cm Pb4Li
and
45cm Pb
HFIR
10-4
10-3
10-2
10-1
1
V PKA ENERGY, T - MEV

Figure VI.14

where $\bar{\chi}_i$ is the neutron spectrum averaged differential PKA production cross section from the i^{th} reaction.

i, goes over all nuclear reactions considered; elastic, inelastic, (n,α), etc.

$\bar{\chi}_i$ is calculated from

$$\bar{\chi}_i = \frac{\int \chi_i(E,T)\ \phi(E)\ dE}{\int \phi(E)\ dE} \qquad 6.2$$

and

$$\chi_i(E,T) = \sigma_i(E)\ K_i(E,T)/\Delta T \qquad 6.3$$

where

$\sigma_i(E)$ is the i^{th} reaction cross section at neutron energy E,

$K_i(E,T)$ is the probability that a neutron of energy E transfers energy T to the recoiling atom as a result of the nuclear reaction i, and $\phi(E)$ is the flux of neutrons with energy E.

The results shown in Figures VI.1 and VI.2 are sometimes difficult to interpret when many different spectra are used so we have integrated, normalized to unity and replotted the data in Figures VI.3 and VI.4. These latter figures show the fraction of PKA's with energy greater than T as a function of the PKA energy T and it is easier to see similarities and differences between spectra from such plots. Figures VI.5 - VI.8 are similar to Figures VI.1 - VI.4, respectively, except they are for the element chromium. Differential and fractional PKA distributions for the element nickel are displayed in Figures VI.9

and VI.10 while Figures VI.11 - VI.14 give the fractional PKA distribution results for niobium and vanadium.

Since the object of this Chapter was to see how close one could make the PKA spectra in a fusion reactor first wall to that characteristic in already available neutron test facilities, let us consider the EBR-II and HFIR PKA spectra separately.

EBR-II PKA Spectra

It can be seen from Figures VI.3, 4, 7, 8, 10, 11, 12, 13, and 14 that the PKA spectrum in a fast neutron facility such as EBR-II is much harder than in a thermal reactor like HFIR up to ∿100 keV and in an unprotected fusion first wall up to ∿10 keV. Above PKA energies of 10 keV, the unprotected fusion reactor first wall PKA spectrum is much harder than in EBR-II and that, of course, is the major concern of materials scientists faced with simulation of such damage. The insertion of an ISSEC structure between the neutron source and the first wall does a great deal to soften the high energy PKA spectra in a fusion reactor and it can be seen in Figures VI.1, 2, 5 and 6 that a 60-70 cm of either liquid Pb or Pb_4Li softens the PKA spectrum sufficiently in Fe and Cr that it is closely simulated by the EBR-II neutron spectrum. However, the softening of the PKA by the ISSECs also occurs at the low energy end and increases the discrepancy below ∿50 keV. For example, in V (Figure VI.13), the probability of producing PKAs with T > 1 keV is almost twice as

large in EBR-II than behind a 25 cm thick Mo or C ISSEC. The use of thicker liquid ISSECs makes the situation even worse on the low energy side while at the same time softening the PKA spectra even further at the high energy side. The probability of producing a vanadium PKA of T > 1 keV is 4 times as great in EBR-II than behind 91 cm thick Pb_4Li liquid ISSEC, and the probability of producing a PKA of T > 100 keV is 10 times greater.

It is clear that the use of ISSECs to protect the first wall not only reduces the absolute damage rate, but it softens the neutron spectra in all the materials considered to the point that the fast neutron facilities produce even harder PKA spectra than found in potential fusion reactor first walls. At this stage of our understanding of the radiation damage process, this is the same as saying that, on a dpa basis, the displacement damage per neutron will be worse in EBR-II than in an ISSEC protected fusion reactor, not less as is the case in most designs considered today!

HFIR PKA Spectra

Unlike the EBR-II case, there are a large number of thermal neutrons present which can cause (n,γ) reactions. The recoils from these reactions can produce large numbers of low energy PKAs and we see from Figure VI.3, for example, that the HFIR PKA spectra is softer than that for the unprotected fusion reactor first wall over the entire energy range. Without any modification to the fusion

neutron spectrum, this can have serious implications for present simulation studies.

However, when solid or liquid ISSECs are used, the softened PKA spectra is closely simulated by the HFIR spectra over a wide range of energies. For example, it is seen from the fractional PKA distribution plots for all the elements considered, that the HFIR spectra closely simulates the PKA spectra below 1 keV and for Cr, Ni and Nb the simulation is quite accurate up to several hundred keV behind a 25 cm of carbon ISSEC.

While the ISSECs cannot reduce the maximum recoil energy, they can reduce the number of those recoils to insignificant levels. Again, it can be seen that 91 cm of Pb_4Li in front of a Ni first wall can reduce the number of PKAs above 100 keV by over a factor of 10 from the HFIR case (Figure VI.10). The similar comparison shows that the HFIR spectrum produces a factor of 10 less PKAs above 100 keV than for the hard fusion case (i.e., the 91 cm of Pb_4Li reduces the number of PKAs above 100 keV by a factor of 100 over the hard fusion spectrum case).

The conclusion that one arrives at after these comparisons is that the displacement damage behind the various ISSECs considered can best be simulated by a thermal reactor spectrum and if anything, the damage per neutron should be less in the fusion reactor than in the fission source. Fast neutron facilities can simulate the high energy PKA spectra but they do not do a very good job of simulating the low energy spectra. If there are processes that are sensitive to large

numbers of low energy collisions (such as stimulated diffusion or annealing of point defects) then the fast neutron spectra may not be suitable for simulation.

Gas to Displacement Damage Calculation

Table VI.1 lists effects of various carbon ISSEC's on the calculated appm He to dpa ratios for the five potential CTR first structural wall materials considered in this study. It is found that this ratio varies from 1-40 for unprotected walls. Appropriate values for a fast reactor (EBR-II) and a thermal reactor (HFIR) test facility are generally much lower ranging from 0.006-0.31 for most elements with 316 SS having a value of 95 in HFIR because of the Ni-58 to Ni-59 conversion and subsequent high thermal capture and (n,α) cross sections.

The general trend for all the elements is to reduce the gas to dpa ratio by a factor of 2-3 with a 12.5 cm carbon thickness. However, that level of reduction still leaves the gas to dpa ratio far greater than that in current fission reactor test facilities. This is amply demonstrated in Figures VI.15 and VI.16 where the values of (appm He/dpa) for ISSEC systems are divided by those in EBR-II and HFIR, respectively. The important point to note here is that even behind $\sim$30 cm of a carbon ISSEC the (gas/dpa) ratio is still $\sim$20-200 higher than for 316 SS in HFIR and the discrepancy is even larger for the EBR-II case. The lower values tend to be for the higher Z elements.

Table VI.2 gives the appm He/dpa ratio in the 316 SS first structural wall of the model blanket shown in Figure V.11 of Chapter V

Table VI.1

Calculated Ratio of appm He Gas Production to Displaced Atom Density in Potential CTR First Structural Wall Materials

	appm He/dpa				
Material	No ISSEC	12.5 cm C ISSEC	25 cm C ISSEC	EBR-II	HFIR
Al	37.5	14.7		0.10	0.31
V	6.1	3.0		0.0057	0.0094
316 SS	24.8	10.7		0.11	95[a]
Nb	3.9	2.0		0.034	0.073
Mo	7.7	3.9	2.8	0.059	0.12
Ta	0.89	0.34		NA[b]	NA[b]

(a) After 1 year of irradiation

(b) Not Available

NORMALIZED He/DPA RATIOS FOR ISSEC PROTECTED SYSTEMS

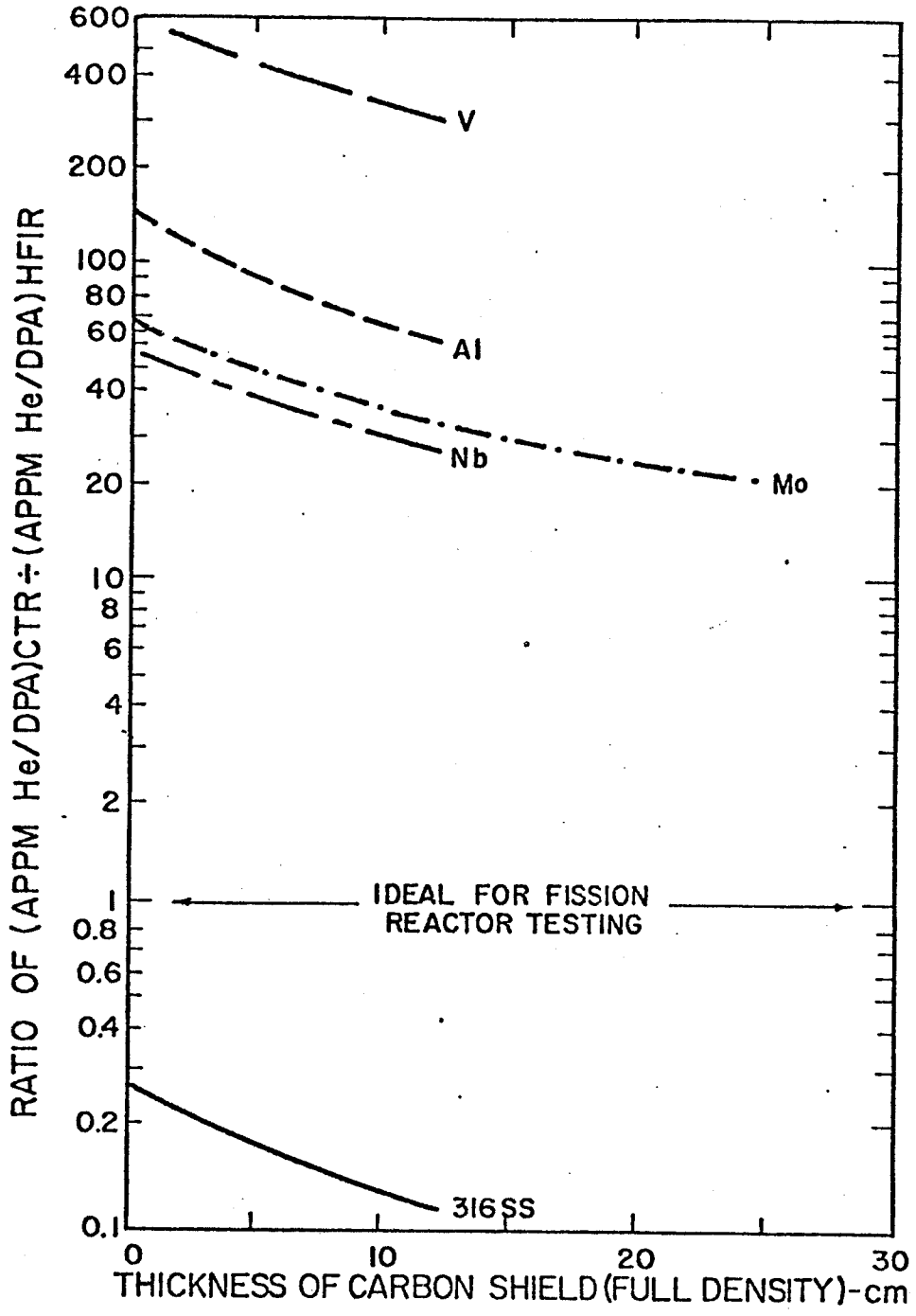

Figure VI.15

NORMALIZED He/DPA RATIOS FOR ISSEC PROTECTED SYSTEMS

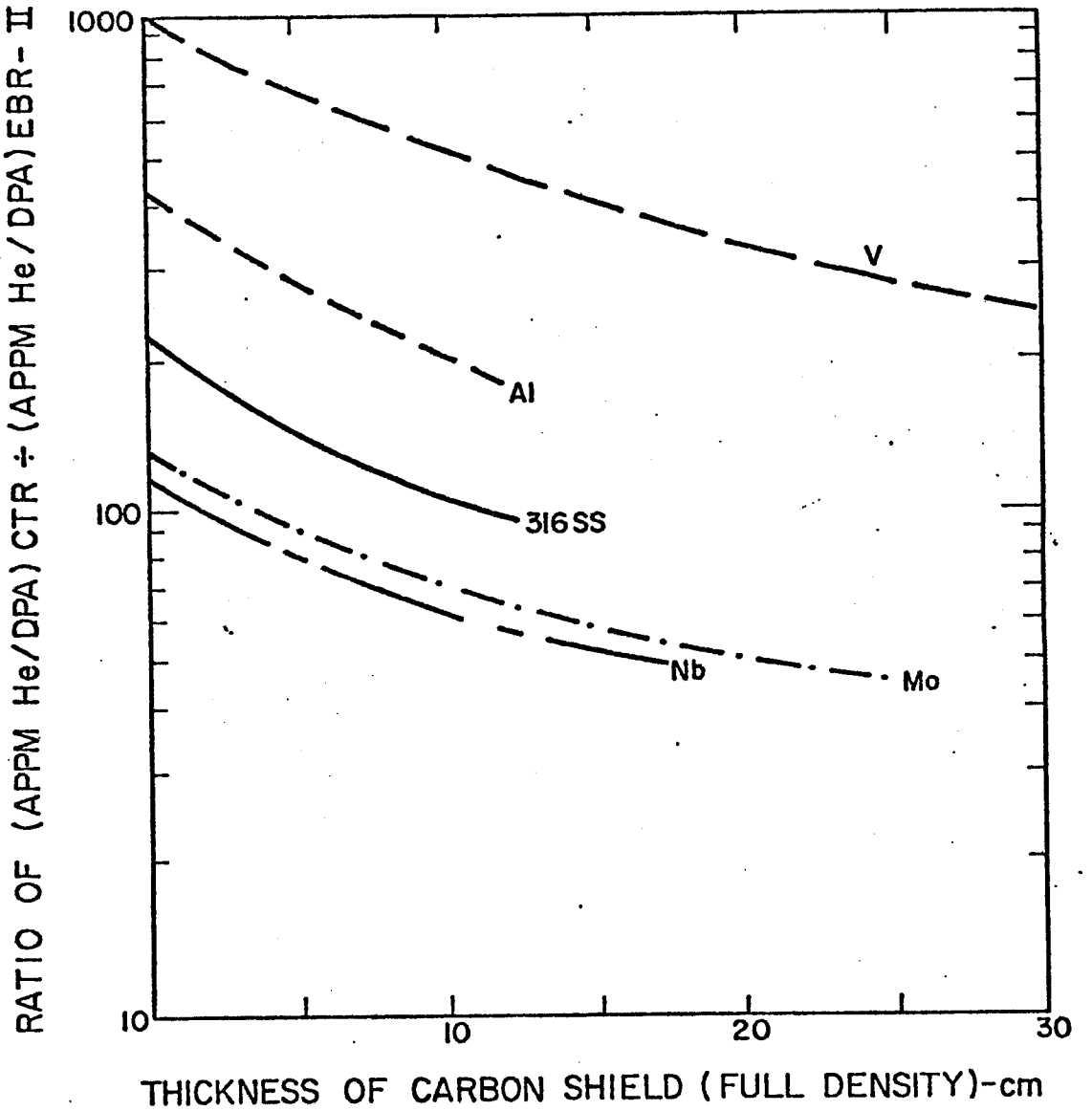

Figure VI.16

Table VI.2

Appm He/dpa Ratio in the 316 SS First Structural Wall
in ISSEC Protected Systems

ISSEC Thickness-cm	ISSEC Material								
	None	C	Mo	Nb	V	W	Li	Pb	Pb_4Li
0	21.6								
5		17.7	11.1	13.1	14.6	12.6			
10		14.6	7.33	8.4	10.6	8.3			
20							15.2	2.9	3.3
25		10.0	3.8	2.9	5.6	4.3			
40							11.4	0.64	0.94
100							4.0	0.01	0.02

with and without various ISSECs. The values in Table VI.2 are divided by 0.11, the appm He/dpa ratio for 316 SS in EBR-II, and plotted in Figure VI.17. We see in this figure that about 73 cm of liquid Pb_4Li or 65 cm of liquid Pb ISSEC exactly reproduces the appm He/dpa ratio from EBR-II in the 316 SS first structural wall of a CTR. One needs almost 3 meters of liquid Li ISSEC, or $\sim$2.5 m C, 125 cm V or W, 130 cm Mo, or $\sim$75 cm of Nb ISSEC to get the same effect. These numbers are really not realistic for solid ISSECs because of the excessive temperatures associated with even conductively cooled shields.

The significance of these results is that a 60-70 cm of liquid Pb or 65-70 cm of liquid Pb_4Li ISSEC reduces the appm He/dpa ratio in the 316 SS first structural wall of an inertial confinement fusion reactor to that value one would get if he irradiated that 316 SS first structural wall sample in EBR-II fast fission test reactor. As discussed previously, the high energy part of the PKA spectrum will also be similar in the two cases. Therefore, the data obtained from the already present fast fission test facilities can be used with much more confidence in the design of fusion reactors if the liquid Pb or Pb_4Li ISSECs were to be used at thicknesses given above. As far as the other solid ISSEC materials (and liquid Li) considered in this study are concerned, the gas to dpa ratio behind any practical thickness of them is still so different than for EBR-II that any process that depends on the interaction of gas atoms and point defects will not be correctly simulated in fission reactors.

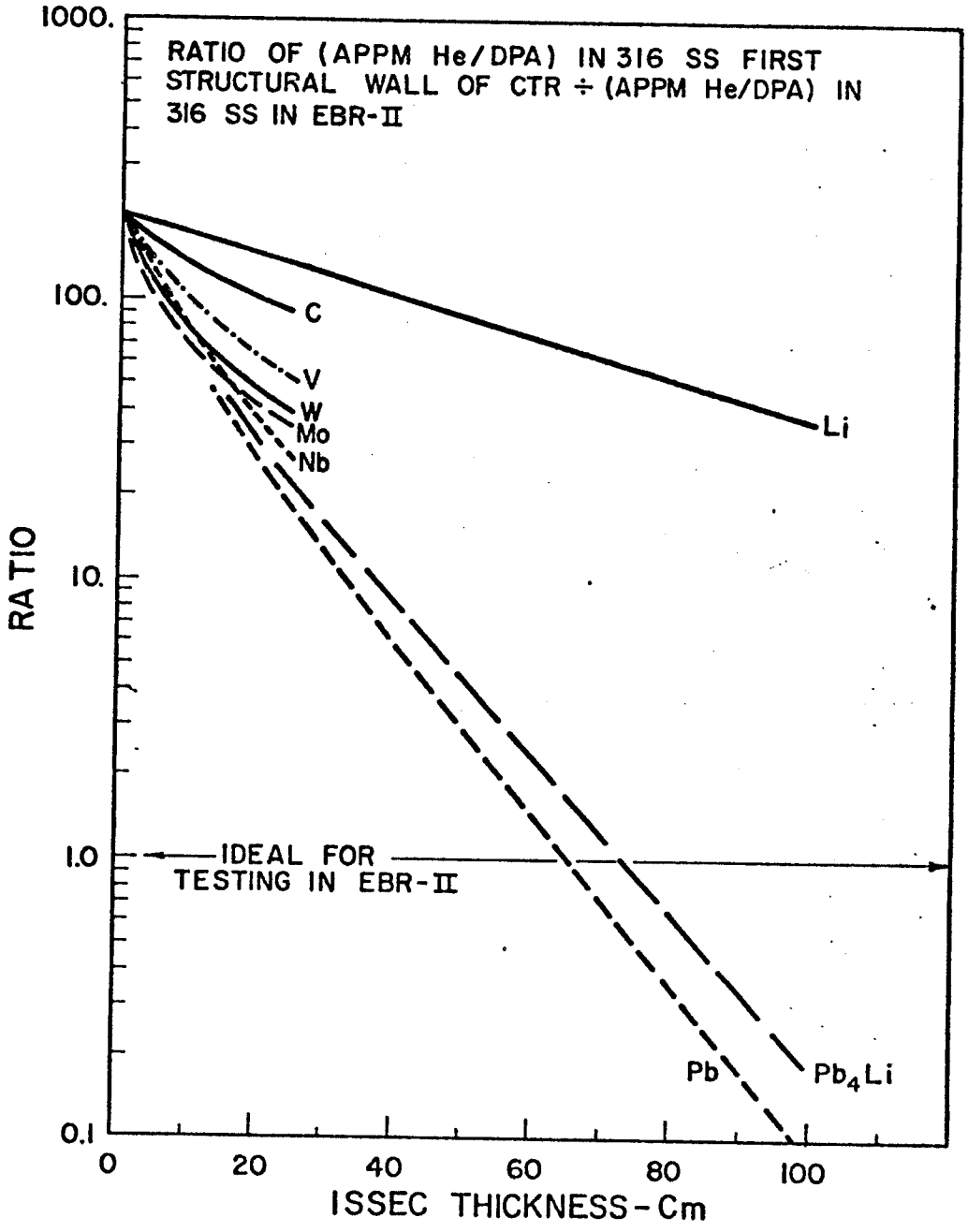
RATIO OF (APPM He/DPA) IN 316 SS FIRST STRUCTURAL WALL OF CTR ÷ (APPM He/DPA) IN 316 SS IN EBR-II
1000.
100.
10.
1.0
0.1
RATIO
C
V
W
Mo
Nb
Li
IDEAL FOR TESTING IN EBR-II
Pb
Pb4Li
0
20
40
60
80
100
ISSEC THICKNESS-Cm

Figure VI.17

An even stronger case could be made for the non-nickel containing elements (Fe, Cr, Nb, and V) in the HFIR spectrum. Even though calculations were not done for these elements with the liquid ISSECs, the Pb and Pb_4Li ISSECs would also reduce the He/dpa ratio down to levels characteristic of the HFIR with ∿50 cm of flowing metal. The simulation of the appropriate fusion PKA spectra is even better in HFIR than in EBR-II. This means that contrary to current thinking, the thermal fission neutron facilities would be extremely valuable as a simulation facility for non Ni containing materials if such materials were to be used behind 50 cm or so of Pb or Pb_4Li material.

One final point is worth noting about the time structure of irradiation in fusion and fission devices. It is well-known that tokamaks are quasi-steady-state machines and from the point of view of the response of materials to the time of irradiation, such reactors could be considered steady-state. On the other hand, liquid ISSECs are originally conceived to be used in laser fusion reactors which are inherently pulsed systems. If one could assume that the time structure of the irradiation in a pulsed device such a laser fusion reactor does not have any drastic effect on the final damage state of the material, the simulation in fission reactors would give accurate results. However, it is expected that the inherent damage incurring in the irradiated material will be different in pulsed and steady-state systems.[138] Even though in the process of slowing down

the neutrons, the ISSECs help spread out the time interval during which neutrons arrive at the first structural wall it will still be far from a steady-state irradiation. Therefore, before one could use the fission reactor data in the design of laser fusion reactors employing liquid ISSECs reliably, one has to answer the question of what effects pulsed irradiation has on the material as opposed to steady-state irradiation.

CHAPTER VII

CONCLUSIONS AND RECOMMENDATIONS

This study has been devoted to the development of effective means to increase the first structural wall lifetimes in both magnetic and inertially confined fusion reactors. It has been shown that either a non-metallic element such as carbon or metals, either in solid or liquid form, can be used to protect the fusion reactor first walls from high energy neutrons as well as charged particles originating either in the magnetically confined plasma or inertially confined micro pellets. The study has been concerned with five distinct areas:

- Development and modification of models and applications of radiation damage theories to more precisely quantify the damage state in a neutron irradiated material,
- The effects of a carbon Internal Spectral Shifter and Energy Converter (ISSEC) on the radiation damage parameters of potential first wall materials for magnetic confinement fusion reactors operating on both D-T and D-D plasma cycles,
- The effects of carbon and high temperature refractory solid metal ISSECs on the 316 SS first structural wall and blanket of a D-T plasma tokamak fusion reactor,
- Application of liquid metals such as Li, Pb and Pb_4Li as ISSECs in inertial confinement laser fusion reactors,

. Demonstration of how fission reactor data on materials can be used more confidently in ISSEC protected systems.

The following points will serve as a summary of the results and conclusions of this study. This will be followed by general recommendations for future research.

VII.A. Summary and Conclusions

VII.A.1. Development and Modification of Radiation Damage Models

The displacement damage calculations code DISCS and the input preparation code for the DISCS, INPUTPP have been modified in such a way that the nuclear reactions (n,γ), $(n,n'p)$ and $(n,n'\alpha)$ are also included in the displacement cross section and PKA spectrum calculations. The approach used for the $(n,n'c)$ reactions is based on the sequential emission of neutron and charged particle, and some approximate nuclear evaporation models to determine the energy of the emitted particles. The approach used for the (n,γ) reaction is new and is completely based on data given in ENDF-B files. The codes DISCS and INPUTPP are reassigned the names DISCSM and INPUTPM, respectively, after the modifications. Some of the more important conclusions from this part of the study are as follows:

1) Because of the high energy threshold and coulomb barrier effects associated with the $(n,n'c)$ reactions, neither the displacement cross sections nor the PKA energy probability distributions in fusion reactor neutron spectra were drastically changed by the

inclusion of these reactions in the calculations. However, such changes will be important for PKA spectrum calculations in neutron environments expected in (D-Be), (D-Li) high energy neutron sources.

2) The effect of the (n,γ) reactions is to make the displacement cross sections finite at neutron energies below $\sim$1 keV and to shift the PKA probability distribution in neutron spectra to lower energies. However, this effect is found to be less than 1% in hard fusion neutron spectra and about 2% in neutron spectra degraded by 25 cm solid carbon ISSEC.

3) New routines which process the displacement cross section and PKA spectrum data from the DISCSM code are written and connected to DISCSM and other codes included in the MODISS computer package which is put together for calculations of this study.

VII.A.2. The Effects of a Carbon ISSEC on the Radiation Damage Parameters of Potential First Structural Wall Materials

In this part of the study a variable thickness carbon ISSEC was used in a non-breeding slab geometry blanket design to show the effects of softened fusion neutron spectra on the potential first wall materials; Al, V, 316 SS, Nb, Mo and Ta. The study was carried out for two systems operating on D-T and D-D plasma cycles. The main conclusions from this part of the study are:

VII.A.2.a. About Both D-D and D-T Systems

1) A carbon ISSEC reduces the displacement damage in all

potential first wall materials studied. Reduction factors vary from 3 to 5 with 12.5 cm carbon ISSEC and from 8 to 20 with 25 cm of carbon ISSEC.

2) With the exception of 316 SS, the gas production rates in the first wall are reduced by factors of 7-14 by a 12.5 cm carbon ISSEC, and by factors of 27-80 by a 25 cm carbon ISSEC.

3) Because of the thermal $Ni^{58}(n,\gamma)$ $Ni^{59}(n,\alpha)$ reaction sequence the total accumulated helium gas produced in 316 SS first wall after 10 years of operation is actually higher in D-D plasma case with 12.5 cm carbon ISSEC than it is with no ISSEC. In the D-T case the ISSEC still reduces the helium production in 316 SS first wall but for long operating times (longer than 10 years) the reduction factor drops to <70% of what it would be if only the higher energy (n,α) threshold reactions had been considered.

4) A carbon ISSEC reduces the short term radioactivity in 316 SS, Al and Nb first walls, but increases it in V and Ta.

5) Long term radioactivity is reduced in 316 SS, Al and V but it is increased in Nb and Ta.

VII.A.2.b. Conclusions about D-D vs. D-T

1) Displacement damage is higher for D-D system per (MW/m^2) neutronic wall loading.

2) Gas production rates are lower (15-60%) in D-D system except for helium production in 316 SS.

3) Thermally induced activation is aggravated by a carbon ISSEC in D-D system, i.e., those materials that have increased radioactivity in ISSEC protected systems will have it higher in D-D case than in D-T.

A final general conclusion from this part of the study is that there is no significant advantage of the 'D-D' plasma cycle over the 'D-T' cycle with respect to radiation damage.

VII.A.3. Effects of Carbon and Solid Metal ISSECs in D-T Plasma Tokamak Fusion Reactors

The use and performance of carbon, Mo, Nb, V, and W metal ISSECs in a D-T plasma cycle, 316 SS structure tokamak fusion reactor has been investigated with a breeding model blanket design in cylindrical geometry, and the study has led to the following conclusions:

1) All ISSECs considered reduce the displacement damage in the 316 SS first structural wall. Reduction factors vary between 2-5 for a 10 cm thick ISSEC, between 5-50 for a 25 cm thick spectral shifter.

2) The gas production rates in the first structural wall are also reduced by ISSECs. Helium production rates are reduced by factors of 3.2 - 12 with a 10 cm thick ISSEC and by factors of 12 to 275 with a 25 cm thick ISSEC. The reductions in hydrogen production rates are 2.5 to 12.7 and 8 to 235, respectively with 10 cm and 25 cm shield thickness.

3) The short and intermediate term radioactivity, Biological Hazard Potential (BHP) and afterheat of the 316 SS first wall are

reduced by all ISSECs, and the long-term activities are actually increased by a 10 cm or thicker carbon ISSEC.

4) All five ISSECs reduce the breeding ratio in the model blanket used in this part of the study. Reduction factors vary between 1.25 and 2.1 for a 10 cm thick ISSEC and between 2.1 and 13.6 for a 25 cm thick ISSEC.

5) Mo, Nb, and W ISSECs increase the total energy available per fusion in the model blanket while C and V ISSECs decrease it.

6) The radioactivity of the total blanket (including the ISSEC) at shutdown is higher than the unprotected case for W, Mo, Nb and V ISSECs but it is lower with C ISSEC. At 1-10 years after shutdown the blanket has about the same radioactivity with and without an ISSEC. At long time after shutdown (greater than 100 years), a Mo ISSEC system has the most radioactivity followed by the Nb ISSEC system. Carbon, W, and V ISSEC protected designs have about the same radioactivity as unprotected blankets.

7) Maximum displacement rates in the ISSECs themselves per 1 MW/m^2 neutron wall loading per year vary between 8.4 for Nb and 12.5 dpa/yr for V. Maximum helium production rates vary between 3.7 for W and 2300 appm/yr for C.

8) The radioactivity at shutdown of all metal ISSECs is about the same order of magnitude (1-10 Ci/W), and is higher than that of C ISSEC by a factor of about 10^4. At long times after shutdown (longer than 100 years) radioactivity in C, W and V ISSEC has

decayed away while in Mo it is ∿0.1% of its value at shutdown and in Nb about 0.01% of its shutdown value.

9) Most ISSECs cooled only by thermal radiation are limited by their vapor pressure and the maximum allowable thicknesses are 9.5 cm for C, 7.5 cm for Mo, and 4.5 cm for V for a 1 MW/m^2 neutronic and 4 W/cm^2 surface heat loading. Niobium and tungsten are limited to 9 and 12.5 cm by vapor pressure and 8.5 and 6 cm by breeding ratio considerations, respectively.

10) A conduction plus radiation cooled ISSEC can have greater thickness up to 15 cm or higher depending on the specific design.

11) From a thorough investigation of all four metal ISSECs considered, including their capability of reducing radiation damage, maximum allowable thicknesses, cost, availability, vacuum properties, plasma - ISSEC surface interactions, etc., molybdenum appears to be the best overall for a metal ISSEC(compared to W, Nb and V).

12) The same investigation revealed that a definitive choice between a carbon and molybdenum ISSEC is difficult to make at this time as both materials have strong points but in different areas.

VII.A.4. The Performance of Liquid Metals Li, Pb, and Pb_4Li as ISSECs in Laser Fusion Reactors

The liquid metals Li, Pb, and Pb_4Li have been proposed, in connection with the waterfall concept, to protect the laser fusion

reactor first walls from neutrons, charged particles, X-rays and shock waves. This study revealed that in addition to protecting the first wall, liquid ISSECs can also increase the tritium breeding ratio and energy multiplication in the system. Conclusions from this part of the study are broken down with respect to each ISSEC material considered:

VII.A.4.a. Conclusions for Liquid Li ISSEC

1) Li is the least effective of the three liquid ISSECs considered in reducing the displacement damage and gas production rates in the 316 SS first structural wall.

2) If the first wall is operating at 300°C, it is estimated that a 52 cm thick liquid Li zone gives enough protection to the 316 SS first structural wall so that from the radiation damage point of view it can last for 30 years at 5 MW/m^2 nominal wall loading and 70% plant factor. If the wall is operating at 500°C, about 85 cm thick lithium zone is needed, and at 600°C the required Li thickness goes up to about 200 cm.

3) A high tritium breeding ratio is obtained. In fact, the breeding ratio in just the ISSEC itself goes over 1.0 for liquid Li thicknesses greater than 30 cm.

VII.A.4.b. Conclusions for Liquid Pb ISSEC

1) Enhances the thermal output of the system by increased energy multiplication.

2) A thickness of 47-67 cm of Pb is estimated to give enough protection to the 316 SS first structural wall so that from radiation damage considerations alone it can last up to 30 years at 5 MW/m^2 loading and 70% plant factor if the first wall operated at temperatures 300-600°C.

3) The percentage of energy deposited in a given thickness of Pb is not as great as it is for the other two liquid ISSEC materials considered.

VII.A.4.c. Conclusions for Liquid Pb_4Li ISSEC

1) Enhances the thermal output of the system by increased energy multiplication.

2) The lead-lithium eutectic is the most effective of the three materials considered in reducing the radiation damage to the first structural wall. From radiation damage point of view a 37 to 65 cm ISSEC is estimated to give the 316 SS first wall a 30 year lifetime if it operated between 300°C and 600°C at 5 MW/m^2 neutron wall loading and 70% plant factor.

3) For thicknesses greater than 50 cm, the breeding ratio inside the ISSEC is over 1.0.

4) For the same thickness, both the percentage and the absolute amount of energy deposited in ISSEC is higher than both the pure Li and Pb cases.

From the conclusions already stated in Sections VII.A.4.a.,b., and c. and the ones that will be given in Section VII.A.5., we conclude that the liquid ISSEC material with the best overall characteristics is Pb_4Li and the thickness to be used is 50 to 75 cm.

VII.A.5. Prospects for Fission Reactor Testing of Fusion Reactor Materials

1) The probability of getting a PKA with energy greater than about 0.1 MeV is 3-4 orders of magnitude higher in an unsoftened fusion first wall neutron spectrum than it is in either EBR-II or HFIR fission reactor neutron spectrum.

2) The only ISSEC materials that can bring down the high energy part of the PKA distribution in a fusion reactor first wall neutron spectrum to EBR-II or HFIR levels are Pb and Pb_4Li with thicknesses around 55 cm and 65 cm, respectively. With the other ISSEC materials considered in this study either the required thickness becomes too large (>2 m) or heat transfer limitations prohibit the ISSECs from operating at the required thicknesses.

3) The calculated appm He/dpa ratio in Al, V, Nb and Mo first walls is much higher in a hard fusion reactor neutron spectrum (or even behind ∿30 cm of carbon), than it is in either EBR-II or HFIR spectrum. Because of the $Ni^{58}(n,\gamma)Ni^{59}(n,\alpha)$ reaction sequence, 316 SS has a higher appm He/dpa ratio in HFIR than in fusion spectrum.

4) Either a 65 cm of liquid Pb or 73 cm of liquid Pb_4Li ISSEC reduces the appm He/dpa ratio in the 316 SS structural first wall of a CTR to same value one would have obtained in 316 SS in EBR-II. The other ISSEC materials require unreasonably large thicknesses to do the same. For example, with Li one needs about 3 meters, with carbon 2.5 meters, V, W or Mo about 125 cm, and Nb around 73 cm. As stated previously such large thicknesses of solid ISSECs are not possible because of heat transfer problems.

5) An overall conclusion of this phase of the work is that if the time dependence of the radiation damage in a laser fusion reactor is not overriding, the structural materials to be used in laser fusion reactors employing liquid Pb and Pb_4Li ISSECs at thicknesses of 50-75 cm can be tested in fast fission test facilities already present today. This would also allow the vast amount data that have already been obtained in such facilities to be used in the design of future fusion facilities.

VII.B. Recommendations for Future Research

VII.B.1. Recommendations for Displacement Damage Studies

1) Secondary displacement functions used in the calculation of the displacement cross sections should be improved to include the effects of recombination and clustering of interstitials and vacancies. The actual damage state of the irradiated material, especially in the case of neutron and heavy ion irradiations, would be much better described by such displacement functions.

2) Displacement cross sections calculated by various authors should be consolidated and one general displacement cross section library which includes the cross sections for most elements and alloys of technological importance should be established. In this way the displacement damage results reported in fusion research or in data obtained from high energy neutron sources when they become available would be consistent and easy to compare.

3) The displacement damage calculations should be extended to higher neutron energies (higher than 20 MeV) either when the experimental nuclear reaction cross sections become available in ENDF or by making use of the calculated reaction cross sections. This would be important in the calculation of PKA spectra in neutron spectra soon to be available from high energy (D-Li) or (D-Be) neutron sources where neutrons can have energies up to 35 MeV or higher.

VII.B.2. Recommendations on Future Work With Carbon or Metallic Solid ISSECs

1) Plasma-carbon surface interactions should be investigated experimentally at appropriate ion energies and surface temperatures. In particular the experiments should be carried out at or above 1200-1400°C range to determine the rate at which carbon reacts chemically with the incident hydrogenic ions.

2) The effects of high energy neutron irradiations at temperatures 1500°C or higher in the metal ISSECs themselves should be investigated.

3) For solid ISSECs, either carbon or metal, better mechanical attachment and heat transfer schemes than the ones presented in this study should be designed to allow them to have larger thicknesses and better first wall protection. Active cooling of ISSECs in addition to cooling by conduction and thermal radiation should be seriously considered.

VII.B.3. Recommendations on Work With Liquid ISSECs

1) Corrosion characteristics of liquid ISSECs, Pb, Pb_4Li with 316 SS as well as other potential first wall materials should be studied at temperatures 400-500°C.

2) Pumping power losses due to liquid Pb and Pb_4Li ISSECs should be determined.

3) The question about the transmission of the laser light through the vapor generated in the reaction chamber after each micro-explosion should be settled.

4) The effect of pulsing on the final damage state of the neutron irradiated materials should be studied to find out how accurately one can use the materials data obtained in fission reactors in the design of the laser fusion reactors employing liquid Pb or Pb_4Li ISSECs.

References

1. G.L. Kulcinski, R.G. Brown, R.G. Lott, and P.A. Sanger, Nucl. Tech., 22, 20 (1974).

2. A Fusion Power Plant, R.G. Mills, Ed., MATT-1050, April 1974.

3. W. Danner, Max-Planck Institute fur Plasmaphysik Report #IPR 4/130, February 1975.

4. B. Badger, et al., "UWMAK-I, A Wisconsin Toroidal Fusion Reactor Design," Fusion Research Program, University of Wisconsin, UWFDM-68, Vol. 1 and 2.

5. B. Badger, et al., "UWMAK-II, A Conceptual Tokamak Power Reactor Design," Fusion Research Program, University of Wisconsin, UWFDM-112, October 1975.

6. G.L. Kulcinski, J.R. Young, "The Influence of First Wall Lifetime on the Cost of Electricity in UWMAK Type Fusion Reactors," Proc. Int. Confer. on Rad. Eff. and Tritium Tech., Gatlinburg, Tenn., October 1-3, 1975. Also Report UWFDM-140, Nuclear Engr. Dept., Univ. of Wis., Madison, Wisconsin, October 1975.

7. J.A. Maniscalco, et al., "Design Studies of a Laser Fusion Power Plant," IAEA Conference and Workshop on Fusion Reactor Design, October 10-21, 1977, Madison, Wisconsin. See also the Lawrence Livermore Laboratory report UCRL-80424 by W.R. Meier and J.A. Maniscalco.

8. R.W. Conn, G.L. Kulcinski, H. Avci, and M. El-Maghrabi, Nucl. Tech. 26, 125 (1975). Also report UWFDM-115, Nucl. Engr. Dept., Univ. of Wis., Madison, Wisconsin, October 1974.

9. G.L. Kulcinski, R.W. Conn, H.I. Avci, D.K. Sze, "Production of CTR Metallic First Walls by Neutron Spectral Shifting," Report UWFDM-127, Nuclear Engr. Dept., Univ. of Wis., June 1975. Also Trans. Am. Nucl. Soc., 21, 50 (1975).

10. H.I. Avci and G.L. Kulcinski, "The Response of ISSEC Protected First Walls to DT and DD Plasma Neutrons," Proc. Int. Confer. on Rad. Eff. and Tritium Tech. for Fusion Reactors at Gatlinburg, Tenn. October 1-3, 1975. Also Report UWFDM-135, Nucl. Engr. Dept., Univ. of Wis., Madison, Wisconsin, October 1975.

11. H.I. Avci, Y. Gohar, T. Y. Sung, G.L. Kulcinski, and C.W. Maynard, Nuclear Engineering and Design, 45, 285 (1978). Also Report UWFDM-202.

12. H.I. Avci and G.L. Kulcinski, "The Effect of a Liquid ISSEC on Radiation Damage Parameters in Laser Fusion Reactor First Walls," Report UWFDM-205, Nuclear Engr. Dept., Univ. of Wis., Madison, Wisconsin, April 10, 1977. (revised August 1977)

13. H.I. Avci and G.L. Kulcinski, "Comparison of Liquid ISSECs, Li, Pb, and Pb_4Li for Use in Laser Fusion Reactors," Report UWFDM-208, Nucl. Engr. Dept., Univ. of Wis., Madison, Wisconsin, May 1977. (revised August 1977).

14. H.I. Avci and G.L. Kulcinski, Trans. Am. Nuc. Soc., 28, 40 (1978).

15. G.L. Kulcinski, R.W. Conn, G. Lang, Nucl. Fusion, 15, 327 (1975). Also report UWFDM-108.

16. D.K. Sze, R.W. Conn, "Heat Transfer and Neutronics of ISSEC and Partial ISSEC Blanket Designs," Report UWFDM-128, Nucl. Engr. Dept., Univ. of Wis., Madison, Wisconsin, June 1975. Also Trans. Am. Nucl. Soc., 21, 34 (1975).

17. "An Engineering Design Study of a Reference Theta-Pinch Reactor (RTPR)" LA-5336; ANL-8019. Joint report of Los Alamos Scientific Lab. and Argonne National Lab. (March, 1974).

18. A.P. Fraas, "Conceptual Design of the Blanket and Shield Region and Related Systems for a Full Scale Toroidal Fusion Reactor," ORNL-TM-3096, Oak Ridge National Lab., May 1973.

19. H.B. Steward, et al., "Utilization of the Thorium Cycle in the HTGR," Proc. Int'l Conf. Peaceful Uses of Atomic Energy, 4th Geneva Conf. (1971).

20. G. Hopkins, In Proc. 1st Top. Meet. on the Technology of Cont. Nucl. Fus., San Diego, April 1974 (Conf. - 740402 - p2, USAEC) Vol. 2, P. 437.

21. D. Steiner, "The Neutron Induced Activity and Decay Power of the Niobium Structure in a D-T Fusion Reactor Blanket," ORNL-TM-3094, Oak Ridge National Lab. (1974).

22. W.F. Vogelsang, G.L. Kulcinski, R.G. Lott, and T.Y. Sung, Nucl. Tech., 22, 379 (1974).

23. D.J. Dudziak and R.A. Krakowski, Vol. 1, P. 548 of reference 20.

24. R.W. Conn, T.Y. Sung, and M.A. Abdou, Nucl. Tech., 26, 391 (1975).

25. M.A. Abdou, L.W. Wittenberg, and C.W. Maynard, Nucl. Tech., 26, 400 (1975).

26. J.R. Powell, et al., "Studies of Fusion Reactor Blankets with Minimum Radioactive Inventory and with Tritium Breeding in Solid Lithium Compounds," BNL-18236, Brookhaven National Lab., (1973).

27. G.R. Odette and D.R. Doiron, Nuclear Tech., 29, 346 (1976).

28. M.T. Robinson, in Radiation Induced Voids in Metals, p. 397, J.W. Corbett and L.C. Ianniello Eds., National Tech. Information Series CONF-710601, April 1972.

29. M.T. Robinson and I.M. Torrens, Phys. Rev., B, 9, 12, 5008 (1974).

30. "Recommendation for Displacement Calculations for Reactor/ Accelerator Studies in Austenitic Steels," Nucl. Engr. Design, 33, 91 (1975).

31. D. Doran, J. Beeler, N. Dudey, and M. Fluss, "Report of the Working Group on Displacement Models and Procedures for Damage Calculations," HEDL-TME 73-76, Westinghouse Hanford Company (1973).

32. J. Beeler, Phys. Rev., 150, 2, 470 (1966).

33. G.A. Kinchin and R.S. Pease, Rept. Prog. Phys., 18, 1 (1955).

34. M.T. Robinson, Phil. Mag. 12, 741 (1965) and 17, 639 (1968).

35. J. Lindhard, M. Scharff, and H. Schiott, Mat. Phys., Medd. Dan Vid Selsk., 33, 14 (1963).

36. J. Beeler, J. Test. Eval., 33, 230 (1975).

37. D. Doran, R. Simons, and W. McElroy, "Spectral Effects in Neutron and Charged Particle Irradiations," Proc. ASTM Symp. Effects of Radiation on Structural Materials, Gatlinburg, Tenn., June 1974.

38. D. Doran, "Fundamentals of Displacement Production in Irradiated Metals," HEDL-SA-1012, Westinghouse Hanford Company (1975).

39. M. Norgett, "Effects of Replacement Sequences in Cascade Simulation and Annealing," TPD AERE-TPS 60, Atomic Energy Research Establishment, Harwell (1973).

40. L.R. Greenwood, Argonne National Laboratory, Argonne, Illinois (private communication).

41. W. Sheely, Nucl. Sci, Eng., 29, 165 (1967).

42. J.D. Jenkins, Nucl. Sci. Eng., 41, 155 (1970).

43. D.G. Doran, Nucl. Sci. Eng., 49, 130 (1972).

44. D.G. Doran, and N.J. Graves, "Displacement Cross Section and PKA Spectra: Tables and Applications," HEDL-TME 76-70, Westinghouse Hanford Company (1976).

45. T.A. Gabriel et al., Nucl. Sci. Eng., 61 21 (1976).

46. D.M. Parkin and A.N. Goland, Rad. Eff., 28, 31 (1976).

47. K. Kikuchi and M. Kawai, Nuclear Matter and Nuclear Reactions, North-Holland Publishing Co., (1968).

48. I. Dostrovsky, Z. Fraenkel, and G. Friedlander, Phys. Rev., 116, 683 (1959).

49. M.K. Drake, Ed., "Data Formats and Procedures for the ENDF Neutron Cross Section Library," Report BNL 50274 (T-601), Brookhaven National Laboratory (1970). See also O. Ozer and D. Graber, ENDF/B Summary Documentation" BNL-17541 and ENDF-201, Brookhaven National Laboratory, July 1973.

50. W.W. Engle, Jr., "A Users Manual for ANISN," K-1693, Oak Ridge Gaseous Diffusion Plant.

51. T.Y. Sung and W.F. Vogelsang, "DKR: A Radioactivity Calculation Code for Fusion Reactors," Report UWFDM-170, September 1976.

52. W.A. Beckman, "HEAT: Heat Transfer Computer Program in Fortran V Language," EES Report No. 37, Mechanical Engr. Dept., University of Wisconsin, Madison, Wisconsin (1972).

53. G.E. Myers, "FEM2D: A Finite Element Program for Solving Two-Dimensional Conduction Problems," Mechanical Engr. Dept., University of Wisconsin, Madison, Wisconsin (1976).

54. D.J. Dudziak, "Fusion Reactor Nuclear Analysis - Methods and Applications," 8th Symp. on Fusion Technology, Noordijkerhout, The Netherlands, June 1974.

55. R.W. Wright, et al., "SUPERTOG: A Program to Generate Fine Group Constants and P_n Scattering from ENDF/B," ORNL-TM-2679, Oak Ridge National Laboratory (1969).

56. N.M. Greene, et al., "AMPX: A Modular Code System for Generating Coupled Multi-Group Neutron-Gamma Libraries from ENDF/B," ORNL-TM-3706, Oak Ridge National Laboratory.

57. D. Steiner, "Analysis of a Bench Mark Calculation of Tritium Breeding in a Fusion Reactor Blanket: The United States Contribution," ORNL-TM-4177, April 1973.

58. Y. Gohar, C.W. Maynard, T. Wu, "Validation Study of the UNIVAC 1110 Version of the CTR-PMCS - Nuclear Data Library and Codes Package," Report UWFDM-209, June 1977.

59. M. Abdou, C.W. Maynard, and R.Q. Wright, "MACK: A Program to Calculate Neutron Energy Release Parameters (fluence to kerma factors) and Multi-Group Neutron Reaction Cross Sections from Nuclear Data in ENDF Format," ORNL-TM-3994.

60. J.R. Knight and F.R. Mynatt, "MUG: A Program for Generating Multi-Group Photon Cross Sections," CTC-17, January 1970.

61. T.Y. Sung, "Radioactivity Calculations in Fusion Reactors," Ph.D. Thesis, University of Wisconsin-Madison (1976).

62. T.Y. Sung, and W.F. Vogelsang, "Decay Chain Data Library for Radioactivity Calculations," Report UWFDM-171, September 1976.

63. USNRC, "Standards for Protection Against Radiation," NRC Rules and Regulations, Title 10, Part 20 (1975).

64. D.J. Hughes, et al., "Neutron Cross Sections," 2nd Ed., BNL-325 (1958) and Supplement.

65. C.M. Lederer, et al., Table of Isotopes, 6th Ed., John Wiley & Sons, Inc. (1967).

66. W.A. Beckman, Solar Energy, 13, 293 (1971).

67. D.G. Doran, Nucl. Sci. Eng. 52, 398 (1973).

68. S. Pearlstein, private communication, See also S. Pearlstein, J. Nuclear Energy, 27, 81, (1973).

69. G.L. Kulcinski, D.G. Doran, and M.A. Abdou, ASTM STP 570 (1975), pp. 329-351.

69a. M.T. Robinson, "The Energy Dependence of Neutron Radiation Damage in Solids," BNES Nucl. Fus. React. Conf., Culham Laboratories, Sept. 1969.

70. G. H. Miley, Univ. of Illinois, private communication.

71. D.M. Plaster, R.T. Santoro, and W.E. Ford III, "Coupled 100 Group Neutron and 21 Group Gamma Ray Cross Sections for EPR Calculations," RONL-TM-4872, April 1975.

72. W.C. Morgan, J. Nucl. Mat., 51, 209 (1974).

73. B. Badger, et al., UWMAK-III, A Noncircular Tokamak Power Reactor Design," Report UWFDM-150, Fusion Technology Program, Nuclear Engr. Dept., Univ. of Wisconsin, Madison (July 1976).

74. G.B. Engle and W.P. Eatherly, High Temperatures and High Pressure, 7, 319, 1969.

75. J.H. Cox and J.W. Helm, Carbon, 7, 319 (1969).

76. W.J. Gray and W.C. Morgan, BNWL-B-288 and BNWL-B-289, June 1973.

77. W.N. Reynolds, et al., "Radiation Damage in Graphite at 1200^{o}C," 2nd Conf. on Indust. Carbon and Graphite, Soc. Chem. Ind., April 1965.

78. B.T. Kelly, et al., "Fast Neutron Induced Dimensional Changes in Graphites and Carbons," Ibid.

79. B.T. Kelly, "Dimensional Changes and Lattice Parameter Changes in Graphite Crystals Due to Interstitial Atoms and Vacancies," Ibid.

80. M.R. Everett, et al., "Graphite Materials Data for High Temperature Nuclear Reactors," 3rd Conf. on Ind. Carbon and Graphite, Soc. Chem. Ind., April 1970.

81. G.L. Tingey, W.C. Morgan and E.M. Woodroff, "Near-Isotropic Graphites for Helium Cooled Reactors - A Review," BNWL-B-478 (Feb. 1976).

82. J.W. Helm and J.M. Davidson, "Effect of Neutron Exposure on the Distortion of Reactor Graphite," Carbon 1, 435 (1964).

83. J.W. Helm, "Radiation Effects in Graphite at High Temperatures," Carbon 3 493 (1966).

84. M. Van Den Berg, M. R. Iverett and A. Kingsbury, "12th Biennial Conf. on Carbon," Pittsburgh, Penn., 1975, p. 307.

85. W.C. Morgan, "A Note on the Dimensional Change Rates of Graphite Irradiated Above 900^{o}C," BNWL, 1976 (private communication).

86. G.J. Thomas, W. Bauer, P.L. Mattern and B. Granoff, "He and H Implantation of Vitrous Silica and Graphite," Report SAND 75-8718, Sandia Lab., Albuquerque, N.M. Also Proc. Am. Chem. Soc. Mtg., Chicago, Illinois, August 21-22, 1975.

87. J. B. Holt, et al., "Helium Generation and Diffusion in Graphite," Lawrence Livermore Lab., Livermore, California, April 1976.

88. J. Scott, Oak Ridge National Lab., private communication.

89. C.L. Smithells, Metals Reference Book, Plenum Press, N.Y. (1967).

90. The Industrial Graphite Engineering Handbook, Union Carbide Co. (1970).

91. I. Sviatoslavsky, Nucl. Engr. Dept., Univ. of Wisconsin-Madison, private communication.

92. B. Benenati, P. Tichler and J.R. Powell, "Low Activity Aluminum Blanket," Report BNL 21159, Brookhaven National Lab., March 1976.

93. D. Steiner, et al., "ORNL Fusion Power Demonstration Study: Interim Report," ORNL-TM-5813, Oak Ridge National Lab., Oak Ridge, Tennessee.

94. J. Davis, McDonnell-Douglas Astronautics Co. - East (private communication.

95. G.S. Allison, "Assessment of Materials Needs for Fusion Reactors," Report BNWL-1933, Battelle Northwest Lab., Richland, Washington (July 1976).

96. J.N. Hartley, et al., "Materials Availability for Fusion Power Plant Construction," Report BNWL-2016 (Sept. 1976), Ibid.

97. R. Behrish, Nuclear Fusion, 12, 695 (1972).

98. C.L. Mantell, Carbon and Graphite Handbook, Interscience, New York (1968).

99. G.A. Beitel, "The Use of Graphite in High and Ultra-High Vacuum - A Review," J. Vac. Science and Tech., Vol. 8, No. 5, 647 (1971).

100. G.P. Lang and V.L. Holmes, "Gas Content and Sticking Probabilities for Fibrious Forms of Graphite as Applied to Fusion Reactors," Nuclear Fusion, 16, 162 (1976).

101. R. Behrish, to be published, 1976 Erice Summer School on Tokamaks.

102. H. Vernickel, EURATOM Association, Garching b. Munchen, West Germany (private communication).

103. B. Feinberg and R.S. Post, "Graphite Surface Erosion and Blistering," Report UWFDM-141, Nuclear Engineering Department, University of Wisconsin, Madison, August 1975.

104. M. Balooch and D.R. Olander, J. Chem. Phys. 63, No. 11, December 1975.

105. I.P. Busharov, E.A. Gorbatov, V.M. Gusev, M.I. Geseva and Y.V. Martynenko, "Chemical Atomization of Graphite by H^+ Ions," The I.V. Kurchatov Order of Lenin Institute of Atomic Energy, Moscow (1975).

106. S. Veprek and M.R. Hague, "On the Chemical Erosion of the First Wall in the Next Generation of Tokamak Devices for Controlled Fusion," Univ. of Zurich, Zurich, Switzerland.

107. B.J. Wood and A. Wise, J. Phys. Chem. 73, 1348 (1969).

108. J. Bohdansky et al., "Erosion of Different First Wall and Limiter Materials by Low Energy Hydrogen Ions," Fus. Tech., Proc. of 9th Symp., p. 541, Pergamon Press (1976).

109. R. Ekern, S.K. Das and M. Kaminsky, "Temperature Dependence of Surface Damage in Graphite Cloth Irradiated with Deuterons and Helium Ions," 2nd Inter. Confer. on Surface Effects on Contr. Fus. Devices, San Francisco, California, February 1976.

110. S.K. Erents, C.M. Braganza and G.M. McCracken, "Methane Formation During the Interaction of Energetic Protons and Deuterons With Carbon," CLM-P451, February 1976.

111. J. Roth, et al., J. Nucl. Mat. 63, 222 (1976).

112. N. Laegreid and G.K. Wehner, J. Appl. Phys. 32, 365 (1961) and D. Rosenberg and G.K. Wehner, J. Appl. Phys. 33, 1842 (1962).

113. G. Carter and J.S. Colligen, Ion Bombardment of Solids (American Elseveier Publishing Co., New York: 1968), p. 323, p. 325.

114. O. Almen and G. Bruce, Nucl. Inst. and Methods 11, 279 (1961).

115. M. Kaminsky and S.K. Das, "14.1 MeV Neutron Sputtering of Polycrystalline and Monocrystalline Niobium with Different Microstructures," J. Nucl. Mat., 60, 111 (1976). Also in ANL CTR quarterly progress report, Nov. 1975.

116. O.K. Harling, et al., "Recent Neutron Sputtering Results and the Status of Neutron Sputtering," J. Nucl. Mat. 63, 422 (1976) (see bibliography in this reference for earlier work by this group).

117. R. Behrish, "Neutron Sputtering," 6th Inter. Conf. on "Atomic Collisions in Solids," Amsterdam, September 22-26, 1975.

118. L.H. Jenkins, et al., Appl. Phys. Letters, 26, 426 (1975).

119. M. Kaminsky and S.K. Das, "Sputtering of Vanadium and Niobium Under 14 MeV Neutron Impact," 2nd Inter. Conf. on Surface Eff. in Cont. Fus. Devices, San Francisco, February 16-20, 1976.

120. R.J. Garber, G.P. Dolya, V.M. Kolyada, A.A. Molden, and A.I. Foderenko, JETP Lett., 7, 296 (1968).

121. S.K. Erents and G.M. McCracken, CLM-P-323, September 1972.

122. H. Verbeck and W. Eckstein, "Applications of Ion Beams to Metals," Ed. S.T. Picraux, E.P. Eernisse, and F.L. Vook, Plenum Publ. Corp., N.Y., p. 597 (1974).

123. G.M. McCracken and S.K. Erents, CLM-P-359, November 1973.

124. W. Bauer and G.A. Thomas, SLL-73-5266, June 1973.

125. R.W. Knoll, M.S. Thesis, University of Wisconsin, Madison, August 1974.

126. M. Kaminsky and S.K. Das, Radiation Effects, 18, 245 (1973).

127. R. Behrish, et al., Appl. Phys. Letters, 27, No. 4, p. 199 (1975).

128. J. Roth, R. Behrish, B.M.U. Scherzer, J. Nucl. Mat., 57, 365 (1975). Also page 573 in reference 78.

129. S.K. Das and M. Kaminsky, "Defects and Defect Clusters in BCC Metals and Their Alloys," Nucl. Met., 18, 240 (1973).

130. M. Kaminsky and S.K. Das, Nucl. Nucl. Tech., 22, 373 (1974).

131. D. Kaletta, J. Nucl. Material, 63, 347 (1976).

132. R. Wright, R. Varma and D.M. Gruen, "Raman Scattering and SEM Studies of Graphite, CVD Pyrolitic and Vitreous Carbon, etc.," 2nd Inter. Confer. on Surface Effects on Contr. Fus. Devices, San Francisco, Calif., February 16-20, 1976.

133. L.H. Rovner and K.Y. Chen, "Surface Erosion of C and SiC by 0.5-3.5 MeV He^+," reference 132. Also Report GA-A13812, General Atomic Co., San Diego, California.

134. J. Roth, R. Behrish, and B.M.U. Scherzer, J. Nucl. Mat., 57, 365 (1975).

135. Gmelins Handbuch Der Anorganischen Chemie Blei-Teil C3, System #47, Pub. 1970 - p. 979.

136. J.A. Maniscalco, et al., "Civilian Applications of Laser Fusion," Report UCRL-52349, November 1977.

137. R.W. Conn, K. Okula, A.W. Johnson, "Minimizing Radioactivity and Other Features of Elemental and Isotopic Tailoring of Materials for Fusion Reactors," Nucl. Tech. (in press).

138. N.M. Ghoniem and G.L. Kulcinski, "Swelling of Metals Under Pulsed Irradiation," UWFDM-179, October 1976.

Table A.1

Sample card input to the INPUTPM program for the element niobium

```
1189
NIOBIUM 1189
0,930E+02 0,410E+02 0,36E-08 0,600E-08 0,930E-01 0,930E+01 0,300E+01
100  0,0
  1  1  2  1  5  0  1  1
     1     1
           106
 ,2200+01  ,4140+00  ,5316+00  ,6826+00  ,8764+00  ,1125+01  ,1445+01  ,1855+01
 ,2382+01  ,3059+01  ,3928+01  ,5044+01  ,6476+01  ,8315+01  ,1068+02  ,1371+02
 ,1760+02  ,2260+02  ,2902+02  ,3727+02  ,4785+02  ,6144+02  ,7889+02  ,1013+03
 ,1301+03  ,1670+03  ,2145+03  ,2754+03  ,3536+03  ,4540+03  ,5830+03  ,7485+03
 ,9611+03  ,1234+04  ,1585+04  ,2035+04  ,2613+04  ,3355+04  ,4307+04  ,5531+04
 ,7102+04  ,9119+04  ,1171+05  ,1503+05  ,1930+05  ,2479+05  ,3183+05  ,4087+05
 ,5248+05  ,6738+05  ,8652+05  ,1111+06  ,1228+06  ,1357+06  ,1500+06  ,1657+06
 ,1832+06  ,2024+06  ,2237+06  ,2472+06  ,2732+06  ,3020+06  ,3337+06  ,3688+06
 ,4076+06  ,4505+06  ,4979+06  ,5502+06  ,6081+06  ,6721+06  ,7427+06  ,8208+06
 ,9072+06  ,1003+07  ,1108+07  ,1225+07  ,1353+07  ,1496+07  ,1653+07  ,1827+07
 ,2019+07  ,2231+07  ,2466+07  ,2725+07  ,3012+07  ,3329+07  ,3679+07  ,4066+07
 ,4493+07  ,4966+07  ,5488+07  ,6065+07  ,6703+07  ,7408+07  ,8187+07  ,9048+07
 ,1000+08  ,1105+08  ,1221+08  ,1350+08  ,1492+08  ,1600+08  ,1700+08  ,1800+08
 ,1900+08  ,2000+08
1189   2 151
1189   3   2
1189   3  16
1189   3  22
1189   3  51
1189   3  52
1189   3  53
1189   3  54
1189   3  55
1189   3  56
1189   3  57
1189   3  58
1189   3  59
1189   3  60
1189   3  61
1189   3  62
1189   3  91
1189   3 102
1189   3 103
1189   3 107
  0    0   0
           52
 ,2200-07  ,4140-06  ,8764-06  ,1855-05  ,3928-05  ,8315-05  ,1760-04  ,3727-04
 ,7889-04  ,1670-03  ,3536-03  ,7485-03  ,1485-02  ,3355-02  ,7102-02  ,1503-01
 ,3183-01  ,6738-01  ,1228+00  ,1657+00  ,2237+00  ,3020+00  ,4076+00  ,5502+00
 ,7427+00  ,1003+01  ,1353+01  ,1827+01  ,2466+01  ,2725+01  ,3012+01  ,3329+01
 ,3679+01  ,4066+01  ,4493+01  ,4966+01  ,5488+01  ,6065+01  ,6703+01  ,7408+01
 ,8187+01  ,9048+01  ,1000+02  ,1105+02  ,1221+02  ,1350+02  ,1492+02  ,1600+02
 ,1700+02  ,1800+02  ,1900+02  ,2000+02
2000  8,8260  9,200
1;NPRTME ALFA
4,003  2,000  88,91  39,00   0,9400E+00  0,12E-12
 2000   1,951

1,007  1,000  93,00  40,00 0,7250E+00  0,0
N,P
4,003  2,000  90,00  39,00  0,9400E+00  0,120E-12
N,A
```

Table A.2

Part of an output from the INPUTPM (input to the DISCSM) for the element niobium

```
1.          1 1189
2.       NIOBIUM 1189
3.         .930+002  .410+002  .360-004  .600-004  .930-001  .930+001  .300+001
4.            1    1    2    1    5    0    1    1
5.            1    1
6.                 1
7.                 2
8.         .10000-004 .10000+001 .20000+008 .10000+001
9.                 2
10.        .10000-008          16
11.        .00000     .00000     .12500+006 .57408-007 .37500+006 .64296-006
12.        .62500+006 .41533-007 .87500+006 .13678-006 .11250+007 .82667-007
13.        .13750+007 .13578-006 .21250+007 .31749-006 .28750+007 .20267-006
14.        .43750+007 .88857-007 .46250+007 .11482-006 .48750+007 .78873-007
15.        .51250+007 .11382-006 .60000+007 .29952-007 .71250+007 .14976-007
16.        .72140+007 .00000
17.        .20000+008          16
18.        .00000     .00000     .12500+006 .57408-007 .37500+006 .64296-006
19.        .62500+006 .41533-007 .87500+006 .13678-006 .11250+007 .82667-007
20.        .13750+007 .13578-006 .21250+007 .31749-006 .28750+007 .20267-006
21.        .43750+007 .88857-007 .46250+007 .11482-006 .48750+007 .78873-007
22.        .51250+007 .11382-006 .60000+007 .29952-007 .71250+007 .14976-007
23.        .72140+007 .00000
24.          100   51
25.        .22000-007.00000
26.        .5664+001    1    1
27.        .0000
28.           12     .254950+001
29.         -.0290  -.7400  -.8100  -.9590 -1.0700 -1.3150 -1.4884 -1.6740 -1.9470
30.        -2.1590 -2.3350 -2.5190
31.        .0000  .0000  .0000  .0000  .0000  .0000  .0000  .0000  .0000  .0000
32.        .0000  .0000  .0000
33.             2000     8.8260     9.2000
34.        .0000
35.             4.003      2.000     88.910     39.000 N,NPRIME ALFA
36.        .9400+000 .1200-012
37.             2000     1.9510     8.8260
38.        .00000
39.        .11223+01
40.             1.007      1.000     93.000     40.000 N,P
41.        .7250+000 .0000     .7190+000
42.        .00000
43.             4.003      2.000     90.000     39.000 N,A
44.        .9400+000 .1200-012 .4914+001
45.        .00000
46.        .41400-006,00000
47.        .5664+001    1    1
48.        .0000
49.        .0000  .0000  .0000  .0000  .0000  .0000  .0000  .0000  .0000  .0000
50.        .0000  .0000  .0000
51.             .0000
52.        .00000
53.        .22644+000
54.        .00000
55.        .00000
```

Table A.3.1

Damage cross sections for niobium at 14.92 MeV neutron energy calculated by the DISCM code

DAMAGE CROSS SECTIONS

FORNIOBIUM 1189

ENERGY (MEV)	MODEL	ELASTIC	INELASTIC	N,2N	N,N'LR	(N,2N)SUM	CHARGE 1	CHARGE 2	SUM(B)	SUM(KEV-B)
1.492+001										
	LINDHARD	5.439+002	.000	9.762+002	3.873+002	1.364+003	3.872+001	5.686+001	2.003+003	3.004+002
	KINCHIN-PEASE	7.130+002	.000	1.527+003	4.896+002	2.017+003	4.712+001	2.647+001	2.803+003	2.523+002
	TDAM	1.053-001	1.053-001	8.633-002	1.072-001	1.936-001	1.098-001	5.955-001	1.110+000	
	CROSS SECTIONS	2.185+000	.000	1.225+000	4.092+001		3.960-002	9.240-003		
	AVERAGE T	6.128-002	.000	1.907-001	2.341-001		2.436-001	8.545-001		
	LOWER CUT OFF INTERGRATION ENERGY IS		.000	MEV						

	N,N'A	N,N'P	N,GAMA	TOTAL(B)	TOTAL(KEV-B)
LINDHARD	.000	.000	5.889-003	2.003+003	3.004+002
KINCHIN-PEASE	.000	.000	1.221-002	2.803+003	2.523+002
TDAM	.000	.000	3.706-008	1.110+000	
CROSS SECTIONS	2.625-003	.000	7.635-004		
AVERAGE T	.000	.000	1.014-004		

Table A.3.2

χ(T) versus the Nb PKA energy, T at 14.92 MeV neutron energy as calculated by the DISCSM code

T	K(T)										
(MEV)	ELASTIC	INELASTIC	N,2N	NNPUP	SUM	N,P	N,ALPHA	N,N'A	N,N'P	N,GAMA	TOTAL
.000	1.472+002	.000	.000	.000	.000	.000	.000	.000	.000	.000	1.472+002
1.693-002	3.984+001	.000	2.205-001	4.883-001	7.087-001	7.491-002	.000	.000	.000	.000	4.062+001
3.385-002	9.065+000	.000	8.724-001	9.420-001	1.814+000	8.557-002	.000	.000	.000	.000	1.096+001
5.078-002	1.920+000	.000	1.871+000	9.420-001	2.813+000	8.557-002	.000	.000	.000	.000	4.818+000
6.771-002	5.780-001	.000	1.830+000	9.420-001	2.772+000	8.557-002	.000	.000	.000	.000	3.435+000
8.464-002	2.851-001	.000	3.916+000	9.420-001	4.858+000	8.557-002	.000	.000	.000	.000	5.229+000
1.016-001	2.065-001	.000	4.358+000	9.420-001	5.300+000	8.557-002	.000	.000	.000	.000	5.592+000
1.185-001	2.692-001	.000	4.942+000	9.420-001	5.884+000	8.557-002	.000	.000	.000	.000	6.239+000
1.354-001	4.088-001	.000	4.365+000	9.420-001	5.307+000	8.557-002	.000	.000	.000	.000	5.801+000
1.523-001	5.456-001	.000	5.281+000	9.420-001	6.223+000	8.557-002	.000	.000	.000	.000	6.854+000
1.693-001	6.496-001	.000	6.307+000	9.420-001	7.249+000	8.557-002	1.183-003	.000	.000	.000	7.985+000
1.862-001	7.386-001	.000	5.105+000	9.420-001	6.047+000	8.557-002	9.434-003	.000	.000	.000	6.881+000
2.031-001	8.329-001	.000	5.008+000	9.420-001	5.950+000	8.557-002	1.274-002	.000	.000	.000	6.881+000
2.201-001	9.203-001	.000	4.798+000	9.420-001	5.740+000	8.557-002	1.409-002	.000	.000	.000	6.760+000
2.370-001	9.580-001	.000	3.817+000	9.420-001	4.759+000	8.557-002	1.465-002	.000	.000	.000	5.817+000
2.539-001	9.030-001	.000	2.969+000	9.420-001	3.911+000	8.557-002	1.489-002	.000	.000	.000	4.915+000
2.708-001	7.481-001	.000	1.999+000	9.420-001	2.941+000	8.557-002	1.499-002	.000	.000	.000	3.789+000
2.878-001	5.377-001	.000	3.053+000	9.420-001	3.995+000	8.557-002	1.500-002	.000	.000	.000	4.634+000
3.047-001	3.550-001	.000	2.860+000	9.420-001	3.802+000	8.557-002	1.500-002	.000	.000	.000	4.257+000
3.216-001	2.839-001	.000	1.489+000	9.420-001	2.431+000	8.557-002	1.500-002	.000	.000	.000	2.815+000
3.385-001	3.667-001	.000	1.314+000	9.420-001	2.256+000	8.557-002	1.500-002	.000	.000	.000	2.724+000
3.555-001	5.774-001	.000	1.599+000	9.420-001	2.541+000	8.557-002	1.500-002	.000	.000	.000	3.219+000
3.724-001	8.259-001	.000	1.093+000	9.420-001	2.035+000	8.557-002	1.500-002	.000	.000	.000	2.961+000
3.893-001	9.945-001	.000	8.923-001	9.420-001	1.834+000	8.557-002	1.500-002	.000	.000	.000	2.929+000
4.063-001	9.934-001	.000	2.401-001	9.420-001	1.182+000	8.557-002	1.500-002	.000	.000	.000	2.276+000
4.232-001	8.081-001	.000	2.359-001	9.168-001	1.153+000	8.557-002	1.500-002	.000	.000	.000	2.061+000
4.401-001	5.171-001	.000	1.858-001	5.158-001	7.015-001	7.541-002	1.500-002	.000	.000	.000	1.309+000
4.570-001	2.619-001	.000	9.427-002	2.783-001	3.725-001	5.424-002	1.500-002	.000	.000	.000	7.036+001
4.740-001	1.760-001	.000	7.267-002	1.471-001	2.198-001	3.509-002	1.500-002	.000	.000	.000	4.459+001
4.909-001	3.041-001	.000	8.054-002	7.632-002	1.569-001	2.120-002	1.500-002	.000	.000	.000	4.972-001
5.078-001	5.555-001	.000	.000	3.885-002	3.885-002	1.218-002	1.500-002	.000	.000	.000	6.215+001
5.247-001	7.368-001	.000	.000	1.941-002	1.941-002	6.723-003	1.500-002	.000	.000	.000	7.779+001
5.417-001	6.771-001	.000	.000	9.502-003	9.502-003	3.583-003	1.500-002	.000	.000	.000	7.052+001
5.586-001	3.945-001	.000	.000	4.538-003	4.538-003	1.841-003	1.500-002	.000	.000	.000	4.158+001
5.755-001	1.771-001	.000	.000	2.091-003	2.091-003	9.121-004	1.500-002	.000	.000	.000	1.951+001
5.925-001	4.027-001	.000	.000	9.025-004	9.025-004	4.263-004	1.500-002	.000	.000	.000	4.191+001
6.094-001	9.804-001	.000	.000	3.349-004	3.349-004	1.814-004	1.500-002	.000	.000	.000	9.959+001
6.263-001	6.228-001	.000	.000	6.624-005	6.624-005	5.317-005	1.500-002	.000	.000	.000	6.379+001
6.432-001	.000	.000	.000	.000	.000	.000	1.500-002	.000	.000	.000	1.500-002
6.602-001	.000	.000	.000	.000	.000	.000	1.500-002	.000	.000	.000	1.500-002
6.771-001	.000	.000	.000	.000	.000	.000	1.500-002	.000	.000	.000	1.500-002
6.940-001	.000	.000	.000	.000	.000	.000	1.500-002	.000	.000	.000	1.500-002
7.109-001	.000	.000	.000	.000	.000	.000	1.500-002	.000	.000	.000	1.500-002
7.279-001	.000	.000	.000	.000	.000	.000	1.500-002	.000	.000	.000	1.500-002
7.448-001	.000	.000	.000	.000	.000	.000	1.500-002	.000	.000	.000	1.500-002
7.617-001	.000	.000	.000	.000	.000	.000	1.500-002	.000	.000	.000	1.500-002
7.787-001	.000	.000	.000	.000	.000	.000	1.500-002	.000	.000	.000	1.500-002
7.956-001	.000	.000	.000	.000	.000	.000	1.500-002	.000	.000	.000	1.500-002
8.125-001	.000	.000	.000	.000	.000	.000	1.500-002	.000	.000	.000	1.600-002
8.294-001	.000	.000	.000	.000	.000	.000	1.500-002	.000	.000	.000	1.600-002
8.464-001	.000	.000	.000	.000	.000	.000	1.500-002	.000	.000	.000	1.500-002
8.633-001	.000	.000	.000	.000	.000	.000	1.500-002	.000	.000	.000	1.500-002
8.802-001	.000	.000	.000	.000	.000	.000	1.500-002	.000	.000	.000	1.500-002

Table A.3.2 (cont.)

8.972-001	.000	.000	.000	.000	.000	.000	1.500-002	.000	.000	.000	1.500-002
9.141-001	.000	.000	.000	.000	.000	.000	1.500-002	.000	.000	.000	1.500-002
9.310-001	.000	.000	.000	.000	.000	.000	1.500-002	.000	.000	.000	1.500-002
9.479-001	.000	.000	.000	.000	.000	.000	1.500-002	.000	.000	.000	1.500-002
9.649-001	.000	.000	.000	.000	.000	.000	1.500-002	.000	.000	.000	1.500-002
9.818-001	.000	.000	.000	.000	.000	.000	1.500-002	.000	.000	.000	1.500-002
9.987-001	.000	.000	.000	.000	.000	.000	1.500-002	.000	.000	.000	1.500-002
1.016+000	.000	.000	.000	.000	.000	.000	1.500-002	.000	.000	.000	1.500-002
1.033+000	.000	.000	.000	.000	.000	.000	1.500-002	.000	.000	.000	1.500-002
1.049+000	.000	.000	.000	.000	.000	.000	1.500-002	.000	.000	.000	1.500-002
1.066+000	.000	.000	.000	.000	.000	.000	1.500-002	.000	.000	.000	1.500-002
1.083+000	.000	.000	.000	.000	.000	.000	1.500-002	.000	.000	.000	1.500-002
1.100+000	.000	.000	.000	.000	.000	.000	1.500-002	.000	.000	.000	1.500-002
1.117+000	.000	.000	.000	.000	.000	.000	1.500-002	.000	.000	.000	1.500-002
1.134+000	.000	.000	.000	.000	.000	.000	1.500-002	.000	.000	.000	1.500-002
1.151+000	.000	.000	.000	.000	.000	.000	1.500-002	.000	.000	.000	1.500-002
1.168+000	.000	.000	.000	.000	.000	.000	1.500-002	.000	.000	.000	1.500-002
1.185+000	.000	.000	.000	.000	.000	.000	1.500-002	.000	.000	.000	1.500-002
1.202+000	.000	.000	.000	.000	.000	.000	1.500-002	.000	.000	.000	1.500-002
1.219+000	.000	.000	.000	.000	.000	.000	1.500-002	.000	.000	.000	1.500-002
1.236+000	.000	.000	.000	.000	.000	.000	1.500-002	.000	.000	.000	1.500-002
1.253+000	.000	.000	.000	.000	.000	.000	1.500-002	.000	.000	.000	1.500-002
1.270+000	.000	.000	.000	.000	.000	.000	1.500-002	.000	.000	.000	1.500-002
1.286+000	.000	.000	.000	.000	.000	.000	1.500-002	.000	.000	.000	1.500-002
1.303+000	.000	.000	.000	.000	.000	.000	1.500-002	.000	.000	.000	1.500-002
1.320+000	.000	.000	.000	.000	.000	.000	5.588-002	.000	.000	.000	5.588-002
1.337+000	.000	.000	.000	.000	.000	.000	2.621-002	.000	.000	.000	2.621-002
1.354+000	.000	.000	.000	.000	.000	.000	5.277-002	.000	.000	.000	5.277-002
1.371+000	.000	.000	.000	.000	.000	.000	3.666-002	.000	.000	.000	3.666-002
1.388+000	.000	.000	.000	.000	.000	.000	2.482-002	.000	.000	.000	2.482-002
1.405+000	.000	.000	.000	.000	.000	.000	1.611-002	.000	.000	.000	1.611-002
1.422+000	.000	.000	.000	.000	.000	.000	9.732-003	.000	.000	.000	9.732-003
1.439+000	.000	.000	.000	.000	.000	.000	5.055-003	.000	.000	.000	5.055-003
1.456+000	.000	.000	.000	.000	.000	.000	1.631-003	.000	.000	.000	1.631-003
1.473+000	.000	.000	.000	.000	.000	.000	6.431-010	.000	.000	.000	6.431-010
1.490+000	.000	.000	.000	.000	.000	.000	.000	.000	.000	.000	.000
1.507+000	.000	.000	.000	.000	.000	.000	.000	.000	.000	.000	.000
1.523+000	.000	.000	.000	.000	.000	.000	.000	.000	.000	.000	.000
1.540+000	.000	.000	.000	.000	.000	.000	.000	.000	.000	.000	.000
1.557+000	.000	.000	.000	.000	.000	.000	.000	.000	.000	.000	.000
1.574+000	.000	.000	.000	.000	.000	.000	.000	.000	.000	.000	.000
1.591+000	.000	.000	.000	.000	.000	.000	.000	.000	.000	.000	.000
1.608+000	.000	.000	.000	.000	.000	.000	.000	.000	.000	.000	.000
1.625+000	.000	.000	.000	.000	.000	.000	.000	.000	.000	.000	.000
1.642+000	.000	.000	.000	.000	.000	.000	.000	.000	.000	.000	.000
1.659+000	.000	.000	.000	.000	.000	.000	.000	.000	.000	.000	.000
1.676+000	.000	.000	.000	.000	.000	.000	.000	.000	.000	.000	.000
1.693+000	.000	.000	.000	.000	.000	.000	3.493-010	.000	.000	.000	3.493-010

Table A.4

POINTWISE NIOBIUM DISPLACEMENT CROSS SECTIONS AS CALCULATED BY THE DISCSN CODE

(BARNS)

ENERGY (MEV)	ELASTIC	INELST	N,2N	N,2NP	N,P	N,ALFA	N,N'A	N,N'P	N,GAMA	TOTAL
.2200-007	.000	.000	.000	.000	.000	.000	.000	.000	.238	.238
.4140-006	.000	.000	.000	.000	.000	.000	.000	.000	.047	.047
.8764-006	.000	.000	.000	.000	.000	.000	.000	.000	.032	.032
.1855-005	.000	.000	.000	.000	.000	.000	.000	.000	.022	.022
.3928-005	.000	.000	.000	.000	.000	.000	.000	.000	.015	.015
.8315-005	.000	.000	.000	.000	.000	.000	.000	.000	.011	.011
.1760-004	.000	.000	.000	.000	.000	.000	.000	.000	.007	.007
.3727-004	.000	.000	.000	.000	.000	.000	.000	.000	.005	.005
.7889-004	.000	.000	.000	.000	.000	.000	.000	.000	.003	.003
.1670-003	.000	.000	.000	.000	.000	.000	.000	.000	.002	.002
.3536-003	.000	.000	.000	.000	.000	.000	.000	.000	.002	.002
.7485-003	.000	.000	.000	.000	.000	.000	.000	.000	.016	.016
.1585-002	.455	.000	.000	.000	.000	.000	.000	.000	.029	.484
.3355-002	6.299	.000	.000	.000	.000	.000	.000	.000	.042	6.341
.7102-002	6.153	.000	.000	.000	.000	.000	.000	.000	.028	6.181
.1503-001	11.993	.000	.000	.000	.000	.000	.000	.000	.010	12.003
.3183-001	24.373	.001	.000	.000	.000	.000	.000	.000	.003	24.376
.6738-001	55.418	.014	.000	.000	.000	.000	.000	.000	.012	55.445
.1228+000	119.790	.086	.000	.000	.000	.000	.000	.000	.019	119.895
.1657+000	148.264	.193	.000	.000	.000	.000	.000	.000	.016	148.473
.2237+000	183.676	.344	.000	.000	.000	.000	.000	.000	.014	184.035
.3020+000	224.605	.597	.000	.000	.000	.000	.000	.000	.013	225.215
.4076+000	265.364	1.208	.000	.000	.000	.000	.000	.000	.011	266.584
.5502+000	309.628	2.451	.000	.000	.000	.000	.000	.000	.010	312.089
.7427+000	315.837	3.575	.000	.000	.000	.000	.000	.000	.009	319.020
.1003+001	270.460	65.384	.000	.000	.000	.000	.000	.000	.006	335.849
.1353+001	235.246	147.079	.000	.000	.000	.000	.000	.000	.003	382.328
.1827+001	232.596	231.428	.000	.000	.000	.000	.000	.000	.002	463.936
.2466+001	247.155	368.822	.000	.000	.000	.000	.000	.000	.001	615.978
.2725+001	254.102	392.930	.000	.000	.000	.000	.000	.000	.001	647.034
.3012+001	280.444	420.588	.000	.000	.000	.000	.000	.000	.001	701.033
.3329+001	257.549	448.132	.000	.000	.000	.000	.000	.000	.001	705.681
.3679+001	280.631	473.947	.000	.000	.000	.000	.000	.000	.001	754.579
.4066+001	308.348	503.723	.000	.000	.000	.000	.000	.000	.001	812.072
.4493+001	351.570	537.091	.000	.000	.000	.000	.000	.000	.001	888.661
.4966+001	392.820	561.048	.000	.000	.000	.000	.000	.000	.000	953.868
.5488+001	412.187	578.841	.000	.000	.000	.000	.000	.000	.000	991.028
.6065+001	487.733	624.309	.000	.000	.000	.000	.000	.000	.000	1112.043
.6703+001	488.170	668.487	.000	.000	82.365	.000	.000	.000	.000	1239.022
.7408+001	484.082	709.190	.000	.000	9.572	.000	.000	.000	.000	1203.244
.8187+001	483.285	.000	2.972	.000	14.005	.000	.000	.000	.000	500.262
.9048+001	472.571	.000	69.393	718.965	18.090	.000	.000	.000	.000	1279.019
.1000+002	510.928	.000	257.386	802.687	23.458	.000	.000	.000	.000	1394.459
.1105+002	451.296	.000	515.624	431.289	28.412	.000	.000	.000	.000	1426.621
.1221+002	467.530	.000	749.138	335.042	33.032	.086	.000	.000	.000	1584.829
.1350+002	370.667	.000	897.512	348.326	36.730	188.576	.000	.000	.000	1841.811
.1492+002	543.890	.000	976.168	387.338	38.718	56.864	.000	.000	.000	2002.978
.1600+002	559.312	.000	1045.450	417.223	39.658	39.551	2.184	.000	.000	2103.377
.1700+002	619.401	.000	1034.042	444.149	40.477	31.021	2.603	.000	.000	2171.889
.1800+002	630.065	.000	1032.815	470.572	41.450	29.402	3.058	.000	.000	2207.362
.1900+002	685.661	.000	1007.108	496.010	42.473	27.761	3.593	.000	.000	2262.606

Table A.5

GROUP AVERAGED DISPLACEMENT CROSS SECTIONS OF NIOBIUM AS CALCULATED BY THE XGRPAVE PROGRAM

(BARNS)

GROUP	UPPER ENERGY (MEV)	ELASTIC	INELST	N,2N	N,2NP	N,P	N,ALFA	N,N'A	N,N'P	N,GAMA	TOTAL
	.2200-007										
1	.4140-006	.000	.000	.000	.000	.000	.000	.000	.000	.100	.100
2	.8764-006	.000	.000	.000	.000	.000	.000	.000	.000	.039	.039
3	.1855-005	.000	.000	.000	.000	.000	.000	.000	.000	.027	.027
4	.3928-005	.000	.000	.000	.000	.000	.000	.000	.000	.018	.018
5	.8315-005	.000	.000	.000	.000	.000	.000	.000	.000	.013	.013
6	.1760-004	.000	.000	.000	.000	.000	.000	.000	.000	.009	.009
7	.3727-004	.000	.000	.000	.000	.000	.000	.000	.000	.006	.006
8	.7889-004	.000	.000	.000	.000	.000	.000	.000	.000	.004	.004
9	.1670-003	.000	.000	.000	.000	.000	.000	.000	.000	.003	.003
10	.3536-003	.000	.000	.000	.000	.000	.000	.000	.000	.002	.002
11	.7485-003	.000	.000	.000	.000	.000	.000	.000	.000	.008	.008
12	.1585-002	.290	.000	.000	.000	.000	.000	.000	.000	.022	.312
13	.3355-002	3,098	.000	.000	.000	.000	.000	.000	.000	.035	3,132
14	.7102-002	6,235	.000	.000	.000	.000	.000	.000	.000	.035	6,271
15	.1503-001	8,712	.000	.000	.000	.000	.000	.000	.000	.020	8,732
16	.3183-001	17,416	.000	.000	.000	.000	.000	.000	.000	.007	17,423
17	.6736-001	37,973	.007	.000	.000	.000	.000	.000	.000	.007	37,987
18	.1228+000	84,404	.047	.000	.000	.000	.000	.000	.000	.015	84,466
19	.1657+000	133,317	.137	.000	.000	.000	.000	.000	.000	.017	133,472
20	.2237+000	165,086	.269	.000	.000	.000	.000	.000	.000	.015	165,366
21	.3020+000	203,119	.464	.000	.000	.000	.000	.000	.000	.014	203,597
22	.4076+000	243,968	.888	.000	.000	.000	.000	.000	.000	.012	244,867
23	.5502+000	286,391	1,799	.000	.000	.000	.000	.000	.000	.011	288,201
24	.7427+000	312,387	2,985	.000	.000	.000	.000	.000	.000	.010	315,382
25	.1003+001	294,073	32,934	.000	.000	.000	.000	.000	.000	.007	327,014
26	.1353+001	253,730	104,196	.000	.000	.000	.000	.000	.000	.004	357,931
27	.1827+001	233,945	187,146	.000	.000	.000	.000	.000	.000	.002	421,093
28	.2466+001	239,465	296,696	.000	.000	.000	.000	.000	.000	.002	536,163
29	.2725+001	259,571	369,678	.000	.000	.000	.000	.000	.000	.001	631,248
30	.3012+001	257,220	406,578	.000	.000	.000	.000	.000	.000	.001	663,799
31	.3329+001	259,021	434,181	.000	.000	.000	.000	.000	.000	.001	693,203
32	.3679+001	268,898	460,828	.000	.000	.000	.000	.000	.000	.001	729,723
33	.4066+001	294,259	488,567	.000	.000	.000	.000	.000	.000	.001	782,847
34	.4493+001	329,600	520,120	.000	.000	.000	.000	.000	.000	.001	849,729
35	.4966+001	371,851	568,869	.000	.000	.000	.000	.000	.000	.000	920,721
36	.5488+001	402,332	569,796	.000	.000	.000	.000	.000	.000	.000	972,129
37	.6065+001	449,320	601,196	.000	.000	.000	.000	.000	.000	.000	1050,517
38	.6703+001	487,948	646,830	.000	.000	40,496	.000	.000	.000	.000	1174,474
39	.7408+001	486,357	684,499	.000	.000	46,575	.000	.000	.000	.000	1221,431
40	.8187+001	483,893	360,503	1,461	.000	11,752	.000	.000	.000	.000	857,609
41	.9048+001	470,017	.000	35,830	393,492	16,014	.000	.000	.000	.000	883,193
42	.1000+002	491,430	.000	161,823	661,795	20,729	.000	.000	.000	.000	1335,777
43	.1105+002	481,608	.000	384,357	518,414	25,494	.000	.000	.000	.000	1410,272
44	.1221+002	459,270	.000	630,439	383,966	30,648	.042	.000	.000	.000	1504,409
45	.1350+002	419,909	.000	822,084	341,573	34,650	92,754	.000	.000	.000	1711,170
46	.1492+002	455,835	.000	936,185	367,567	37,707	123,817	.000	.000	.000	1921,052
47	.1600+002	551,511	.000	1010,006	402,106	39,182	88,308	1,079	.000	.000	2052,593
48	.1700+002	589,053	.000	1039,804	430,548	40,063	35,329	2,391	.000	.000	2137,188
49	.1800+002	624,682	.000	1033,435	457,232	40,959	30,219	2,828	.000	.000	2189,356
50	.1900+002	657,613	.000	1020,077	483,178	41,937	28,589	3,323	.000	.000	2234,739
51	.2000+002	713,221	.000	998,364	508,621	42,980	26,948	3,858	.000	.000	2289,992

DIFFERENTIAL NB PKA SPECTRUM AT 14.9 MEV NEUTRON ENERGY

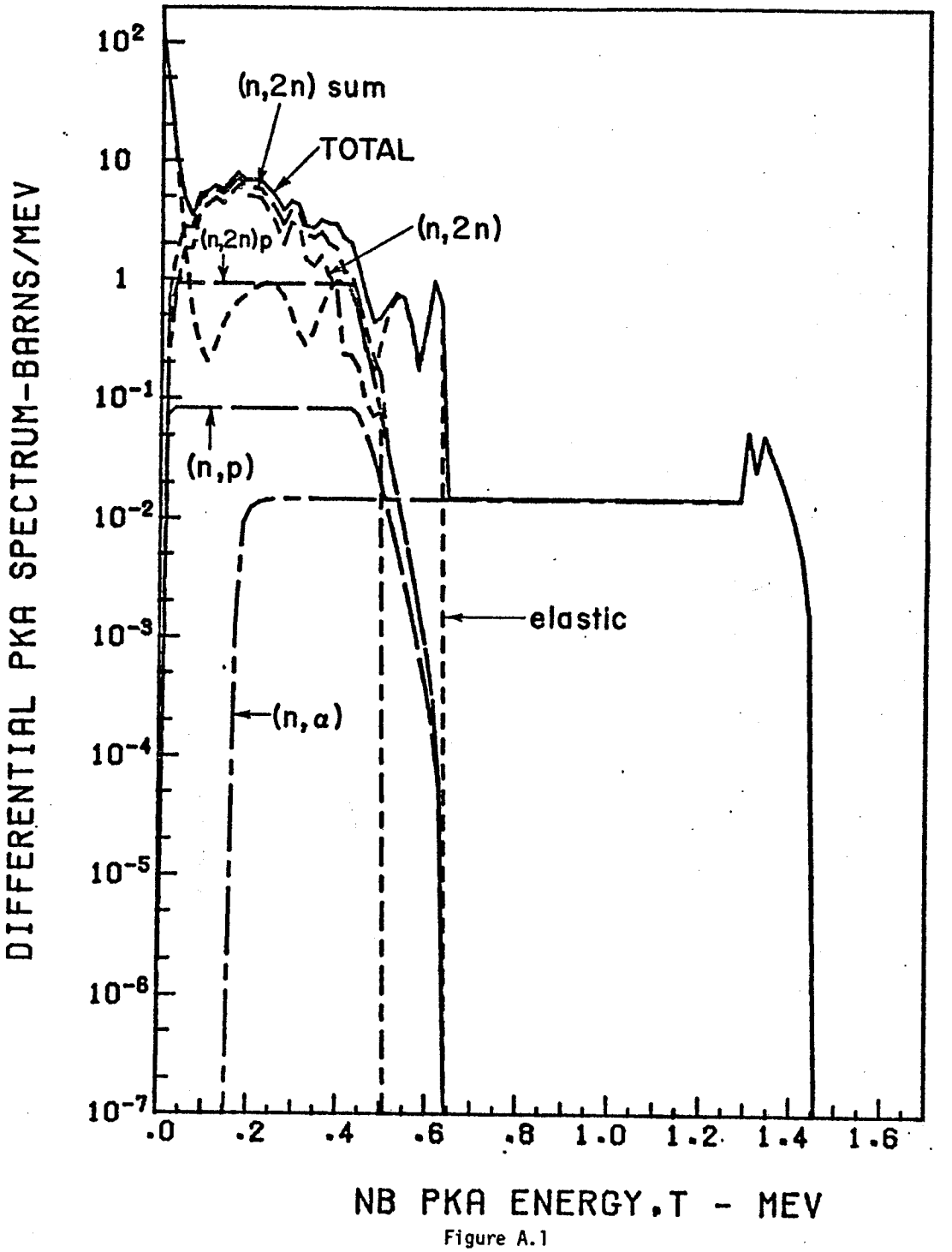

Figure A.1

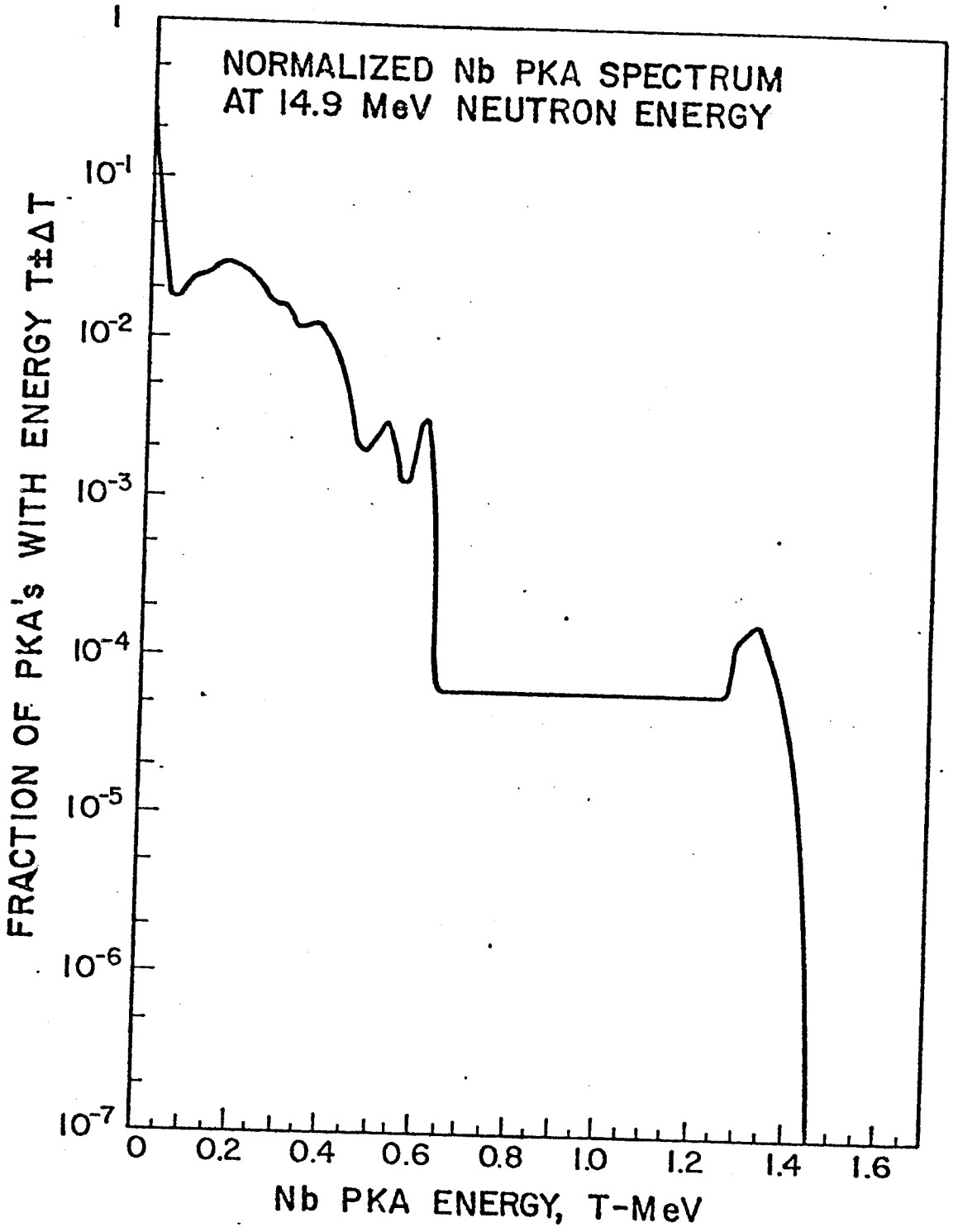
NORMALIZED Nb PKA SPECTRUM
AT 14.9 MeV NEUTRON ENERGY
FRACTION OF PKA's WITH ENERGY T±ΔT
1
10-1
10-2
10-3
10-4
10-5
10-6
10-7
0
0.2
0.4
0.6
0.8
1.0
1.2
1.4
1.6
Nb PKA ENERGY, T-MeV

Figure A.2

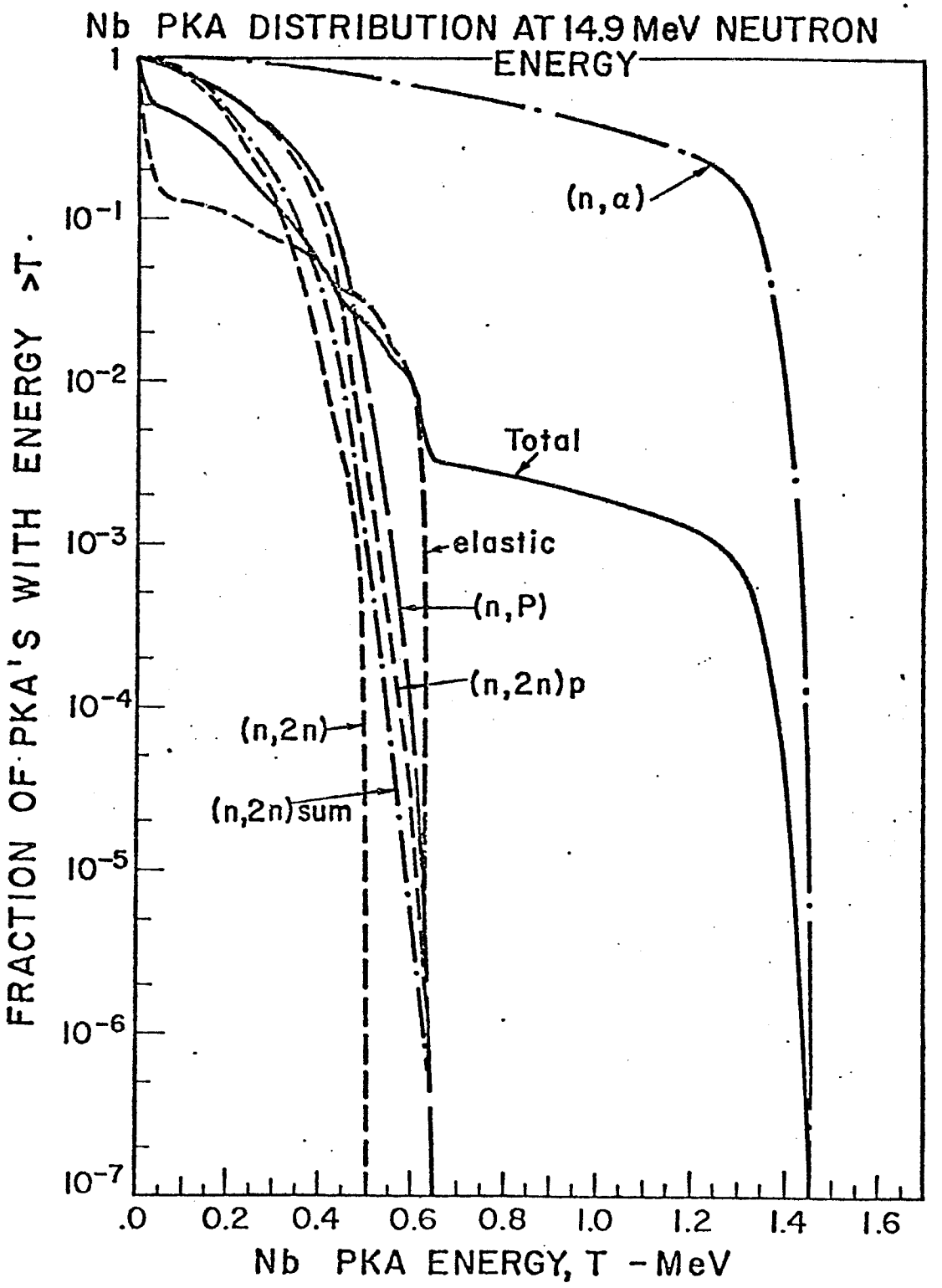
Nb PKA DISTRIBUTION AT 14.9 MeV NEUTRON ENERGY
FRACTION OF PKA'S WITH ENERGY >T.
1
10^{-1}
10^{-2}
10^{-3}
10^{-4}
10^{-5}
10^{-6}
10^{-7}
(n,α)
Total
elastic
(n,P)
(n,2n)p
(n,2n)
(n,2n)sum
.0
0.2
0.4
0.6
0.8
1.0
1.2
1.4
1.6
Nb PKA ENERGY, T - MeV

Figure A.3

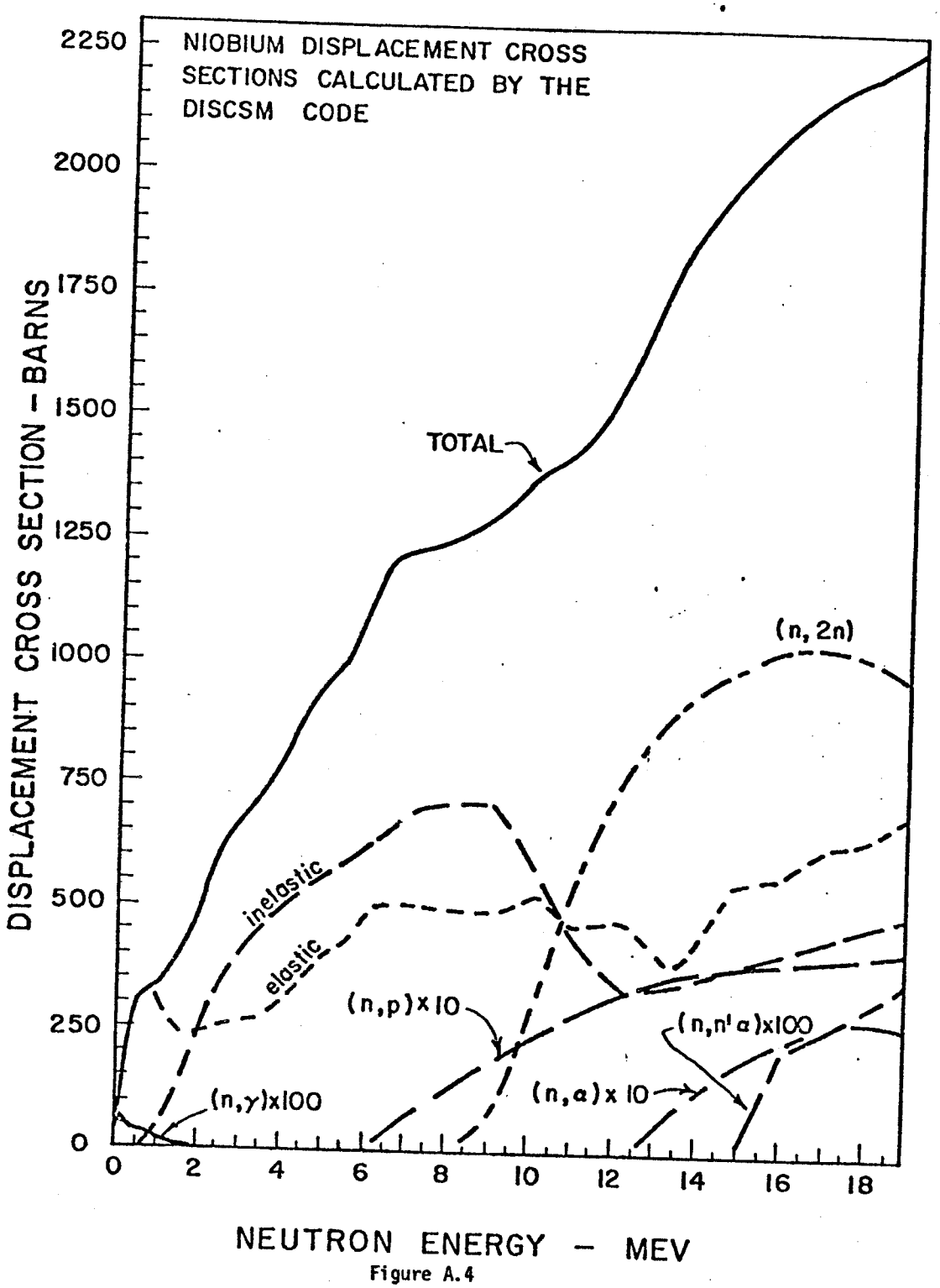
NIOBIUM DISPLACEMENT CROSS SECTIONS CALCULATED BY THE DISCSM CODE
DISPLACEMENT CROSS SECTION - BARNS
NEUTRON ENERGY - MEV
TOTAL
(n, 2n)
inelastic
elastic
(n,p)x10
(n,n'α)x100
(n,γ)x100
(n,α)x 10
2250
2000
1750
1500
1250
1000
750
500
250
0
0
2
4
6
8
10
12
14
16
18

Figure A.4

DIFFERENTIAL Nb PKA PROBABILITY DISTRIBUTION IN HARD FUSION NEUTRON SPECTRUM

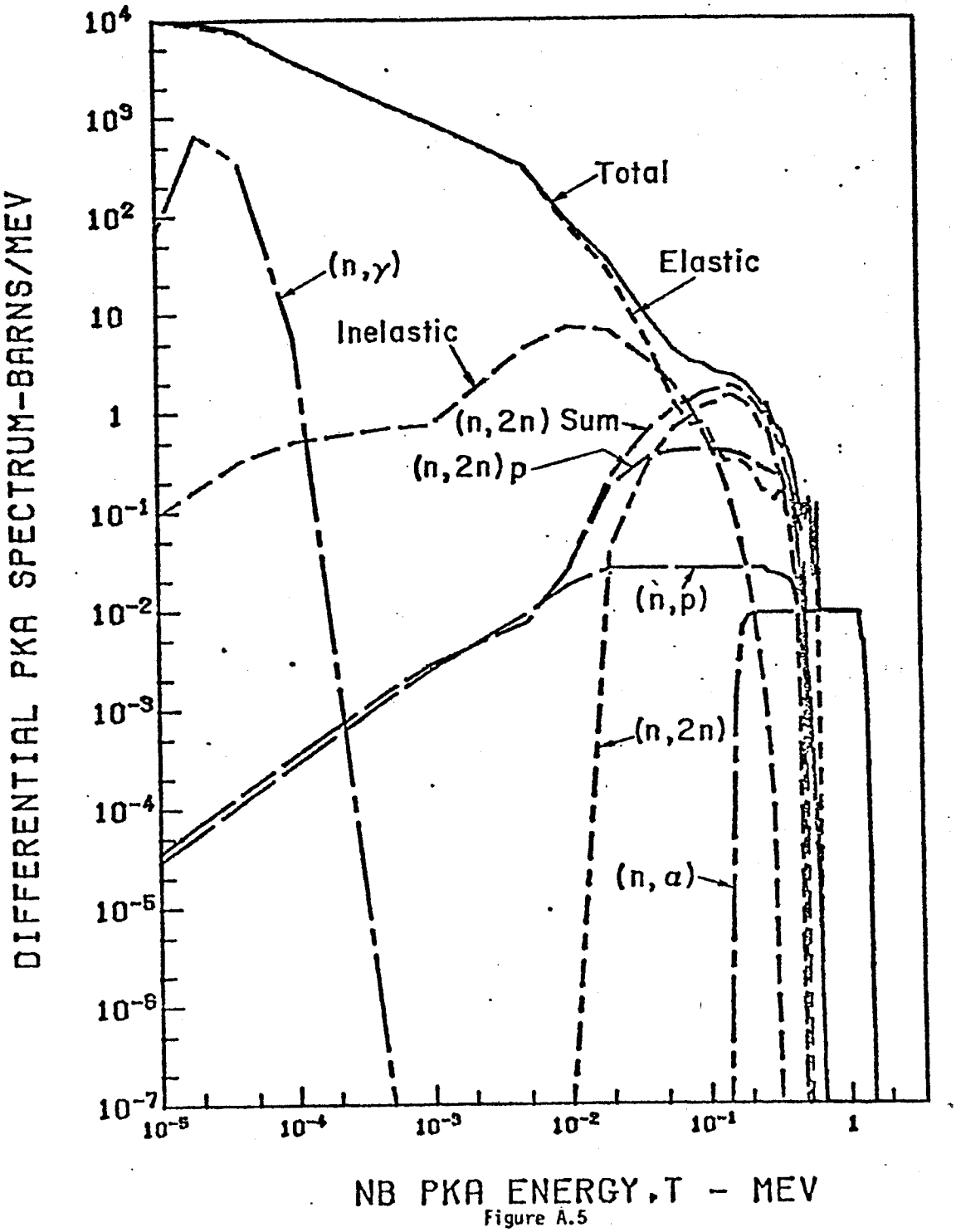

Figure A.5

Nb PKA PROBABILITY DISTRIBUTION IN UNSOFTENED FUSION NEUTRON SPECTRUM

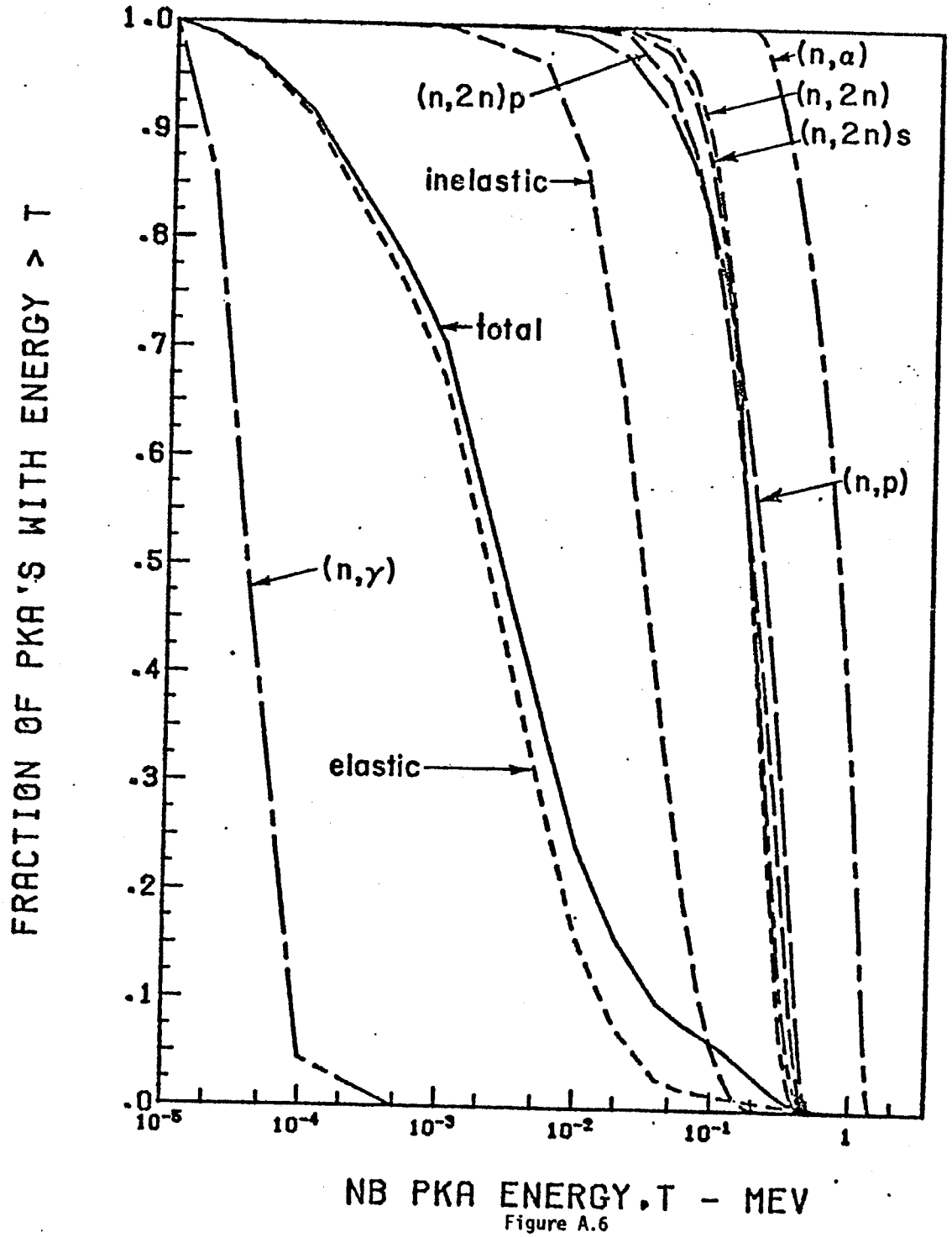

Figure A.6

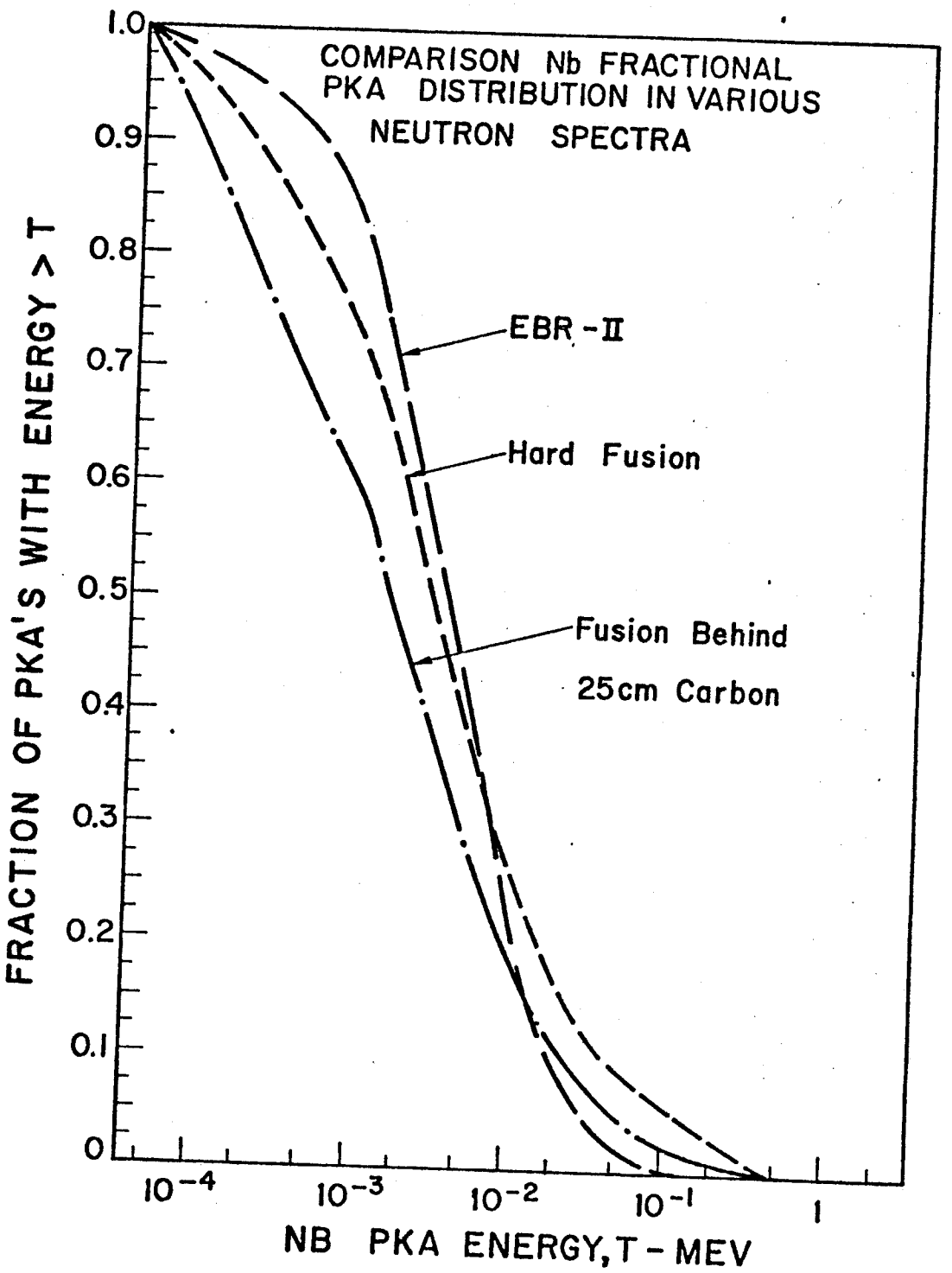
COMPARISON Nb FRACTIONAL
PKA DISTRIBUTION IN VARIOUS
NEUTRON SPECTRA
EBR-II
Hard Fusion
Fusion Behind
25cm Carbon
FRACTION OF PKA'S WITH ENERGY > T
NB PKA ENERGY, T - MEV
1.0
0.9
0.8
0.7
0.6
0.5
0.4
0.3
0.2
0.1
0
10^-4
10^-3
10^-2
10^-1
1

Figure A.7

Appendix B

Neutron and Gamma Multigroup Energy Structures Used in This Study

Table B.1

Neutron 46 Multigroup Structure in eV Group Limits

Group	E(Top)	E(Low)	E(Mid-Point)
1	1.4918 (+7)	1.3499 (+7)	1.4208 (+7)
2	1.3499 (+7)	1.2214 (+7)	1.2856 (+7)
3	1.2214 (+7)	1.1052 (+7)	1.1633 (+7)
4	1.1052 (+7)	1.0000 (+7)	1.0526 (+7)
5	1.0000 (+7)	9.0484 (+6)	9.5242 (+6)
6	9.0484 (+6)	8.1873 (+6)	8.6178 (+6)
7	8.1873 (+6)	7.4082 (+6)	7.7977 (+6)
8	7.4032 (+6)	6.7032 (+6)	7.0557 (+6)
9	6.7032 (+6)	6.0653 (+6)	6.3843 (+6)
10	6.0653 (+6)	5.4881 (+6)	5.7767 (+6)
11	5.4881 (+6)	4.9659 (+6)	5.2270 (+6)
12	4.9659 (+6)	4.4933 (+6)	4.7296 (+6)
13	4.4933 (+6)	4.0657 (+6)	4.2795 (+6)
14	4.0657 (+6)	3.6788 (+6)	3.8722 (+6)
15	3.6788 (+6)	3.3287 (+6)	3.5038 (+6)
16	3.3287 (+6)	3.0119 (+6)	3.1703 (+6)
17	3.0119 (+6)	2.7253 (+6)	2.8686 (+6)
18	2.7253 (+6)	2.4660 (+6)	2.5956 (+6)
19	2.4660 (+6)	1.8268 (+6)	2.1464 (+6)
20	1.8268 (+6)	1.3534 (+6)	1.5901 (+6)
21	1.3534 (+6)	1.0026 (+6)	1.1700 (+6)
22	1.0026 (+6)	7.4274 (+5)	3.726 (+5)
23	7.4274 (+5)	5.5023 (+5)	6.4648 (+5)
24	5.5023 (+5)	4.0762 (+5)	4.7892 (+5)
25	4.0762 (+5)	3.0197 (+5)	3.5480 (+5)
26	3.0197 (+5)	2.2371 (+5)	2.6284 (+5)
27	2.2371 (+5)	1.6573 (+5)	1.9472 (+5)
28	1.6573 (+5)	1.2277 (+5)	1.4425 (+5)
29	1.2277 (+5)	6.7379 (+4)	9.5080 (+4)
30	6.7379 (+4)	3.1828 (+4)	4.9604 (+4)
31	3.1828 (+4)	1.5034 (+4)	2.3431 (+4)
32	1.5034 (+4)	7.1017 (+3)	1.1068 (+4)
33	7.1017 (+3)	3.3546 (+3)	5.2281 (+3)
34	3.3546 (+3)	1.5846 (+3)	2.4696 (+3)
35	1.5846 (+3)	7.4852 (+2)	1.1666 (+3)
36	7.4852 (+2)	3.5358 (+2)	5.5105 (+2)
37	3.5358 (+2)	1.6702 (+2)	2.6030 (+2)
38	1.6702 (+2)	7.8893 (+1)	1.2296 (+2)
39	7.8893 (+1)	3.7267 (+1)	5.8080 (+1)
40	3.7267 (+1)	1.7603 (+1)	2.7435 (+1)
41	1.7603 (+1)	8.3152 (+0)	1.2959 (+1)
42	8.3153 (+0)	3.9279 (+0)	6.1216 (+0)
43	3.9379 (+0)	1.8554 (+0)	2.8917 (+0)
44	1.8554 (+0)	8.7643 (-1)	1.3659 (+0)
45	8.7643 (-1)	4.1399 (-1)	6.4521 (-1)
46	4.1399 (-1)	2.2000 (-2)	2.1800 (-1)

Table B.2

Gamma 21 Multigroup Structure in MeV

Group Boundaries

Group	E(Top)	E(Low)	E(mid-point)
1	1.4E01	1.2E01	1.30E01
2	1.2E01	1.0E01	1.10E01
3	1.0E01	8.0E00	9.00E00
4	8.0E00	7.5E00	7.75E00
5	7.5E00	7.0E00	7.25E00
6	7.0E00	6.5E00	6.75E00
7	6.5E00	6.0E00	6.25E00
8	6.0E00	5.5E00	5.75E00
9	5.5E00	5.0E00	5.25E00
10	5.0E00	4.5E00	4.75E00
11	4.5E00	4.0E00	4.25E00
12	4.0E00	3.5E00	3.75E00
13	3.5E00	3.0E00	3.25E00
14	3.0E00	2.5E00	2.75E00
15	2.5E00	2.0E00	2.25E00
16	2.0E00	1.5E00	1.75E00
17	1.5E00	1.0E00	1.25E00
18	1.0E00	4.0E-01	7.00E-1
19	4.0E-01	2.0E-01	3.00E-1
20	2.0E-01	1.0E-01	1.50E-1
21	1.0E-01	1.0E-02	5.00E-2